SUSCEPTIBILITY AND MAGNETORESISTANCE MEASUREMENTS ON FERRO- AND ANTIFERRO-MAGNETIC MATERIALS

by

Subhas Kumar DEY, B.Sc., M.Sc.(India).

A thesis submitted for the
Degree of Doctor of Philosophy
in the University of London.

Department of Electrical Engineering,
Imperial College of Science and Technology.

September, 1966.

ABSTRACT

This thesis is in two parts: Part I is concerned with magnetoresistivity, Part II with susceptibility.

The magnetoresistance of ferromagnetic metals at saturation can be described by analogous expressions to those used for magnetostriction, both effects being represented by even-rank tensors. In practice, however, magnetoresistance measurements need careful interpretation because of the use of rod-shaped specimens which exhibit considerable shape anisotropy. A complete derivation of the magnetoresistivity expressions is presented for the appropriate crystal symmetries.

Experimentally, a potentiometer measuring circuit of 10^{-9} volt/mm sensitivity has been constructed, using a temperature bath constant to 0.005° C. Measurements have been performed on Ni, Fe, Co and Gd polycrystals and on a Ni single crystal, for various fields and orientations. The results have led to a significant improvement in the agreement between the polycrystalline magnetoresistive coefficients and the values obtained from single-crystal measurements in cubic materials. In addition, all five saturation constants of nickel have been evaluated. This work led to the development, and experimental verification, of an analytical expression relating the forced magnetoresistance in nickel to the variation of resistivity with spontaneous magnetization.

The values for $(\frac{\Delta\rho}{\rho})_{\parallel}$ and $(\frac{\Delta\rho}{\rho})_{\perp}$ are positive for cobalt

and negative for gadolinium. Furthermore, $(\Delta\rho_{\parallel} - \Delta\rho_{\perp})/\rho$ is negative in gadolinium and the magnetoresistivity displays an $H^{2/3}$ field dependence near the Curie temperature. These results, hitherto unreported, fit well in the existing theories.

In Part II, antiferromagnetic susceptibility measurements are reported for $LiFeO_2$ and $CdMn_2O_4$. The system $Cd_xMn_{3-x}O_4$ (except for $x = 1$) is found to exhibit para-/antiferro-/ferri-magnetic transitions on cooling to 4.2° K. A modified Sucksmith ring balance is described and details of the appropriate low-temperature techniques are given. After a brief account of Néel ferrimagnetism (collinear-spins), the Yafet-Kittel triangular spin theory is successfully used to explain the results. Two publications relating to this Part are submitted as Appendix III and IV.

ACKNOWLEDGEMENTS

I wish to express my deep gratitude to my supervisor, Professor J. C. Anderson, for valuable discussions, guidance and encouragement throughout this research. I am also indebted to him and to Imperial College for providing the necessary facilities and the financial support, in the form of a research appointment.

I would also like to thank Dr. V. Halpern for his assistance with the theoretical interpretation of some of the susceptibility results. Thanks are also extended to members of the Materials Laboratory for their co-operation and to the technical staff of the department.

Finally, I wish to thank Miss P. J. Carter for typing the thesis.

C O N T E N T S

CHAPTER I

INTRODUCTION

1.1 Summary

Since its discovery by Sir William Thomson in 1856, the change in resistance which accompanies the magnetization of a ferromagnetic specimen has been frequently investigated. In most materials the magnetoresistance corresponds to an increase of resistivity when the current and the magnetization are in the same direction and a decrease when they are at right angles to each other. Near the Curie point, however, a negative magnetoresistance is obtained with the magnetization in any direction relative to the current. The magnitude of the change in resistivity at saturation magnetization is usually a few per cent ($\sim$ 2%) at room temperature, although at low temperatures much larger changes have been observed.

Like magnetostriction, magnetoresistance is independent of the sense in which the field acts. Thus $\frac{\Delta \rho}{\rho}$ and $\frac{\Delta l}{l}$ both are unaffected by the 180° reversal of a magnetic domain: substantial changes in these properties can, however, occur in the upper region of the magnetization curve where the changes in magnetization are mainly due to domain rotations (Fig. 1). Measurements have shown that, in general, as the applied field is gradually increased, the longitudinal magnetoresistance slowly rises to a saturation limit, but the rise is initially much slower than that of the magnetization

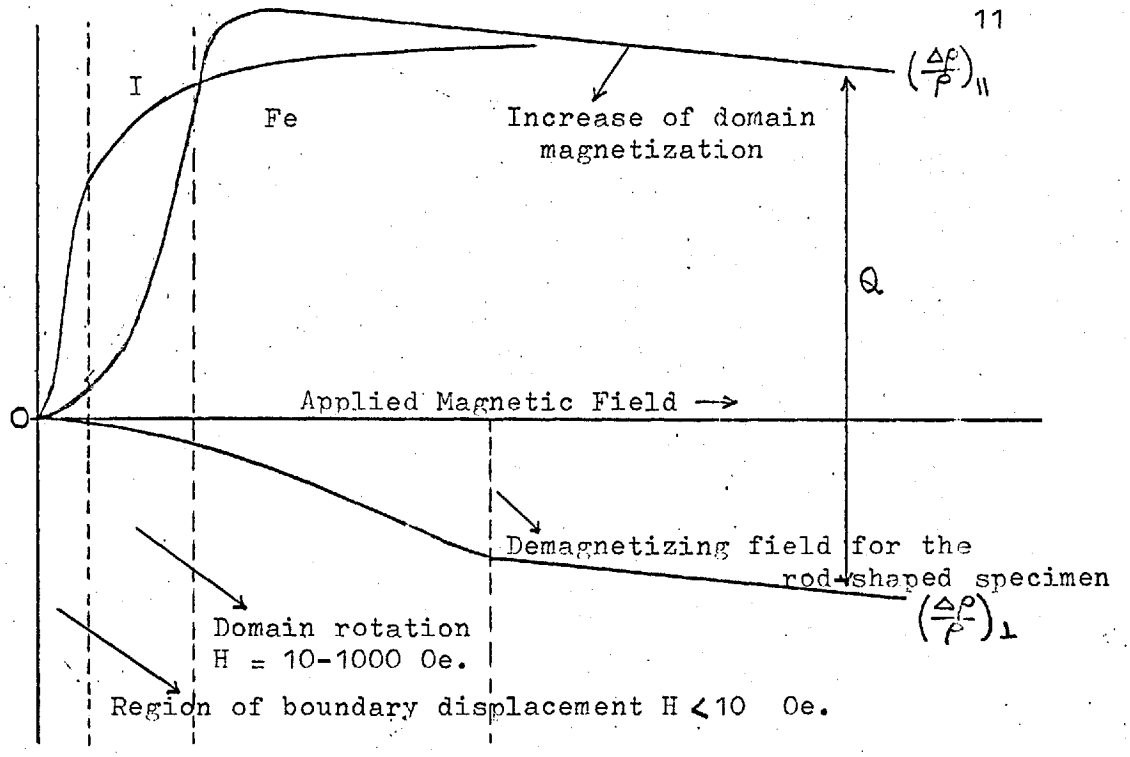

Fig. 1. Schematic representation of magnetization and magnetoresistance of iron as a function of applied field.

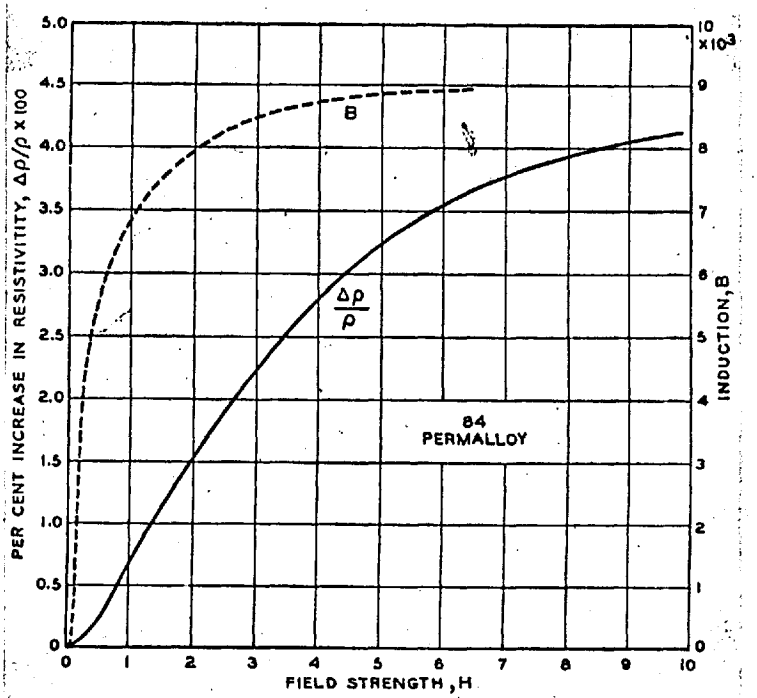

Fig. 2. Increase in resistivity with magnetization in 84 Permalloy. After Bozorth[60].

curve and this lag persists up to the peak value (Fig. 2). In high fields, in the region above what is called technical saturation, both the longitudinal and transverse magnetoresistance decrease almost linearly with the field, the small negative slope being practically the same for all orientations - a characteristic of ferromagnetics shared with a few alloys.

As pointed out by Smit[1], the observed magnetoresistance can, in principle, be classified into three types:

(a) The normal effect, the increase in resistivity that is observed even in non-ferromagnetic metals and alloys. This is due to the Lorentz force acting on the conduction electrons, which gives them curved paths: it appears appreciably at low temperatures even in low fields.

(b) This may be called the orientation effect and it results from the change in the direction of intrinsic magnetization in a crystallite. The anisotropy of the resistivity below technical saturation is analogous to that of the magnetostriction, both being described by tensors that depend on the orientation of the magnetization vector.

(c) The third effect is the decrease of resistivity in strong fields and is analogous to isotropic volume or "forced" magnetostriction caused by a field-induced increase in the spontaneous magnetization. This effect is therefore expected to be most pronounced just below the Curie temperature and it should disappear at the absolute zero.

When the applied field is removed, the resistivity is found to be somewhat greater than its value when the specimen is unmagnetised. This increase of resistivity at the remanent induction is usually, however, a small fraction of the maximum value at saturation. For polycrystalline nickel, $(\frac{\Delta\rho}{\rho})_{rem.}$ is about 15% of the saturation value[2] although in many alloys it is small enough to escape observation. The magnetoresistance thus exhibits some hysteresis when displayed as a function of either the magnetic field or the magnetization (Fig. 3). Special a.c. demagnetizing coils were used in the present investigation to overcome this effect.

1.2 Brief survey of previous work

The variation of resistivity with magnetic field in different crystallographic directions was first investigated in iron by Webster[3] and by Shirakawa[4]. The latter made measurements from room temperature down to -196° C and Gondo and Funatogawa[5] extended the range from room temperature to the Curie point. Measurements on single crystal of nickel were first made by Kaya[6] and later by Döring[7], both at room temperature. The magnetoresistance of polycrystalline nickel below saturation was studied extensively by Gerlach and co-workers[8] and above saturation at different temperatures by Potter[9], who also made similar measurements on iron and Heusler alloys[10]. Magnetoresistance measurements on nickel and iron polycrystals were also reported by Matuyama[11] between -196° C and Curie temperature and by Fedenev

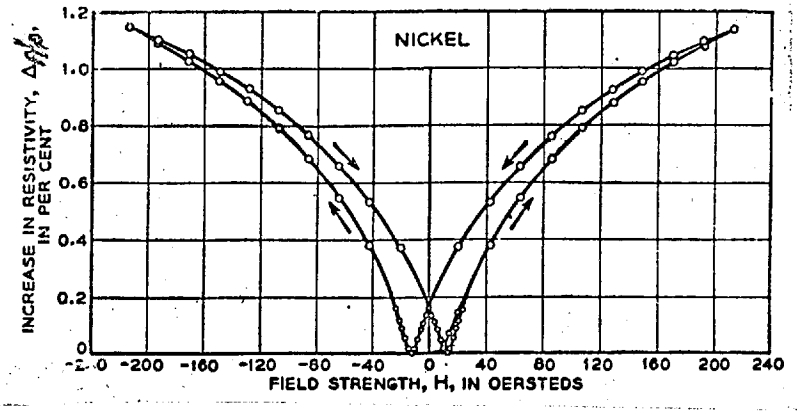

Fig. 3. Hysteresis of resistivity as plotted against field-strength; after Bozorth (60).

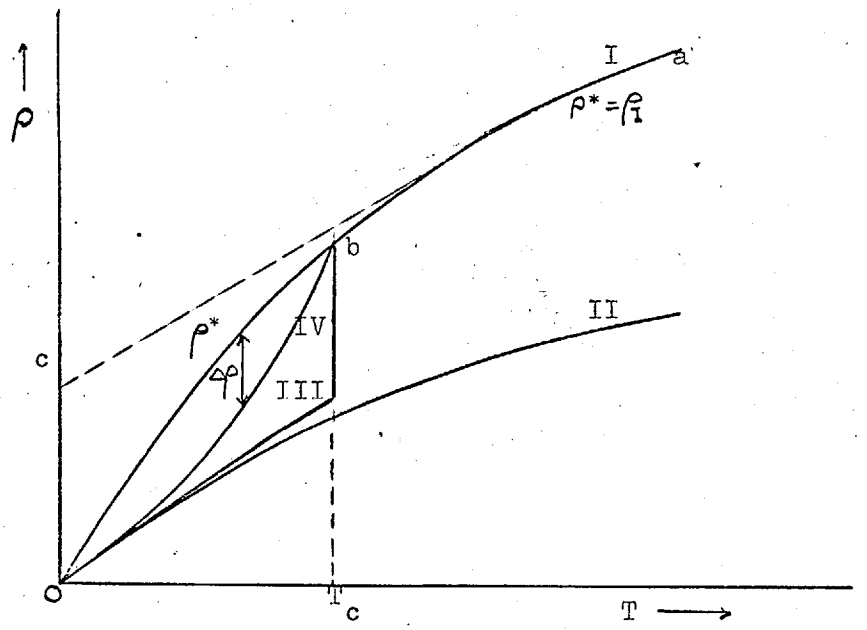

Fig. 4. Schematic diagram illustrating the definition of the resistivities ρ_I, ρ_{II}, ρ_{III} and ρ_{IV}.

and Uskov[12]. Among the very recent work, mention may be made that of Kimura and Tatsumoto[13] on silicon-iron between -196° C and Curie point, of Ôhara[14] on single crystal of iron at low temperatures, of Kikoin and Igosheva[15] and, lastly, of Coleman and Isin[16] who used iron whiskers in fields up to 50 kOe and in a temperature range from 1° K to 1000° K.

There have been few measurements on hexagonal materials, presumably because of difficulty in getting single-crystal specimens of good quality and of requiring very high field to reach saturation. The longitudinal magnetoresistance of polycrystalline cobalt was measured by Alam[17], Matuyama[11], Bates[18] and de Mandrot[19]. There are as yet no single-crystal measurements on either cobalt or gadolinium. After the completion of the work described in this thesis, two articles were published on the magnetoresistance of polycrystalline gadolinium by Lüthi and Grüneisen[20] and by Babushkina[21]. The former is concerned only with the longitudinal magnetoresistance at 4.2° K using pulsed fields up to 200 kOe: an oscilloscope display is used and it is claimed to be possible to determine, in principle, that part of the zero-field electrical resistivity which comes from the electron spin-wave scattering. The second paper deals with resistivity measurements in fields up to 16 kOe and between 4° K and 400° K: the curve of $\frac{\Delta\rho}{\rho}$ against temperature reveals two more maxima in addition to the expected peak at the Curie point due to the paramagnetic transition process, and the high temperature measurements indicate a square law

variation with field. The peculiarities of the magnetic properties of gadolinium near the Curie point have also been investigated by Belov[22] who reported two magnetoresistance maxima in the temperature interval 210-290° K, one of them corresponding to the Curie point.

Among the earlier theories of magnetoresistance, mention may be made to those of Akulov[23], Peierls[24], Englert[25], Gerlach[8], Jones and Zener[26], Davies[27], Bozorth[28], Sondheimer and Wilson[29], Köhler[30], Snoek[31] and Smit[32]. Domain theory was first applied by Gans and Harlem[33] and later extended by Döring, Hironi and Hori[34], Parker[35] and Chikazumi[36]. Among the later contributions are those of Hajdu[37], Kondo[38] and Jones and Sondheimer[39]. In this thesis the theory of magnetoresistance in cubic and hexagonal crystals has been developed from a phenomenological approach on a line similar to that used for magnetostriction[77].

Kaya's[6] results on the longitudinal and transverse magnetoresistance of nickel along the three principal crystallographic directions were later used by Döring[7] to evaluate the five constants k_1 .... k_5 of his general expression for the magnetoresistance in single crystal in which the easy directions of magnetization are the ternary axes (equation 3.42). These values are in good agreement with those obtained by him from his own measurements[7] on eight single crystals of nickel. In a similar way Hironi and Hori[34] derived the constants for iron from the data of Webster[3] and Shirakawa[4]. No measurements have yet been made

on the temperature dependence of these five constants for nickel or for iron. The reliability of these earlier results in reflecting the true magnetic properties of the materials is discussed in the next section.

1.3 Purpose of the present study

Although many experimental studies have been made in the past it may be pointed out that, even for polycrystalline specimens, the variety of significant data that may be obtained is unfortunately restricted. The resistivity in a given direction can only be measured by establishing a uniform electric current density in that direction, and this may only be readily achieved by employing a long rod-shaped specimen. To investigate the magnetoresistance at various angles to the applied magnetic field it is therefore necessary to alter the angle between the field and the axis of the rod. Consequently, for a given value of field, the geometry of the specimen exerts a considerable influence on its magnetic state. Except in very large applied fields, the magnetization will only be collinear with the field when the latter is applied either parallel or perpendicular to the axis of the rod, and nearly all the existing investigations on polycrystalline materials are concerned only with the measurement of the corresponding changes in the "longitudinal" and "transverse" resistivities, $\Delta\rho_{//}$ and $\Delta\rho_{\perp}$.

It has frequently been pointed out[40,41] that it is the difference $(\Delta\rho_{//} - \Delta\rho_{\perp})$ - the so-called ferromagnetic anisotropy -

that is the important constant of the material, rather than these changes in resistivity themselves. This is because, at any applied field, the values of $\Delta\rho_{\parallel}$ and $\Delta\rho_{\perp}$ depend upon the resistivity in the reference demagnetized state, and in many materials this state differs significantly from the ideal demagnetized state in which the ferromagnetic domains are distributed at random. However, it is erroneous to assume that the variation of $(\Delta\rho_{\parallel} - \Delta\rho_{\perp})$ with applied field characterizes the magnetoresistive behaviour of a ferromagnetic substance completely or that the influence of the demagnetized state has been completely removed by this procedure.

In most experimental investigations of magnetoresistance the quantities $\Delta\rho_{\parallel}$ and $\Delta\rho_{\perp}$ are determined separately and the demagnetization of the specimen is also accomplished separately, the demagnetizing fields being applied parallel to the rod-shaped specimen in one set of measurements and perpendicular in the other. There is therefore no reason to believe that the two demagnetized states are the same for each set of measurements nor that $(\Delta\rho_{\parallel} - \Delta\rho_{\perp})$ is independent of these demagnetized states. Even if a common demagnetized state can be employed, the influence of the reference state may not be completely eliminated for the quantities of fundamental importance are the fractional changes in resistivity, $\frac{\Delta\rho}{\rho}$, or their differences. However, since the resistance in any demagnetized state is, in general, large compared with the magnetoresistance (any $\Delta\rho$), the influence of the reference state on the quantity $(\Delta\rho_{\parallel} - \Delta\rho_{\perp})/\rho$ is not usually large.

A further complication is presented by the fact that $\Delta\rho_{\parallel}$ and $\Delta\rho_{\perp}$ do not exhibit saturation in high fields. At normal temperatures and above the point of technical saturation, both quantities exhibit a uniform decrease with increasing applied field that is known as the forced magnetoresistance. The magnetoresistive behaviour of a polycrystal cannot therefore be characterized by a single saturation value of ($\Delta\rho_{\parallel}$ - $\Delta\rho_{\perp}$). Nor is the value at <u>any</u> given field of significance by itself, because the geometry of the specimen may produce marked differences in the resulting magnetic state, both between different specimens and for various field orientations with the same specimen. It is clear therefore that considerable care is needed if experimental data are to be interpreted so as to provide an unambiguous description of the magnetoresistive behaviour of polycrystalline ferromagnetics. It is largely for this reason that this work was undertaken. It was felt that there were some uncertainties and possibly inaccuracies in the values of the five magnetoresistance constants of nickel and iron in view of the poor agreement found, on the basis of existing data, between the experimental and the theoretical values of the polycrystalline magnetoresistance coefficient (the latter being related to the single-crystal constants). It is of primary importance that all measurements are made at saturation as this enables the constants to be evaluated without any need to use a reference state and hence the uncertainty about the demagnetized state disappears. However, in order that the magnetization within the specimen be uniform for

all directions of magnetization, the surface must be one of second degree, i.e. an ellipsoid. Uniform magnetization is not therefore expected in the case of rod or bar-shaped specimens with a high demagnetizing factor unless the field is very large. The influence of the shape anisotropy of the specimen on the field dependence of magnetoresistance at different orientations is one missing feature in the earlier measurements.

The various points mentioned above are considered while analysing the experimental results obtained in the present investigations. This part of the thesis includes measurements on the four ferromagnetic materials Ni, Fe, Co and Gd (all in the shape of cylindrical rods) using a normal four-probe technique. A method of measuring magnetoresistance coefficients of cubic materials by using two arbitrarily shaped flat samples has been described by Mathews and Doherty[42], following an earlier report by Van der Pauw[43]. Since, however, the method involves the measurement of resistivity in zero field and also in fields parallel and (in particular) perpendicular to the plane of the disc, it provides no overall advantage over the present method. A detailed consideration of the nature and the extent of demagnetizing field inside a specimen placed at different orientation to the magnetizing field has been made for the case of uniform magnetization (zero susceptibility) and is given in Appendix II . The account also describes how one piece of single crystal of nickel, suitably oriented, was used to give sets of measurements in three different crystallographic planes from which

all the five magnetoresistance constants can be evaluated. The single crystal of nickel was cut, in the form of a slice, from a larger piece that had been thoroughly polished and had been oriented and checked by the normal X-ray technique. The final results give lower values for the magnetoresistance constants than those obtained by previous workers, improve the agreement between the single-crystal and polycrystalline coefficients referred to earlier and have revealed some new and interesting facts in the case of hexagonal cobalt and gadolinium. These are discussed in Chapter 6.

CHAPTER II

THE RESISTIVITY

2.1 The non-magnetic reference state

The quantity of fundamental importance is not the change in resistivity referred to any demagnetized state, but the fractional change in resistivity $\xi = \frac{\Delta\rho}{\rho}$ referred to the non-magnetic state in which the magnetic interactions have been annihilated. This later quantity - the fractional change in resistance associated with the creation of the spontaneous magnetization - is called the spontaneous magnetoresistance. It is dimensionless and, from symmetry considerations, may be expressed in the form

$$\xi = \frac{\Delta\rho}{\rho} = k_o + k_1 S(\alpha_1^2\beta_1^2) + 2k_2 S(\alpha_1\alpha_2\beta_1\beta_2) + k_3 S(\alpha_1^2\alpha_2^2) + k_4 S(\alpha_1^4\beta_1^2) + 2k_5 S(\alpha_1\alpha_2\alpha_3^2\beta_1\beta_2) \qquad (2.1)$$

for the case of a single crystal of a cubic ferromagnetic material magnetized to saturation. Here α_1, α_2, α_3 are the direction cosines, relative to the crystal axes, of the magnetization vector and ρ is the resistivity in the direction characterised by the direction cosines β_1, β_2, β_3. The operator $S(\ )$ implies the summation of the three terms obtained by a cyclic permutation of suffixes on the expression within the brackets. This reference to an undeformed crystal lattice which is originally non-magnetic is

also used to define the spontaneous magnetostriction. Although it is not, of course, realisable experimentally there are, in fact, several ways of estimating the change in resistivity associated with the destruction of the spontaneous magnetization. The most obvious method is to measure the resistivity of a single crystal over a temperature range which includes the Curie point, when the change in resistivity may be seen superimposed on the normal increase of resistivity with temperature. At temperatures reasonably far below the Curie point, the coefficient k_o is approximately 0.5 whilst the coefficients $k_1 \ldots k_5$ are usually some ten times smaller in magnitude (see page 146). The change in resistivity given by equation (2.1) is thus substantially isotropic and does not depend strongly either on the direction of magnetization or on the direction in which the resistivity is measured. An estimate of the value of k_o may therefore be made from measurements on <u>polycrystals</u> and, in fact, existing data on the temperature dependence of the resistivity of ferromagnetics refer exclusively to polycrystalline materials. Further, the values of k_o obtained from measurements on polycrystals will be considerably closer to the single-crystal values than is indicated by the comparison of k_o with $k_1 \ldots k_5$ mentioned above, for more detailed calculations indicate that the actual discrepancy would be nearly one order of magnitude smaller than these latter coefficients (e.g. -0.0069 for nickel compared to k's $\approx$ 0.055).

Although the coefficients $k_o \ldots k_5$ are called the

magnetoresistance constants, they are, in reality, only constant for a given temperature and for a given value of applied field - it being assumed that the field is large enough to saturate the single crystal so that the magnetoresistive behaviour of the whole specimen is governed by equation (2.1). As stated earlier, the fractional change in resistivity, ξ , decreases linearly with field in high fields and the rate of change $\xi' = \partial\xi/\partial H$ is found to be substantially independent of the direction of magnetization or the direction of observation. For polycrystals, the corresponding fractional change in resistivity ξ_{poly} also changes linearly at a rate ξ'_{poly} which is very nearly the same as the value ξ' obtained with single-crystal specimens of the same material. The variation of resistivity with temperature is considered in detail in section 6.3, where it is shown that it is possible to derive a relation connecting the temperature dependence of ξ'_{poly} , and hence of ξ and k_o, with the field dependence of these quantities, that is with the "forced" magnetoresistance.

2.2 The temperature dependence of the electrical resistivity of polycrystalline ferromagnetics

The electrical resistivity of a ferromagnetic transition or rare-earth metal exhibits, in general, a conspicuous anomaly in the region of the ferromagnetic Curie point, the variation of resistivity with temperature being more pronounced just below this temperature than just above it. This is depicted schematically in

Figure 4. Above the Curie point, T_c, that is in the region a to b, the temperature dependence of the resistivity is similar to that observed in non-ferromagnetic metals. Below the Curie point, the onset of ferromagnetism is accompanied by a reduction in the ideal resistivity, which may therefore be written in the form

$$\rho = \rho^{*} (1 + \xi_{\sigma}), \qquad (2.2)$$

where ξ_{σ}, a negative parameter which vanishes above the Curie point, depends upon the spontaneous magnetization - and hence upon temperature - and where ρ^{*} exhibits a resistivity which is not disturbed in any way by the onset of ferromagnetism. Thus ρ^{*} represents the resistivity of the hypothetical non-ferromagnetic phase of the metal referred to in the previous section. The coefficient $\xi_{\sigma} \simeq k_o$ may be regarded as being temperature dependent, the material passing through a succession of different ferromagnetic states each characterised by the spontaneous magnetization I_s. Thus, below the Curie point, k_o may be evaluated by comparing the resistivity of the ferromagnetic with that of a "normal" non-ferromagnetic metal. The difficulty involved in this procedure, however, lies in predicting the dependence of ρ^{*} on temperature below the Curie point. Several attempts were made in the past to do this.

In 1930 Gerlach and Schneiderhahn[8] drew attention to a connection between the spontaneous magnetization of a ferromagnetic and its electrical resistance. In the neighbourhood of the Curie point the resistivity of nickel is reduced in an applied magnetic

field by a quantity which is proportional to the change in magnetic energy. Similar results were obtained by Potter[9] for iron and Heusler alloy. Gerlach and Schneiderhahn assumed that the resistivity of nickel could also be related to the spontaneous magnetization throughout the whole range of temperatures from the absolute zero to the Curie point. On rather incomplete evidence Gerlach concluded that above the Curie point the variation of resistivity with temperature was linear and by extrapolating a line, such as ab of Figure 4, to lower values of temperatures the distance $\Delta\rho$ was found to be fairly accurately proportional to the square of the spontaneous magnetization. It was therefore concluded that when the metal entered the ferromagnetic state the resistance fell by an amount which was proportional to the magnetic energy.

An objection to this conclusion was put forward by Potter who pointed out that the extrapolated portion bc of the line ab cannot represent the resistivity of a "normal" non-ferromagnetic metal since it predicts a finite resistivity at the absolute zero. He also found difficulty in believing that there was such a close connection between the resistivity and the spontaneous magnetization since the results of Svensson[44] indicated a sharp discontinuity in the temperature coefficient of resistance of nickel in a temperature range as small as 0.1° C at the Curie point, whilst measurements of magnetic energy indicate that the Curie temperature is not sharply defined but extends over a much larger temperature range. Further, the resistivity curves for both nickel and iron are markedly

concave to the temperature axis above the Curie point and Potter[45] concluded that "this fact presumably invalidates Gerlach's extrapolation and consequently his formal theory concerning the connection between resistance and energy of spontaneous magnetization". Whilst there can be no doubt that it invalidates Gerlach's extrapolation it is clear that the form of the relation between resistivity and I_s is still open. For example, the relation

$$k_o \propto I_s^2 , \tag{2.3}$$

may not be far from actual relationship for, although ρ tends to zero at the absolute zero, the ratio $\frac{\Delta\rho}{\rho}$ need not, since the resistivity of both ferromagnetic and non-ferromagnetic metals go to zero together. The difficulty lies in accurately measuring k_o at very low temperatures in order to test the validity of the above equation.

The failure of Gerlach's original linear extrapolation is at first sight rather surprising since Grüneisen[46] has shown that for most pure metals the dependence of resistivity on temperature is given to a close approximation by a universal function of the absolute temperature. Grüneisen's empirical formula, originally derived by Bloch[47], is

$$\rho \propto g\left(\frac{T}{\Theta}\right) \frac{T}{\Theta^2} , \tag{2.4a}$$

where

$$g\left(\frac{T}{\Theta}\right) = 4\left(\frac{T}{\Theta}\right)^4 \int_0^{\Theta/T} \frac{x^5\,dx}{(e^x - 1)(1 - e^{-x})} , \tag{2.4b}$$

and where the characteristic temperature Θ which gives the best

fit with the resistivity measurements is generally close, although not exactly equal, to the Debye temperature for specific heats. Equation (2.4) predicts that the resistivity will be proportional to the absolute temperature, T, at high temperatures and to T^5 at low temperatures ($T \ll \Theta$). Experimental measurements confirm that ρ/T is sensibly constant at high temperatures for most of the non-ferromagnetic metals, increases with T in the case of noble metal and decreases with T in some of the transition metals (including palladium). It is thus clear that Gerlach's original linear extrapolation fails because, above the Curie point, the curve of resistivity versus temperature (e.g. for nickel) is concave to the temperature axis. In conjunction with the fact that resistivity of the transition metals is exceptionally high, this indicates that there must be an additional term or contribution to the resistivity which itself does not obey Grüneisen's relation.

The explanation both of the departure from linearity of the resistivity versus temperature curves of the transition metals and of the difference between the resistivity of a ferromagnetic and the value obtained by extrapolation from above the Curie point, was first given by Mott[48]. Depending on whether the resistivity process invokes an s-d transition mechanism[48, 49] or a spin-disorder mechanism[50, 51, 52, 53, 54], Mott and Stevens[55] later were able to draw a distinction between the band structures of close-packed (e.g. nickel and cobalt) and body-centred (e.g. chromium and iron) transition metals. The two cases correspond to the vanishing

of ρ^{*} and $(1 + \xi)$ respectively at very low temperatures so that in either case the actual resistivity ρ disappears.

2.2.1. The resistivity of close-packed transition metals

Mott pointed out that the poor conductivity of these transition metals is due to the overlap of a narrow d-band (in which the atomic d functions predominate) with a more normal s-band. Since the d wave functions of the individual atoms overlap relatively little, the d-band is abnormally narrow (with a correspondingly large density of states) and the contribution of the d-electrons to the conductivity is very small. However, although almost the entire current is carried by the s-electrons, the vacant levels in the d-band have a considerable effect on the conductivity since the s-electrons can be scattered into energy levels both in the s-band (s-s transitions) and in the d-band (s-d transitions). Since the transition probability is proportional to the density of energy levels in the final state, which is large for the d-levels, the s-d transitions will give rise to a large scattering probability and the resistivity of the transition metal will be much larger than the normal resistivity arising from s-s transitions.

If the transition metal, is in addition, ferromagnetic, Mott's theory again predicts an increase in resistivity due to s-d transitions. Above the Curie point this increase in resistivity arises in exactly the same way as it does in a non-ferromagnetic transition metal. Below the Curie point, however, the ferromagnetic

is spontaneously magnetized and the two half d-bands appropriate to atomic spins parallel and antiparallel to the local magnetization are occupied to different extents. The number of vacant levels in the d-band is therefore a function of temperature and at low temperatures all the levels in the parallel half d-band are occupied as this results in a lower potential energy. At the absolute zero the weight factor for the unfilled levels corresponds to only one direction of spin and is therefore half of what it is above the Curie point. Mott ascribed the reduction in resistivity which accompanies the onset of ferromagnetism to the decrease in the number of s-electrons which are able to make spin-conserving transitions to vacant levels in the d-bands. At low temperatures only one-half of the electrons can undergo s-d transitions. The resistance is thus smaller than that of the corresponding non-ferromagnetic transition metal although, of course, it is still much larger than that of a normal metal in which only s-s transitions are operative.

If these ideas are correct then the variation of ρ^{*} with temperature should arise both from s-s and s-d transitions but mainly from the latter: for a non-ferromagnetic metal, ρ^{*} represents its actual resistivity. At any temperature, ρ^{*} is determined by the band structure of the metal, which is assumed to be sensibly unaffected by changes in temperature, and by the distribution of electrons over the energy levels, which is, of course, temperature dependent. For a ferromagnetic metal, ρ^{*} represents the actual resistivity above the Curie point, T_c, and the

resistivity of the 'normal' non-ferromagnetic metal below T_c. The decrease of ρ/T with T observed in the transition metals may be expected to occur when the density of states for the (unfilled) half d-band decreases appreciably with increasing energy resulting in a reduction in the scattering of the s-electrons with higher thermal energies. Indirect evidence for the validity of Mott's theory also comes from the investigations of several other workers[56,57,58]. It is now generally accepted that for nickel (and for palladium and the Ni-Pd alloys) s-d transitions are mainly responsible for the high resistivity and for the difference between ρ and ρ^{*}.

A procedure commonly adopted in the past for obtaining the dependence of ρ^{*} on temperatures below T_c for nickel was based on the experimentally observed fact that (in Ni and Pd) the two resistivities are approximately proportional for an extended range of temperatures above the Curie point, T_c, of nickel. Further, nickel and palladium occupy similar positions in the periodic table: both elements and their alloys have about 0.6 holes per atom in the d-band and presumably there is a similar equality in the number of conduction electrons per atom. Hence by adopting the same constant of proportionality below T_c, a curve may be obtained which represents the resistivity of 'normal' non-ferromagnetic nickel[59,60,61,62]. It has been shown by Birss and the present writer[63] that although this procedure is legitimate at temperatures just below T_c it is invalid at lower temperatures. An alternative procedure is therefore

suggested whereby the constants of the two equations representing the resistivities of palladium, ρ_{Pd}, and of 'normal' non-ferromagnetic nickel, ρ^{*}_{Ni}, namely

$$\rho_{Pd} = B_1 \, g\left(\frac{T}{\Theta_1}\right) T + C_1 T^2 + D_1 T^3 \,, \qquad (2.5a)$$

$$\rho^{*}_{Ni} = B_2 \, g\left(\frac{T}{\Theta_2}\right) T + C_2 T^2 + D_2 T^3 \,, \qquad (2.5b)$$

are first determined from the measurements of the temperature variation of the resistivities of these two metals at high temperatures since the function $g\left(\frac{T}{\Theta}\right)$ tends to unity for $T \gg \Theta$. The inclusion of the T^2 and T^3 terms in equation (2.5) is explained in the following way:

According to Grüneisen's universal function, for a given metal, if Θ is constant, ρ/T should be constant at high temperatures. The increase of ρ/T with T can be ascribed to the thermal expansion of the metal which gives rise to a decrease of Θ with T given by

$$\frac{1}{\Theta}\frac{d\Theta}{dT} = \frac{d\,\ell n\,\Theta}{dV}\frac{dV}{dT} = -\left(\frac{1}{V}\frac{dV}{dT}\right)\left(-\frac{d\,\ell n\,\Theta}{d\,\ell n\,V}\right) = -\alpha\gamma \,,$$

where α is the volume coefficient of thermal expansion and γ is the Grüneisen constant. At high temperatures, $\alpha\gamma$ is small and approximately constant, whence

$$\Theta^{-2} \propto e^{2\alpha\gamma T} = (1 + 2\alpha\gamma T) \,,$$

whilst $g(T/\Theta) = 1$ in equation (2.4a) so that

$$\rho \propto T(1 + 2\alpha\gamma T) \,. \qquad (2.6)$$

At temperatures of the order $\textcircled{H}$ and below, g is no longer unity and the variation of g with $\textcircled{H}$ must be taken into account. For example, if $\alpha\gamma$ is assumed to be constant at very low temperatures (for which $g \propto (T/\textcircled{H})^4$), equation (2.4a) yields $\rho \propto T^5/\textcircled{H}^6$, or

$$\rho \propto T^5 (1 + 6\alpha\gamma T) . \qquad (2.7)$$

However, the thermal expansion coefficient α vanishes at very low temperatures and hence so does the correction to the resistivity for the decrease of $\textcircled{H}$ with T accompanying thermal expansion: moreover the correcting term $2\alpha\gamma T$ may already be neglected compared with unity when T falls to temperatures of the order $\textcircled{H}$ or below. It may therefore be seen that, at <u>all</u> temperatures, a correcting term of the form CT^2 may be added to the value

$$\rho = B\, g\left(\frac{T}{\textcircled{H}}\right) T , \qquad (2.8)$$

given by equation (2.4a), where B is a constant and C is the approximately constant value of $2\alpha\gamma B$ appropriate to high temperatures.

To allow for the decrease of ρ/T with T observed in the transition metals, a further correction term must be applied of the form DT^3, where D depends[64] upon the shape of the d-band in the neighbourhood of the Fermi limit (Mott writes the term DT^3 as $-\frac{1}{6}\pi^2 T (T/T_o)^2$ thereby defining a "degeneracy temperature" for the d-band, which is about 3500° K for palladium).

At low temperatures it is found, that if the resistivity[72] of palladium is represented by equation (2.5a), the function $g(T/\textcircled{H})$ is not given exactly by equation (2.4b). A new function $G(T/\textcircled{H})$ is therefore defined which brings (2.5a) into exact agreement with the

experimental data where G differs from g appreciably only at low temperatures (see Table 1). The values of G so obtained may then be used to obtain the temperature variation of ρ^{*}_{Ni} by substituting G for g in equation (2.5b). This would seem to be the only satisfactory method of exploiting the similarity of palladium and nickel to predict ρ^{*}_{Ni} from ρ_{Pd}, and it may be seen that the method relies partly on the existence of accurate measurements of ρ_{Ni} and ρ_{Pd} at high temperatures.

The results of the application of this procedure to some new measurements on nickel made by this writer[63] give values of ξ_2 which are in good agreement with other values which are derived from theoretical calculations using the band-structure calculations of Fletcher[65]. The new values of ξ_2 are subsequently used (in section 6.3.) for the verification of the relationship developed in section 6.3 connecting the temperature dependence of ξ_2 with the 'forced' magneto-resistance.

2.2.2 The resistivity of body-centred transition metals

For the body-centred metals such as chromium and iron, Mott and Stevens suggest that the d-band is split into two parts one associated with rather diffuse wave functions of t_g symmetry (i.e. of type xyf(r)) and the other with compact wave functions of e_g symmetry (i.e. of type $(x^2 - y^2)f(r)$). The conductivity is ascribed to the electrons in the t_g band and the magnetic properties to the e_g electrons, for Mott and Stevens suggest that these 'magnetic'

TABLE 1

$T/\textcircled{H}$	$g(T/\textcircled{H})$	$G(T/\textcircled{H})$	g/G
10.0	0.9994	0.9994	1.0000
5.0	0.9978	0.9978	1.0000
2.0	0.9862	0.9862	1.0000
1.75	0.9822	0.9822	1.0000
1.50	0.9757	0.9757	1.0000
1.25	0.9653	0.9727	0.9924
1.0	0.9465	0.9687	0.9771
0.9	0.9351	0.9593	0.9748
0.8	0.9196	0.9476	0.9705
0.7	0.8962	0.9281	0.9656
0.6	0.8581	0.8945	0.9593
0.5	0.8073	0.8412	0.9597
0.4	0.7230	0.7551	0.9575
0.3	0.5756	0.6211	0.9267
0.2	0.3217	0.3998	0.8047
0.1	0.04655	0.1130	0.4120
0.05	0.00311	0.02326	0.1337

electrons do not form a band and do not contribute to the conductivity. This model is based on the interpretation of experimental data for the transition metals, particularly X-ray determinations of electron densities[66,67,68]. The conclusion that the valence electrons may be divided into two classes - conduction electrons distributed throughout the metal and magnetic d-electrons localized near each atom - has also been reached by others, notably Griffith[69] and Lomer and Marshall[70].

If these ideas are correct, the magnetic properties of the body-centred transition metals are due to the existence of essentially localized magnetic electrons whilst current is carried by conduction electrons with t_g wave-functions hybridized with 4s and possibly 4p functions. The resistivity of these metals will therefore be mainly due to scattering of the conduction electrons by the disordered spins of the magnetic electrons[50,51]. Thus, above the Curie point, the spins of the magnetic electrons will be orientated at random and the associated resistivity will be constant, whilst at the absolute zero all the spins will be aligned and this resistivity will vanish leaving only the small contribution of the transitions between conducting states. These conclusions of Mott and Stevens have not met with general acceptance in relation to the metal iron but there is little doubt that the spin-disorder mechanism is correctly invoked in explaining the resistivities of the rare earth metals such as gadolinium. For example, the resistivity of gadolinium follows a line such as ab of Figure 4 above the Curie point which

shows little dependence on temperature. This suggests that the increase in resistivity over that due to s-s transitions should not be ascribed to s-d transitions but rather to a component of the resistivity which is constant above the Curie point and which decreases monotonically to zero as the temperature is lowered from $T=T_c$ to $T=0$.

For gadolinium, the dependence of ρ^* on temperature below the Curie point may be determined more readily than for nickel. For such metals, although the spin-disorder mechanism predominates, the resistivity arises nevertheless from a combination of electron-phonon and electron-magnon interactions. However, above the Curie point the electron-magnon contribution is constant (corresponding to completely disordered spins) whilst electron-phonon interactions give rise to an additional dependence of resistivity on temperature which is essentially linear and of moderate slope. It is therefore possible to fit the experimental data at high temperatures ($\rho = \rho^*$) to an equation of the form

$$\rho^*_{Gd} = A_3 + B_3 g(T/\Theta_3)T + C_3 T^2 + D_3 T^3 \quad , \qquad (2.9)$$

where g is given by equation (2.4b). Again, it may be noted that predictions of ρ^*_{Gd} below the Curie point may only be made if accurate measurements of resistivity at high temperatures are available. The results of the application of the above equation to some new data on gadolinium, taken by this writer, have been described elsewhere[63].

2.2.3 The influence of the Weiss molecular field on the form of the curve of resistivity versus temperature

It is particularly instructive to consider how the form of the curve of resistivity versus temperature is altered by variations in a parameter $Z = X + Y$, where $Y = qI_s$ is the Weiss molecular field and $X = H - NI$ is the effective internal field (N being a demagnetizing factor). This variation is shown schematically in Figure 4.

Curve I is the curve appropriate to $Z = 0$, that is to the hypothetical non-ferromagnetic phase of the material under investigation. At the absolute zero, the separation between the levels in the parallel and antiparallel half d-bands of the ferromagnetic metal reaches a limiting value and the saturation magnetization I_s attains its maximum value I_{so}. If this limiting separation were assumed to remain constant at all temperatures, then the resistivity would only change as a result of the variation with temperature of the distribution of electrons over the levels. Thus if curve II is drawn from the relation $\rho_{II} = \frac{1}{2} \rho_I$, then it represents the resistivity of an "artificial" ferromagnetic for which the 3d spins remain in perfect alignment at all temperatures and for which the Curie temperature and q are both infinite. Curve II corresponds therefore to $Z = \infty$.

Now, in reality, actual ferromagnetics exhibit large and finite values of q, the Weiss molecular field constant, rather than infinite values. Thus the resistivity curve of a ferromagnetic with

a finite value of q must lie between I and II, and its distance from II decreases as the degree of alignment increases. If an "ideal" ferromagnetic is considered for which q is large and finite and $I_s = I_{so}$ for all temperatures below the Curie point, T_c, it may be seen that the degree of spin alignment is little different from the perfect alignment of the "artificial" ferromagnetic. This is because I_s/I_{so} is a measure of the degree of alignment and this quantity is given by a Brillouin function, one characteristic of which is that it changes very slowly for large values of the argument. Thus the resistivity curve for an "ideal" ferromagnetic - curve III - will be almost the same as curve II except that it will exhibit a finite Curie temperature, T_c, corresponding to a finite value of the Weiss molecular field coefficient. Curve III thus corresponds to a large finite value of the parameter Z.

For an actual ferromagnetic, q is substantially constant, except in a small range of temperatures at the Curie point, but I_s varies from I_{so} to zero, causing a considerable variation in the degree of spin alignment and hence of the resistivity - depicted by curve IV. Curve IV thus corresponds to constant q and variable I_s, that is to a variable value of the parameter Z. However, an increase in the total field Z, leading to an increase in spin alignment, can be achieved not only by reducing the temperature so that I_s and hence Y are increased but also by increasing the internal magnetic field X acting on the material. Thus, if the form of the dependence of the curves of Figure 4 upon Z can be

ascertained, the variation of resistivity with temperature may be related to the dependence of resistivity on magnetic field, that is to the "forced magnetoresistance". This is attempted in section 6.3.

2.3 Resistivity in an external magnetic field

For an ideal polycrystal, the spontaneous magnetoresistance associated with the creation of the spontaneous magnetization may be expressed in the form[40]

$$\xi = P + Q\cos^2 x + R\cos^4 x + \ldots \quad , \qquad (2.10)$$

where x is the angle between the saturation magnetization vector and the direction in which the magnetoresistance is measured. The coefficients P, Q, R, ... are purely formal and subject only to the limitations of crystal symmetry. An advantage of formulating the fundamental equation in terms of the spontaneous magnetoresistance ξ rather than in terms of quantities referred to the ideal demagnetized state, such as $\Xi_{\parallel} = \Delta\rho_{\parallel}/\rho$ or $\Xi_{\perp} = \Delta\rho_{\perp}/\rho$, is that it eliminates an undesirable tendency to interpret the forced magnetoresistance in terms of a field dependence of the Ξ's, quantities which contain a part that depends on the demagnetized state and which cannot therefore be field dependent.

Experimental data are always interpreted by taking only the first two terms of equation (2.10), although the justification for terminating the series at any stage of the expansion must, of course, always rely upon a comparison with the experimental data themselves. From a consideration of the linear relationship observed

between the increase in resistivity and the square of the magnetization for a material under substantial tension, Bozorth[60] concluded that no terms higher than that in $\cos^2 x$ need be included for the description of the magnetoresistive behaviour of the material. However, present measurements indicate a weak dependence on the $\cos^4 x$ term which will be discussed in Chapter 6. A similar expression is usually employed to describe the polycrystalline magnetostriction and, in this case, an expression of the form $P + Q \cos^2 x$ fits the experimental data quite well at least for nickel. The spontaneous polycrystalline magnetostriction may also be obtained by averaging the strain in the individual crystallites over all directions. For cubic and hexagonal materials it has been shown that even if the expressions for the single-crystal magnetostriction are not limited to second powers of cosines of angles an expression of the form $P + Q \cos^2 x$ is obtained provided that it is assumed, in this averaging process, that the stress is uniform throughout the polycrystal so that the strains in the individual crystallites may be added together linearly[71]. A similar procedure can be followed to derive expressions for polycrystalline magnetoresistance from single-crystal equations. The justification for employing a corresponding linear averaging process for magnetoresistance rests on the fact that it is the resistivities rather than the changes in resistivity that must be averaged and, since the magnetoresistance is usually small compared with the resistance itself, the exact method of averaging is not very important. Thus, for instance, either resistivity or con-

ductivity can be averaged without making a significant difference to the resulting expression, as shown by the following approximate equality

$$\rho/\rho_o = (1 + \frac{\Delta\rho}{\rho_o}) = (1 - \frac{\Delta\sigma}{\sigma_o}) \simeq (1 + \frac{\Delta\sigma}{\sigma_o})^{-1} = \frac{\sigma_o}{\sigma} , \qquad (2.11)$$

where ρ is the resistivity and σ is the conductivity. Theoretically, the first method of averaging corresponds to the evaluation of the electric field average over a large number of individual crystallites in the direction of the current assuming that the current is continuous everywhere. The second approach corresponds to a current density average assuming that the electric field is continuous.

Assuming, then, that the polycrystalline magnetoresistance can be adequately represented by the first two terms of equation (2.10), the somewhat artificial situation may be considered in which a given polycrystalline specimen is placed in a given orientation relative to a fixed saturating applied field. If the resistivity is measured at various angles x to the saturation magnetization vector then the spontaneous magnetoresistance may be expressed in the form

$$\bar{\xi} = P + (3/2)\,\bar{\Xi}_s \cos^2 x , \qquad (2.12)$$

where the constant Q has been replaced by $\frac{3}{2}\bar{\Xi}_s$ because of the familiar association of $\bar{\Xi}_s$ with the fractional change in resistance between the ideal demagnetized state and the state in which the polycrystal is magnetized to saturation parallel to the measuring direction. It should be noted that, since the angular relationship

between the specimen and the field is assumed to be fixed, it is the direction of measurement which must be varied to alter the angle x.

The formulation contained in equation (2.12) is inconvenient for three reasons. First it does not correspond to the usual experimental arrangement in which the direction of measurement remains fixed relative to the specimen and the direction of the applied field is varied. Secondly it does not take into account possible variations in the saturating applied magnetic field H and thirdly it does not permit a ready comparison between data obtained with different specimens of the same material.

As mentioned in section 2.1, if the magnetoresistance is measured in high fields (but still with the same specimen) it is usual to observe that $\bar{\rho}$ decreases linearly with field for a given value of the angle x. Equation (2.12) may therefore be modified thus

$$\bar{\rho}(x,H) = \bar{\rho}(x,H_o) + (H-H_o)\left(\frac{\partial \bar{\rho}}{\partial H}\right)_{H = H_o} \qquad (2.13a)$$

or

$$\bar{\rho}_H = P_{H_o} + (H-H_o)\frac{\partial P}{\partial H} + \frac{3}{2}\cos^2 x \left\{ \left(\bar{\Delta}_s\right)_{H_o} + (H-H_o)\frac{\partial \bar{\Delta}_s}{\partial H} \right\}. \qquad (2.13b)$$

The two unknown quantities $\partial P/\partial H$ and $\partial \bar{\Delta}_s/\partial H$ may be determined by observing the rate of change with H of $\bar{\rho}_{\parallel}$ $(x = 0)$ and $\bar{\rho}_{\perp}(x = \pi/2)$.

In practice it may be desirable to measure $\bar{\rho}$ on different specimens of the same material or - what is more likely - to compare

values of $\bar{\xi}$ obtained with a particular specimen for which the parameter x has been altered by keeping the direction of measurement fixed and varying the direction of the applied magnetic field. For these cases equations (2.13) cannot be employed directly because of the dependence of the magnetic state of the ferromagnetic on the geometry of the specimen. However, this difficulty can be overcome by observing that the dependence of magnetic state on internal magnetic field, X, is always the same for any specimen and for any direction in the specimen, provided only that the internal field is uniform. Thus if the dependence of H of equation (2.12) is replaced by a dependence on the internal field

$$X = H - NI \ , \tag{2.14}$$

where N is the demagnetizing factor, then the equation

$$\bar{\xi}_X = P_{X_o} + (X - X_o)\frac{\partial P}{\partial X} + \frac{3}{2}\cos^2 x \left\{ \left(\bar{\Xi}\right)_{X_o} + (X - X_o)\frac{\partial \bar{\Xi}}{\partial X} \right\} , \tag{2.15}$$

is obtained. Equation (2.15) may be used with confidence for the customary experimental arrangements and also for comparing results obtained with different specimens of the same material provided the internal field is uniform. A further simplification is afforded by defining the values of P and $\bar{\Xi}_s$ in equation (2.12) as those obtained by extrapolation of the linear high-field portion of the magnetoresistance curves to zero internal field ($X_o = 0$). Thus

$$\bar{\bar{\xi}}_{x} = P + X\frac{\partial P}{\partial X} + \frac{3}{2}\cos^2 x\left\{\bar{\bar{\Xi}}_s + X\frac{\partial \bar{\bar{\Xi}}_s}{\partial X}\right\}, \qquad (2.16)$$

where it should be noted that, experimentally, this equation is somewhat artificial since the polycrystal is not saturated at X = 0. If measurements above the point of technical saturation reveal that $\partial \bar{\bar{\xi}}_{\parallel} / \partial H$ and $\partial \bar{\bar{\xi}}_{\perp} / \partial H$ are exactly equal so that $\frac{\partial P}{\partial X} = \frac{\partial P}{\partial H}$ is finite whilst $\frac{\partial \bar{\bar{\Xi}}_s}{\partial X} = \frac{\partial \bar{\bar{\Xi}}_s}{\partial H}$ is zero then equation (2.16) simplifies to

$$\bar{\bar{\xi}}_{x} = P + X\frac{\partial P}{\partial X} + \frac{3}{2}\bar{\bar{\Xi}}_s \cos^2 x , \qquad (2.17)$$

C H A P T E R III

TRANSPORT EQUATIONS

3.1 Galvanomagnetic effects

Broadly speaking, the effects that manifest themselves when a conductor carrying a primary current is placed in a magnetic field, H, define the galvanomagnetic and thermomagnetic properties of the conductor. When H = 0, the electrical and thermal properties of an isotropic conductor may be adequately described by four basic quantities, namely, the electrical conductivity, the thermal conductivity, the thermoelectric power and the Peltier coefficient. In the presence of a magnetic field, several other phenomena are exhibited, the most important of which are the Hall effect and magnetoresistance associated with the electric current, the magneto-conductivity and thermoelectric power change associated with the thermal current and the Ettingshausen-Nernst effect associated with the flow of either current. To give precise definitions of these effects, it is necessary to define the conditions under which measurements are taken.

Since the present investigation is primarily concerned with the magnetoresistance effect in ferromagnetics, no attempt will be made to include thermomagnetic terms in the subsequent development of the phenomenological theory; in other words, it will be assumed that conditions are perfectly isothermal so that no thermal

gradients exist anywhere. Of the remaining two transport phenomena, namely electrical conductivity and the Hall effect, the former has been discussed in detail in the previous chapter. The Hall effect in an isotropic solid is the electric field which appears perpendicular to the current and the magnetic field when the latter is applied. It will be shown that this quantity can be described by the antisymmetrical part of the general tensor representing the electrical resistivity, and hence is eliminated in the normal experimental arrangements to measure magnetoresistivity.

3.2 The phenomenological description

The fundamental equation in the phenomenological theory is the generalized form of Ohm's law

$$E_i = \rho_{ij} J_j \quad (i = 1,2,3) , \qquad (3.1a)$$

where the current density and electric field vectors, $\underline{J}$ and $\underline{E}$ respectively, are represented by their components in a Cartesian co-ordinate system (x_1,x_2,x_3) and where ρ_{ij} is the electrical resistivity tensor. Here, as throughout the rest of this part of the thesis, the standard convention implying summation over repeated indices has been adopted. The resistivity matrix is the reciprocal of the conductivity matrix, the corresponding conductivity tensor, σ_{ik}, being given by the inverse relation

$$J_i = \sigma_{ik} E_k \quad (i = 1,2,3) . \qquad (3.1b)$$

Now a second rank tensor, such as ρ_{ij}, can be divided into a symmetrical part, ρ^s_{ij}, and an antisymmetrical part, ρ^a_{ij}, so

that equation (3.1a) becomes

$$E_i = \rho^s_{ij} J_j + \rho^a_{ij} J_j \ , \tag{3.2}$$

where

$$\rho^s_{ij} = \tfrac{1}{2} (\rho_{ij} + \rho_{ji}) = \rho^s_{ji} \ , \tag{3.3a}$$

and

$$\rho^a_{ij} = \tfrac{1}{2} (\rho_{ij} - \rho_{ji}) = - \rho^a_{ji} \ . \tag{3.3b}$$

It has been shown by Onsager[73] and others[74,75,76] that a reciprocal relationship exists for the resistivity and other similar coefficients which are functions of the magnetic field vector, $\underline{H}$, by virtue of the property of microscopic reversibility, and that this leads to the results

$$\rho_{ij} (\underline{H}) = \rho_{ji} (-\underline{H}) \ , \tag{3.4a}$$

$$\sigma_{ij} (\underline{H}) = \sigma_{ji} (-\underline{H}) \ . \tag{3.4b}$$

From equation (3.3) it follows therefore that

$$\rho^s_{ij} (\underline{H}) = \rho^s_{ij} (-\underline{H})$$

and

$$\rho^a_{ij} (\underline{H}) = -\rho^a_{ij} (-\underline{H})$$

that is, the symmetric tensor must contain only even powers of the magnetic field and the antisymmetric tensor only odd powers.

For ferromagnetics, however, the magnetization is not proportional to the field so that it is more useful to develop the expression for ρ_{ij} or σ_{ik} in a power series of α_i , the direction cosines of the magnetization vector, rather than in a power series of the magnetic field. Furthermore, in a normal experimental arrangement, as in the present case, it is the current

density that is maintained constant whilst the electric field is allowed to adjust itself and is determined from voltage measurements. It is convenient, therefore, in order to be able to correlate directly theory and experimental results, that the full analysis be given for the resistivity tensor rather than for the conductivity tensor. Thus, with a saturating magnetic field, $\underline{H} = H\,\underline{\alpha}$ (with components $H_i = H\,\alpha_i$) applied to the crystal, it is possible to write

$$\rho^{s}_{ij}\,(\underline{\alpha}) = \rho^{M}_{ij} + a_{ijlm}\,\alpha_l\,\alpha_m + a_{ijlmno}\,\alpha_l\,\alpha_m\,\alpha_n\,\alpha_o + \cdots\cdots , \tag{3.5a}$$

and

$$\rho^{a}_{ij}\,(\underline{\alpha}) = a_{ijl}\,\alpha_l + a_{ijlmn}\,\alpha_l\,\alpha_m\,\alpha_n + \cdots\cdots , \tag{3.5b}$$

or, alternatively,

$$E^{s}_{i} = \rho^{M}_{ij}\,J_j + a_{ijlm}\,J_j\,\alpha_l\,\alpha_m + a_{ijlmno}\,J_j\alpha_l\,\alpha_m\,\alpha_n\,\alpha_o + \cdots\cdots , \tag{3.6a}$$

and

$$E^{a}_{i} = a_{ijl}\,J_j\,\alpha_l + a_{ijlmn}\,J_j\,\alpha_l\,\alpha_m\,\alpha_n + \cdots\cdots . \tag{3.6b}$$

Here, ρ^{M}_{ij} corresponds to the non-magnetic reference state discussed in Section 2.2. The higher rank tensors, a_{ijl} , a_{ijlm} , ... are known as galvanomagnetic coefficients. They can be expressed explicitly in terms of the conductivity coefficients of the analogous equation

$$J_i = \sigma^{M}_{ik}\,E_k + b_{ikl}\,E_l\,\alpha_l + b_{iklm}\,E_k\,\alpha_l\,\alpha_m + \cdots\cdots , \tag{3.7}$$

by using the relations

$$\rho_{ij}\,(\underline{\alpha})\,\sigma_{jk}\,(\underline{\alpha}) = \delta_{ik} , \tag{3.8a}$$

where δ_{ik} is the Kronecker delta, defined by

$$\delta_{ik} = 1 \text{ when } i = k \ ,$$

$$\delta_{ik} = 0 \text{ when } i \neq k \ . \qquad (3.8b)$$

Equation (3.2) indicates that the resultant electric field, $\underline{E}$, consists of two parts, $\underline{E}^a$ (with components E_i^a) which changes sign when the saturating magnetic field - and therefore the magnetization - is reversed and $\underline{E}^s$ (with components E_i^s) which remains unchanged on reversing the field. It will be further shown in section 3.2.2 that these two parts represent respectively a generalized Hall effect and a generalized magnetoresistance. Equations (3.6) imply that the electric field $\underline{E}$ depends upon the direction of the saturating magnetic field but not on its magnitude. In a ferromagnetic or ferrimagnetic material there are generally two contributions to the galvanomagnetic effects - one arising from the presence of the spontaneous magnetization and the other from the magnetic field. It is the former contribution that is given by the equation (3.6)[77].

3.2.1 Application of symmetry : definitions

It should be noted that the tensor components occurring in equations (3.5) are all subject to the limitations imposed by the macroscopic or point-group symmetry of the crystalline material in question. The relation between the symmetry of a crystal and the symmetry of its macroscopic physical properties is furnished by Neumann's principle which states that any type of symmetry that is exhibited by the point group of the crystal is also possessed by

every physical property of the crystal. This leads to the requirement that the resistivity or the conductivity tensor must be invariant under all the permissible symmetry operations appropriate to the particular crystal class.

The starting point in the application of symmetry is the matrix, in Cartesian co-ordinate system Ox_i ($i = 1,2,3$), expressing a right-handed rotation through an angle θ about an axis with direction cosines m_i (relative to Ox_i). This leads to new co-ordinates x'_i given by[78]

$$x'_i = l_{ip}\, x_p \,, \tag{3.9a}$$

where

$$[l_{ip}] =$$

$$\begin{bmatrix} \cos\theta + m_1^2(1-\cos\theta) & m_1m_2(1-\cos\theta)+m_3\sin\theta & m_1m_3(1-\cos\theta)-m_2\sin\theta \\ m_2m_1(1-\cos\theta)-m_3\sin\theta & \cos\theta + m_2^2(1-\cos\theta) & m_2m_3(1-\cos\theta)+m_1\sin\theta \\ m_3m_1(1-\cos\theta)+m_2\sin\theta & m_3m_2(1-\cos\theta)-m_1\sin\theta & \cos\theta + m_3^2(1-\cos\theta) \end{bmatrix} \tag{3.9b}$$

For a rotation of the co-ordinate axes given by the above matrix, the components $d_{ijk..n}$ of a tensor transform according to the relations

$$d'_{ijk..n} = l_{ip}\, l_{jq}\, l_{kr} \ldots l_{nu}\, d_{pqr..u} \,, \tag{3.10}$$

where the number of suffixes attached to $d_{ijk..n}$ determines the rank of the tensor. Quantities which transform according to (3.10) are referred to as true or polar tensors since they do not change sign upon a transformation that changes the hand of the co-ordinate

axes. Such a transformation corresponds, for example, to a combination of a rotation of the axes and a reversal of their sense (i.e. the inversion $x'_i = - x_i$). However, many physical quantities do change their sign upon such a transformation and therefore obey the transformation law

$$d'_{ijk..n} = \pm l_{ip} l_{jq} l_{kr} \cdots l_{nu} d_{pqr..u} , \qquad (3.11)$$

these are referred to as axial tensors. Examples of a polar vector (tensor of the first rank) and an axial vector are provided respectively by a displacement and a vector product of two polar vectors. The latter is really a true (i.e. polar) antisymmetrical second-rank tensor, but in three dimensions it has only three components and can therefore be represented by an (axial) vector.

Another concept of importance for the present purpose is that of a physical (or field) tensor, a terminology which is used to differentiate it from the property (or matter) tensor, such as the resistivity or conductivity tensor of equations (3.1). For example, the vectors $\underline{E}$ and $\underline{J}$ of the same equations are physical tensors of the first rank. The invariance of the linear equation - e.g. equation (3.1) - relating the influence and the resultant physical effect under the operation of space-inversion enables the property tensor to be immediately classified as polar or axial provided the physical tensors are so classified. An extension of this simple idea to the invariance of Maxwell's equations immediately yields the results that $\underline{E}$ and $\underline{J}$ are polar vectors while $\underline{H}$ is an axial vector.

A complication to the symmetry problem is introduced by the consideration of time-inversion, which reverses the direction of spin and of current whilst leaving that of charge invariant. Its significance arises from the fact that an orderly distribution of spin magnetic moment may constitute a further repetitive feature of the crystal (on a non-zero time-average basis) that is not included in the description of the geometrical symmetry. This leads to a four-dimensional problem involving generalized transformations in space-time. An excellent treatment of the subject is given by Birss[79], who has shown that non-magnetic crystals (e.g. diamagnetic, paramagnetic) are time-symmetric, that is they are invariant under time-inversion and for these cases the time-inversion operator, R, is an additional symmetry operator. For ferromagnetic, ferrimagnetic and certain antiferromagnetic crystals, R cannot be a symmetry operator since time-inversion reverses the spontaneous magnetization, but this does not preclude the combination of R and a spatial operator being a symmetry operator for these crystals. Property tensors which fall into the above two classes - invariant and anti-invariant under time-inversion - are designated by Birss as i- and c-tensors respectively. It follows from the above that since E_i and J_j of equations (3.6) are the components of a polar i-vector and a polar c-vector respectively, the galvanomagnetic tensors ρ^{*}_{ij} a_{ijlm} , a_{ijlmno} .. , of even rank, are polar c-tensors whilst a_{ijl} , a_{ijlmn} .. , of odd rank, are axial i-tensors.

To determine the form of a property tensor, a practice

that is commonly followed is to impose successively the limitations of crystal symmetry on to the general tensor until all the symmetry requirements are satisfied. The surviving terms then determine the form of the tensor appropriate to the particular crystal class. The mathematical formulation of this process is provided by equation (3.10) where $d_{ijk..n}$ now represents a polar property tensor. Expressed in the more appropriate form,

$$d_{ijk..n} = \sigma_{ip}\, \sigma_{jq} \cdots \sigma_{nu}\, d_{pqr..u} , \qquad (3.12a)$$

where σ is one of a set of matrices (to be successively applied) that correspond to particular permissible symmetry operations. For the axial tensor, the corresponding equation may be written as

$$d_{ijk..n} = |\sigma|\, \sigma_{ip}\, \sigma_{jq} \cdots \sigma_{nu}\, d_{pqr..u} , \qquad (3.12b)$$

where $|\sigma|$ is the determinant of the symmetry matrix σ and is equal to + 1 or - 1 for proper or improper rotations respectively. It is apparent that there will be as many equations as there are symmetry operators. However, an application of ordinary rules of matrix multiplication enables all the permissible symmetry matrices appropriate to a particular crystal class (e.g. 48 for class m3m) to be obtained from suitable combinations of at most four basic matrices, which are known as generating matrices. Since these generating matrices already take account of the full number of symmetry elements they are sufficient to secure maximum simplification in the form of the tensor $d_{ijk..n}$. The members of a set of generating matrices, however, are not unique for a particular

crystal class but may be suitably chosen from a convenient group. Three generating matrices, for the crystal class $\frac{4}{m}$, $\bar{3}$, $\frac{2}{m}$ (O_h) , to which the ferromagnetic metals iron and nickel belong, are

$$\sigma^1 = \left[\bar{1}\right] = \begin{bmatrix} -1 & 0 & 0 \\ 0 & -1 & 0 \\ 0 & 0 & -1 \end{bmatrix}, \quad \sigma^7 = \left[4_z\right] = \begin{bmatrix} 0 & 1 & 0 \\ -1 & 0 & 0 \\ 0 & 0 & 1 \end{bmatrix},$$

$$\sigma^9 = \begin{bmatrix} 0 & 1 & 0 \\ 0 & 0 & 1 \\ 1 & 0 & 0 \end{bmatrix}. \qquad (3.13)$$

The numbering of the matrices is arbitrary and is taken from Birss[79]. For crystals of the class $\frac{6}{m}$, $\frac{2}{m}$, $\frac{2}{m}$ (D_{6h}), to which the ferromagnetic metals cobalt and gadolinium belong, four generating matrices are

$$\sigma^1 = \left[\bar{1}\right] = \begin{bmatrix} -1 & 0 & 0 \\ 0 & -1 & 0 \\ 0 & 0 & -1 \end{bmatrix}, \quad \sigma^2 = \left[2_y\right] = \begin{bmatrix} -1 & 0 & 0 \\ 0 & 1 & 0 \\ 0 & 0 & -1 \end{bmatrix},$$

$$\sigma^3 = \left[2_z\right] = \begin{bmatrix} -1 & 0 & 0 \\ 0 & -1 & 0 \\ 0 & 0 & 1 \end{bmatrix}, \quad \sigma^6 = \left[3_z\right] = \begin{bmatrix} -\frac{1}{2} & \frac{\sqrt{3}}{2} & 0 \\ -\frac{\sqrt{3}}{2} & -\frac{1}{2} & 0 \\ 0 & 0 & 1 \end{bmatrix},$$

(3.14)

where the x_3 axis is taken to be parallel to the hexagonal c-axis of the crystal. Since the inversion, $\bar{1}$, is a symmetry operator in both these crystal classes (i.e. they are centrosymmetrical), polar

TABLE 2

CUBIC SOLIDS

Tensor Rank	Relation among the Components	No. of Independent Components	No. after Particularization
First	$x = y = z = 0$,	0	0
Second	$xx = yy = zz$,	1	1
Third	$xyz = -yxz = yzx$ $= -zyx = zxy = -xzy$,	1	1
Fourth	$xxxx = yyyy = zzzz$, $xxyy = xxzz = yyzz = zzyy$ $= zzxx = yyxx$ (3) ,	4	3
Fifth	$-xxxyz = +xxxzy = -yyyzx$ $= +yyyxz = -zzzxy = +zzzyx$ (10) ,	10	2
Sixth	$xxxxxx = yyyyyy = zzzzzz$, $xxxxyy = xxxxzz = yyyyzz$ $= zzzzyy = zzzzxx = yyyyxx$ (15) , $xxyyzz = xxzzyy = yyzzxx$ $= zzyyxx = zzxxyy = yyxxzz$ (15) .	31	6

TABLE 3

HEXAGONAL

Tensor Rank	Relations among the Components	No. of Independent Components	No. after Particularization
First	$x = y = z = 0$	0	0
Second	$xx = yy$, $zz = zz$,	2	2
Third	$xyz = - yxz$, $yzx = - xzy$, $zxy = - zyx$,	3	2
Fourth	$xxxx = xxyy + xyxy + yxxy$ $= yyyy$, $zzzz = zzzz$, $xxyy = yyxx$ (3) , $xxzz = yyzz$ (6) ,	10	6
Fifth	$yxzzz = - xyzzz$ (10) , $yyxyz = - xxyxz$ (yyxy:5) , $yxyyz = - xyxxz$ (yxyy:5) , $xyyyz = - yxxxz$ (xyyy:5) , $xxxyz = - xxyxz - xyxxz$ $= - yxxxz$ (xxxy:5) , $yyyxz = xxyxz + xyxxz$ $+ yxxxz$ (yyyx:5) ,	25	4
Sixth	$zzzzzz = zzzzzz$, $yyzzzz = xxzzzz$ (15) , $yyxxzz = xxyyzz$ (45) , $xxxxzz = xxyyzz + xyxyzz$ $+ xyyxzz$ (xxxx:15) ,		

(continued)

Tensor Rank	Relations among the Components	No. of Independent Components	No. after Particularization
Sixth (cont)	yyyyzz = xxyyzz + xyxyzz + xyyxzz (yyyy:15),		
	yxyxyy = xxxxxx - yyyyyy - xxxyxy - xxxyyx + xxyxxy + xxyxyx + xyyxxx - yxxyxx + yxyxxx ,		
	xyxyxx = xxyxxy - xxxyxy - xxxyyx + xxyxyx + xyyxxx + yxyxxx - yxxyxx ,		
	yxyyyx = 2yyyyyy - xxxxxx - xxxxyy - xxyxxy - xxyxyx - xyxxyx - xyyxxx + yxxyxx ,		
	xyyyyx = xxxxxx - yyyyyy - xxxyxy + xxyxyx + xyxxyx + xyyxxx - yxxyxx ,		
	xyyyxy = 2yyyyyy - xxxxxx - xxxxyy - xxxyyx - xxyxyx - xyxxyx ,	72	11
	yxxxyx = 3yyyyyy - 2 xxxxxx - xxxxyy - xxxyyx - xxyxyx - xyxxyx ,		
	yxxxxy = xxyxyx - xxxyxy + xyxxyx + xyyxxx - yxxyxx ,		
	xyxxxy = 3yyyyyy - 2xxxxxx - xxxxyy - xxyxxy - xxyxyx - xyxxyx - xyyxxx + yxxyxx ,		
	yyyyxx = xxxxxx - yyyyyy + xxxxyy(:9),		
	yyxxyy = 2yyyyyy - xxxxxx - xxyxxy - xxyxyx - xyyxxx - yxyxxx ,		
	xxyyyy = xxxxxx - yyyyyy + xxxxyy + xxxyxy + xxxyyx - xyyxxx - yxyxxx ,		
	yyxxxx = xxxxyy + xxxyxy + xxxyyx - xyyxxx - yxyxxx ,		
	xxyyxx = 3yyyyyy - 2xxxxxx - xxyxxy - xxyxyx - xyyxxx - yxyxxx.		

tensors of odd rank and axial tensors of even rank vanish identically ($d_{ijk..n} = -d_{ijk..n} = 0$). Tables can now be constructed giving the forms of the general tensors of rank 1,2,3,4,5 and 6 by systematic substitution into equations (3.12) of the generating matrices given in (3.13) and (3.14). For simplicity, only the non-zero components with their inter-relations are shown in column 2 of Tables 2 and 3. In presenting these tables, the compact notations of Fieschi and Fumi[80] and Fieschi[81] have been used according to which the suffixes, instead of the coefficients, are written down using x,y,z in place of 1,2,3. The figure (3) after xxyy in Table 3 denotes the three distinct relations which are obtained after unrestricted permutation of the suffixes. Similar meanings apply to the other figures. Notations of the type (yyxy:5) in Table 3 indicate the five permutations of the given relation subject to the condition that the order of the first four indices of each of its terms is unaltered. The notation (:9) indicates a set of nine equations which are obtained by nine permutations on each term of the given equation, the permutations on yyyyxx, for example, being yyyyxx, yyxyxy, yyxyyx, yyyxxy, yyyxyx, yxyyxy, xyxyyy, xyyxyy, yxxyyy. For axial tensors of fifth rank and polar tensors of sixth rank, the relations among the non-zero components are taken from Fieschi and Fumi.

When the general tensors ρ^{*}_{ij} , a_{ijlm} , ... are identified with the resistivity tensors, a further simplification of the above scheme of coefficients results from a consideration of "intrinsic

symmetry". For example, in the term $a_{ijlm}\,\alpha_l\,\alpha_m$ in equation (3.5a), α_l and α_m are interchangeable so that $a_{ijlm} = a_{ijml}$. Similarly i and j can be interchanged. The number of independent components which remains after particularisation is shown in column 4 of the tables.

3.2.2 The Hall effect and magnetoresistance

Table 2 shows that for the cubic group O_h there is only one independent component for the third rank axial tensor, all the six non-zero coefficients being equated to one another with their proper sign. This takes into account the fact that the first two of the three indices are antisymmetric. If a linear relationship is assumed between the components of $\rho^a_{ij}(\underline{\alpha})$ and $\underline{\alpha}$, then equation (3.6b) gives

$$\begin{bmatrix} E^a_1 \\ E^a_2 \\ E^a_3 \end{bmatrix} = \begin{bmatrix} 0 & a_{123}\,\alpha_3 & -a_{123}\,\alpha_2 \\ -a_{123}\,\alpha_3 & 0 & a_{123}\,\alpha_1 \\ a_{123}\,\alpha_2 & -a_{123}\,\alpha_1 & 0 \end{bmatrix} \begin{bmatrix} J_1 \\ J_2 \\ J_3 \end{bmatrix}. \tag{3.15}$$

If the second and fourth rank tensors are also included the total electric field $\underline{E}$ can be given in the component form

$$\begin{aligned} E_1 &= \rho^{\mathrm{H}} J_1 + a_{123}(J_2\alpha_3 - J_3\alpha_2) + \lambda J_1 + \varepsilon\alpha_1\,\underline{J}\cdot\underline{\alpha} + \eta J_1\alpha_1^2 , \\ E_2 &= \rho^{\mathrm{H}} J_2 + a_{123}(J_3\alpha_1 - J_1\alpha_3) + \lambda J_2 + \varepsilon\alpha_2\,\underline{J}\cdot\underline{\alpha} + \eta J_2\alpha_2^2 , \\ E_3 &= \rho^{\mathrm{H}} J_3 + a_{123}(J_1\alpha_2 - J_2\alpha_1) + \lambda J_3 + \varepsilon\alpha_3\,\underline{J}\cdot\underline{\alpha} + \eta J_3\alpha_3^2 , \end{aligned} \tag{3.16}$$

where

$$\lambda = a_{2211}, \qquad \varepsilon = 2a_{2323}, \qquad \eta = (a_{1111} - 2a_{2323} - a_{2211})$$

and the suffixes on ρ^{*} are now dropped since the resistivity in zero magnetic field is isotropic in cubic crystals. In a more compact vector form, equation (3.16) becomes

$$\underline{E} = \rho^{*}\,\underline{J} + R_H(\underline{J} \times \underline{\alpha}) + \lambda \underline{J} + \varepsilon\,(\underline{J}\cdot\underline{\alpha})\,\underline{\alpha} + \eta\, T\, \underline{J}\,, \qquad (3.17)$$

where $R_H = a_{123}$ and T is a diagonal matrix with elements α_1^2, α_2^2, and α_3^2. Equation (3.17) can be rewritten as

$$\underline{E} = \rho^{*}\,(\,\underline{J} + c(\underline{J} \times \underline{\alpha}) + d\,\underline{J} + e\,(\underline{J}\cdot\underline{\alpha})\,\underline{\alpha} + f\,T\,\underline{J}\,)\,, \qquad (3.18a)$$

where $c = a_{123}/\rho^{*}$, $d = a_{2211}/\rho^{*}$, $e = 2a_{2323}/\rho^{*}$, and $f = (a_{1111} - 2a_{2323} - a_{2211})/\rho^{*}$.

The above form, which is due to Pearson and Suhl[82], provides the inverse relation to the expression developed by Seitz[83] for the magnetoconductivity in cubic solids, namely

$$\underline{J} = \sigma^{*}\,\underline{E} + \alpha(\underline{E} \times \underline{H}) + \beta\, H^2 \underline{E} + \gamma(\underline{E}\cdot\underline{H})\,\underline{H} + \delta\, T\, \underline{E}\,, \qquad (3.18b)$$

where, as before, the co-ordinate axes are coincident with the crystal axes and the Seitz coefficients are connected with the basic magnetoconductivity components of equation (3.7) by the relations

$$\sigma^{*} = \sigma_{11}^{*}\,, \quad \alpha = b_{123}\,, \quad \beta = b_{2211}\,, \quad \gamma = 2b_{2323},$$

$$\delta = b_{1111} - 2b_{2323} - b_{2211}\,.$$

The five different nonvanishing magnetoconductivity components, resulting from the retention of terms involving up to second powers of the magnetic field, may be expressed in terms of the five galvanomagnetic coefficients by using the reciprocal relation (vide eqn. 3.8)

$$\rho_{ij}(\underline{\alpha})\,\sigma_{jp}(\underline{\alpha}) = \delta_{ip}\ , \tag{3.19}$$

where $\rho_{ij}(\underline{\alpha})$ and $\sigma_{jp}(\underline{\alpha})$ are given by

$$\rho_{ij}(\underline{\alpha}) = \rho^{*}_{ij} + a_{ijl}\,\alpha_l + \tfrac{1}{2}\,(a_{ijlm} + a_{ijml})\,\alpha_l\alpha_m\ ,$$

$$\sigma_{jp}(\underline{\alpha}) = \sigma^{*}_{jp} + b_{jpm}\,\alpha_m + \tfrac{1}{2}\,(b_{jplm} + b_{jpml})\,\alpha_l\alpha_m\ . \tag{3.20}$$

After carrying out the summation over j and equating the two sides of equation (3.19) for terms in $\alpha(o)$, α and α^2, the relations

$$\sigma^{*} = \frac{1}{\rho^{*}}\ ,$$

$$b_{123} = -\,a_{123}/(\rho^{*})^2\ , \qquad b_{2211} = -\,\frac{a_{2211}}{(\rho^{*})^2} - \frac{a^2_{123}}{(\rho^{*})^3}$$

$$b_{1111} = -\,\frac{a_{1111}}{(\rho^{*})^2}\ , \qquad b_{2323} = -\,\frac{a_{2323}}{(\rho^{*})^2} + \tfrac{1}{2}\,\frac{a^2_{123}}{(\rho^{*})^3}\ , \tag{3.21}$$

are obtained. Thus the constants of equation (3.18a) are related to the Seitz coefficients by the following expressions

$$\rho^{*} = \frac{1}{\sigma^{*}}\ , \qquad e = -\,(\gamma - \frac{\alpha^2}{\sigma^{*}})/\sigma^{*}\ ,$$

$$c = -\,\frac{\alpha}{\sigma^{*}}\ , \qquad f = -\,\frac{\delta}{\sigma^{*}}\ , \qquad d = -\,(\beta + \frac{\alpha^2}{\sigma^{*}})/\sigma^{*}\ . \tag{3.22}$$

For isotropic media, it can be shown that

$$a_{1111} = a_{2211} + 2a_{2323}\ , \tag{3.23}$$

so that the parameter in equation (3.17) is zero and the equation reduces to the form

$$\underline{E} = \rho^{*} + R_H(\underline{J} \times \underline{\alpha}) + \lambda\,\underline{J} + \varepsilon\,(\underline{J}\cdot\underline{\alpha})\,\underline{\alpha}\ . \tag{3.24}$$

Equation (3.24) indicates that the leading term in $\underline{E}^a$ represents an electric field which is perpendicular to both the current density and the magnetic field. $\underline{E}^a$ may therefore be associated with a

generalized Hall voltage where the Hall coefficient, R_H (= a_{123}), is associated with the nondirectional Hall effect, whilst the fifth rank axial tensor a_{ijlmn} gives directional contributions to it. The term $\lambda\, \underline{J} + \varepsilon(\underline{J}\cdot\underline{\alpha})\, \underline{\alpha}$ constitutes a vector which has no component perpendicular to both $\underline{J}$ and $\underline{H}$. In fact, when $\underline{J}$ and $\underline{H}$ are perpendicular, this vector is collinear with $\underline{J}$. $\underline{E^s}$ may therefore be associated with a generalized magnetoresistance. Equation (3.24) also indicates that the longitudinal magnetoresistance in isotropic solids should vanish if $(\lambda + \varepsilon) = 0$. For anisotropic media, $\underline{E^a}$ is always perpendicular to the current (but not necessarily to the magnetic field) whilst $\underline{E^s}$ is not always parallel to the current.

The analysis contained in equations (3.15) to (3.18) could be extended to include the dependence of the Hall coefficient on terms quadratic in the magnetic field, in which case the fifth rank axial tensor is invoked. It would then be necessary to add to the first component E_1 of equation (3.16) three terms of the form

$$h(J_2\alpha_3^3 - J_3\alpha_2^3) + d'\alpha_1^2\,(J_2\alpha_3 - J_3\alpha_2) + a'\alpha_2\alpha_3\,(J_2\alpha_2 - J_3\alpha_3)\ , \tag{3.25a}$$

where

$$\begin{aligned} h &= a_{23111} = yzxxx\ , \\ d' &= -3a_{13211} = -3xzyxx\ , \\ a' &= -3a_{21113} = -3yxxxz\ . \end{aligned} \tag{3.25b}$$

The above results are obtained after particularization of the general tensor components so that the last three of the five indices which correspond to the powers of the magnetic field are inter-

changeable on account of the intrinsic symmetry. Similar equivalent expressions should be added to the other two equations in (3.16). It can be shown that for an isotropic medium, further limitations to the number of independent coefficients are brought about by the following sets of relations (after particularization)

$$a = b = c = d = i = j = -\frac{1}{3} h \ ,$$
$$e = f = g = 0, \qquad (3.26)$$

where the letters a, b, c, d, e, f, g, h, i and j are used, for simplicity, to denote the 10 independent relations which are obtained by the unrestricted permutations on each term of the compact expression of Fieschi and Fumi, the permutation on xxxzy, for example, being yxxxz, xzxxy, xzxyx, xzyxx, xxzxy, xxzyx, xxxzy, yzxxx, yxzxx, yxxzx. A comparison of (3.25b) with (3.26) immediately shows that the three parameters h, d' and a' are equal to each other in the case of isotropic solid so that (3.25a) becomes the first component of the vector

$$\underline{J} \times \alpha \qquad (3.27)$$

remembering that $\alpha_1^2 + \alpha_2^2 + \alpha_3^2 = 1$. (3.28)

3.2.3 Formulation of the expression for the magnetoresistivity

As stated earlier, in many galvanomagnetic measurements the current density is maintained constant by applying a voltage between the opposite ends of a bar or a rod-shaped specimen that has been cut so as to be parallel to a known crystallographic direction. The effect of this is to produce an electric field, $\underline{E}$,

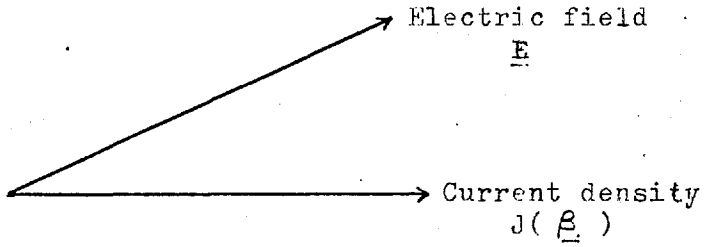

Fig. 5. Diagram illustrating the definition of the resistivity $\rho(\underline{\alpha},\underline{\beta})$ in the direction of $\underline{J}$.

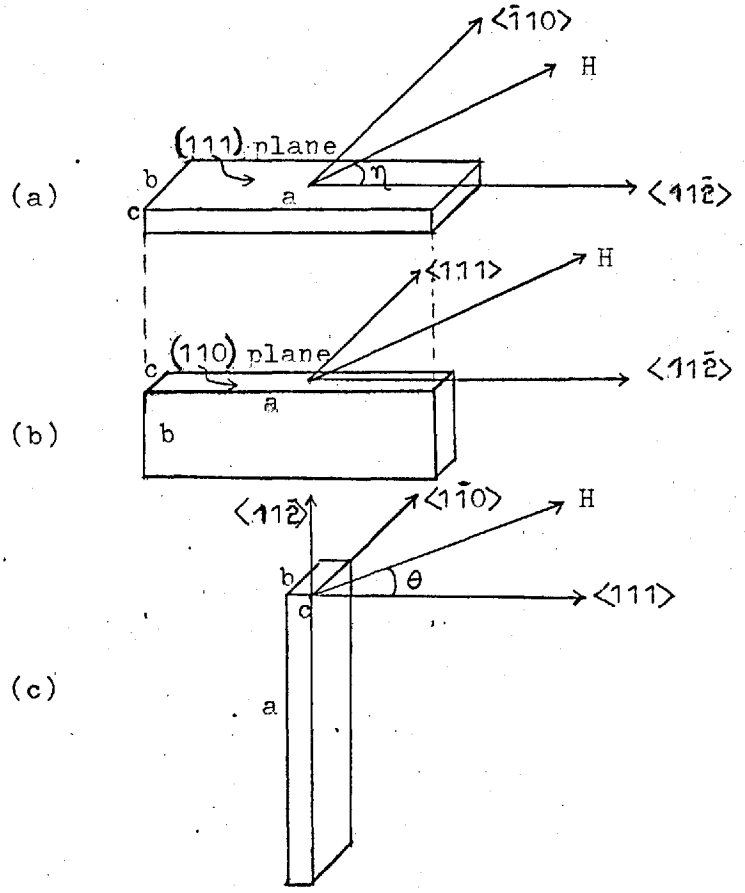

Fig. 6. Diagrams illustrating the three different orientations of the specimen of nickel relative to the plane of magnetization used in the measurement of the five saturation magnetoresistive constants.

in the crystal with, in general, components both parallel and transverse to $\underline{J}$. The resistivity ρ in the direction of $\underline{J}$ is then defined to be the component of $\underline{E}$ parallel to $\underline{J}$ divided by J, that is, $E_{\parallel}/J$. If now β_1, β_2, β_3 denote the direction cosines of $\underline{J}$, then $J_i = \beta_i J$ and the component of $\underline{E}$ parallel to $\underline{J}$ is $(\underline{J}.\underline{E})/J$ (Fig. 5), or, in suffix notation, $(J_i E_i)/J$. The resistivity $\rho(\underline{\alpha},\underline{\beta})$ in the direction $\underline{\beta}$, associated with magnetization in the direction $\underline{\alpha}$ is, therefore, given by

$$\rho(\underline{\alpha},\underline{\beta}) = \frac{(J_i E_i)}{J^2} = \frac{\rho_{ij} J_i J_j}{J^2} = \rho_{ij}\,(\underline{\alpha})\,\beta_i\,\beta_j\,. \qquad (3.29)$$

However, since $\rho^a_{ij}\,(\underline{\alpha})\,\beta_i\,\beta_j = 0$ by definition, all terms involving the Hall constants and their higher-order terms vanish and hence the effective resistivity contains contributions only from the magnetoresistivity part $\rho^s_{ij}\,(\underline{\alpha})\,\beta_i\,\beta_j$, which is an even function of the α_i.

3.3 The spontaneous magnetoresistance of the cubic crystals

For the crystal class $\frac{4}{m}$, $\bar{3}$, $\frac{2}{m}$ the effects of particularization imposed by intrinsic symmetry on the forms of general polar tensors of even rank have already been summarized in Table 2. The spontaneous magnetoresistance is given by the expression

$$\begin{aligned}\rho(\underline{\alpha},\underline{\beta}) = \rho_{ij}(\underline{\alpha})\beta_i\beta_j = {} & \rho_{11}\beta_1^2 + \rho_{22}\beta_2^2 + \rho_{33}\beta_3^2 + \rho_{23}\beta_2\beta_3 \\ & + \rho_{32}\beta_3\beta_2 + \rho_{31}\beta_3\beta_1 + \rho_{13}\beta_1\beta_3 \\ & + \rho_{12}\beta_1\beta_2 + \rho_{21}\beta_2\beta_1\,, \qquad (3.30)\end{aligned}$$

where the ρ_{ij}'s are given, to a fourth order in the α's by equation

(3.5a). The forms of the galvanomagnetic tensors ρ^{*}_{ij}, a_{ijlm}, a_{ijlmno} may now be conveniently displayed by setting out the suffixes of the nonzero components in the following schemes:

ij	11	22	33	23	32	31	13	12	21
	11	11	11	0	0	0	0	0	0

(3.31)

ij / $\alpha_l\alpha_m$	11	22	33	23	32	31	13	12	21
α_1^2	1111	2211	2211	0	0	0	0	0	0
α_2^2	2211	1111	2211	0	0	0	0	0	0
α_3^2	2211	2211	1111	0	0	0	0	0	0
$\alpha_2\alpha_3$	0	0	0	2323	2323	0	0	0	0
$\alpha_3\alpha_1$	0	0	0	0	0	2323	2323	0	0
$\alpha_1\alpha_2$	0	0	0	0	0	0	0	2323	2323

(3.32)

$\alpha_l\alpha_m\alpha_n\alpha_o$ \ ij	11	22	33	23	32	31	13	12	21
α_1^4	111	211	211	0	0	0	0	0	0
α_2^4	211	111	211	0	0	0	0	0	0
α_3^4	211	211	111	0	0	0	0	0	0
$\alpha_2^2\alpha_3^2$	321	121	121	0	0	0	0	0	0
$\alpha_3^2\alpha_1^2$	121	321	121	0	0	0	0	0	0
$\alpha_1^2\alpha_2^2$	121	121	321	0	0	0	0	0	0
$\alpha_1^2\alpha_2\alpha_3$	0	0	0	414	414	0	0	0	0
$\alpha_2^2\alpha_3\alpha_1$	0	0	0	0	0	414	414	0	0
$\alpha_3^2\alpha_1\alpha_2$	0	0	0	0	0	0	0	414	414
$\alpha_2^3\alpha_3$	0	0	0	661	661	0	0	0	0
$\alpha_3^3\alpha_1$	0	0	0	0	0	661	661	0	0
$\alpha_1^3\alpha_2$	0	0	0	0	0	0	0	661	661
$\alpha_3^3\alpha_2$	0	0	0	661	661	0	0	0	0
$\alpha_1^3\alpha_3$	0	0	0	0	0	661	661	0	0
$\alpha_2^3\alpha_1$	0	0	0	0	0	0	0	661	661

(3.33)

In order to cut down the number of suffixes in the case of sixth rank tensors, the customary practice is to replace reversible pairs of subscripts by single numbers thus

$$(11) = 1;\quad (22) = 2;\quad (33) = 3;\quad (23) = (32) = 4;$$
$$(13) = (31) = 5;\quad (12) = (21) = 6,$$

(3.34)

and this has been followed in the scheme. However, to avoid confusion and for the sake of greater clarity this compact form of presentation of the suffixes will not be pursued elsewhere except in the schemes for the hexagonal case.

It follows, using equations (3.5a), (3.31), (3.32) and (3.33), that

$$\begin{aligned}
\rho_{11}(\underline{\alpha}) &= h_o + h_1\alpha_1^2 + h_2\alpha_1^4 + h_3\alpha_2^2\alpha_3^2 \,, \\
\rho_{22}(\underline{\alpha}) &= h_o + h_1\alpha_2^2 + h_2\alpha_2^4 + h_3\alpha_3^2\alpha_1^2 \,, \\
\rho_{33}(\underline{\alpha}) &= h_o + h_1\alpha_3^2 + h_2\alpha_3^4 + h_3\alpha_1^2\alpha_2^2 \,, \\
\rho_{23}(\underline{\alpha}) &= \rho_{32}(\underline{\alpha}) = \alpha_2\alpha_3\,(L_o + L_1\alpha_1^2) \,, \\
\rho_{31}(\underline{\alpha}) &= \rho_{13}(\underline{\alpha}) = \alpha_3\alpha_1\,(L_o + L_1\alpha_2^2) \,, \\
\rho_{12}(\underline{\alpha}) &= \rho_{21}(\underline{\alpha}) = \alpha_1\alpha_2\,(L_o + L_1\alpha_3^2) \,,
\end{aligned} \tag{3.35}$$

where the coefficients h_o, h_1, h_2, h_3, L_o and L_1 are given by

$$\begin{aligned}
h_o &= \overset{*}{\rho}_{11} + a'_{2211} + a'_{221111} \,, \\
h_1 &= a'_{1111} - a'_{2211} - 2a'_{221111} + a'_{112211} \,, \\
h_2 &= a'_{111111} + a'_{221111} - a'_{112211} \,, \\
h_3 &= a'_{332211} - 2a'_{221111} \,, \\
L_o &= a'_{2323} + a'_{122111} \,, \qquad L_1 = a'_{231123} - a'_{122111} \,.
\end{aligned} \tag{3.36}$$

Because of the multiplicity involved in some of the functions of α's in the expansion of equation (3.5a), the primed coefficients used in (3.36) are contracted forms of the corresponding tensor components and are similar to the scheme of subscripts set out in (3.31), (3.32) and (3.33). Thus for example, $a'_{2323} = 2a_{2323}$ since $\alpha_2\alpha_3$, $\alpha_3\alpha_1$ or $\alpha_1\alpha_2$ appears twice in $a_{ijlm}\alpha_l\alpha_m$ but only once in the

summation implied in (3.32).

If now equations (3.30) and (3.35) are combined, the well-known expression for the magnetoresistivity of cubic crystals results, viz:

$$\rho(\underline{\alpha},\underline{\beta}) = k_o + k_1 S(\alpha_1^2\beta_1^2) + 2k_2 S(\alpha_1\alpha_2\beta_1\beta_2) + k_3 S(\alpha_1^2\alpha_2^2) + k_4 S(\alpha_1^4\beta_1^2) + 2k_5 S(\alpha_1\alpha_2\alpha_3^2\beta_1\beta_2) \ , \qquad (3.37)$$

where the saturation magnetoresistive constants $k_o \ldots k_5$ are connected with the tensor components through the following relations

$$\begin{aligned} k_o &= h_o \ , & k_3 &= h_3 \ , \\ k_1 &= h_1 - h_3 \ , & k_4 &= h_2 + h_3 \ , \\ k_2 &= L_o \ , & k_5 &= L_1 \ . \end{aligned} \qquad (3.38)$$

3.3.1 The demagnetized state as reference state

Equation (3.37) may also be taken to represent the fractional change in resistivity referred to the non-magnetic state in which the magnetic interactions have been annihilated. What is of interest, however, is $\frac{\Delta\rho}{\rho}$ where ρ is the average resistivity in the initially demagnetized state. As the actual distribution of domains in the demagnetized state is uncertain, an ideal demagnetized state is customarily considered in which the domains are oriented in equal numbers along each of the crystallographically equivalent directions of easy magnetization. $\frac{\Delta\rho}{\rho}$ thus represents the change in resistivity between the ideal demagnetized state and one of saturation magnetization as a single domain in the direction $\underline{\alpha}$.

If the easy directions are the quaternary axes $\langle 100 \rangle$, as

in iron, then for domains aligned parallel or antiparallel to the [100] direction, the change of resistivity in the direction $\underline{\beta}$ is given, from (3.37), by

$$(\rho)_i(\underline{\beta}) = k_o + k_1\beta_1^2 + k_4\beta_1^2 \,. \tag{3.39a}$$

Similarly, for the [010] direction

$$(\rho)_i(\underline{\beta}) = k_o + k_1\beta_2^2 + k_4\beta_2^2 \,, \tag{3.39b}$$

and for the [001] direction

$$(\rho)_i(\underline{\beta}) = k_o + k_1\beta_3^2 + k_4\beta_3^2 \,. \tag{3.39c}$$

If the magnetoresistivities of all the individual domains are now added together algebraically with their proper weight factor, then the resistivity in the ideal demagnetized state is

$$(\rho)_i = k_o + \tfrac{1}{3}k_1 + \tfrac{1}{3}k_4 \,. \tag{3.40}$$

In a similar way, if the ternary axes are the directions of easy magnetization, as in nickel, then

$$(\rho)_i = k_o + \tfrac{1}{3}k_1 + \tfrac{1}{3}k_3 + \tfrac{1}{9}k_4 \,. \tag{3.41}$$

Thus, the magnetoresistivity referred to the ideal demagnetized state is given by the expression

$$\begin{aligned}\frac{\Delta\rho}{\rho} = \frac{\rho(\underline{\alpha},\underline{\beta}) - (\rho)_i}{(\rho)_i} &= k_1\left\{S(\alpha_1^2\beta_1^2) - \tfrac{1}{3}\right\} \\ &+ 2k_2 S(\alpha_1\alpha_2\beta_1\beta_2) \\ &+ k_3^{*} \quad \text{for Fe} \quad \text{or} \\ &+ k_3^{*}(s - \tfrac{1}{3}) \quad \text{for Ni} \\ &+ k_4\left\{S(\alpha_1^4\beta_1^2) + \tfrac{2}{3}s - \tfrac{1}{3}\right\} \\ &+ 2k_5 S(\alpha_1\alpha_2\alpha_3^2\beta_1\beta_2) \,,\end{aligned} \tag{3.42}$$

where

$$s = \alpha_1^2\alpha_2^2 + \alpha_2^2\alpha_3^2 + \alpha_3^2\alpha_1^2 \quad \text{and} \quad k_3^{*} = k_3 - \frac{2}{3} k_4 \,.$$

This is the same form as that given by Becker and Döring[59] for the magnetostriction of cubic crystals with the coefficients k_1, k_2, k_3^{*}, k_4 and k_5 replaced by h_1, h_2, h_3, h_4 and h_5 respectively. The expression should be compared with equation (3.37) which gives the change in resistivity referred not to the demagnetized state but to an undeformed crystal lattice which is originally non-magnetic, when it is spontaneously magnetized as a single domain in the specified direction.

3.3.2 Case of isotropic magnetoresistivity

If the expression for magnetoresistivity is terminated at terms involving second powers of α's, then

$$\frac{\Delta\rho}{\rho} = k_1\left\{S(\alpha_1^2\beta_1^2) - \frac{1}{3}\right\} + 2k_2\, S(\alpha_1\alpha_2\beta_1\beta_2) \,. \qquad (3.43a)$$

By common practice, when the directions $\underline{\alpha}$ and $\underline{\beta}$ are both parallel to $\langle 100\rangle$ or $\langle 111\rangle$ direction, $\frac{\Delta\rho}{\rho}$ is denoted by $(\frac{\Delta\rho}{\rho})_{100}$ and $(\frac{\Delta\rho}{\rho})_{111}$ respectively. Thus, from (3.43a)

$$(\frac{\Delta\rho}{\rho})_{100} = \frac{2}{3} k_1 \quad \text{and} \quad (\frac{\Delta\rho}{\rho})_{111} = \frac{2}{3} k_2 \,.$$

Hence, the simplest two-constant equation of magnetoresistivity is

$$\frac{\Delta\rho}{\rho} = \frac{3}{2}(\frac{\Delta\rho}{\rho})_{100}\left\{S(\alpha_1^2\beta_1^2) - \frac{1}{3}\right\} + 3\,(\frac{\Delta\rho}{\rho})_{111}\, S(\alpha_1\alpha_2\beta_1\beta_2) \,. \qquad (3.43b)$$

If now a further approximation is made namely, $(\frac{\Delta\rho}{\rho})_{100} = (\frac{\Delta\rho}{\rho})_{111} = \square_{11}$, then (3.43b) becomes

$$\frac{\Delta\rho}{\rho} = \frac{3}{2}\square_{11}(\cos^2\eta - \frac{1}{3}) \,, \qquad (3.43c)$$

where $\cos\eta = \alpha_i\beta_i$ is the angle between the magnetization vector

and the direction of measurement. Since this expression contains no reference to the crystal axes, it therefore represents isotropic magnetoresistivity. The material then has uniaxial properties with the magnetization vector as axis of symmetry. For a polycrystalline material with random orientations of the crystallites, the same symmetry is observed. This is discussed in section 3.5.1.

3.4 The spontaneous magnetoresistance of hexagonal crystals

In this case the co-ordinate axes x_1, x_2 and x_3 may be assumed to coincide with the $[1\bar{2}.0]$, $[10.0]$ and $[00.1]$ crystallographic axes. As before, the number of independent components of the even (except second) rank tensors are reduced by the process of particularization (Table 3) and may now be displayed by setting out the suffixes of the nonvanishing terms in the following scheme.

ij	11	22	33	23	32	31	13	12	21
	11	11	33	0	0	0	0	0	0

(3.44)

$\alpha_l\alpha_m$ \ ij	11	22	33	23	32	31	13	12	21
α_1^2	1111	1122	3311	0	0	0	0	0	0
α_2^2	1122	1111	3311	0	0	0	0	0	0
α_3^2	1133	1133	3333	0	0	0	0	0	0

continued

$\alpha_l\alpha_m$ \ ij	11	22	33	23	32	31	13	12	21
$\alpha_2\alpha_3$	0	0	0	2323	2323	0	0	0	0
$\alpha_3\alpha_1$	0	0	0	0	0	2323	2323	0	0
$\alpha_1\alpha_2$	0	0	0	0	0	0	0	1212	1212
	where $a'_{1212} = 2a_{1212}$ $a'_{1111} = a'_{1122} + a'_{1212}$								

(3.45)

$\alpha_l\alpha_m\alpha_n\alpha_o$ \ ij	11	22	33	23	32	31	13	12	21
α_1^4	111*	211	311	0	0	0	0	0	0
α_2^4	122	222	311	0	0	0	0	0	0
α_3^4	133	133	333	0	0	0	0	0	0
$\alpha_2^2\alpha_3^2$	132	232	332	0	0	0	0	0	0
$\alpha_3^2\alpha_1^2$	232	132	332	0	0	0	0	0	0
$\alpha_1^2\alpha_2^2$	121	221	321	0	0	0	0	0	0
$\alpha_1^2\alpha_2\alpha_3$	0	0	0	441	441	0	0	0	0
$\alpha_2^2\alpha_3\alpha_1$	0	0	0	0	0	441	441	0	0
$\alpha_3^2\alpha_1\alpha_2$	0	0	0	0	0	0	0	636	636
$\alpha_2^3\alpha_3$	0	0	0	441	441	0	0	0	0
$\alpha_3^3\alpha_1$	0	0	0	0	0	535	535	0	0

*For the explanation of the compact notation, see (3.34).

continued

$\alpha_l\alpha_m\alpha_n\alpha_o$ \ ij	11	22	33	23	32	31	13	12	21
$\alpha_1^3\alpha_2$	0	0	0	0	0	0	0	616	616
$\alpha_3^3\alpha_2$	0	0	0	535	535	0	0	0	0
$\alpha_1^3\alpha_3$	0	0	0	0	0	441	441	0	0
$\alpha_2^3\alpha_1$	0	0	0	0	0	0	0	626	626

where $a'_{211} = 2a'_{111} - 3a'_{222} + a'_{121}$

$a'_{122} = 3a'_{111} - 4a'_{222} + a'_{121}$

$a'_{221} = 6a'_{111} - 6a'_{222} + a'_{121}$

$a'_{321} = 2a'_{311}$

$a'_{232} = a'_{132} + a'_{636}$

$a'_{616} = -4a'_{111} + 6a'_{222} - a'_{121}$

$a'_{626} = 2a'_{222} - a'_{121}$

(3.46)

As before, because of the multiplicity involved in some of the functions of α's, the primed coefficients a'_{ijlm}, a'_{ijlmno} are contracted forms of the corresponding components of the tensors. The use of contracted forms alters the relation between the non-vanishing components for hexagonal crystals. For example, the equation $a_{1111} = a_{1122} + 2a_{1212}$ for the fourth rank tensor becomes $a'_{1111} = a'_{1122} + a'_{1212}$ corresponding to a multiplicity for $\alpha_1\alpha_2$ of two.

Using equation (3.5a) in conjunction with (3.44), (3.45) and (3.46) and the relations among the α's, one obtains

$$\rho_{11} = L_o + (L_1 - L_3)\alpha_1^2 + (L_2 - L_3)\alpha_2^2 + 8L_3\alpha_1^2\alpha_2^2 + (L_4 + L_3)\alpha_2^2\alpha_3^2 + (L_5 + L_3)\alpha_3^2\alpha_1^2 ,$$

$$\rho_{22} = L_o + (L_2 + L_3)\alpha_1^2 + (L_1 + L_3)\alpha_2^2 - 8L_3\alpha_1^2\alpha_2^2 + (L_4 - L_3)\alpha_3^2\alpha_1^2 + (L_5 - L_3)\alpha_2^2\alpha_3^2 ,$$

$$\rho_{33} = M_o + M_1 (\alpha_1^2 + \alpha_2^2) + M_2 (\alpha_1^2 + \alpha_2^2) \alpha_3^2 ,$$

$$\rho_{23} = \alpha_2\alpha_3 (N_o' + N_1' \alpha_3^2) = \rho_{32} ,$$

$$\rho_{31} = \alpha_3\alpha_1 (N_o' + N_1' \alpha_3^2) = \rho_{13} ,$$

$$\rho_{12} = \alpha_1\alpha_2 \left[(L_1 - L_2) - (L_4 - L_5)\alpha_3^2 + 4L_3 (\alpha_1^2 - \alpha_2^2) \right] = \rho_{21} , \qquad (3.47)$$

where the constants are given by

$$L_o = \rho_{11}^{*} + a'_{1133} + a'_{113333} ,$$

$$L_1 = a'_{1111} - a'_{1133} + \frac{1}{2} a'_{111111} + \frac{1}{2} a'_{222222} - a'_{113333} ,$$

$$L_2 = a'_{1122} - a'_{1133} + \frac{5}{2} a'_{111111} + a'_{112211} - \frac{7}{2} a'_{222222} - a'_{113333}$$

$$L_3 = - \frac{1}{2} a'_{111111} + \frac{1}{2} a'_{222222} ,$$

$$L_4 = - \frac{5}{2} a'_{111111} + \frac{7}{2} a'_{222222} - a'_{112211} - a'_{113333} + a'_{113322} ,$$

$$L_5 = - \frac{1}{2} a'_{111111} - \frac{1}{2} a'_{222222} - a'_{113333} + a'_{113322} + a'_{123312} ,$$

$$M_o = \rho_{33}^{*} + a'_{3333} + a'_{333333} ,$$

$$M_1 = - a'_{3333} + a'_{3311} - a'_{333333} + a'_{331111} ,$$

$$M_2 = - a'_{333333} - a'_{331111} + a'_{333322} ,$$

$$N_o' = a'_{2323} + a'_{232311} ,$$

$$N_1' = - a'_{232311} + a'_{133331} . \qquad (3.48)$$

Combining now equations (3.30) and (3.47), the expression for the spontaneous magnetoresistivity in hexagonal crystals may be written

in the form

$$\begin{aligned}\rho(\underline{\alpha},\underline{\beta}) = {} & R_o + R_1\beta_3^2 \\ & + \left[R_2 + R_3\alpha_3^2\right](1 - \alpha_3^2) \\ & + \left[R_4 + R_5\alpha_3^2\right](1 - \alpha_3^2)\,\beta_3^2 \\ & + \left[R_6 + R_7\alpha_3^2\right](\alpha_1\beta_1 + \alpha_2\beta_2)\alpha_3\beta_3 \\ & + \left[R_8 + R_9\alpha_3^2\right](\alpha_1\beta_1 + \alpha_2\beta_2)^2 \\ & + R_{10}(2\alpha_1\alpha_2\beta_1 + \alpha_1^2\beta_2 - \alpha_2^2\beta_2)^2 \,, \end{aligned} \tag{3.49}$$

where the magnetoresistive constants are connected with the tensor components through the relations

$$\begin{aligned} R_o &= L_o \,, & R_2 &= L_2 - L_3 \,, \\ R_1 &= M_o - L_o \,, & R_3 &= L_4 + L_3 \,, \\ R_4 &= M_1 - L_2 + L_3 \,, \\ R_5 &= M_2 - L_4 - L_3 \,, \\ R_6 &= 2N'_o \,, \\ R_7 &= 2N'_1 \,, \\ R_8 &= L_1 - L_2 \,, \\ R_9 &= L_5 - L_4 \,, \\ R_{10} &= 2L_3 \,. \end{aligned} \tag{3.50}$$

The fourth-order equation (3.49) contains only one term - that multiplied by R_{10} - which is characteristic of hexagonal symmetry. In this case eleven constants are required to describe the magnetoresistance unless the saturation magnetization is parallel or perpendicular to the direction of measurement, in which case the number of constants involved reduces to eight. If the last term of equation (3.49) is omitted, the expression corresponds to cylindrical

symmetry since ρ becomes independent of the orientations of both $\underline{\alpha}$ and $\underline{\beta}$ with respect to the non-hexagonal axes.

3.4.1 The demagnetized state as the reference state

Following the method outlined for cubic crystals, if the easy directions of magnetization are parallel and antiparallel to the hexagonal c axis, the corresponding magnetoresistivity in the ideally demagnetized state may be obtained as

$$(\rho)_i = R_o + R_1\beta_3^2 , \tag{3.51a}$$

while if the basal plane is a plane of easy magnetization, then

$$(\rho)_i = R_o + R_1\beta_3^2 + R_2 + R_4\beta_3^2 + \tfrac{1}{2}(R_8 + R_{10})(1 - \beta_3^2) . \tag{3.51b}$$

Hence the magnetoresistivity, referred to the demagnetized state, is given, in the first case, by the expression (3.49) with the first two terms removed and, in the second case, by the equation

$$\begin{aligned}\frac{\Delta\rho}{\rho} = & -\left\{R_2 + R_3 (1 - \alpha_3^2)\right\}\alpha_3^2 \\ & + \left\{- R_4 + R_5 (1 - \alpha_3^2)\right\}\alpha_3^2\beta_3^2 \\ & + \left\{R_6 + R_7 \alpha_3^2\right\}(\alpha_1\beta_1 + \alpha_2\beta_2)\,\alpha_3\beta_3 \\ & + R_8\left\{(\alpha_1\beta_1 + \alpha_2\beta_2)^2 - \tfrac{1}{2}(1 - \beta_3^2)\right\} + R_9\,\alpha_3^2\,(\alpha_1\beta_1 + \alpha_2\beta_2)^2 \\ & + R_{10}\left\{(2\,\alpha_1\alpha_2\beta_1 + \alpha_1^2\beta_2 - \alpha_2^2\beta_2)^2 - \tfrac{1}{2}(1 - \beta_3^2)\right\} ,\end{aligned} \tag{3.51c}$$

where, as before, the fractional change in resistivity has been considered.

3.4.2 Second-order equation for cylindrical symmetry

The approximation involving only second-order terms in the α's, which corresponds to equation (3.43a) for cubic crystals, may be obtained by setting $\alpha_3 = 0$ within the four sets of square brackets in (3.49) and omitting the last term. The resulting expression then becomes

$$\frac{\Delta\rho}{\rho} = (R_2 + R_4\,\beta_3^2)(1 - \alpha_3^2) + \left\{R_6\alpha_3\beta_3 + R_8(\alpha_1\beta_1 + \alpha_2\beta_2)\right\}(\alpha_1\beta_1 + \alpha_2\beta_2) \,. \quad (3.52)$$

A similar expression for magnetostriction in the hexagonal system was first derived by Mason[84] who used a different grouping of terms and obtained

$$\begin{aligned}\lambda = {} & \lambda_A\left\{(\alpha_1\beta_1 + \alpha_2\beta_2)^2 - (\alpha_1\beta_1 + \alpha_2\beta_2)\,\alpha_3\beta_3\right\} \\ & + \lambda_B\left\{(1 - \alpha_3^2)(1 - \beta_3^2) - (\alpha_1\beta_1 + \alpha_2\beta_2)^2\right\} \\ & + \lambda_C\left\{(1 - \alpha_3^2)\,\beta_3^2 - (\alpha_1\beta_1 + \alpha_2\beta_2)\,\alpha_3\beta_3\right\} \\ & + 4\lambda_D\,(\alpha_1\beta_1 + \alpha_2\beta_2)\,\alpha_3\beta_3 \,. \end{aligned} \quad (3.53)$$

The relations connecting the constants λ_A, λ_B, λ_C, λ_D and the constants appearing in equation (3.52) are

$$R_2 = \lambda_B \,, \qquad R_6 = 4\lambda_D - \lambda_C - \lambda_A \,,$$
$$R_4 = \lambda_C - \lambda_B \,, \qquad R_8 = \lambda_A - \lambda_B \,,$$

or

$$\lambda_A = R_2 + R_8 \,, \qquad \lambda_C = R_2 + R_4 \,,$$
$$\lambda_B = R_2 \,, \qquad \lambda_D = \tfrac{1}{4}(2R_2 + R_4 + R_6 + R_8) \,. \quad (3.54)$$

Four constants are thus required to describe the effect. It is

to be noted that, unlike the case of the cubic crystal, equation (3.52) cannot be reduced to the form (3.43c) or even to the more general form

$$\frac{\Delta\rho}{\rho} = P + Q\cos^2\eta \ . \qquad (3.55)$$

The four constants of the second-order magnetostriction equation (3.53) have been measured by Bozorth and Sherwood[85] and appear to be in reasonable agreement with observations on polycrystalline cobalt. A difficulty arises, however, because such large fields are necessary to saturate the specimens. Within this limitation, Bozorth and Sherwood concluded that the simple equation conforming to cylindrical symmetry is an adequate approximation of the magnetostriction of cobalt. No measurements have yet been made of magnetoresistance on single crystals of this material but the present results for polycrystalline cobalt indicate approximate values of P and Q. This is discussed in section 6.4 .

3.5 The magnetoresistivity of polycrystals

If the individual crystallites in a polycrystal are assumed to be oriented at random over all directions, it is possible to derive a relationship between the single-crystal and polycrystalline saturation magnetoresistance constants by averaging equation (3.37) both for saturated and for demagnetized states. The details of the averaging procedure are similar to the corresponding treatment of polycrystalline magnetostriction[71] and so only the results of this process will be quoted here.

3.5.1 The polycrystalline magnetoresistivity of cubic materials

The average resistivity is

$$(\bar{\rho}) = k_o + \frac{1}{5} k_1 - \frac{1}{5} k_2 + \frac{1}{5} k_3^{M} + \frac{23}{105} k_4 - \frac{1}{35} k_5$$

$$+\left\{\frac{2}{5} k_1 + \frac{3}{5} k_2 + \frac{12}{35} k_4 + \frac{3}{35} k_5\right\}\cos^2 \eta \ , \qquad (3.56)$$

where η is the angle between the magnetizing vector and the direction of measurement. The corresponding (spontaneous) magnetoresistivity in the ideally demagnetized state where the domains are aligned in equal numbers parallel to directions of easy magnetization, is, for iron,

$$(\bar{\rho})_i = k_o + \frac{1}{3} k_1 + \frac{1}{3} k_4 \ , \qquad (3.57a)$$

and, for nickel

$$(\bar{\rho})_i = k_o + \frac{1}{3} k_1 + \frac{1}{3} k_3^{M} + \frac{1}{3} k_4 \ . \qquad (3.57b)$$

This gives the change in resistance of an ideal polycrystal referred to the demagnetized state as

$$\left(\frac{\Delta\bar{\rho}}{\rho}\right) = \frac{(\bar{\rho}) - (\bar{\rho})_i}{(\bar{\rho})_i} = P + Q \cos^2 \eta \ , \qquad (3.58)$$

where

$$Q = \frac{2}{5} k_1 + \frac{3}{5} k_2 + \frac{12}{35} k_4 + \frac{3}{35} k_5 \ , \qquad (3.59)$$

and where, for iron,

$$P = -\frac{2}{15} k_1 - \frac{1}{5} k_2 + \frac{1}{5} k_3^{M} - \frac{4}{35} k_4 - \frac{1}{35} k_5 \ , \qquad (3.60a)$$

and, for nickel,

$$P = -\frac{2}{15} k_1 - \frac{1}{5} k_2 - \frac{2}{15} k_3^{M} - \frac{4}{35} k_4 - \frac{1}{35} k_5 \ , \qquad (3.60b)$$

If it is possible to put $k_3^{M} = 0$ then equation (3.58) can be put in a somewhat different form for

$$\left(\frac{\Delta\bar{\rho}}{\rho}\right) = Q\left(\cos^2 \eta - \frac{1}{3}\right) \qquad (3.61)$$

and $(\frac{\overline{\Delta\rho}}{\rho})$ will attain a saturation value when $\eta = 0$ for all the domain magnetization vectors, or

$$(\frac{\overline{\Delta\rho}}{\rho})_S = \overline{\Xi}_S = \frac{2}{3} Q \text{ , giving } (\frac{\overline{\Delta\rho}}{\rho}) = \frac{3}{2} \overline{\Xi}_S (\cos^2 \eta - \frac{1}{3}) \text{ .} \tag{3.62}$$

An equation of the same form as (3.61) is generally taken as governing the saturation magnetostriction of polycrystals and is the one which Becker and Döring[59] obtained by assuming that the term in $k_3^{\#}$, representing the isotropic volume magnetostriction, could be neglected. This is a reasonable assumption for nickel and for certain nickel-rich alloys. However, the previous magnetoresistive data, as well as the present measurements, indicate that, even for nickel, the term in $k_3^{\#}$ cannot be neglected, so that polycrystalline magnetoresistance may not be represented by equation (3.61) or (3.62). This is further discussed in section 6.3.1 .

3.5.2 The polycrystalline magnetoresistivity of hexagonal materials

By adopting a similar procedure to that outlined for cubic materials, namely by averaging the expression (3.49) for all random directions of the individual crystallites, the following relation for the saturated state may be obtained

$$\begin{aligned}(\overline{\rho}) = {} & R_o + \frac{1}{3} R_1 + \frac{2}{3} R_2 + \frac{2}{15} R_3 + \frac{4}{15} R_4 + \frac{4}{105} R_5 - \frac{1}{15} R_6 \\ & - \frac{1}{35} R_7 + \frac{1}{15} R_8 + \frac{1}{35} R_9 + \frac{16}{105} R_{10} \\ & + \left\{ - \frac{2}{15} R_4 + \frac{2}{105} R_5 + \frac{1}{5} R_6 + \frac{3}{35} R_7 + \frac{7}{15} R_8 + \frac{1}{21} R_9 \right. \\ & \left. + \frac{8}{105} R_{10} \right\} \cos^2 \eta \text{ .}\end{aligned} \tag{3.63}$$

The corresponding spontaneous magnetoresistivities in the demagnetized states are

$$(\bar{\rho})_i = R_0 + \tfrac{1}{3} R_1 \,, \tag{3.64a}$$

when the easy directions are parallel and antiparallel to the hexagonal c axis, as in cobalt, and

$$(\bar{\rho})_i = R_o + \tfrac{1}{3} R_1 + R_2 + \tfrac{1}{3} R_4 + \tfrac{1}{3} R_8 + \tfrac{1}{3} R_{10} \,, \tag{3.64b}$$

when the basal plane is a plane of easy magnetization.

Thus the fractional change in resistivity of an ideal polycrystal at saturation, when referred to these demagnetized states, is again given by

$$\left(\frac{\bar{\Delta}\rho}{\rho}\right) = \frac{(\bar{\rho}) - (\bar{\rho})_i}{(\bar{\rho})_i} = P + Q \cos^2 \eta \,, \tag{3.65}$$

where, in the former case,

$$P = \tfrac{2}{3} R_2 + \tfrac{2}{15} R_3 + \tfrac{4}{15} R_4 + \tfrac{4}{105} R_5 - \tfrac{1}{15} R_6 - \tfrac{1}{35} R_7 + \tfrac{1}{15} R_8 + \tfrac{1}{35} R_9 + \tfrac{16}{105} R_{10} \,, \tag{3.66a}$$

and, in the latter case,

$$P = -\tfrac{1}{3} R_2 + \tfrac{2}{15} R_3 - \tfrac{1}{15} R_4 + \tfrac{4}{105} R_5 - \tfrac{1}{15} R_6 - \tfrac{1}{35} R_7 - \tfrac{4}{15} R_8 + \tfrac{1}{35} R_9 - \tfrac{19}{105} R_{10} \,, \tag{3.66b}$$

and where, in both cases,

$$Q = -\tfrac{2}{15} R_4 + \tfrac{2}{105} R_5 + \tfrac{1}{5} R_6 + \tfrac{3}{35} R_7 + \tfrac{7}{15} R_8 + \tfrac{1}{21} R_9 + \tfrac{8}{105} R_{10} \,. \tag{3.66c}$$

It is interesting to note that in neither case can equation (3.65) be put into the form of equation (3.61).

CHAPTER IV

EXPERIMENTAL

4.1 Description of the specimens

All the polycrystalline specimens were in the form of cylindrical rods, 1 - 3 mm in diameter and 1.4 cm in length, and were supplied by Johnson, Matthey & Co. These were spectrographically standardized and the results of the analysis of estimated impurity contents in each case are given below.

Element	Type of Impurity	Quantity Present in Parts per Million
Ni	Si	7
	Fe	3
	Bi	2
	Ag	2
	Cu	1
	Ca, Mn, Mg	each less than 1
Fe	Mn	3
	Ni	2
	Si	1
	Cu, Mg, Ag	each less than 1
Co	Fe	5
	Ni	3
	Si	2
	Ca	2
	Cu, Mg, Ag, Na	each less than 1
Gd	Total rare-earth impurities less than 0.1%	

The single crystal of nickel was available in the form of a rectangular slice cut from a larger piece which had been earlier thoroughly polished, oriented and checked in the laboratory employing the back-reflection X-ray Laue photographic principle together with the standard stereographic projection technique. The accuracy of the orientation was half a degree. The two side faces of the bar specimen contained the (11$\bar{1}$) and (110) crystallographic planes with the directions of the principal crystal axes as shown in Figure 6 . The dimensions of the crystal were 14 mm x 1.9 mm x 1.2 mm.

4.2 Principle of measurement

For the measurement of resistivity, the standard method using a potentiometer was employed as this has the basic advantage of excluding the lead and contact resistances from the final measurement (Fig. 7). The problem was thus to measure a low voltage drop along the specimen with sufficient accuracy whilst monitoring the specimen current with the aid of a standard resistance.

The magnetoresistance was measured in terms of the out-of-balance voltage developed across the potential points on the specimen when a field was applied with the current maintained constant. By calibrating the output galvanometer scale in terms of given changes in current when the resistance of the specimen was maintained constant, the fractional change of resistivity in magnetic field could be directly related to the fractional change of current. Thus,

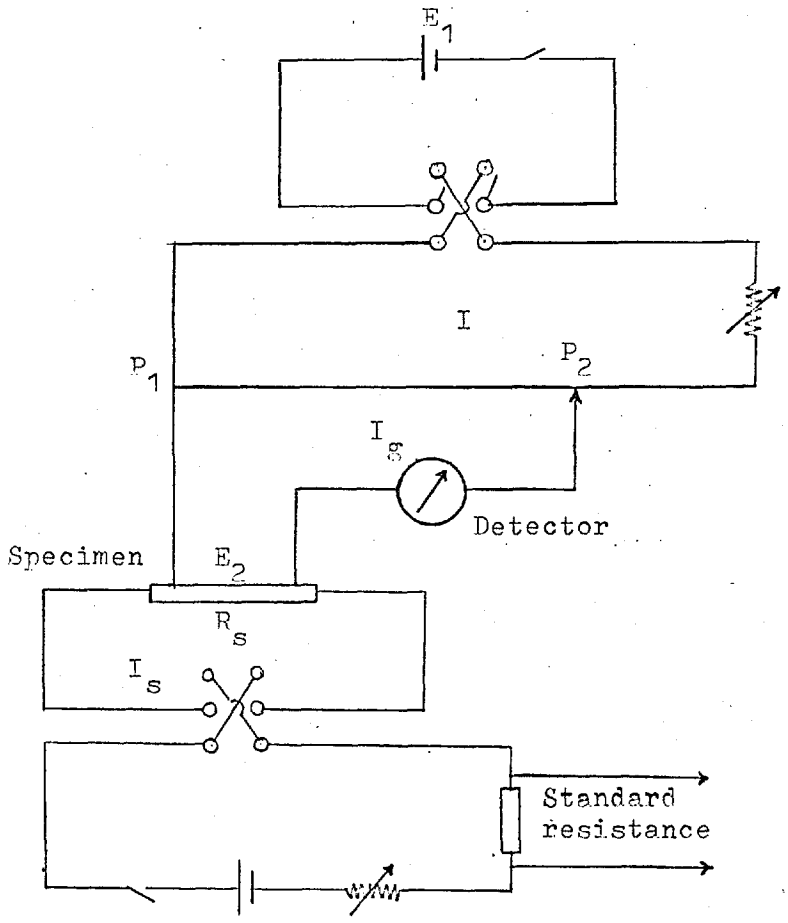

R' = Total resistance of the potentiometer circuit including that of the slide wire.
R = Resistance of the slide wire between P_1 and P_2.
R_g = Resistance of the galvanometer circuit between P_1 and P_2 including the resistance of the specimen and any other resistance.
R_s = Resistance of the specimen alone.

Fig. 7. The basic potentiometer circuit.

$$dE_2 = I_s\, dR_s = E_2 \frac{dR_s}{R_s} \qquad \text{and}$$

$$dE_2 = R_s\, dI_s = E_2 \frac{dI_s}{I_s} \text{ , giving } \frac{dR_s}{R_s} = \frac{dI_s}{I_s} \text{ .} \qquad (4.1)$$

Since I_s and dI_s can be accurately measured, the fractional change of resistivity can be estimated with great precision without any necessity of knowing the actual resistivity of the specimen. This method is obviously preferable to using a null method for each reading as it allows considerable rapidity of operation and it ensures greater stability because steady conditions are maintained in the circuit.

4.2.1 Theory of potential balance

Considering the basic potentiometer circuit (Fig. 7) the current flowing through the galvanometer can be immediately calculated. From Kirchoff's laws the following equations are obtained:

$$E_1 = IR' + I_g R$$

$$E_2 = I_g(R_g + R) + IR \text{ , giving}$$

$$I_g = \frac{E_2 R' - E_1 R}{R'(R_g + R) - R^2} \text{ ,} \qquad (4.2)$$

At balance $I_g = 0$, that is $\frac{E_2}{R} = \frac{E_1}{R'}$ and the current I in the resistance R is equal to $\frac{E_1}{R'}$, no current entering or leaving the galvanometer circuit. The sensitivity depends on the galvanometer

current that flows when a small change is made in the balance condition. This off-balance current can be best calculated by the so-called 'Compensation Theorem' which states[86] "if a network is modified by making a small change ΔR in the resistance of one of its branches, the current increment thereby produced at any point in the network is equal to the current that would be produced at that point by compensating e.m.f., acting in series with the modified branch, whose value is $- I \Delta R$ where I is the original current flowing in the modified branch". This simply means that a current will flow round the galvanometer circuit equal to the out-of-balance voltage divided by the resistance of the galvanometer circuit including the resistance between the potential points. Thus

$$I_g = \frac{E}{R_g + R} \quad \text{where } E = - I \Delta R \,, \qquad (4.3)$$

The current in the potentiometer circuit is likewise changed by $\frac{E}{R}$. Using a Tinsley galvanometer (Type 4500L) of 1000 mm/μA current sensitivity at 1 metre scale distance and of 50Ω coil resistance, the value of I_g (in a potentiometer circuit where R = 50Ω and R_g = 150Ω) for 1 μV out-of-balance voltage is 5.10^{-9} amp. giving a sensitivity of 5 mm galvanometer deflection.

4.2.2 Some difficulties in the measurement of low voltages

The degree of accuracy obtainable with a potentiometer is dependent upon the degree of subdivision of its constituent resistance units that subdivide the potential gradient. However, in order to be able to make use of these subdivisions, special precautions

are necessary. One of the chief difficulties encountered is the thermo-electric potentials which are set up at the various contact points. This can be minimised by using exactly similar metals for both the contact faces (e.g. gold-silver alloy), by accurately adjusting the various resistance coils and maintaining their resistance values with great precision and by using suitable materials (e.g. Manganin) having negligible temperature coefficient of resistance. In addition, there should ideally be no thermo-electric effects between the various component units and the switches and leads which can be of copper or brass. Some of the precision commercial potentiometers, like Pye, Tinsley or the Diesselhorst pattern, incorporating these features, are quite satisfactory for these types of measurement. The use of nickel plated terminals is avoided and clean copper leads and terminals are widely used.

For measurement at temperatures other than room temperature the conditions are generally less steady and it is desirable that the overall time of a measurement be reduced to about half a minute. The response time of the galvanometer should therefore be short. However, a very sensitive galvanometer, in general, suffers from large zero drift and has a larger time period, so that a compromise has to be made to obtain the best results.

The use of a large current or a very long specimen to increase the potential drop is to be avoided because of the consequent greater instability, higher heat dissipation in the material, associated thermo-electric effects at the potential contacts on the

specimen and the possibility of a prohibitive temperature gradient along the specimen. Thus, with a typical sample of 200 μΩ resistance and a safe current of 0.5 amp., it should be possible to use the potentiometer to measure 100 μV with an accuracy preferably higher than 1%.

For magnetoresistivity measurements involving only a 1 or 2% change in resistivity, the sensitivity of the Tinsley galvanometer is not quite adequate and pre-amplification of the out-of-balance current is necessary. This, in the present case, was done with the help of a split photo-cell amplifier unit with a negative feedback arrangement to improve stability and control. This is discussed in Section 4.3.3.

4.3 The magnetoresistivity measurements

4.3.1 Design of the sample holder

The requirement that a uniform magnetic field be maintained over the volume occupied by the specimen usually places a severe limitation on its size, especially when measurements are to be taken in the region of technical saturation. Using a 7" Newport electromagnet with conical pole tips, a maximum field of 21,500 Oe was obtainable at 1" pole gap. This in turn demanded a sufficiently rigid specimen mounting and yet a minimum use of metal parts was desirable to prevent thermal fluctuations due to eddy current heating.

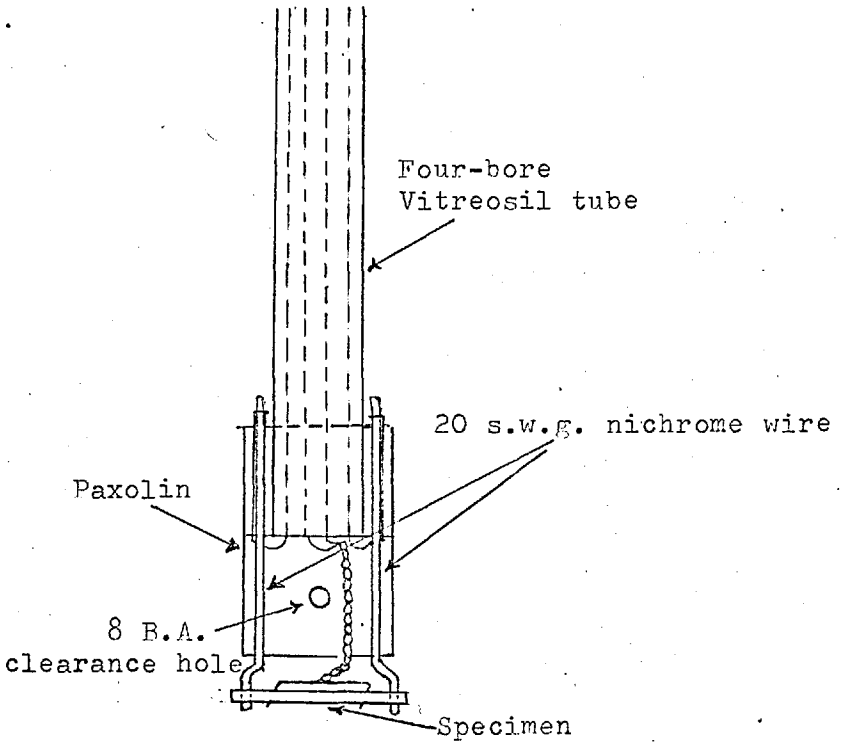

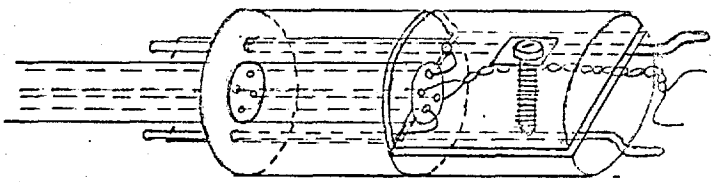

Side view

Fig. 8. Design of the specimen holder

Several insulating materials, like ebonite, amber, bakelite, bees-wax, etc., were tried for making a holder but each one had to be subsequently rejected for one reason or another. The choice ultimately fell on paxolin because of its hardness (sufficient for the present requirement), non-reactivity and insolubility in the particular organic liquid (P-Xylene) which was to be used for the constant temperature bath.

A $\frac{1}{2}$" paxolin rod, about 1" long was drilled to $\frac{1}{2}$" depth and fixed with araldite at the end of a $\frac{1}{4}$" four-bore vitreosil tube as shown in Fig. 8 . The lower portion of the rod was $\frac{3}{8}$" long and this was sliced into two halves parallel to its length with one piece unseparated from the main body of the holder. Two small side holes and slots made in the paxolin enabled two pieces of 20 s.w.g. nichrome wire to be clamped firmly, one on each side of the vitreosil tube, when the cut piece of paxolin was screwed back tightly into the main body of the holder. These wires, which were slightly bent outwards on coming out of the paxolin, were spot-welded on to the specimen and served as the current leads. For the potential leads, 32 s.w.g. nichrome wire with glass insulation was found to be satisfactory. The wires were carefully twisted together in the space between the specimen and the vitreosil tube and a further coating of shellac varnish held them rigidly in position. In addition to this, the plane of the loop where the wires had to be separated for connecting to the specimen was carefully positioned so as to be in the plane of the magnetic field. This, with the

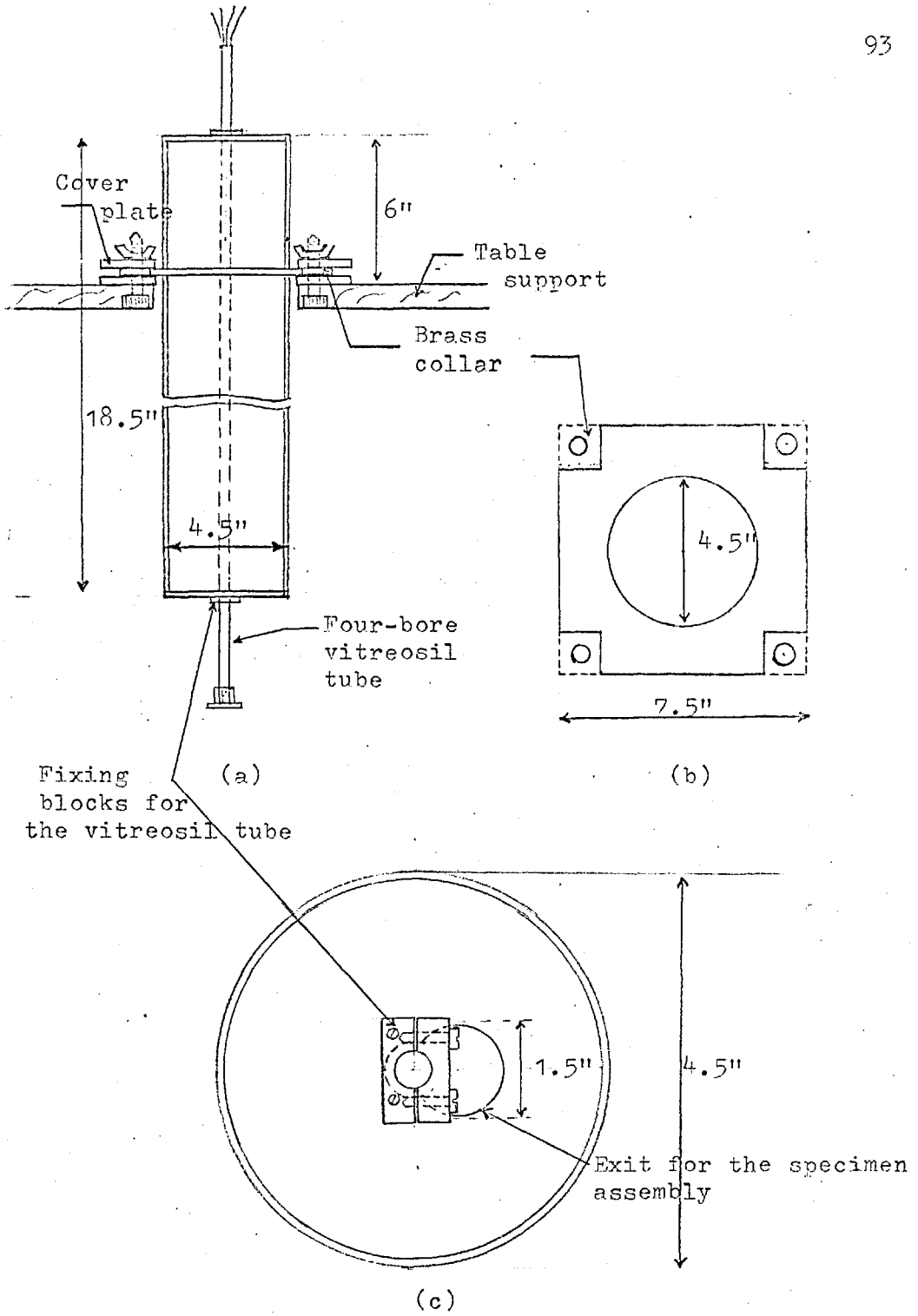

Fig. 9. The arrangement for mounting the specimen

tight binding of the wires, considerably diminished the electromagnetically induced voltage picked up on switching the magnetic field.

4.3.2 Mounting the specimen and the dewar assembly

The four-bore vitreosil tube carrying the specimen assembly, the electrical leads and the cooling arrangement (including the dewar flask containing a constant temperature bath) was itself rigidly mounted along the axis of a hollow brass cylinder, 4.5" in outer diameter and 18.5" in overall length (Fig. 9a). The cylinder was provided with a supporting collar made of a $\frac{1}{4}$" brass plate of size 7.5" square positioned at a distance of 6" from the top. The collar had its four corners machined as shown in Fig. 9b. and it could be placed over a base plate which was permanently fixed to the table and which was fitted with four fixing studs that passed through these corner holes. By allowing sufficient clearance between the cylinder and the holes in the table and in the base plate, the entire unit could be suitably positioned for correct alignment of the specimen and then clamped by means of the cover plate and the fixing nuts. The specimen-supporting tube was fixed only at the lower end plate of the cylinder with the help of two blocks of brass, one of which was always left screwed to the plate and the other of which was removable. The upper end of the tube had a comparatively loose fitting through a felt sleeve in a clearance hole. This arrangement protected the tube against any accidental

break due to shear imposed in assembly.

Two identical eccentric holes, 1.5" in diameter, were cut in the opposite end plates of the cylinder as shown in Fig. 9c , and these enabled the specimen assembly to be easily removed or replaced without the necessity of lifting the entire supporting structure. Finally, a tight fitting cork at the end of the vitreosil tube supported the cooling system and the small dewar flask. These were further securely held in position by extensive thermal lagging (with cotton wool) of the entire space between the bottom of the cylinder and the neck of the dewar.

4.3.3 The photo-cell galvanometer amplifier

One of the most important requirements was to set up a sensitive current detector capable of measuring the small off-balance current while rejecting the background noise. After considering various methods of pre-amplification, a split photo-cell amplifier was finally chosen because it has the advantage of providing its own power with no undesirable signal pick-up and, in addition, it can provide the necessary gain with good linearity and stability in the output current. Amplifiers of this type have been described by many workers (88,89,90). The principle of operation is that the split photo-cell with the two halves connected in series opposition delivers to a secondary galvanometer only the difference between the individual outputs, so that when the illumination of the two halves is unequal a current is produced

whose sign and magnitude depend respectively on the sense and amount of the deflection.

The photo-cell used was of the selenium rectifier type (barrier layer), 27 mm by 40 mm and was split parallel to the shorter side. The whole optical arrangement, shown in Fig. 10 , was mounted on an anti-vibration platform consisting of a heavy concrete block resting on four cork pillars and enclosed in a hard-board box with the inside painted black. A rectangular slit placed close to the focussing lens produced a sharp image on the photo-cell, covering an area equal to that of either half of the cell. This gave the maximum sensitivity and linearity of response. A 150 watt Point-o-lite was used for the source to provide a bright image of the slit on the cell.

The split photo-cell amplifier described above was eventually replaced by a more compact commercial (Tinsley) galvanometer amplifier (developed from the basic design of Preston[89]) but this was not available until a late stage in the investigation. The moving coil of the primary galvanometer is immersed in a liquid which acts as a physical damping medium and at the same time provides bouyancy for the coil. As the liquid in the closed container cannot move bodily, the liquid does not transmit any movement or external disturbance to the coil. The secondary galvanometer was another Tinsley type with a resistance of 511 Ω , a period of 2 secs. and a sensitivity of 1600 mm/μA at 1 metre. This was mounted at a convenient position, and by using a cylindrical lens the image of

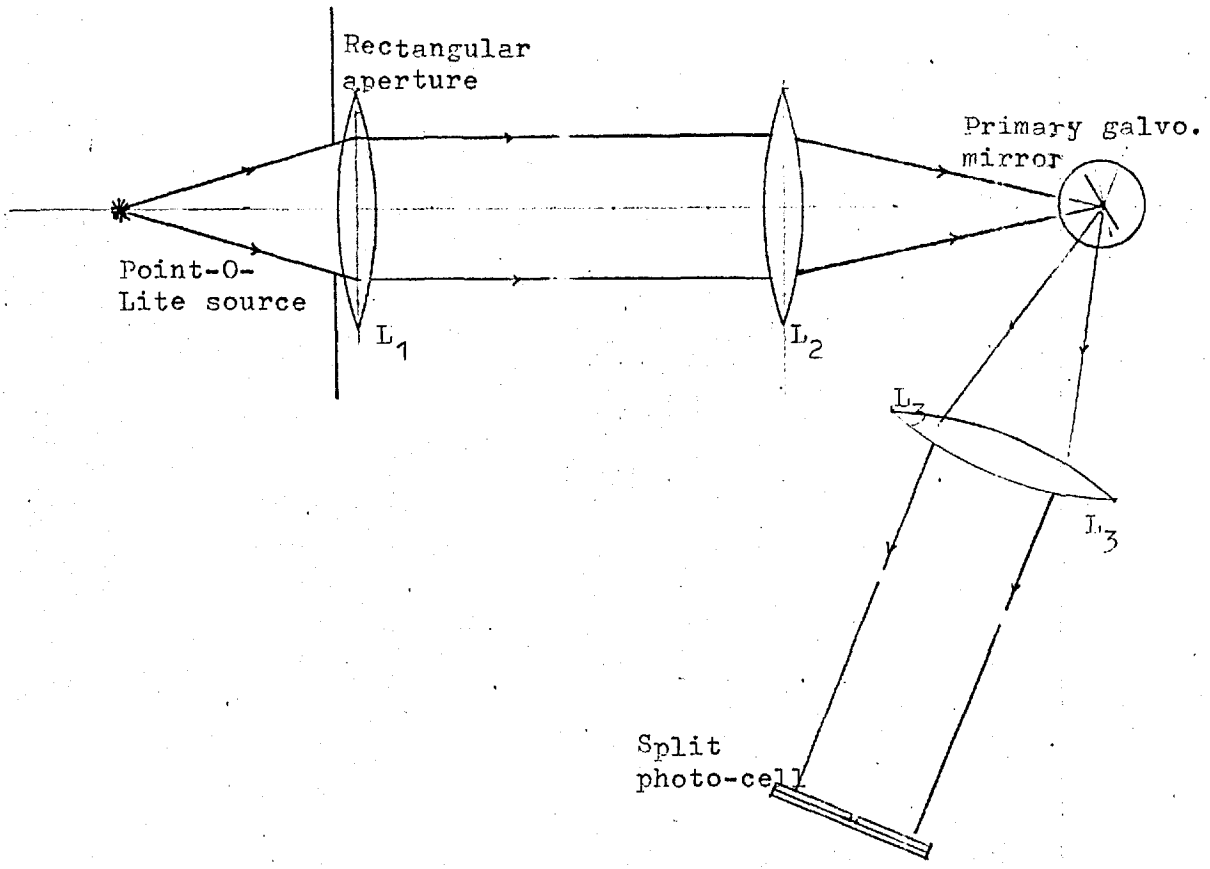

Fig. 10. The optical arrangement for the galvanometer amplifier .

the vertical cross wire was thrown into sharp focus on the final scale, 1.7 metres away. The latter arrangement further increased the over-all amplification of the measuring circuit. In fact, the gain was always so large that it had to be reduced and this was done partly by increasing the amount of negative feedback which, in turn, improved the stability, and partly by adjusting the specimen current which controlled the out-of-balance voltage in the galvanometer circuit. Several tests were carried out to determine the optimum balance between sensitivity and stability before actual measurements were taken.

4.3.4 The constant temperature bath

It should be pointed out that the temperature coefficients of resistance of most of the ferromagnetic metals are of roughly the same magnitude as the magnetoresistance itself. Thus, for nickel, the value of $\frac{1}{R}\frac{dR}{dT}$ is about 0.7% at room temperature, so that if the specimen temperature changes by 0.1° C during the measurement involving a magnetoresistance effect of 1%, an error of 7% is introduced. Unlike prevalent practices[3,4,5,6], it was decided to take the specimen every time from the demagnetized state to the successive stages of magnetization when studying the field dependence of the magnetoresistance: this was in order to avoid any uncertainty as regards zero shift, but it involved, unfortunately, quite an appreciable heating effect on the specimen. Under these circumstances, the use of a constant temperature bath ensuring

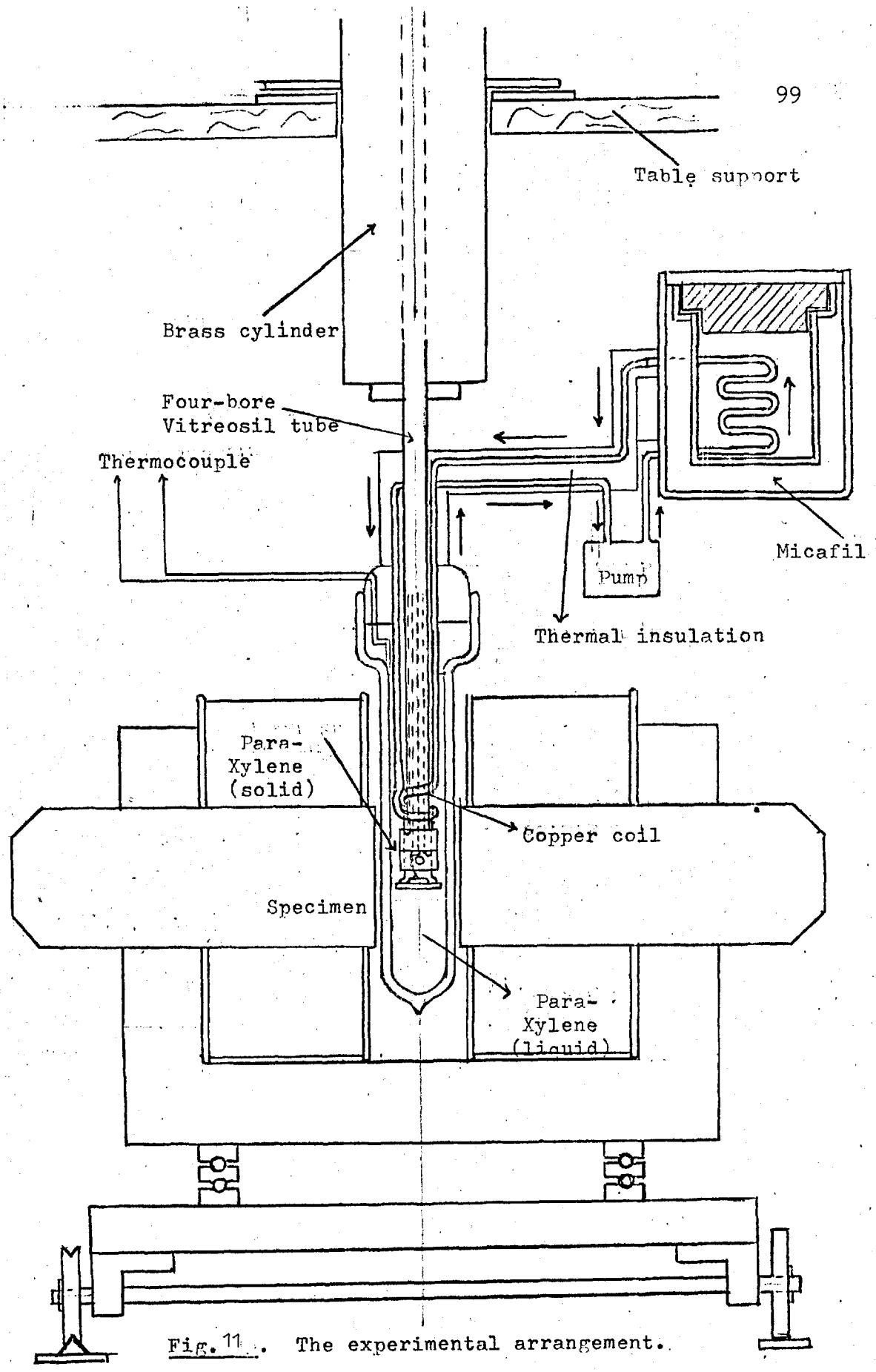

Fig. 11. The experimental arrangement.

thermal steadiness to within 0.005° C was considered to be absolutely necessary. After an extensive search for a suitable solvent, the following arrangement was found to be highly satisfactory.

Para-Xylene, a non-conducting organic solvent (density 0.86; specific heat 0.397 at 30° C and latent heat of solidification 39.3 cals/gm at 16° C), was used for the liquid bath and was contained in a small dewar flask enclosing the specimen, as shown in Fig. 11 . A 1/16" copper tube was then taken through the top of the dewar alongside the vitreosil tube to a small spiral coil near the specimen holder, through which ice-cold water from a nearby storage tank was continuously passed. As the organic liquid has a melting point of 13.2° C, this resulted in local freezing of the liquid in the neighbourhood of the specimen, the extent of which could be controlled by regulating the flow of water down the cooling tube. In a preliminary experiment, a flow rate of 100-120 droplets/min. was found quite sufficient to keep the temperature perfectly steady. With this flow rate, solid Xylene formed in the upper part of the dewar flask with liquid below. It was important that the liquid should have the two phases co-existent as this helped in maintaining a steady temperature even when the water was not flowing at a uniform rate. In fact, it was estimated that neither the normal Joule heating of the specimen nor the magneto-caloric effect associated with the magnetization would produce a significant rise in temperature of the liquid even if the supply of ice-cold water was stopped for half an hour, once thermal equilibrium had

been attained inside the dewar. However, to keep the entire system running for days, a continuous flow system was used in which a small water pump circulated the coolant through a second copper coil immersed in crushed ice in a storage vessel. By using freshly charged accumulators of large capacity (in circuits P and Q, Fig. 14) and by leaving the currents on for 24-48 hours before commencing work, the stability of the specimen temperature was found to be extremely good. Under balanced condition of the bridge, the zero of the final output galvanometer was steady to within 1 part in 500 for a period of half an hour.

4.3.5 The magnet

A water-cooled Newport electromagnet (Type E) was used, having conical pole tips 4.5" in diameter and a gap of 1". Rotation of the field was provided by mounting the magnet on a turntable, graduated in degrees. This, in turn, was mounted on a carriage which could be run on guide rails thus enabling the magnet to be moved clear of the dewar flask and brought back in the same position. For precision location of the specimen in the field, adjustments were made in the specimen support unit described earlier.

The power supply to the magnet was derived from a 400 volt d.c. generator whose field was regulated by means of a voltage divider unit arranged near the working table. For up to 200 volt input, the magnet current was usually altered or reversed with the aid of a suitable control panel consisting of a network of series

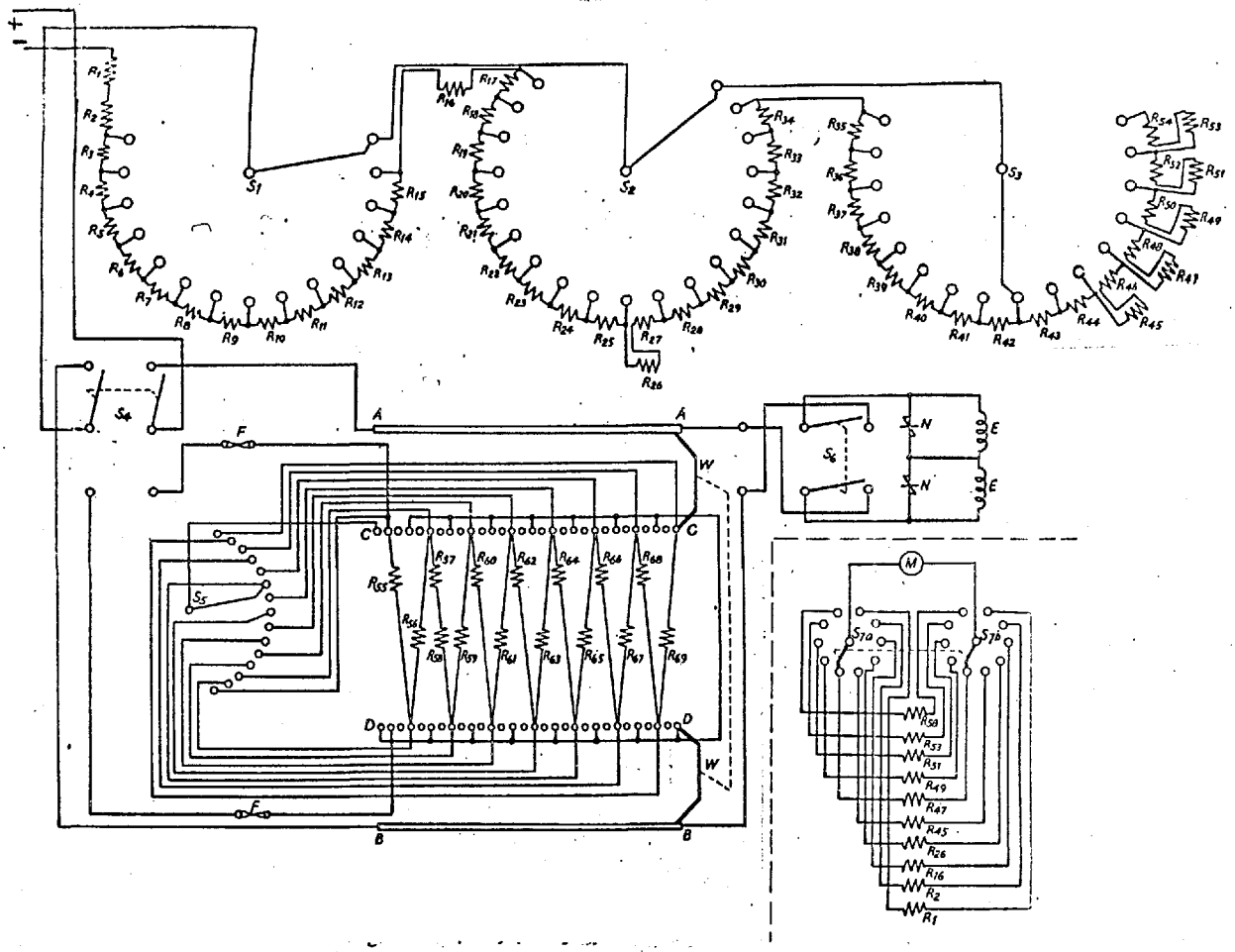

R_1 = 60A Shunt
R_2 = 30A Shunt
R_3 = 0·4Ω
R_4 = 0·4Ω
R_5 = 0·4Ω
R_6 = 0·4Ω
R_7 = 0·6Ω
R_8 = 0·6Ω
R_9 = 0·6Ω
R_{10} = 0·6Ω
R_{11} = 0·8Ω
R_{12} = 0·8Ω
R_{13} = 0·8Ω
R_{14} = 0·8Ω
R_{15} = 0·8Ω
R_{16} = 10A Shunt
R_{17} = 0·5Ω

R_{18} = 0·5Ω
R_{19} = 0·5Ω
R_{20} = 0·5Ω
R_{21} = 0·5Ω
R_{22} = 0·5Ω
R_{23} = 0·5Ω
R_{24} = 0·5Ω
R_{25} = 0·8Ω
R_{26} = 10A Shunt
R_{27} = 0·8Ω
R_{28} = 0·8Ω
R_{29} = 1·0Ω
R_{30} = 1·0Ω
R_{31} = 1·0Ω
R_{32} = 1·0Ω
R_{33} = 1·0Ω
R_{34} = 1·0Ω

R_{35} = 1·29Ω
R_{36} = 1·29Ω
R_{37} = 1·29Ω
R_{38} = 1·29Ω
R_{39} = 1·29Ω
R_{40} = 1·29Ω
R_{41} = 1·29Ω
R_{42} = 1·29Ω
R_{43} = 1·29Ω
R_{44} = 16Ω
R_{45} = 3A Shunt
R_{46} = 44Ω
R_{47} = 1·5A Shunt
R_{48} = 100Ω
R_{49} = 1·0A Shunt
R_{50} = 200Ω
R_{51} = 0·3A Shunt

R_{52} = 400Ω
R_{53} = 0·15A Shunt
R_{54} = 868Ω
R_{55} = 1·6KΩ
R_{56} = 3·3KΩ
R_{57} = 6·6KΩ
R_{58} = 0·03A Shunt
R_{59} = 13KΩ
R_{60} = 20KΩ
R_{61} = 40KΩ
R_{62} = 86·8KΩ
R_{63} = 166KΩ
R_{64} = 334KΩ
R_{65} = 660KΩ
R_{66} = 1·3MΩ
R_{67} = 2MΩ
R_{68} = 4MΩ
R_{69} = 8·7MΩ

S_1 = single-pole 15-way (make-before-break)
S_2 = single-pole 19-way (make-before-break)
S_3 = single-pole 16-way (make-before-break)
S_4 = two-pole 2-way (break-before-make)
S_5 = single-pole 15-way (make-before-break)
S_6 = two-pole 2-way (break-before-make)
S_7 = two-pole 10-way (break-before-make)

Fig. 12. The control unit for the electromagnet. (After Birss and Brown[87]).

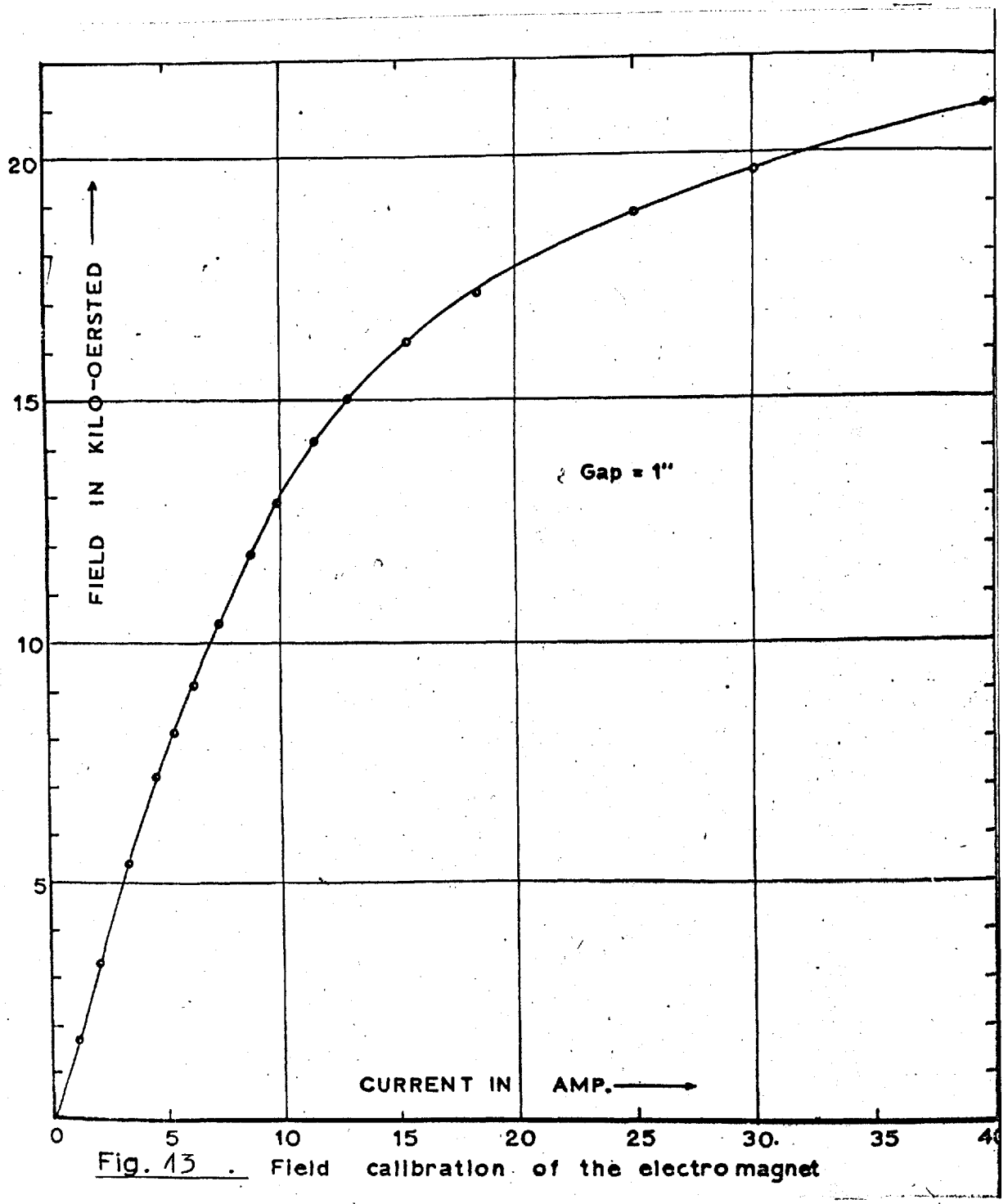

Fig. 13 . Field callbration of the electro magnet

and shunt resistors. This is shown in Fig. 12 .

In Fig. 13 the field calibration of the magnet is given for a 1" pole gap. In the range 30 - 40 amp., current was drawn only for a short period, about 15 secs., and this enabled a few measurements to be made at high fields without overheating the magnet. With the size of the pole tips and the gap used, the field was estimated to be constant to better than 0.6% over a central spherical region 1.5 cm in diameter. A high uniformity of field is, of course, necessary to prevent large translational forces on the specimen.

4.3.6 The circuit arrangement

The general circuit arrangement is shown in Fig. 14. P was the main driving circuit with a number of suitable resistors in series and parallel combinations to provide the necessary coarse and fine control of the specimen current. A standard oil-filled 2 Ω resistor and a commercial Pye potentiometer (Cat. No. 7568) were used to monitor the current. The potentiometer, which has a range from 0 to 1.7 volts can be read directly down to 1μV. Current standardization in the potentiometer circuit is independent of the potentiometer setting. There are three test circuits which can be selected by a double pole switch. The accuracy of the slide wire is half a division and that of the range multiplier is ± 0.02% at 20° C.

The voltage developed across the specimen in the absence of the magnetic field was balanced, by current regulation in the

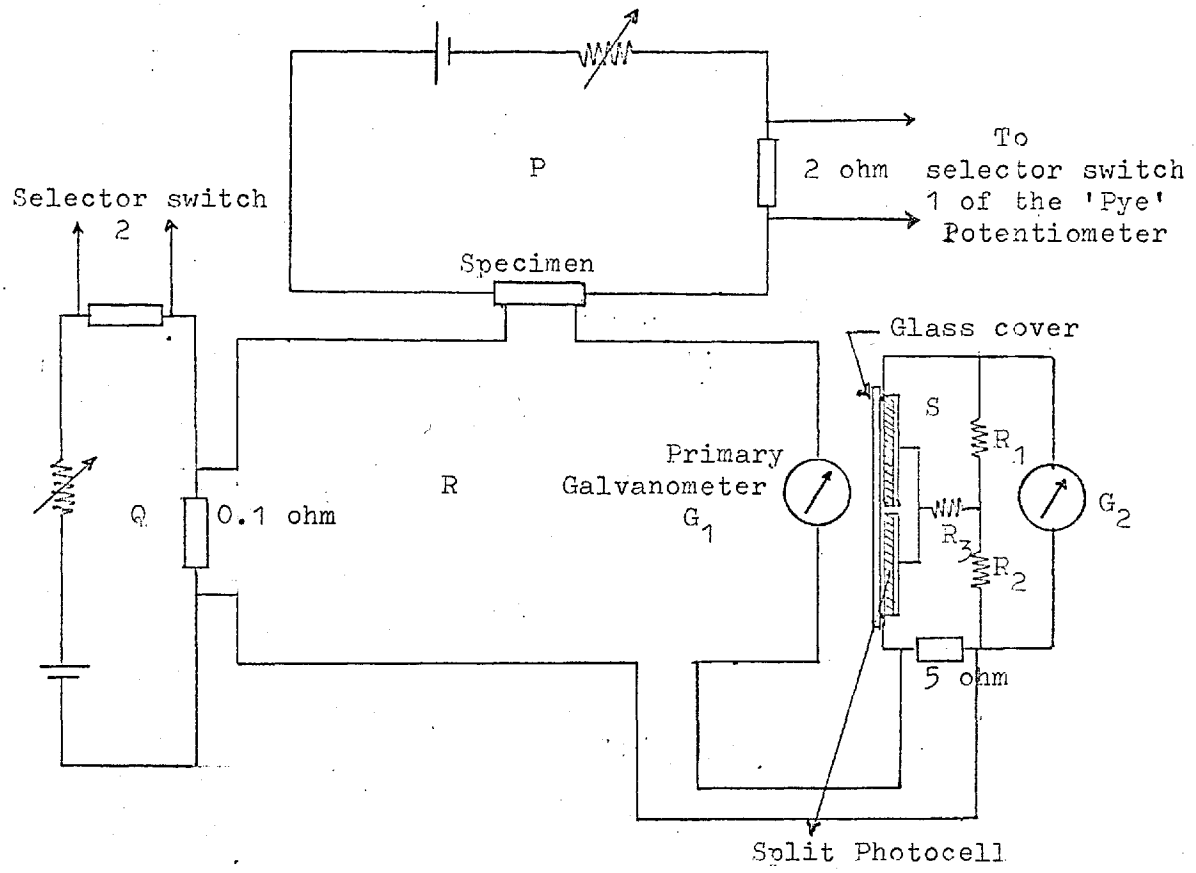

Fig. 14. The circuit arrangement for the measurement of the magnetoresistance.

auxiliary circuit Q, with the backing voltage developed across the standard 0.1Ω resistor. This current could again be monitored by means of the Pye potentiometer. The auxiliary circuit also provided a satisfactory means of compensating for thermal e.m.f.'s in the circuits. Any departure from zero of the current in the test circuit R was indicated by the primary galvanometer G_1 in conjunction with the photo-cell amplifier (the negative feedback loop being as shown). An out-of-balance current in R produced by the change of specimen resistance on application of the magnetic field could then be either reduced to zero each time by varying the specimen current or else the deflection of the galvanometer G_2 could be recorded and related to a resistance change by means of a previous calibration. As shown in Section 4.2, the fractional change of resistance $\frac{dR}{R}$ was then immediately given in terms of the fractional change of current $\frac{dI}{I}$. The latter method was preferred for ease of operation. The change dI in the current and the actual current I was always calculated from the voltage drops across the standard 2Ω resistor. Since the circuit arrangement was capable of providing compensation for stray e.m.f.'s in the circuit, this resulted in considerable simplification since current reversals in the circuit were found unnecessary except for occasional checks. The overall sensitivity of the whole arrangement was better than 10^3 mm/μV or 10^{-9} volt/mm on the final scale, with an input resistance of 45Ω and a typical specimen current of 30 - 50 mA. The noise level was down to 1 mm or 10^{-9} volt and good stability was obtained with extensive thermal

lagging of the different parts of the circuit and with the use of the liquid temperature bath. Under favourable conditions, the drift was found to be less than 2 - 3 mm per hour.

4.3.7 The use of a demagnetizing coil

With the large 7" electromagnet and the type of power unit used, it was found difficult to reduce the residual remanent field below about 25 - 30 Oe and so to demagnetize the specimen completely. Since magnetoresistance is measured as a fractional change in the resistivity due to magnetization in a field, this remanent magnetization of the specimen could produce an error or uncertainty of about 2 - 5% in the measurement. An a.c. Helmholtz-type demagnetizing coil, capable of producing a maximum field of 100 Oe at the centre of the system, was therefore set up to demagnetize the specimen completely using the a.c. field. This coil was mounted in such a way that it could be easily removed to place the magnet in position and then replaced when the specimen was to be demagnetized by it. A 3 amp. variac with series resistors formed a convenient regulated power unit for the coil.

With all the supplies switched on and the system in a steady state, the technique of measurement consisted of first demagnetizing the specimen, removing the coil, adjusting the zero of the scale after balancing the various potentiometer circuits and monitoring the specimen current by reading the voltage across the fixed resistor of 2 Ω. The magnet was then placed in position and

fixed at the desired orientation relative to the direction of measurement. On applying the field, the sense and magnitude of deflection on the scale was noted after checking the constancy of the specimen current. The field was then slowly brought down to zero with few reversals at the last stage to demagnetize the specimen in the existing field. Next, the magnet was removed, the demagnetizing coil brought in and the whole operation repeated for the next reading. This sequence of operations produced one point on one experimental curve, such as those depicted in Fig. 17 . However, by suitably arranging all the control panels to be near at hand, it was possible to keep the time for one such measurement down to about a minute.

CHAPTER V

EXPERIMENTAL RESULTS

5.1 Introduction

The experimental results are described under individual headings for the four ferromagnetic materials investigated, namely, Ni, Fe, Co and Gd. A detailed analysis is given for the cases of nickel and gadolinium, which are representative of solids belonging to the cubic and hexagonal crystal classes respectively.

5.2 Magnetoresistivity

Fig. 15 shows a typical calibration graph of the secondary galvanometer scale deflection against the change of specimen current, dI. The departure from linearity generally increased with increasing feedback, so that an optimum working condition had to be determined by altering the various adjustable parameters, e.g. the specimen current, the resistance in the primary galvanometer circuit, the degree of negative feedback, the galvanometer shunt resistance and so on. In Fig. 16 is shown a plot of the secondary galvanometer deflection when a specimen of nickel was subjected to a constant magnetic field of 7000 Oe and the field was gradually turned through 360°. From this graph it would appear that the longitudinal magnetoresistance effect is much less affected by a small change in the orientation of the field than is the transverse effect. This

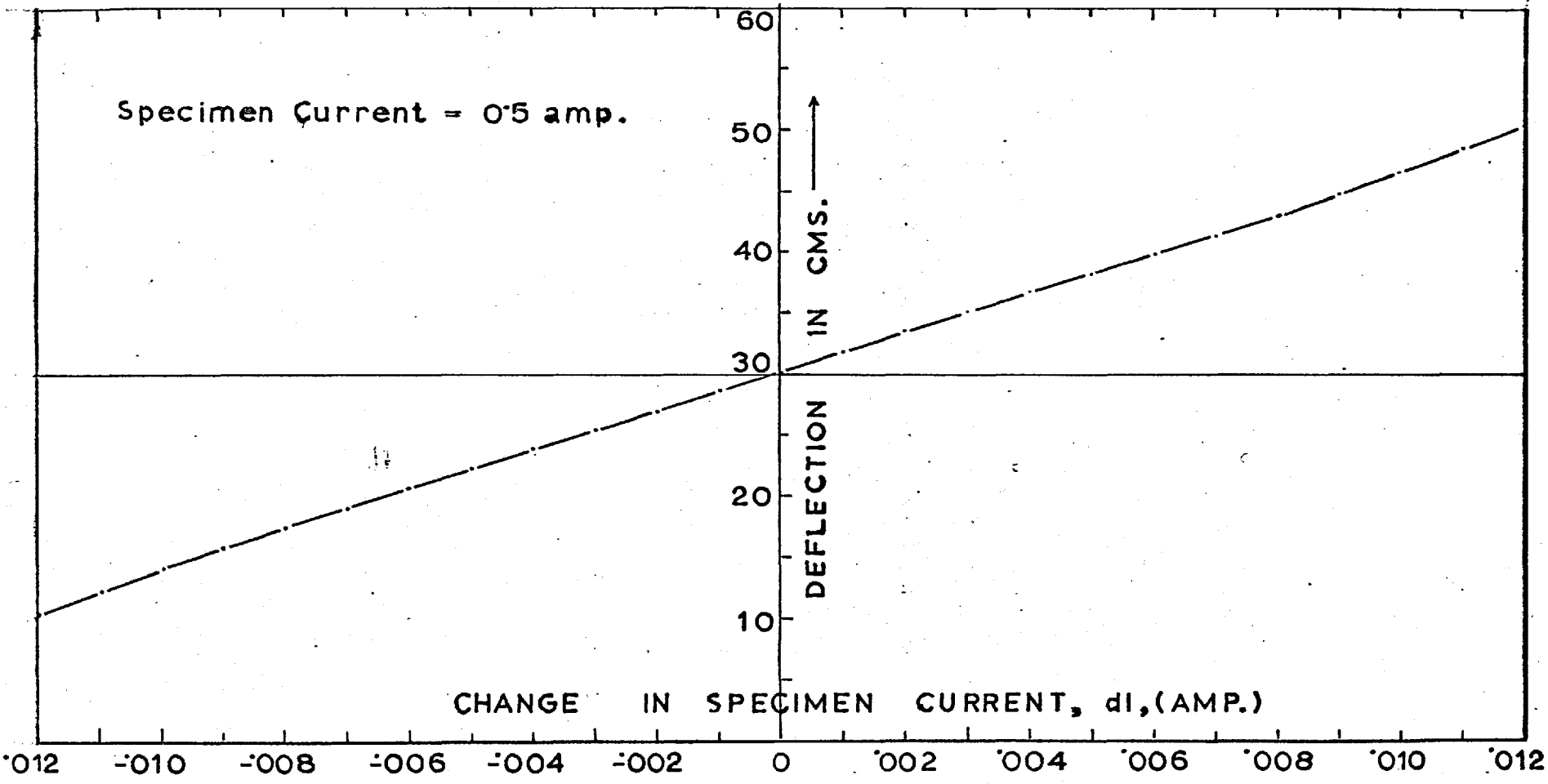

Fig. 15. A typical calibration graph showing the variation of the (secondary) galvanometer deflection with the change of specimen current, ± dI.

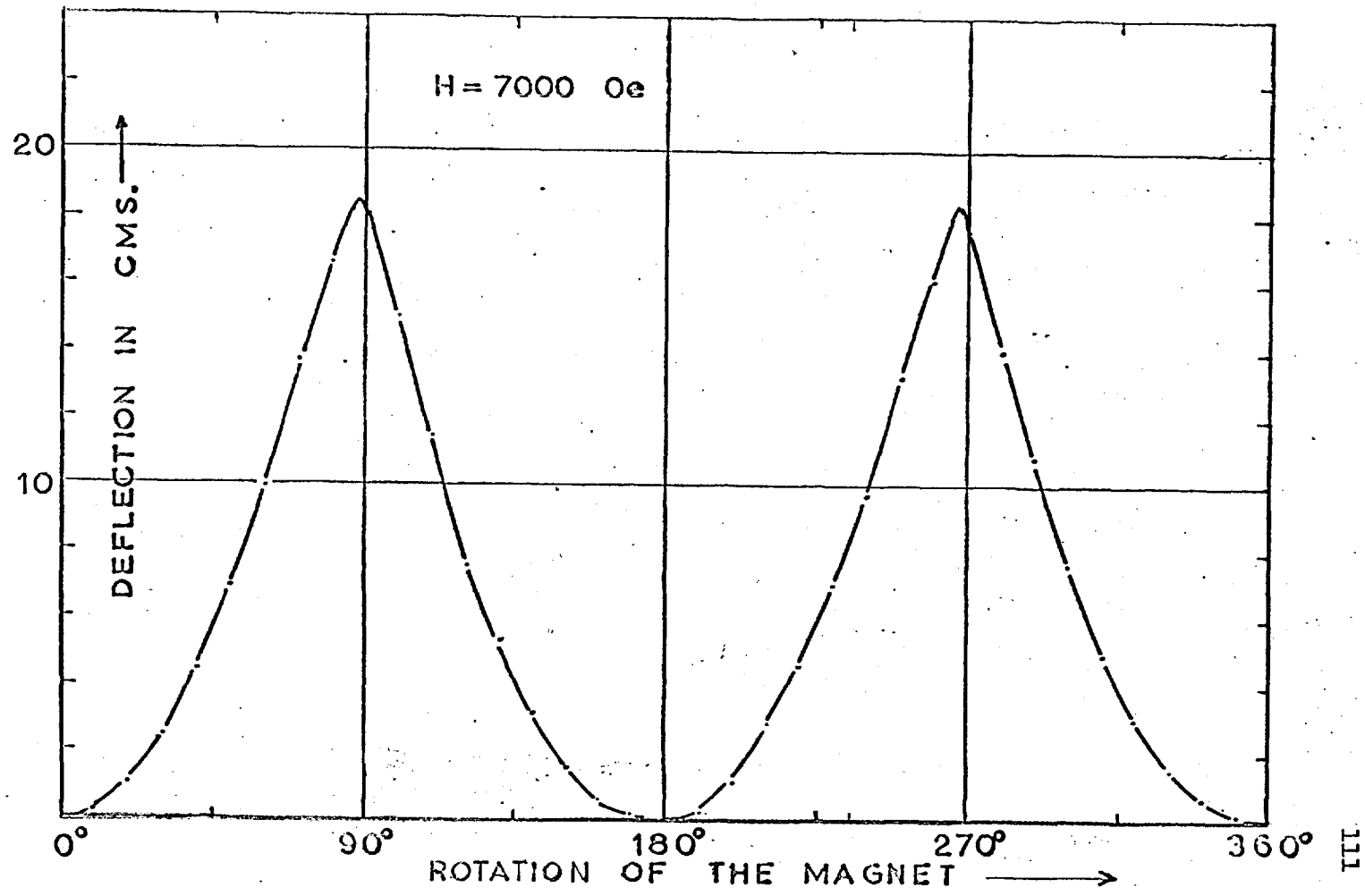

Fig. 16. Variation of the magnetoresistive behaviour of polycrystalline nickel with the orientation of the applied field.

criterion was utilized for checking the correct alignment of the specimen relative to the electromagnet.

5.2.1 Iron

Fig. 17 shows the magnetoresistivity of polycrystalline iron as a function of the applied magnetic field up to a maximum field of 21,500 Oe. The curve marked 0 corresponds to the longitudinal magnetoresistance (x = 0 where x is the angle between the field and the specimen axis) and that marked 90° to transerve effect ($x = 90^{\circ}$). Intermediate positions are indicated in the same way.

The graphs reveal the existence of considerable shape anisotropy in the rod-shaped specimen. Saturation is reached at about 2000 Oe when x = 0 but for increasing x the peaks become wider and move more towards the high field region. It can be seen that the low-field magnetoresistance below saturation is considerably affected by this orientation effect. Above the region of technical saturation, however, the specimen exhibits an isotropic 'forced' magnetoresistance effect ($\bar{\xi}' = \frac{\partial \bar{\xi}}{\partial H}$) that is practically independent of the direction of magnetization. The values of the slopes for the longitudinal and transverse cases are found to be (at 273° K)

$$\bar{\xi}'_{\perp} = -4.18 \times 10^{-8}\ \mathrm{Oe}^{-1}$$

$$\bar{\xi}'_{\parallel} = -4.41 \times 10^{-8}\ \mathrm{Oe}^{-1} \qquad (5.1)$$

The difference in the two values, which is about 5%, is unlikely to be due to experimental error only and may probably be attributed to two, more possible, causes. These are

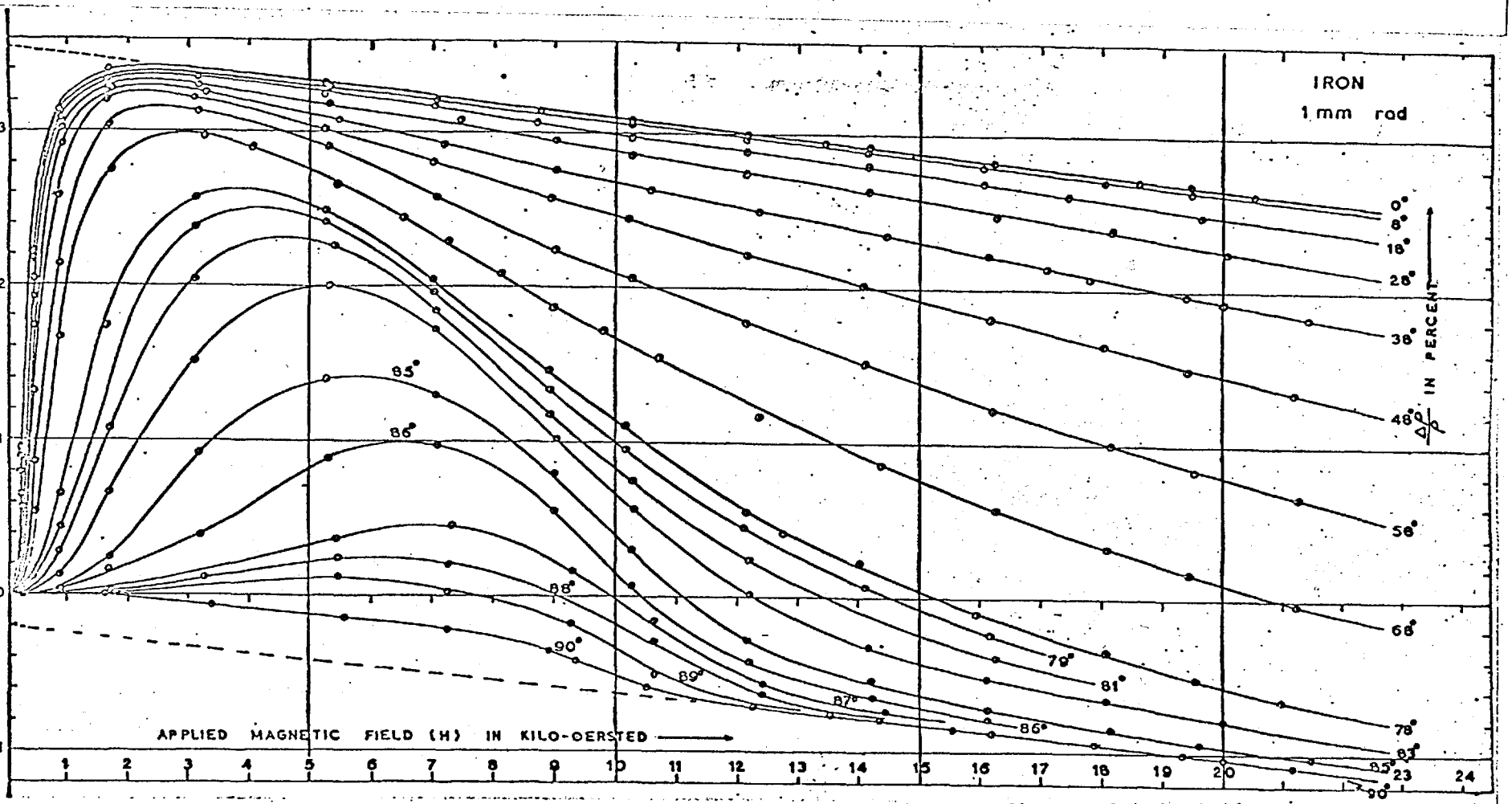

Fig. 17. Magnetoresistivity of polycrystalline iron as functions of field and orientation of the field relative to the specimen axis.

(a) the high demagnetizing field (~ 11,000 Oe) operating at right angles to the rod may prevent the true slope from being reflected in the curve within the range of fields studied, and

(b) there may be a genuine contribution to the forced magnetoresistance from the term $\frac{3}{2}\frac{\partial F_s}{\partial X}$ (2.16), which implies that the coefficient Q is a weakly field-dependent parameter. This is discussed further in the next chapter.

Fig. 18 shows the magnetoresistivity as a function of x, corresponding to saturation in zero (equivalent) internal field. In evaluating the demagnetizing field for various orientations, the simplest case of uniform magnetization has been considered. The demagnetizing field (which is not collinear with the direction of magnetization except when the field is parallel or perpendicular to the axis of the rod) was calculated from the demagnetizing factors along the three principal axes, D_x, D_y, D_z (where $D_x + D_y + D_z = 1$). These latter values were obtained from the existing works on cylindrical rods[91,92,93]. The points for the experimental curve of Fig. 18 were taken from Fig. 17 after correcting for the demagnetizing field appropriate to the particular field orientation, so that all magnetoresistivity values are referred to the same magnetic state, i.e. saturation in zero field. The significance of the solid and broken curves of Fig. 18 is discussed in the next chapter.

5.2.2 Nickel

As before, the magnetoresistivity of polycrystalline nickel

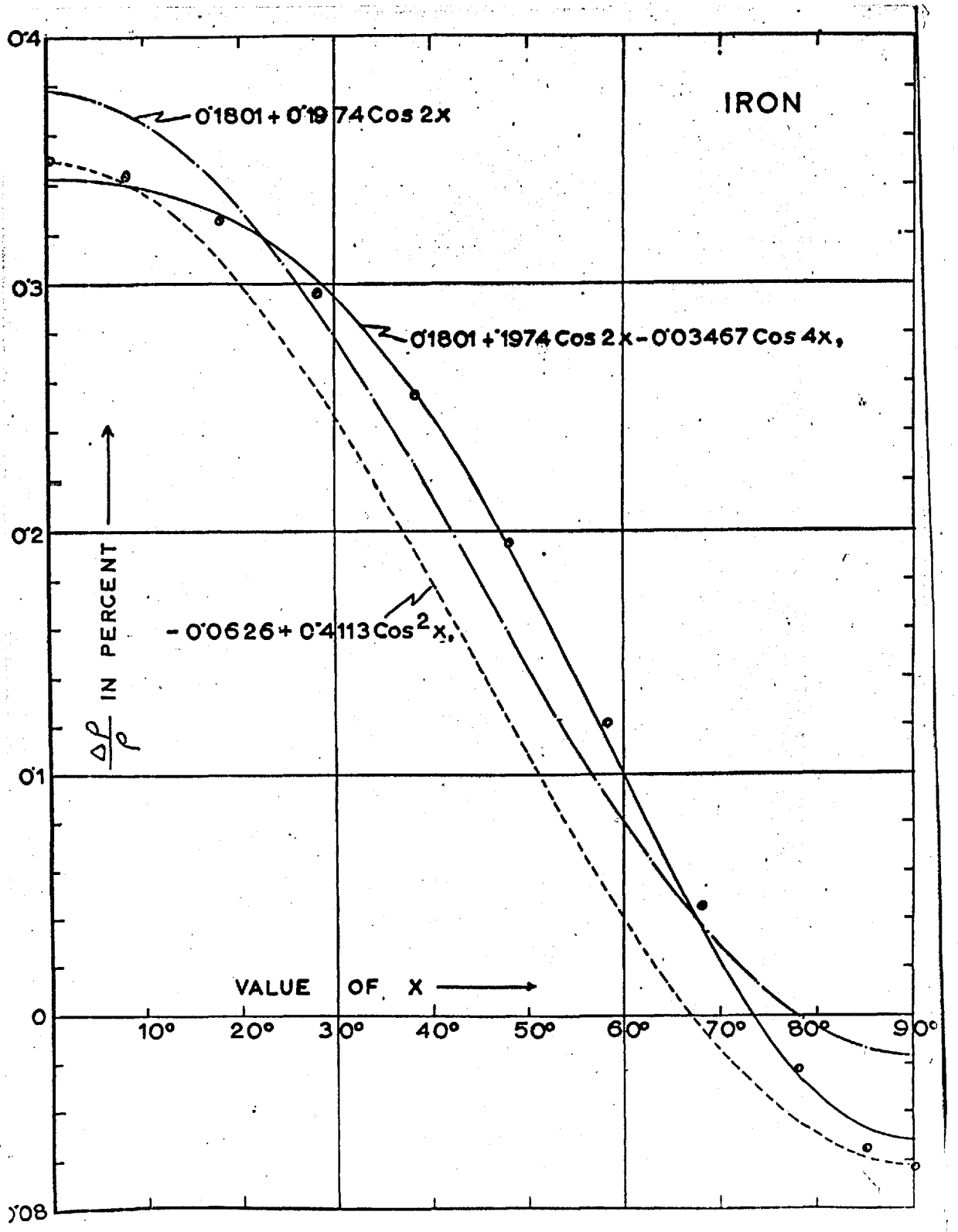

Fig. 18. Saturation magnetoresistivity of iron plotted as a function of x .

as a function of field for various values of x is depicted in Fig. 19. Saturation is reached below 1000 Oe when x = 0 and, unlike the case of polycrystalline iron, the peaks in subsequent magnetoresistivity curves do not show any substantial shift towards higher field as the angle is gradually increased. The transverse magnetoresistance shows no positive peak and attains its saturation value at about 3000 Oe, i.e. the demagnetizing field of the material.

The forced magnetoresistance in nickel is found to be more isotropic than in iron. The values of the slopes for the longitudinal and transverse cases are

$$\bar{\xi}'_{\parallel} = -1.71 \times 10^{-7}\ \mathrm{Oe}^{-1}$$
$$\bar{\xi}'_{\perp} = -1.68 \times 10^{-7}\ \mathrm{Oe}^{-1}\ , \qquad (5.2)$$

with a difference of nearly 1.7%.

In Fig. 20 is shown the values of saturation magnetoresistivity as a function of x at zero (equivalent) internal field. The open circles represent the points taken from Fig. 19 after correcting for the demagnetizing field appropriate to the particular direction of magnetization in a manner similar to that described for iron. The significance of the solid and broken curves in the figure is discussed in the next chapter.

Figs. 21, 22, 23 show the three sets of graphs for the single crystal of nickel which was obtained when the plane of magnetization was the (111), (110) and $(11\bar{2})$ crystallographic planes respectively. The measurement of magnetoresistivity in these three

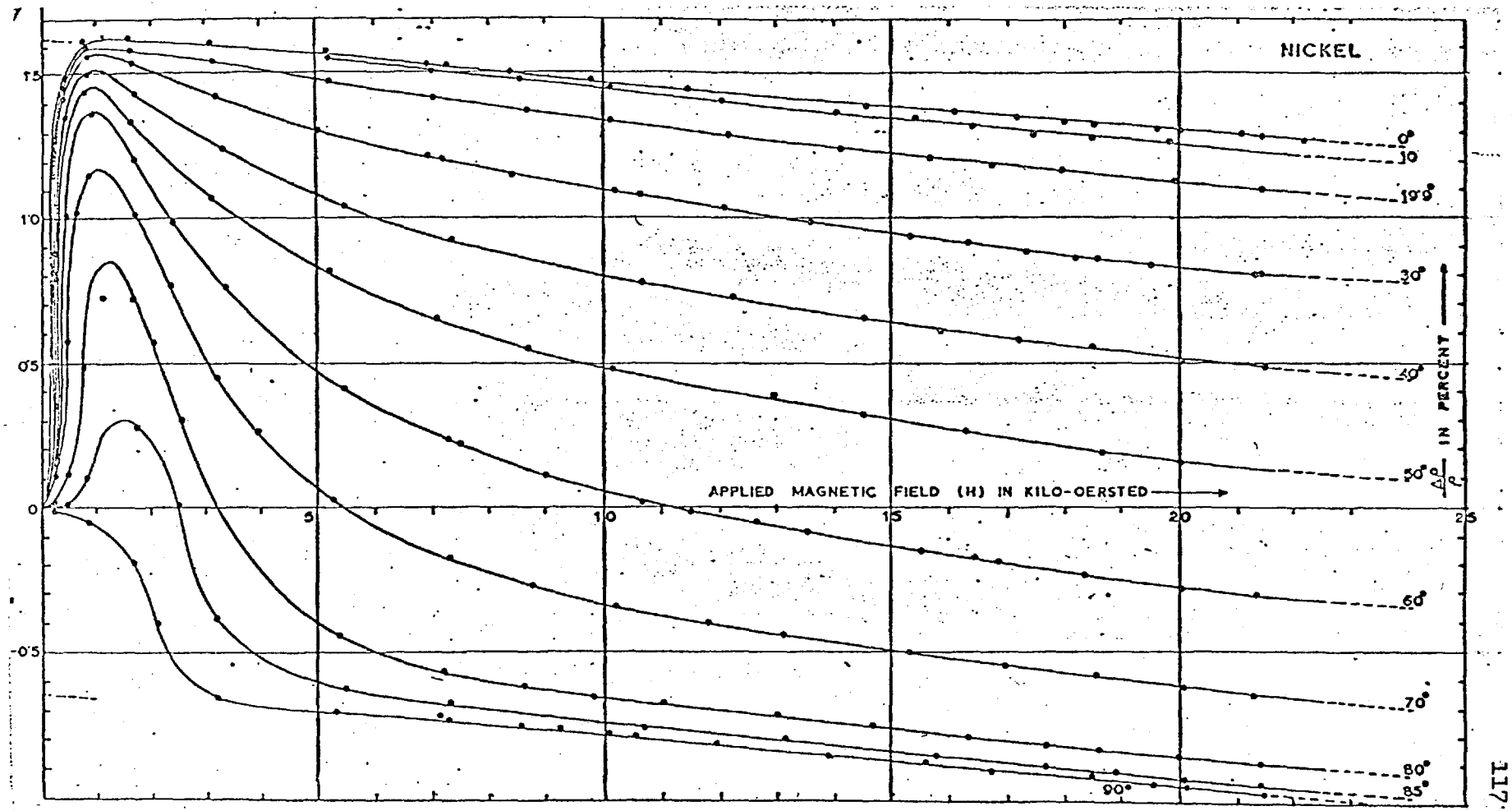

Fig. 19. Magnetoresistivity of polycrystalline nickel as functions of field and orientation of the field relative to the specimen axis.

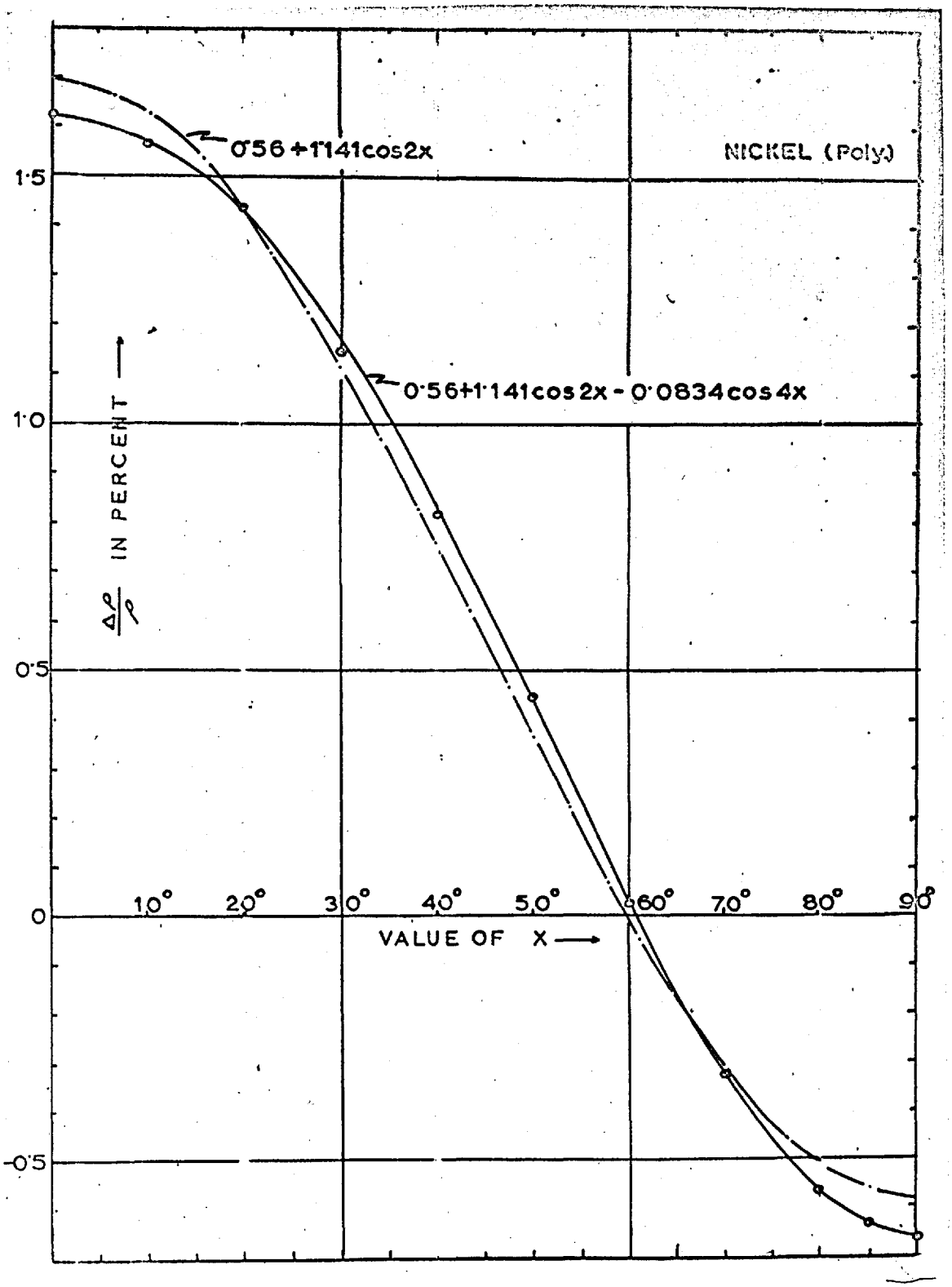

Fig. 20. Saturation magnetoresistivity of polycrystalline nickel at zero internal field plotted against the orientation of the magnetic field relative to the specimen axis.

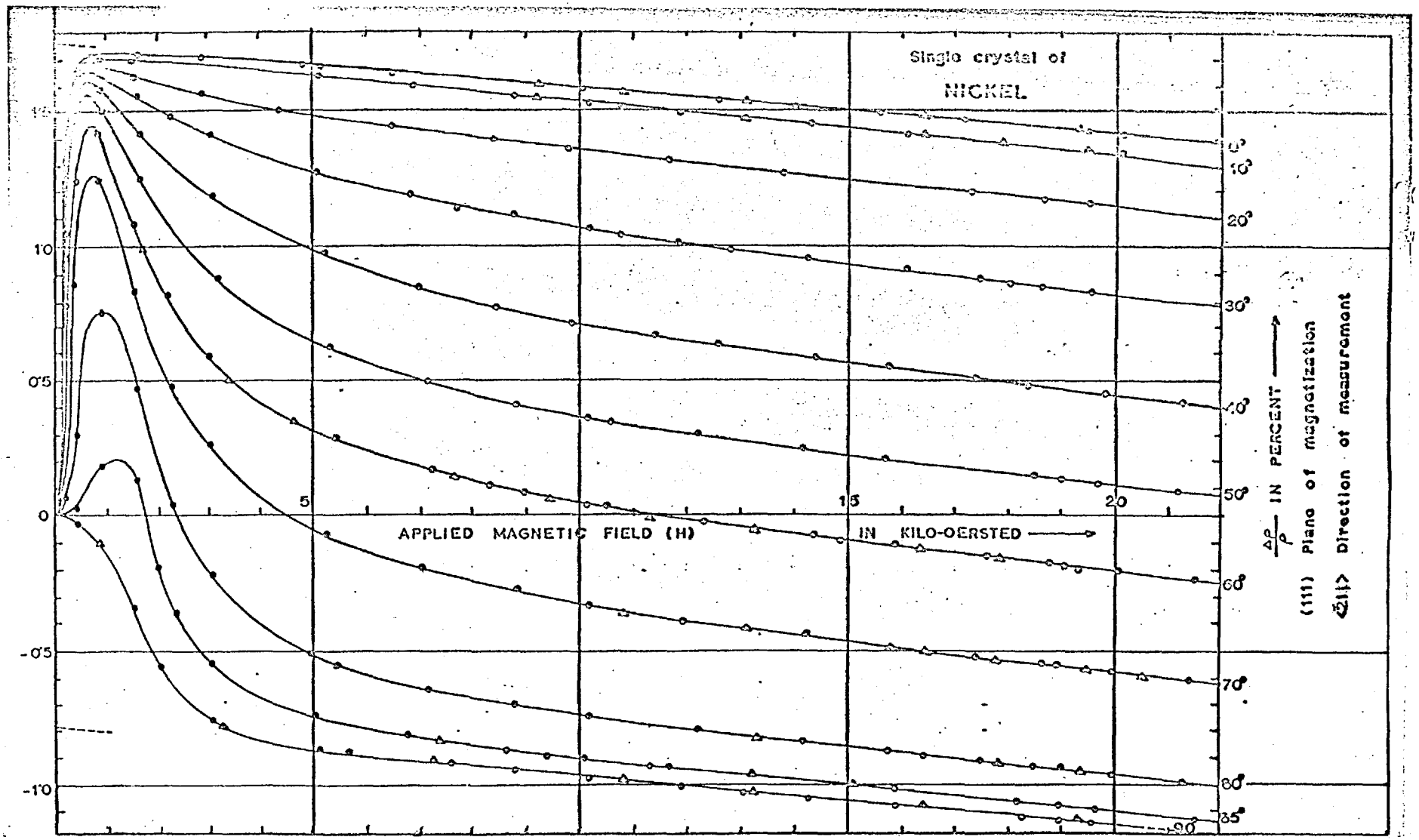

Fig. 21. Magnetoresistivity of single crystal of nickel as measured in the (111) plane; direction of measurement $\langle 2\bar{1}1 \rangle$.

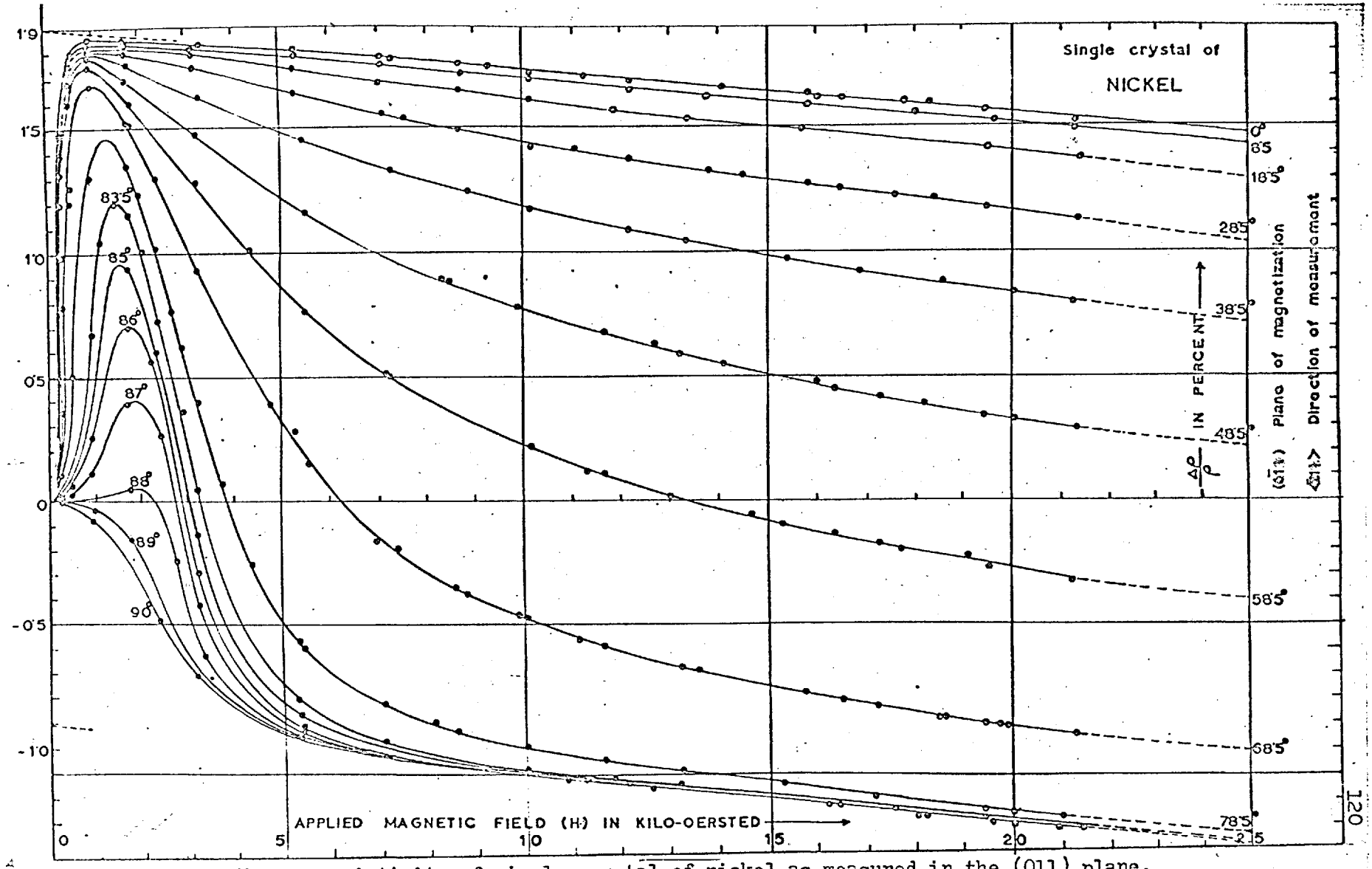

Fig. 22. Magnetoresistivity of single crystal of nickel as measured in the (011) plane.

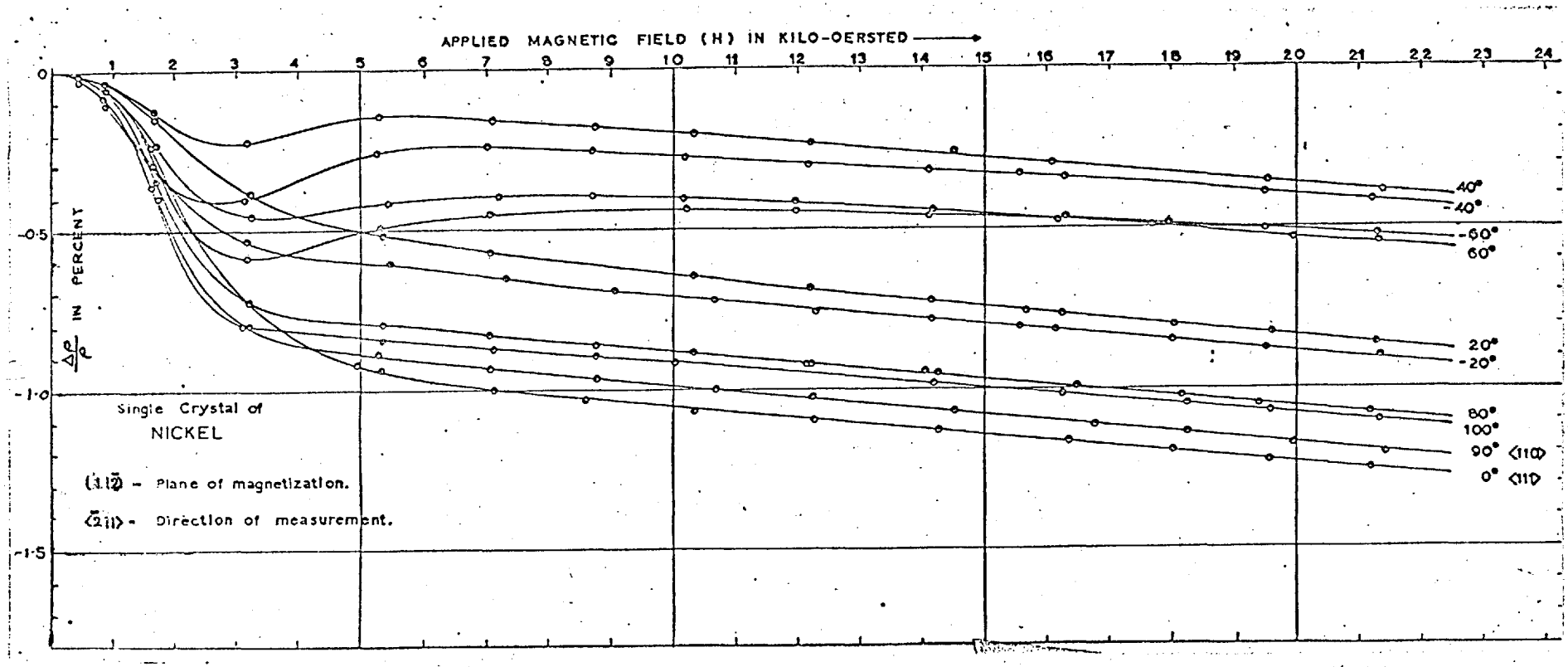

Fig. 23. Transverse magnetoresistivity of single crystal of nickel as measured in the (11$\bar{2}$) plane; direction of measurement <$\bar{2}$11> .

discrete planes, the corresponding measuring directions being each time in a $\langle 11\bar{2} \rangle$ direction enabled, for the first time, the five saturation magnetoresistance constants to be evaluated on the same crystal, as is shown in section 6.3.2. While the general features of the polycrystalline magnetoresistance are retained in the sets of graphs for the (111) and (110) planes, they vary considerably in detail as the direction of magnetization changes relative to the crystallographic axes. The case of transverse magnetoresistance depicted in Fig. 23 is one in which the field and the direction of current are always mutually perpendicular to each other. As in the polycrystalline material, the single crystal forced magnetoresistance decreases linearly with field and is found to be substantially independent of the orientation of the field. The rates of decrease of ξ' with H for the three sets of measurements are

$$(\xi'_{\perp})_{(111)} = -1.86 \times 10^{-7}\ \text{Oe}^{-1}\ , \quad (\xi'_{\parallel})_{(11\bar{2})} = -1.88 \times 10^{-7}\ \text{Oe}^{-1},$$

$$(\xi'_{\parallel})_{(111)} = -1.78 \times 10^{-7}\ \text{Oe}^{-1}\ , \quad (\xi'_{\perp})_{(11\bar{2})} = -1.90 \times 10^{-7}\ \text{Oe}^{-1},$$

$$(\xi'_{\perp})_{(110)} = -1.88 \times 10^{-7}\ \text{Oe}^{-1}\ ,$$

$$(\xi'_{\parallel})_{(110)} = -1.72 \times 10^{-7}\ \text{Oe}^{-1}\ . \qquad (5.3)$$

As before, the geometry of the specimen and the principle of measurement made it necessary to correct these results for the demagnetizing effect before any accurate calculations of the constants could be attempted. The case of an infinitely long specimen of rectangular cross-section has been discussed in Appendix II where an expression was developed for the demagnetizing factor when the plane of magnet-

ization is perpendicular to the axis of the bar. This represents the experimental condition for the case of transverse magneto-resistivity except that the specimen is of finite length and the field is turned between two positions in which it is first parallel to one side of the rectangular cross-section (<111> direction)and then to the other (<110> direction). Taking again the simplest case of a uniformly magnetized isotropic medium, the demagnetizing factors D_x, D_y, D_z along the three principal axes were calculated from the expression developed in Appendix II , namely

$$4\pi D = 2\left\{4\tan^{-1}\frac{1}{p} + 2p\ln p + \frac{1-p^2}{p}\ln(1+p^2)\right\} , \qquad (5.4)$$

where p = ratio of the two adjacent sides of the rectangular section of the bar. The demagnetizing field H_i could then be evaluated for any arbitrary direction of magnetization I inside the body. Fig. 24 shows a typical variation of H_i/I with the angle of orientation of the magnetization vector from <110> direction for the case of the actual specimen.

In Figs. 25, 26 are shown the results which are obtained from Figs. 21, 22 after the necessary corrections have been made for the demagnetizing fields: the values are plotted against the angle between the direction of measurement and the direction of magnetization. Fig. 27 is plotted the same way as Figs. 25, 26 , but the angle is now measured from the <111>direction. In all the three cases, the same magnetic state has been preserved by maintain-

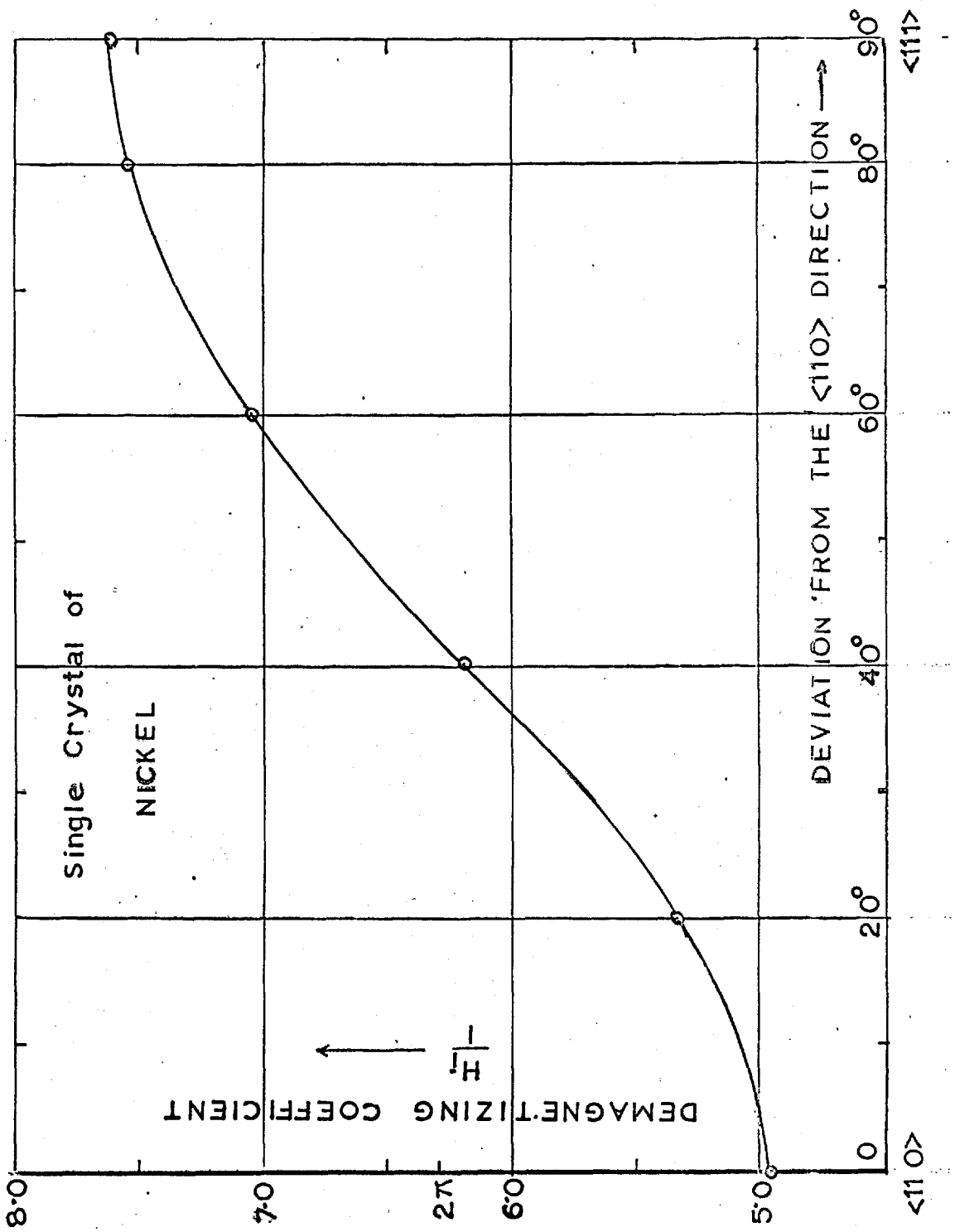

Fig. 24. Variation of the demagnetizing coefficient with the direction of magnetization from the <110> direction for the rectangular cross-section of the Ni single-crystal specimen.

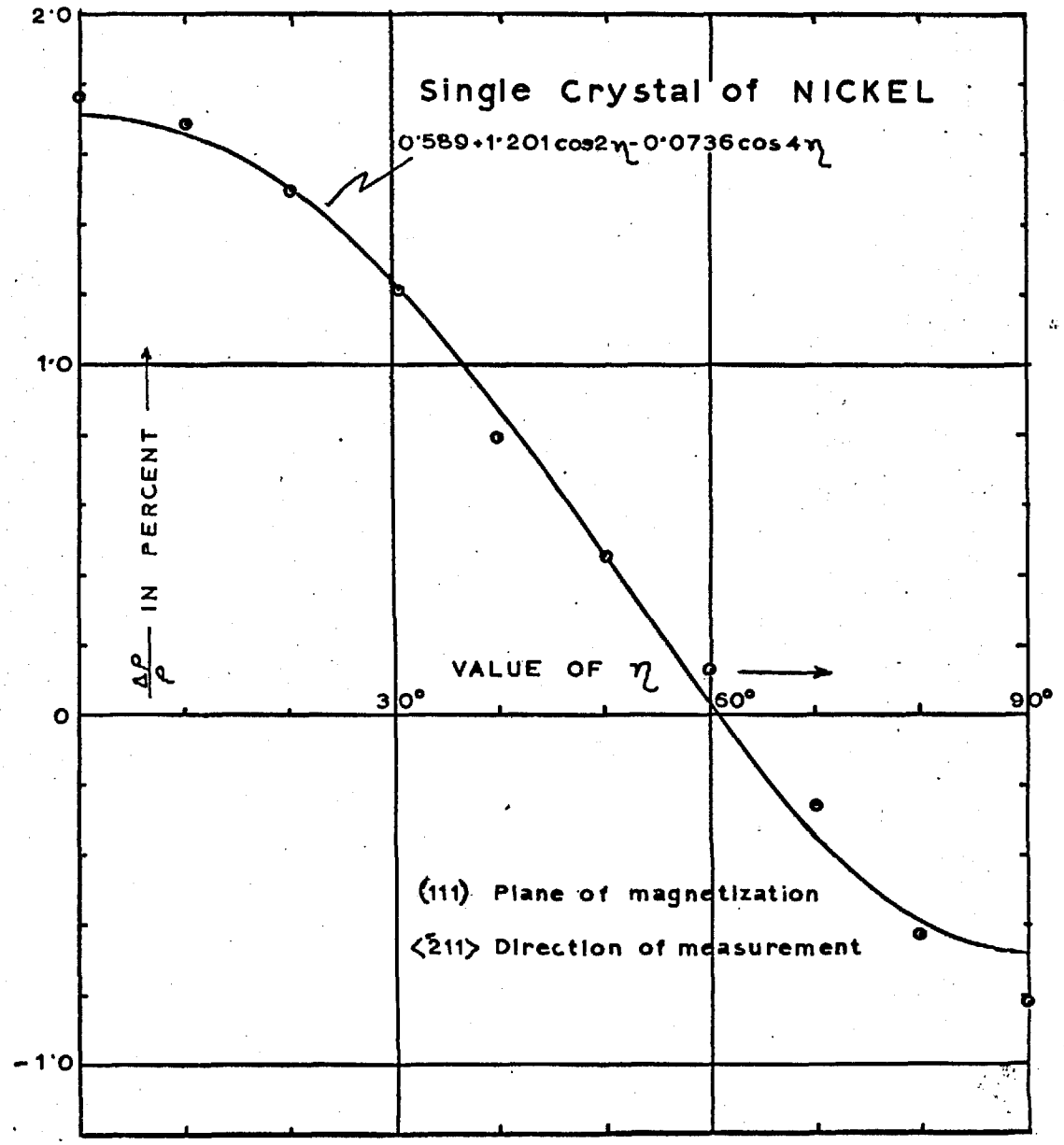

Fig. 25. Saturation magnetoresistivity of nickel in the (111) plane of magnetization as a function of η, (see Fig.6).

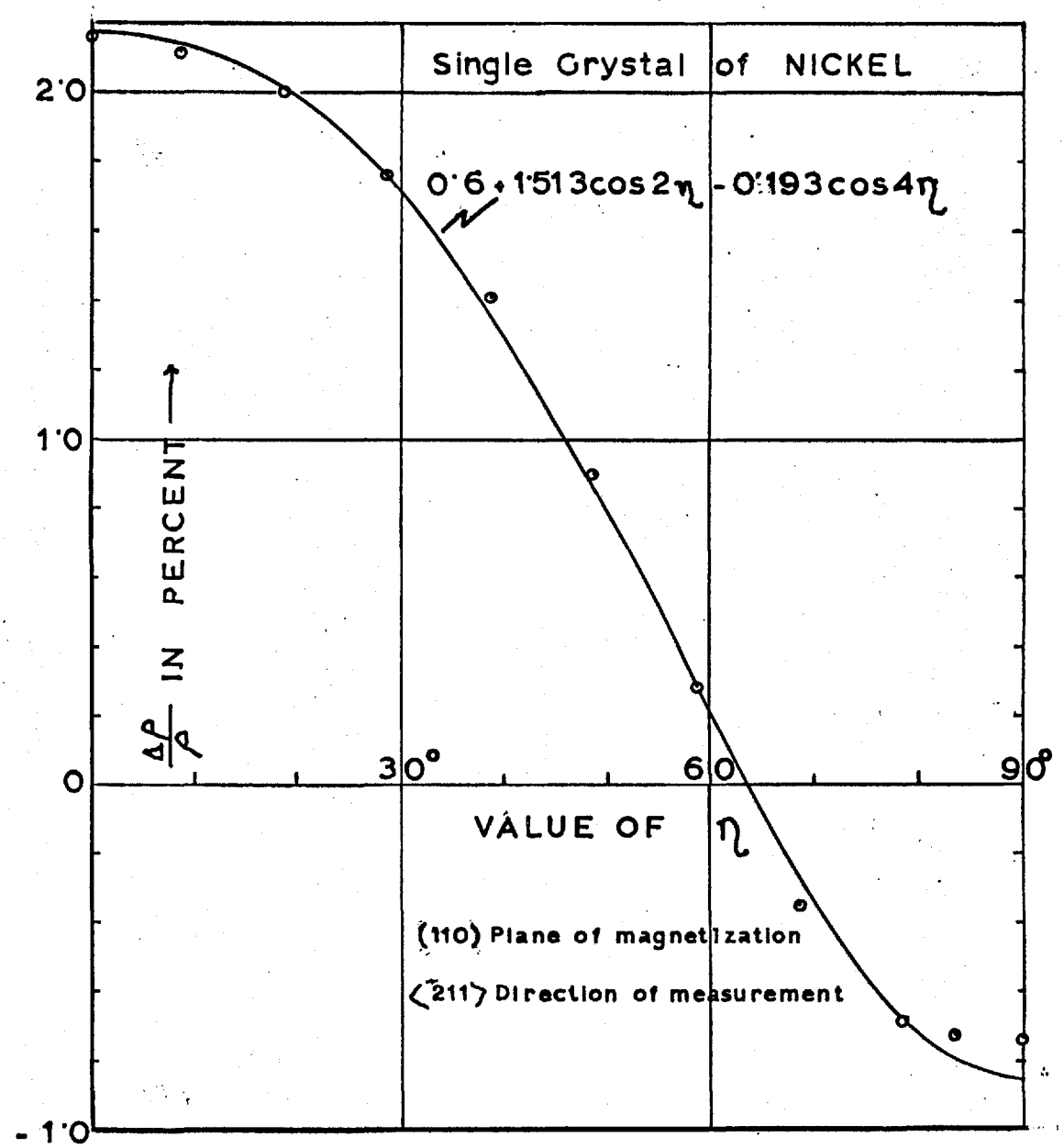

Fig. 26. Saturation magnetoresistivity of nickel in the (110) plane of magnetization as a function of η, (see Fig.6).

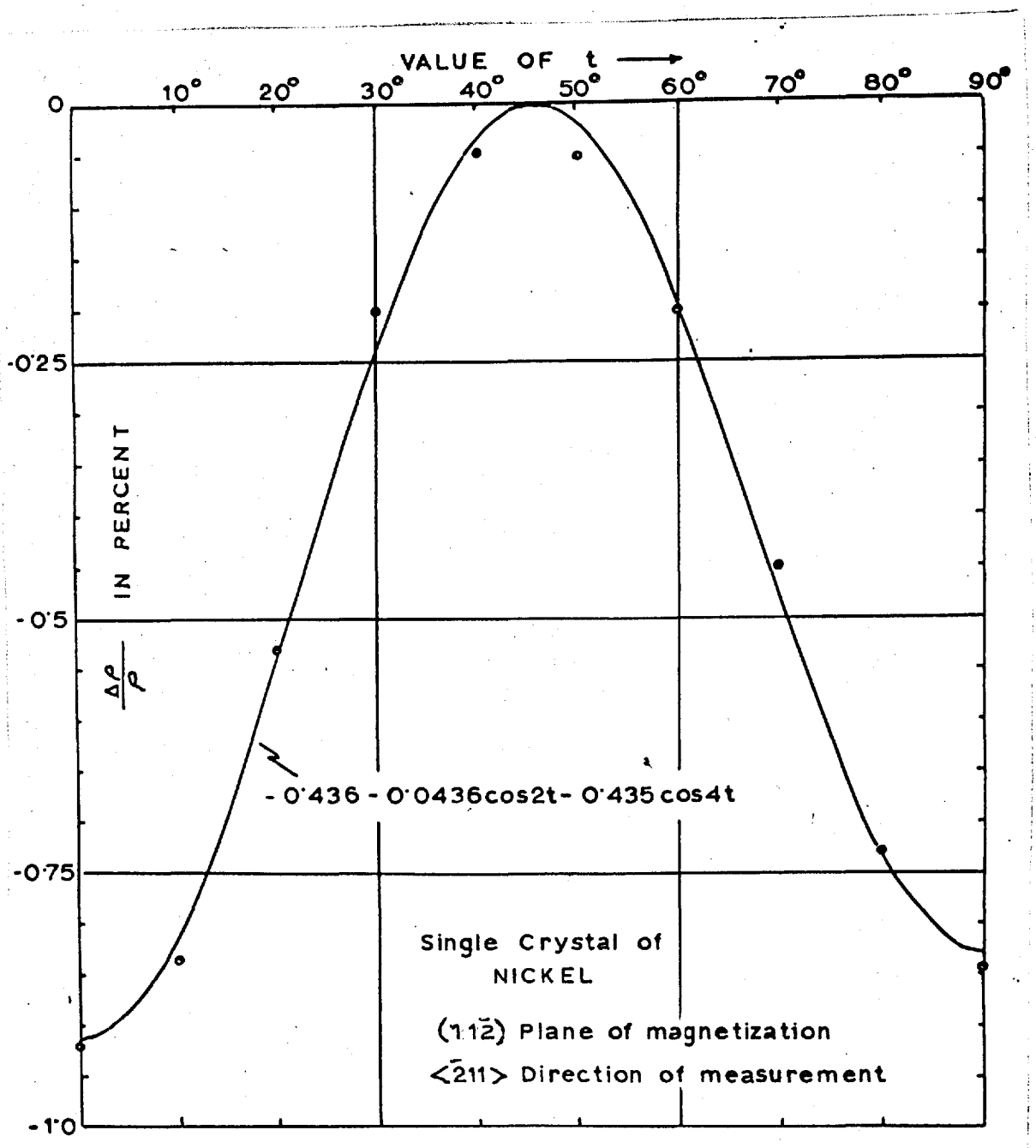

Fig. 27. Transverse magnetoresistivity of nickel at zero (saturation) internal magnetic field in the (11$\bar{2}$) plane of magnetization. The orientation of the field is measured from a <111> direction.

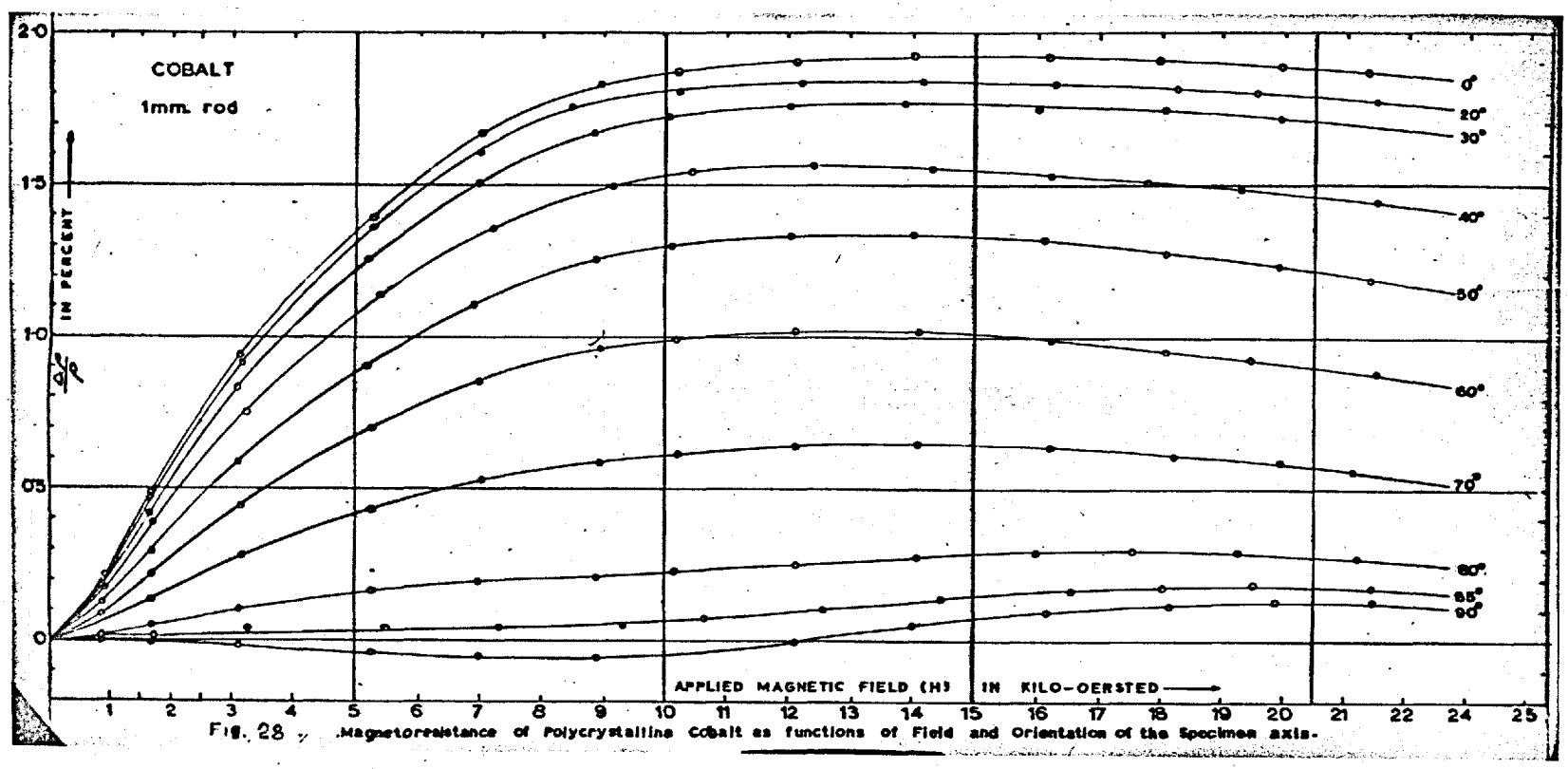

Fig. 28 :- Magnetoresistance of Polycrystalline Cobalt as functions of Field and Orientation of the Specimen axis.

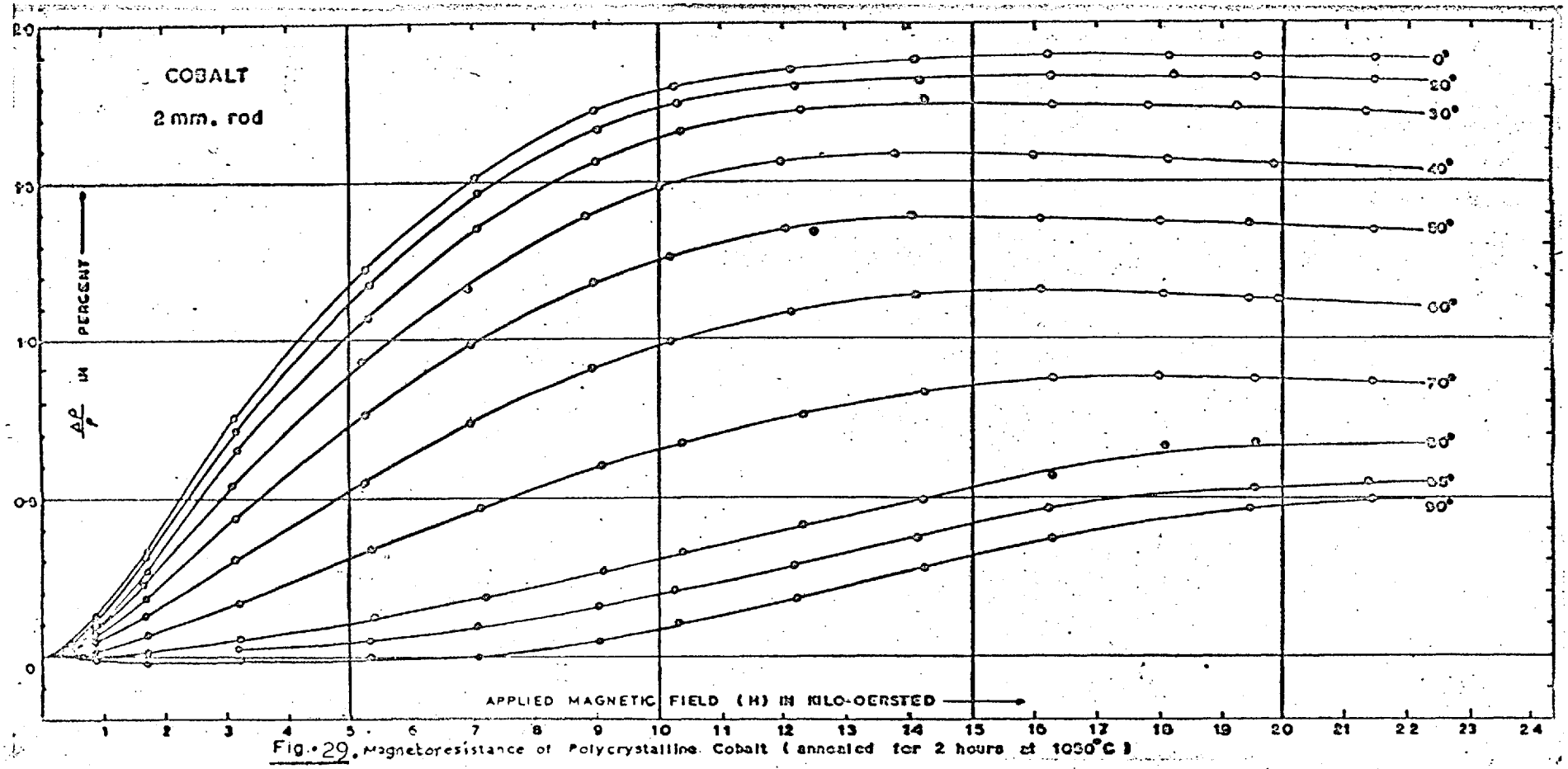

Fig. 29. Magnetoresistance of Polycrystalline Cobalt (annealed for 2 hours at 1050°C)

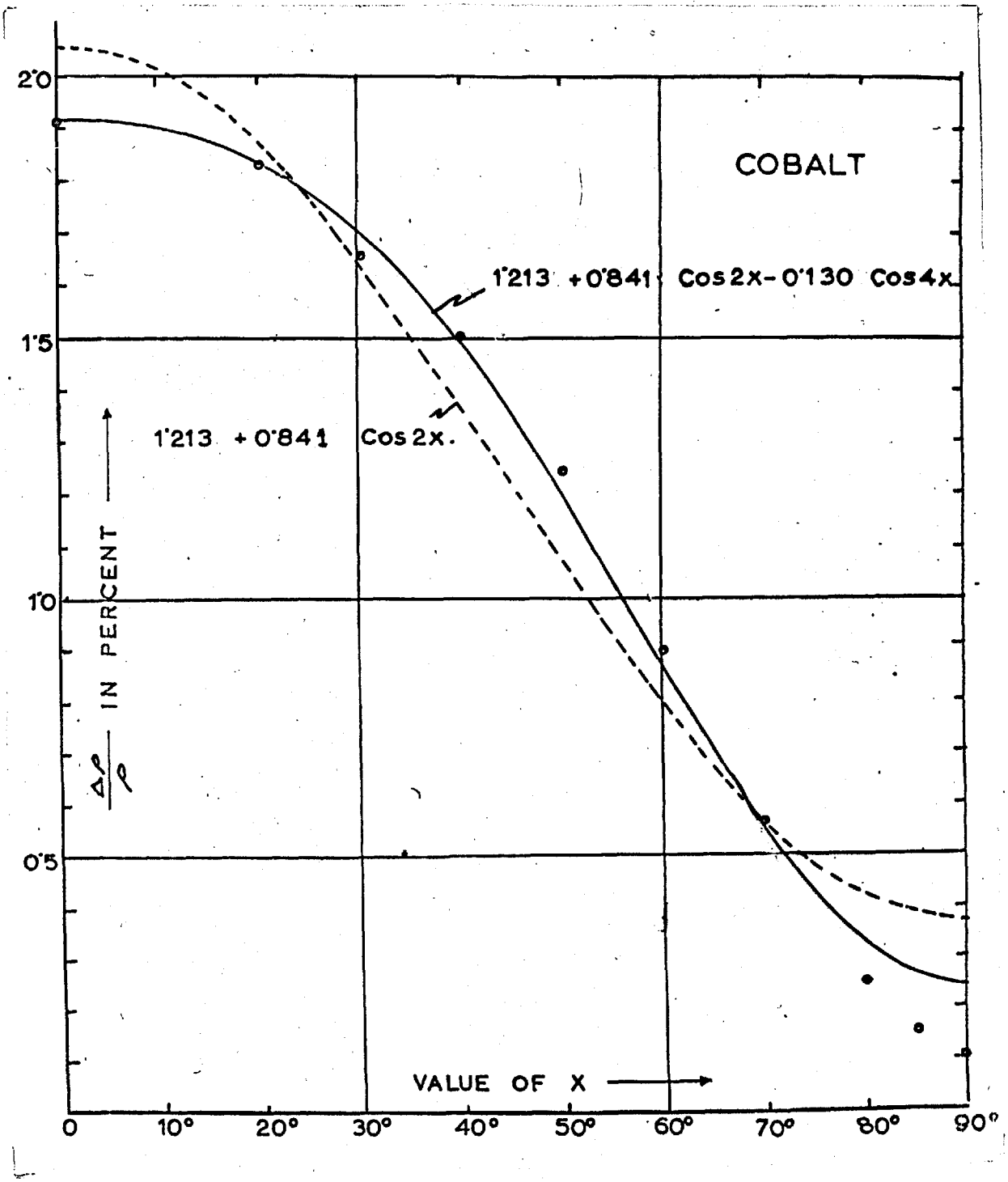

Fig. 30. Saturation magnetoresistivity of cobalt as a function of x (unannealed specimen).

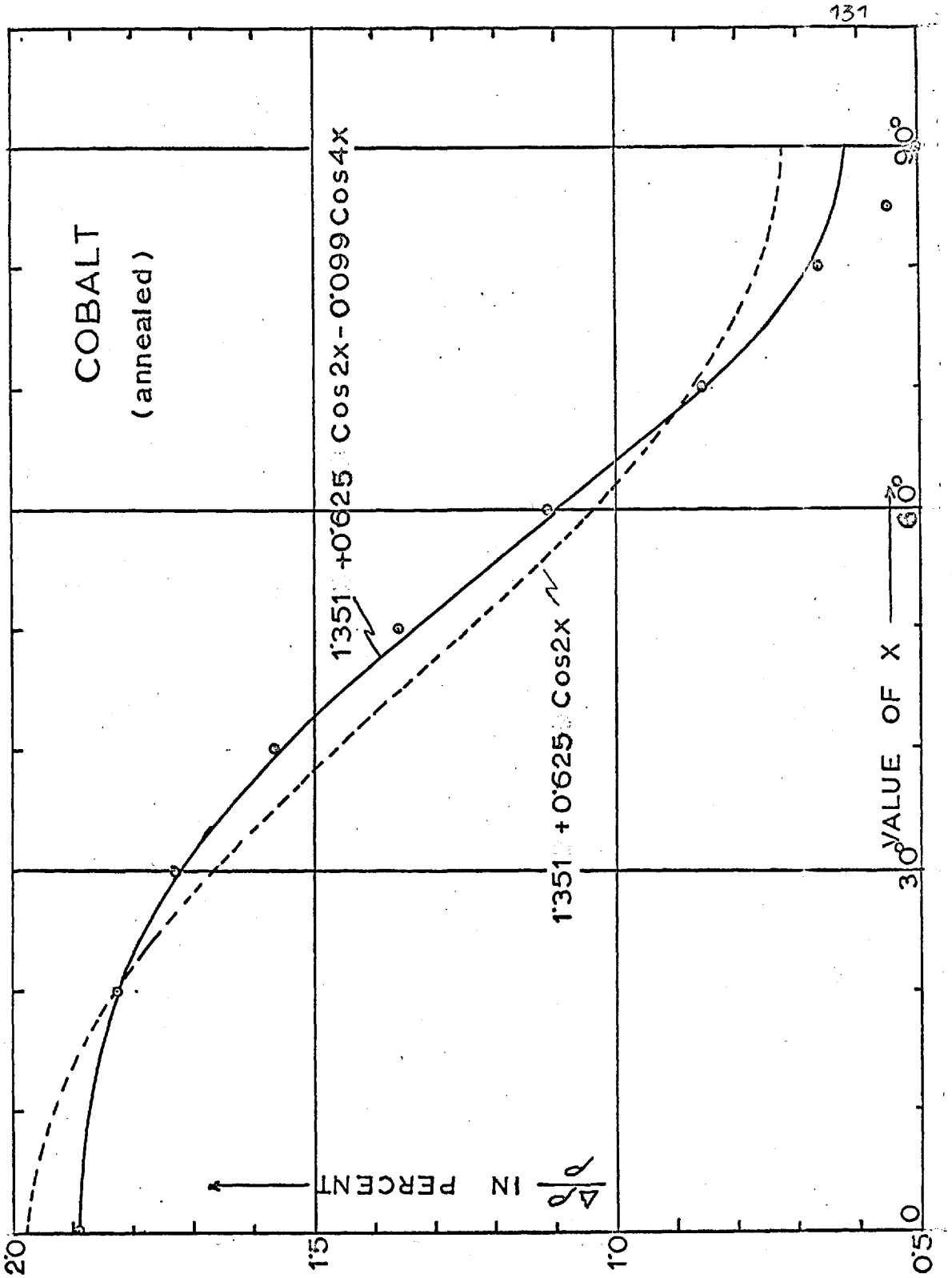

Fig.31. Saturation magnetoresistivity of annealed cobalt as a function of x .

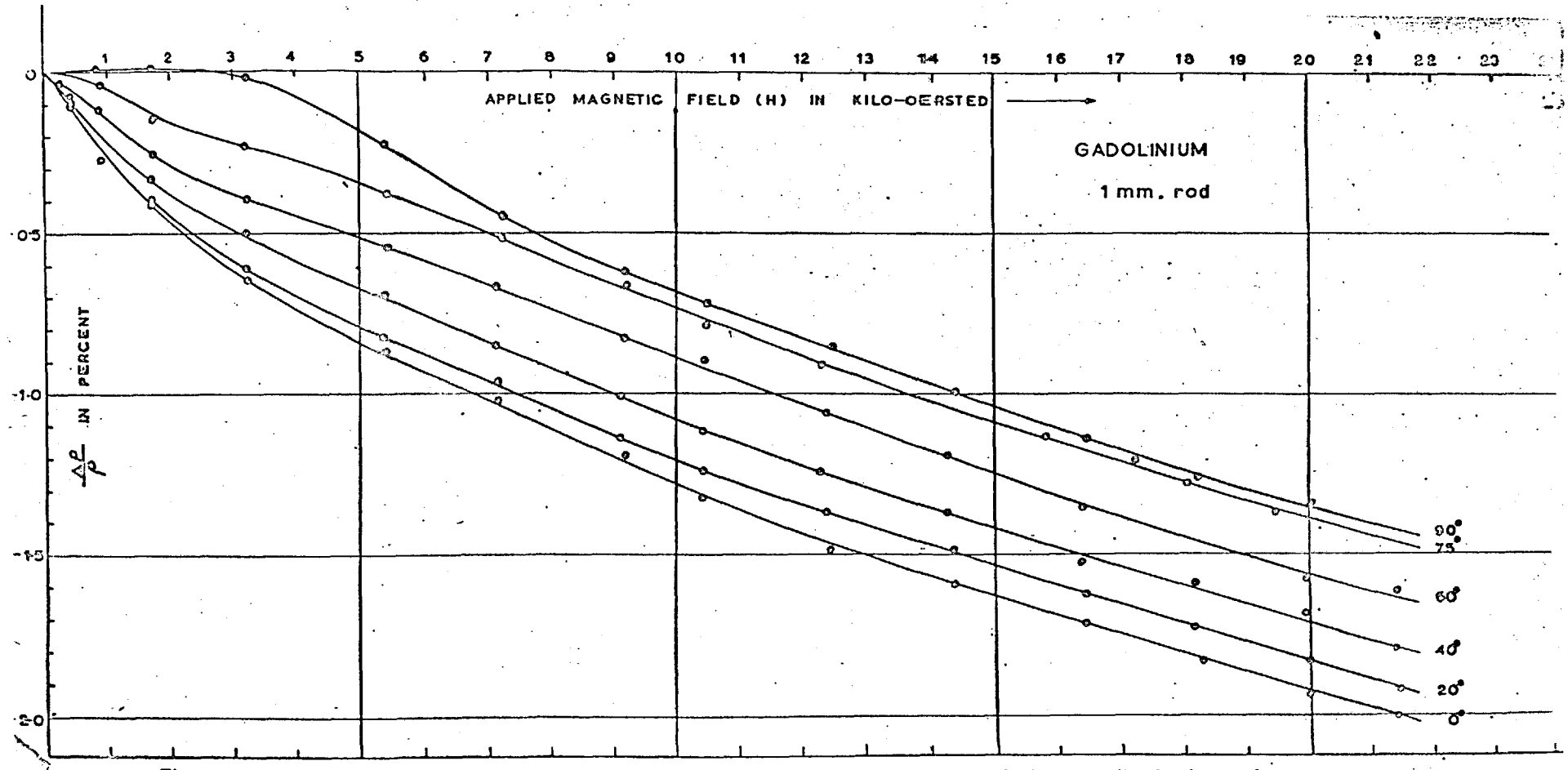

Fig. 32. Magnetoresistance of Polycrystalline Gadolinium as functions of Field and Orientation of the Specimen axis

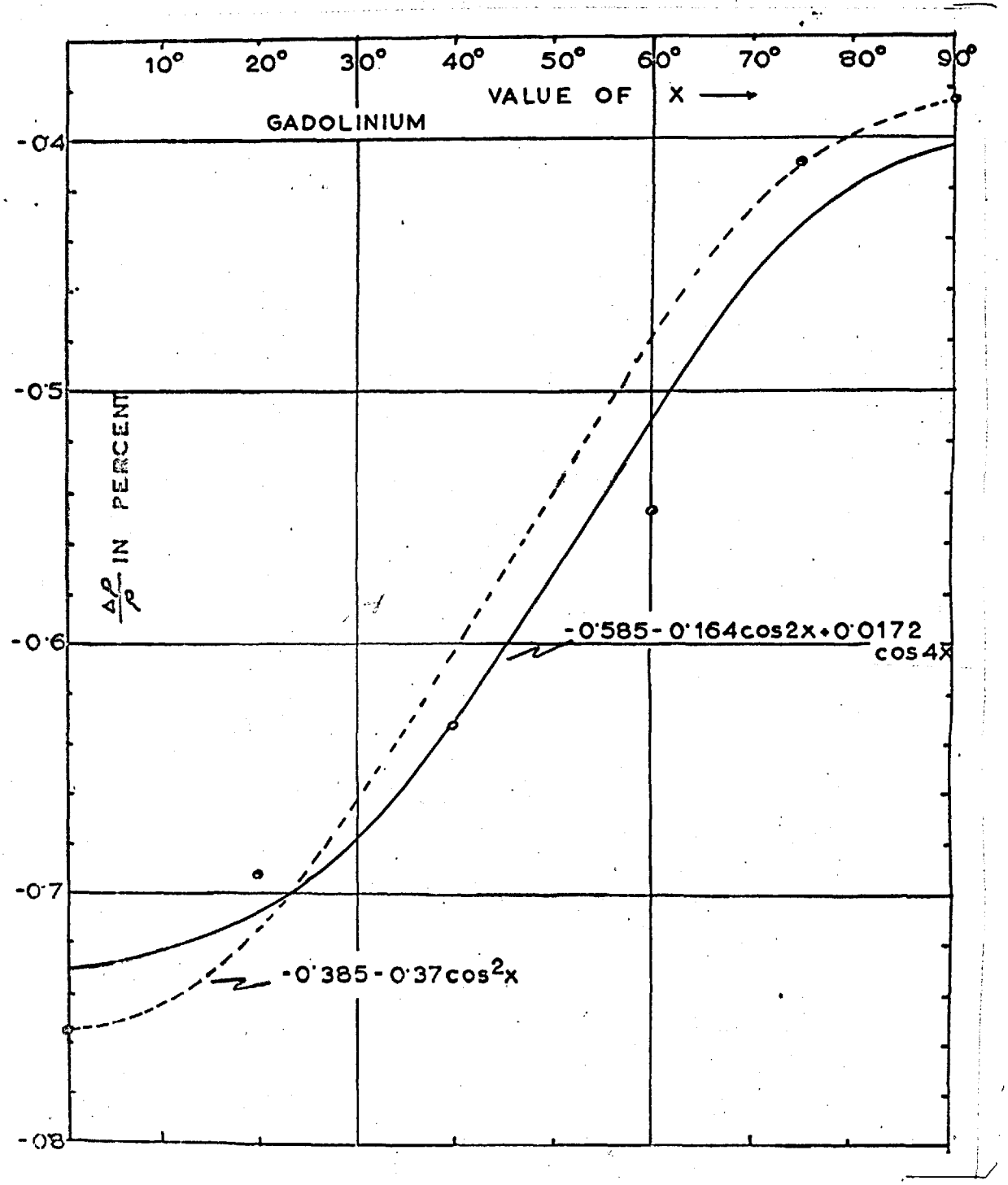

Fig. 33. Saturation magnetoresistivity of gadolinium at zero internal field plotted against the orientaion of the field relative to the specimen axis.

ing the same zero (equivalent) internal field assuming that the magnetization is uniform in all directions inside the specimen. The associated solid curves are derived after applying Fourier analysis to the experimental data to get the best fit. The values of the coefficients so obtained are then used in the final evaluation of the five magnetoresistance constants discussed in section 6.3.2.

5.2.3 Cobalt

In Figs. 28, 29 are given the results for the magnetoresistivity of polycrystalline cobalt before and after annealing to a temperature of 1050° C in vacuo and using two different specimens of diameters 1 mm and 2 mm respectively. In both cases a positive magnetoresistance in high fields is obtained even when the direction of measurement is transverse to the field. This behaviour is rather different from that shown in the earlier results of Bates[18] on many high-coercivity cobalt alloys which reveal negative magnetoresistance in most cases irrespective of whether the field is parallel or perpendicular to the direction of current. It may be seen that the annealing has little effect on the values of the magnetoresistivity.

Figs. 30, 31 give the magnetoresistivity versus angular parameter x of the field after correction for the demagnetizing field. The solid curve is obtained from the application of an analysis to be described in section 6.4.

5.2.4 Gadolinium

The magnetoresistivity curve for polycrystalline gadolinium is shown in Fig. 32 . It may be seen that the difference between the longitudinal and transverse effect is very much smaller than for cobalt or the other materials investigated, and that it is negative rather than positive. The results also indicate a greater field dependence than obtained hitherto. This is to be expected, as the forced effect, largely responsible for the increase of domain magnetization in high fields, is more important near the Curie temperature (T_c = 292° K) and as the present investigation was carried out at 273° K.

Fig. 33 gives the plot of magnetoresistivity values taken from Fig. 32 after correction for the demagnetizing fields. The solid curve, as before, is derived from the application of the Fourier analysis to these data. This is described in section 6.5.

CHAPTER VI

DISCUSSION OF THE RESULTS

6.1 Introduction

The isotropic 'forced' magnetoresistance above the region of technical saturation does not affect appreciably the values of the magnetoresistance coefficients since the rate of linear decrease with H ($=-\frac{\partial \xi}{\partial H}$) is small and is practically independent of the direction of magnetization. Since, however, a considerable influence is exerted by the geometry of the specimen, the range of field over which the linearity is observed can be quite small unless the field is taken to a very high value. The associated large demagnetizing field thus becomes an important factor in the final interpretation of the results particularly where the coefficients are to be determined by changing the direction of saturation magnetization. This is also important when attempting to estimate the value of P (2.12) in the polycrystalline magnetoresistance expression (see also sections 3.5.1 and 3.5.2) for cubic and hexagonal materials. In the preceding chapter, a procedure has been outlined for the derivation of the 'magnetometric' demagnetizing factor and of the internal field for the type of specimens used in the present investigations. The results so obtained on the basis of this calculation are now discussed under separate headings.

6.2 Iron

6.2.1 Polycrystal

The experimental results of the preceding chapter give the values (vide equation (2.13b))

$$\frac{\partial P}{\partial H} = - 4.18 \times 10^{-8}\ \mathrm{Oe}^{-1} ,$$

$$\frac{3}{2}\frac{\partial \bar{\xi}_s}{\partial H} = - 0.227 \times 10^{-8}\ \mathrm{Oe}^{-1} , \qquad (6.1)$$

assuming that the observed difference between the rates of change with H of $\bar{\xi}_{\parallel}(x = 0)$ and $\bar{\xi}_{\perp}(x = \pi/2)$ is attributable to the weak field dependence of the coefficient of the $\cos^2 x$ term in the expression for the spontaneous magnetoresistance of a polycrystalline material.

The value of this coefficient can, however, be determined by reference to the experimental results shown in Fig. 18 , which was obtained in the following manner. Inspection of the family of curves in Fig. 17 clearly shows that except for the longitudinal and transverse cases the graphs for the intermediate positions do not exhibit a true linear effect even at the maximum value of the applied field, but are still influenced by the geometry of the specimen. Consequently, a very large field is necessary in the case of iron if an accurate calculation of the magnetoresistivity coefficients is to be attempted. Subject to this limitation, however, the experimental data were taken from the graphs of Fig. 17 at a constant external field of 22,000 Oe. These values were then extrapolated back to zero internal field by using the demagnetizing

data for the various orientations of the specimen and the mean value for the rate of linear decrease of $\frac{\Delta\rho}{\rho}$ with H. The latter was obtained as the mean of the two values $\left(\frac{\Delta\rho}{\rho}\right)'_{\parallel}$ and $\left(\frac{\Delta\rho}{\rho}\right)'_{\perp}$. The open circles in Fig. 18 represent the final results obtained and substitution of these into the expression $P + Q \cos^2 x$ immediately gives

$$P = -0.00063, \qquad Q = 0.00411 . \tag{6.2}$$

The graph of this expression is given by the broken curve, which reveals only approximate agreement with the open circles. Fourier analysis was therefore carried out to get the best fit with the experimental points. This was attempted in the case of iron as in all the other materials. The theoretical curve is then given in the form

$$\frac{\overline{\Delta\rho}}{\rho} \times 100 = A + B \cos 2x + C \cos 4x + \ldots , \tag{6.3}$$

where the coefficients A, B, C have the values

$$A = 0.1801 ,$$

$$B = 0.1974 ,$$

$$C = -0.03467 . \tag{6.4}$$

The solid curve of Fig. 18 is given by equation (6.3) with the first three terms included while the dash and dot curve represents the graph that would be obtained if the third term were omitted. A comparison of the three curves with the experimental points clearly indicates that the magnetoresistive behaviour of polycrystalline iron is not adequately represented by retaining only the cos2x term in the series expansion. The value of C which is a measure of the coefficient of cos4x term is about 17% of that of B

and is of the opposite sign.

For iron, the five saturation magnetoresistance constants have been given as[34]

$$k_1 = 0.00153, \qquad k_2 = 0.00593 ,$$
$$k_3^{*} = 0.00194, \qquad k_4 = 0.00053 ,$$
$$k_5 = 0.00269 . \tag{6.5}$$

Substitution of these data in (3.59) and (3.60) gives the following values for P and Q

$$P = - 0.00114 , \qquad Q = 0.00458 , \tag{6.6}$$

so that

$$\frac{\overline{\xi_{\parallel}}}{\overline{\xi_{\perp}}} = \frac{P + Q}{P} = - 3.02 . \tag{6.7}$$

This may be compared with the theoretical value of -2 which is obtained by putting $k_3^{*} = 0$, in which case $P = - \frac{Q}{3}$ for cubic materials. The experimental value of Q given in (6.2) for the polycrystalline material now gives (with P =-0.00114 from (6.6))

$$\frac{\overline{\xi_{\parallel}}}{\overline{\xi_{\perp}}} = - 2.61 \tag{6.8}$$

Since any attempt to evaluate P involves reference to the initial demagnetized state, any comparison with the expression containing single crystal constants can be only approximate, and the agreement found for Q, on the basis of the present analysis, is quite satisfactory.

If the simplest two-constant expression for magnetoresistivity is considered (3.43), the polycrystalline saturation value in the longitudinal direction can be related to the corresponding single crystal values along the ⟨100⟩ and ⟨111⟩ directions by the expression

$$\left(\frac{\overline{\Delta\rho}}{\rho}\right)_s = \frac{2}{3}Q = \frac{2}{5}\left(\frac{\Delta\rho}{\rho}\right)_{100} + \frac{3}{5}\left(\frac{\Delta\rho}{\rho}\right)_{111} . \qquad (6.9)$$

In Table 4 , date for $\left(\frac{\Delta\rho}{\rho}\right)_{100}$ and $\left(\frac{\Delta\rho}{\rho}\right)_{111}$ are taken from Webster[3] and Shirakawa[4]. The relation (6.9) is compared with the results from the previous as well as the present measurements on polycrystalline iron. It will be seen that subject to the uncertainty of the initial demagnetized state, the agreement is generally poor, so that the magnetoresistance is not fairly represented by a two-constant equation in the case of iron.

6.3 Nickel

6.3.1 Polycrystal

Fig. 19 shows that the magnetoresistivity curves of nickel, unlike those of iron, decrease fairly linearly with field for all values of x from 0 to 90° in the region of the maximum field used and further that the forced effect is practically isotropic. The graph corresponding to that of Fig. 18 was therefore constructed by referring to Fig. 19 at a zero (equivalent) internal field corresponding to saturation. This is shown in Fig. 20. Application of Fourier analysis to the data of Fig.20 gives, as before, an expression of the form (6.3) in which the coefficients A, B and C are found to have the values

$$A = 0.56 ,$$

$$B = 1.141 ,$$

$$C = -0.0834 . \qquad (6.10)$$

TABLE 4

Comparison between the experimentally observed values of $(\frac{\bar{\Delta\rho}}{\rho})_s$ from polycrystalline measurements and those obtained from the relation $(\frac{\bar{\Delta\rho}}{\rho})_s = \frac{2}{5}(\frac{\Delta\rho}{\rho})_{100} + \frac{3}{5}(\frac{\Delta\rho}{\rho})_{111}$.

	$(\frac{\Delta\rho}{\rho})_{100}$	$(\frac{\Delta\rho}{\rho})_{111}$	Calculated $(\frac{\Delta\rho}{\rho})_s$	Ref.No.	Polycrystal $(\frac{\Delta\rho}{\rho})_s = \frac{2}{3}Q$	Ref.No.
Fe	0.05%	0.40%	0.260%	(3)	0.324%	(11)
	0.005%	0.48%	0.288%	(4)	0.281%	(4)
	-	-	-		0.348%	Present work
Ni	1.971%	2.424%	2.243%	(6)	2.155%	(6)
	-	-	-		1.756%	(11)
	-	-	-		1.63%	Present work

The broken curve in Fig. 20 represents equation (6.3) when only the first two terms are retained. Expressed in power series of cos 2x the corresponding values of the coefficients become

$$Q = 0.00228,$$
$$P = -0.0058. \qquad (6.11)$$

The solid curve is obtained as a result of the inclusion of the cos 4x term and gives a better fit with the open circles. It will thus be seen that the magnetoresistive behaviour of polycrystalline nickel, unlike that of iron, is closely represented by the two-term expression, although for an exact calculation it may be necessary to include the cos 4x term. The value of C which is a measure of the cos 4x term is about 8% of that of B and is of the opposite sign.

Table 4 further shows that the agreement between the experimentally observed value of $\left(\frac{\Delta\rho}{\rho}\right)_s$ for polycrystalline material and that obtained from (6.9) from measurements on single crystals is rather poor so that, for nickel, the two-constant equation (3.43b) depicting the magnetoresistivity should be regarded as only approximate. This is further confirmed by the fact that in nickel the value of k_3^{H} is definitely not zero (section 6.3.2).

In Table 6 are given the values of the five saturation magnetoresistance constants of nickel obtained from the present investigation. On substituting these data in equations (3.59) and (3.60), the values of P, Q and $\frac{P+Q}{P}$ are obtained. These are summarized in Table 5 along with the measured values of Q and of the ratio $\frac{P+Q}{P}$ for polycrystalline nickel. It is certain that the

TABLE 5

Values of the coefficients of the expression $(\frac{\overline{\Delta\rho}}{\rho}) = P + Q\cos^2 x$ as determined from measurements obtained from single crystal constants. For NICKEL.

Polycrystal		Single Crystal			
Ref. No.	Q	From equations (3.59) and (3.60)			$\frac{P+Q}{P}$
		Ref. No.	P	Q	
(25)	0.0305	(6')	-0.00757	0.0371	-3.9
		(7)	-0.00419	0.0254	-5.1
Present work	0.02285	Present work	-0.00207	0.0215	-9.3

ratio, $\frac{P+Q}{P}$, is nowhere near to -2 as predicted by the simplified theory, so that the neglect of the k_3^{*} term is not justified in representing the polycrystalline magnetoresistance of nickel.

6.3.2 Single crystal

The magnetoresistance at saturation is measured as the difference between the changes in resistivity when the crystal is magnetized to saturation in the fixed measuring direction $\langle 11\bar{2} \rangle$ and when saturated at right angles to that direction so as to be independent of the initial domain distributions. The two chosen planes of magnetization are the (111) and (110) planes corresponding to the two adjacent faces of the rectangular shaped crystal, as shown in Fig. 6 . The third setting is when the specimen axis and the plane of magnetization are perpendicular to each other, that is, the measuring direction is again $\langle 11\bar{2} \rangle$ but it is always transverse to the field.

It has been shown in Appendix I that the dependence of magnetoresistivity on the directions of the magnetization vector at saturation, when measured from the $\langle \bar{2}11 \rangle$ direction in the first two cases and from the $\langle 1\bar{1}1 \rangle$ direction in the third case, can be expressed in the following respective forms

$$\left(\frac{\Delta\rho}{\rho}\right)_{(111)\text{Plane}} = A_1 + B_1 \cos 2\eta + C_1 \cos 4\eta \ , \qquad (6.12)$$

$$\left(\frac{\Delta\rho}{\rho}\right)_{(0\bar{1}1)\text{Plane}} = A_2 + B_2 \cos 2\eta + C_2 \cos 4\eta + D_2 \sin 2\eta + E_2 \sin 4\eta \qquad (6.13)$$

and

$$\left(\frac{\Delta\rho}{\rho}\right)_{(\bar{2}11)\,\text{Plane}} = A_3 + B_3 \cos 2\theta + C_3 \cos 4\theta \ , \qquad (6.14)$$

where the constants A_i, B_i, C_i ($i = 1, 2, 3$) and D_2, E_2 are given in terms of the magnetoresistivity constants k_1 .. k_5 by the expressions within the brackets in relations (I.-3), (I.-6a) and (I.-10a) respectively.

In actual practice, the field was applied in various directions from 0 to 90° (in steps of about 10°) and the magnetoresistivity was measured in the fixed irection $\langle 11\bar{2} \rangle$. This enabled the constants B_i, C_i to be evaluated using standard Fourier analysis. It was not necessary to extrapolate the results back to zero internal field as the disposable constants A_i are not needed in the evaluation of the k's.

It may be noted that any one of the three B's, referred to above, is related to the other two by virtue of the fact that the cases $\theta = 90°$ ($\langle 110 \rangle$ direction) and $\theta = 0$ ($\langle 111 \rangle$ direction) in the third setting correspond to $\eta = 90°$ in the first two settings respectively. One is consequently redundant and there are only five independent equations connecting the five magnetoresistive constants.

The occurrence of the sine and cosine terms in equation (6.13) indicates that the expression can still be written down in terms of an even function of η, namely

$$f_{\text{even}}(\eta) = \tfrac{1}{2}\left\{f(\eta) + f(-\eta)\right\}$$
$$= A_2 + B_2 \cos 2\eta + C_2 \cos 4\eta \ , \qquad (6.15)$$

where $f_{\text{even}}(\eta)$ is the mean of the two values of the function for $\pm\eta$. Fourier analysis was, however, performed on the data taken from

TABLE 6

Comparison of the values of the five saturation magnetoresistance constants of nickel obtained from previous and present measurements.

	Döring[6] 1928	Döring[7] 1938	Present work
k_1	0.063	0.0654	0.0589
k_2	0.029	0.0266	0.0192
k_3	-0.036	-0.0320	-0.0382
k_4	-0.051	-0.0540	-0.0416
k_5	0.014	0.0200	0.00755

Fig. 22 and the numerical value for the coefficient of cos 4 η so obtained was used to represent C_2. The final five equations connecting the five saturation magnetoresistance constants with the numerical values of B_1, C_1, C_2, B_3, C_3 are thus

$$\frac{k_1}{6} + \frac{1}{3} k_2 + \frac{1}{9} k_4 + \frac{1}{18} k_5 = 0.01201,$$

$$\frac{1}{36} k_4 + \frac{1}{18} k_5 = - 0.0007358 ,$$

$$\frac{7}{96} k_3^{*} - \frac{7}{288} k_4 - \frac{1}{48} k_5 = - 0.001929 ,$$

$$\frac{k_1 - k_2}{12} + \frac{1}{24} k_3^{*} + \frac{1}{24} k_4 - \frac{1}{18} k_5 = - 0.0004359 ,$$

$$\frac{7}{96} k_3 + \frac{1}{32} k_4 - \frac{5}{144} k_5 = - 0.004345 . \qquad (6.16)$$

Solution of these five simultaneous equations gives the values shown in Table 6. The previous values obtained by Döring from his own measurements[7] and those taken by Kaya[6] are also given for comparison, the latter also being shown under Döring. It will be seen that the present values tend to be lower, and that k_3^{*}, the term usually neglected in magnetostriction, is definitely not small.

6.3.3 Forced Magnetoresistance

Referring to Fig. 4 , if the variation of $\frac{\Delta\rho}{\rho}$ with spontaneous magnetization in zero applied magnetic field ($Z = qI_s = \zeta$) is expressed as an arbitrary function of the product qI_s, thus

$$\frac{\Delta\rho}{\rho} = \frac{\rho_{IV} - \rho_I}{\rho_I} = f(qI_s) = f(\zeta) , \qquad (6.17)$$

then the forced magnetoresistance may be calculated as follows:

Replacing $f(qI_s)$ by $f(Z)$ since the forced magnetoresistance

only occurs when $X > 0$, one obtains

$$\overline{\rho\xi}' = \frac{\partial \overline{\rho\xi}}{\partial H} = \frac{1}{\rho_I} \frac{\partial \rho_{IV}}{\partial X} = \frac{\partial f(Z)}{\partial X}$$

$$= \frac{\partial f(Z)}{\partial Z} \frac{\partial Z}{\partial X}$$

$$= \frac{\partial f(Z)}{\partial Z} (1 + q\frac{dI}{dX}) \quad , \qquad (6.18)$$

where q is assumed to be independent of X and I is given by the relation

$$I = I_s - a_o/H - b_o/H^2 - \ldots + BH \quad ,$$

$$= I_s + BX \quad , \qquad (6.19)$$

in sufficiently high fields[59]. As stated earlier, the term BX is due to the increase in spontaneous magnetization caused by the increased alignment of spins in a domain in high fields. Equation (6.18) relates the forced magnetoresistance to the variation of resistivity with I_s and to the forced magnetization $\frac{dI}{dX} = B$.

For polycrystalline nickel, the values of B and of $\overline{\rho\xi}$ are known for a number of different temperatures near the Curie point, so that it is possible to test the validity of equation (6.18) over an extended temperature range provided that the term $\frac{\partial f(Z)}{\partial Z}$ is accurately known. The first step is to deduce the form of the function $f(qI_s)$ and this may be done by referring to the experimental and the 'normal', non-ferromagnetic curves for nickel as discussed in sections 2.2.1 and 2.2.3. The numerical values of $\overline{\rho\xi}$, so obtained[63], are plotted along with those of I_s^2 in Fig. 34 against temperature and it may be seen that for $X = 0$ the relation

$$(\overline{\rho\xi})_{X=0} = (A - C \times \frac{T}{T_c})\eta^2 \qquad (6.20)$$

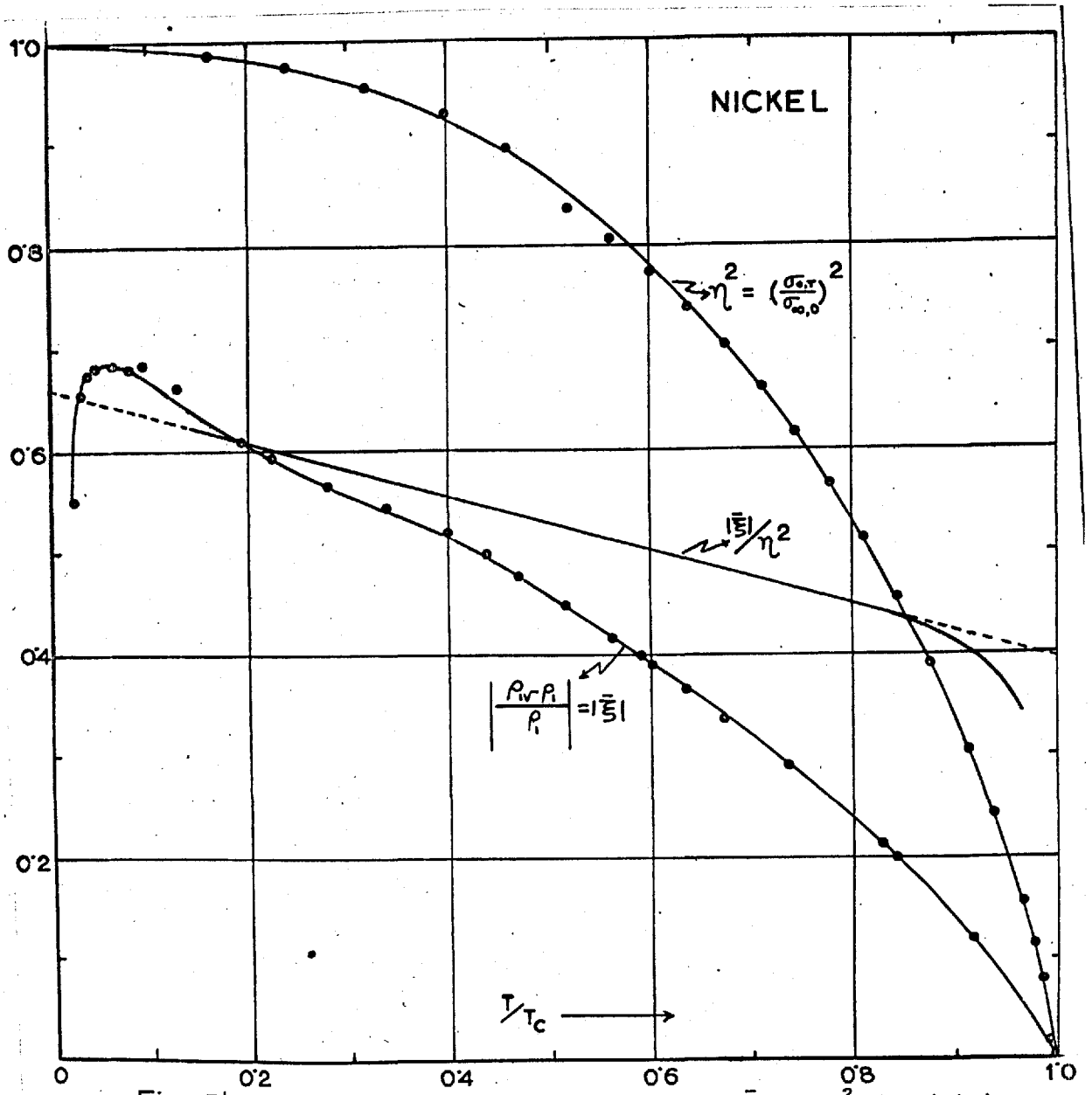

Fig. 34 . Graph showing relation between $\bar{\xi}$ and η^2 for nickel.

is closely followed over a large temperature range in which $\frac{T}{T_c}$ is the reduced temperature (T_c = Curie temperature) and η is the reduced magnetization (= $\frac{\sigma_{o,T}}{\sigma_{,O}}$). Equation (6.20) can be expressed in the form

$$\begin{aligned}(\bar{\bar{\xi}})_{X=0} &= (A_1 - C_1 T)\,\eta^2 \\ &= (A_2 - C_2 T)\,\sigma_{o,T}^2 \\ &= (R - UT)(qd\sigma_{o,T})^2 \end{aligned} \qquad (6.21)$$

where d = density,

$$U = \frac{C_2}{q^2d^2} = \frac{C_1}{q^2d^2\sigma_{\infty,O}^2} = \frac{1}{q^2d^2\sigma_{\infty,O}^2} \times \frac{C}{T_c}$$

and where (qd) is taken to be substantially independent of temperature over this range[94].

The application of an external magnetic field in addition to the Weiss molecular field has the effect of slightly increasing the magnetization and consequently producing a further drop in the anomalous resistivity below the Curie point (cf. $\frac{\partial P}{\partial X}$ in equation (2.17)). The contribution to $\bar{\bar{\xi}}$ arising from the second factor for any given H and T is generally small compared to that from the first except at temperatures approaching the Curie point, where X becomes comparable to and even greater than (qI_s) and where the intrinsic magnetization is most strongly affected by the applied field.

Thus, in so far as it can be assumed that the introduction of X in equation (6.21) in addition to qI_s does not significantly alter the form of the function f(Z), it is still possible to write

$$\left(\frac{\bar{\xi}}{\rho}\right)_Z = f(Z) = (R - UT)\, Z^2 \ . \qquad (6.22)$$

Hence,

$$\frac{\partial f(Z)}{\partial Z} = 2Z\,(R - UT) - UZ^2 \frac{\partial T}{\partial Z}$$

$$= \frac{2}{(qI_s)^2}\, Z \left(\frac{\bar{\xi}}{\rho}\right)_{X=0} - UZ^2 \frac{\partial T}{\partial \zeta} \frac{\partial \zeta}{\partial Z}$$

$$= \frac{2}{(qI_s)} \left(\frac{\bar{\xi}}{\rho}\right)_{X=0} - \frac{C_1 \eta^2}{qd \dfrac{\partial \sigma_{o,T}}{\partial T}} \qquad \text{if } X \ll qI_s \ . \qquad (6.23)$$

From equation (6.18)

$$\frac{\bar{\xi}'}{\rho} = \frac{2}{I_s} \left\{ \left(\frac{\bar{\xi}}{\rho}\right)_{X=0} - \frac{C_1 \eta^2}{d \dfrac{\partial \sigma_{o,T}}{\partial T}} \left(\frac{1}{q} + \frac{dI}{dX}\right) \right\} . \qquad (6.24)$$

Experimentally, a measurement can be made of the dependence of forced magnetoresistance on field, and the slope of this curve is

$$S = \frac{1}{\rho_{IV}} \frac{\partial \rho_{IV}}{\partial X} = \frac{\rho_I}{\rho_{IV}} \frac{\bar{\xi}'}{\rho}$$

giving

$$S = \left\{ \frac{2}{I_s} \frac{\rho_{IV} - \rho_I}{\rho_{IV}} - \frac{\rho_I}{\rho_{IV}} \frac{C_1 \eta^2}{d \dfrac{\partial \sigma_{o,T}}{\partial T}} \right\} \left(\frac{1}{q} + \frac{dI}{dX}\right) \ . \qquad (6.25)$$

An attempt has been made to evaluate q from the above relation using the present data on magnetoresistance and electrical resistance of nickel. Thus, taking

$$1 + \frac{\bar{\xi}}{\rho} = \frac{\rho_{IV}}{\rho_I} = 0.5031 \text{ at } 273^\circ \text{ K}; \quad C_1 = 4.2063 \times 10^{-4};$$

$$\frac{\partial \sigma_{o,T}}{\partial T} = -\,0.0275 \text{ deg}^{-1}; \quad \frac{dI}{dX}^{(95)} = 1.2067 \times 10^{-4} \text{ Oe}^{-1} \ (95)$$

$d = 8.89$ gm/cc at 273° K; $\eta = 0.947$, and $S = -\,1.69 \times 10^{-7} \text{Oe}^{-1}$,

the value of q is found to be 17,182. The equation, however, leads

to a negative value for q at two higher temperatures, 476° K and 551° K, at which the forced magnetoresistance has been previously measured[9]. Although this anomaly could be due to inaccuracies in the estimated values of S (which obtained by using a comparatively low field of 7000 Oe), it is more probable that the form of the function f(Z) ceases to be correctly represented by the equation (6.22) at these temperatures. It is reasonable to believe that the slope of the $f(Z)/Z^2$ versus T graph increases more rapidly than that given by (6.22). Similarly, equation (6.25) is also not expected to give reliable value for q from low temperature measurements.

Taking $J = \frac{1}{2}$, which gives the best theoretical fit with the experimental curve for the variation of spontaneous magnetization with temperature below the Curie point, T_c, the value of q, as calculated from the equation

$$T_c = \frac{(J + 1)\, g\mu_B q I_{so}}{3k}$$

is 18,500[60]. The present magnetoresistance measurements thus give an appropriate value for the Weiss molecular field constant.

6.4 Cobalt

The theory of domain magnetization requires that $(\frac{\overline{\Delta\rho}}{\rho})_{\parallel}$ and $(\frac{\overline{\Delta\rho}}{\rho})_{\perp}$ extrapolated to zero effective field from measurements made in strong fields should have opposite sign. Bate's measurements[18] on many high-coercivity cobalt alloys, however, give negative magnetoresistance irrespective of whether the field is parallel or perpendicular to the direction of the current. The

present measurements, on the other hand, give mostly positive values for all orientations of the field from 0 to 90°. The use of two specimens, 1 mm and 2 mm in diameter, yielded the same results and the main features of the curves were retained when the latter specimen was thoroughly annealed at 1050° C for two hours in vacuo.

The open circles shown in Fig. 30 represent the values of $(\frac{\overline{\Delta\rho}}{\rho})$ for the non-annealed specimen as taken from Fig. 28 at a constant internal field of 14,000 Oe. In view of the very limited range over which the experimental curves of Fig. 28 exhibited linearity, any attempt to extrapolate the resistivity values back to zero internal field was thought to be rather unrewarding. The lack of saturation is seen to be more pronounced with increasing values of x because of the high demagnetizing field operating in this region. For this reason, the last few experimental points in Fig. 30 were considered to be somewhat unreliable and a curve fitting was attempted only for the range 0 - 70°. The associated solid curve is given by the equation

$$(\frac{\overline{\Delta\rho}}{\rho}) \times 100 = A + B \cos 2x + \cos 4x , \qquad (6.26)$$

where $A = 1.213$

$B = 0.841$

$C = -0.130$.

As is seen, this gives a good fit with the experimental points over the range considered.

Fig. 31 shows the results for the annealed specimen and the corresponding effects are found to be somewhat smaller. The

solid curve is again represented by equation (6.26) where the values of the coefficients are now

$$A = 1.351$$

$$B = 0.625$$

$$C = 0.099$$

and give a good agreement with the experimental points except for $x \sim 90^{\circ}$. The associated dotted curves in Figs. 30 and 31 are obtained when only the first two terms of (6.26) are retained. The annealing process has slightly narrowed the gap between the solid curve and the values of $(\frac{\overline{\Delta\rho}}{\rho})$ in the region $x \sim 90^{\circ}$. The value of Q as determined on the basis of the simple expression $P + Q \cos^2 x$ is thus found to be 0.0125 for the case of the annealed specimen. At present, there are no measurements available of the constants of equation (3.66c) so that this value cannot be directly compared with the theory.

6.5 Gadolinium

The magnetic behaviour associated with the exchange interaction effect between conduction electrons and unpaired electrons localized on particular atoms in a crystal is most significant in the rare-earth metals, like gadolinium. Here the 4f electron shell is incomplete, and near the Curie temperature it is further shielded by the outer shells from the influence of the neighbouring atoms. Thus the randomly oriented spins can appreciably scatter the conduction electrons giving rise to an additional term in the resistivity expression. Applying Matthiessen's rule[96], the total resist-

ivity may be written as

$$\rho_T = \rho_{\text{ideal lattice}} + \rho_{\text{impurity}} + \rho_{\text{spin-disorder}}. \quad (6.27)$$

The extra resistance due to spin-disorder scattering may be expected to decrease markedly upon some kind of ordering of the spins and thus to cause a resistivity anomaly below the Curie temperature as discussed in section 2.2.2. However, above the Curie temperature $\rho_{\text{spin-disorder}}$ should be temperature independent and can be evaluated from the rest. Earlier measurements on the electrical resistivity of gadolinium[63] show little dependence on temperature above the Curie point and hence support the mechanism of spin-disorder scattering.

Cadolinium, which is ferromagnetic below 290° K, has a close-packed hexagonal structure (c/a ranging from 1.59 at 370° K to 1.599 at 130° K, which is not far from ideal close packing c/a = 1.633[97]) and a magnetic moment corresponding to $7.5\mu_B$ per atom at the absolute zero. The susceptibility follows closely the Curie-Weiss law at high temperatures, while at lower temperatures definite magnetic ordering effects have been observed[98].

Magnetostriction measurements on both polycrystals and single-crystals by various workers[99,101-103] indicate a linear 'forced' variation with field at temperatures well into the ferromagnetic region, a normal square law dependence at temperatures well above the Curie point and a two-third power law variation near the Curie temperature. Assuming a field-independent susceptibility above the Curie point, the relation between volume magnetostriction

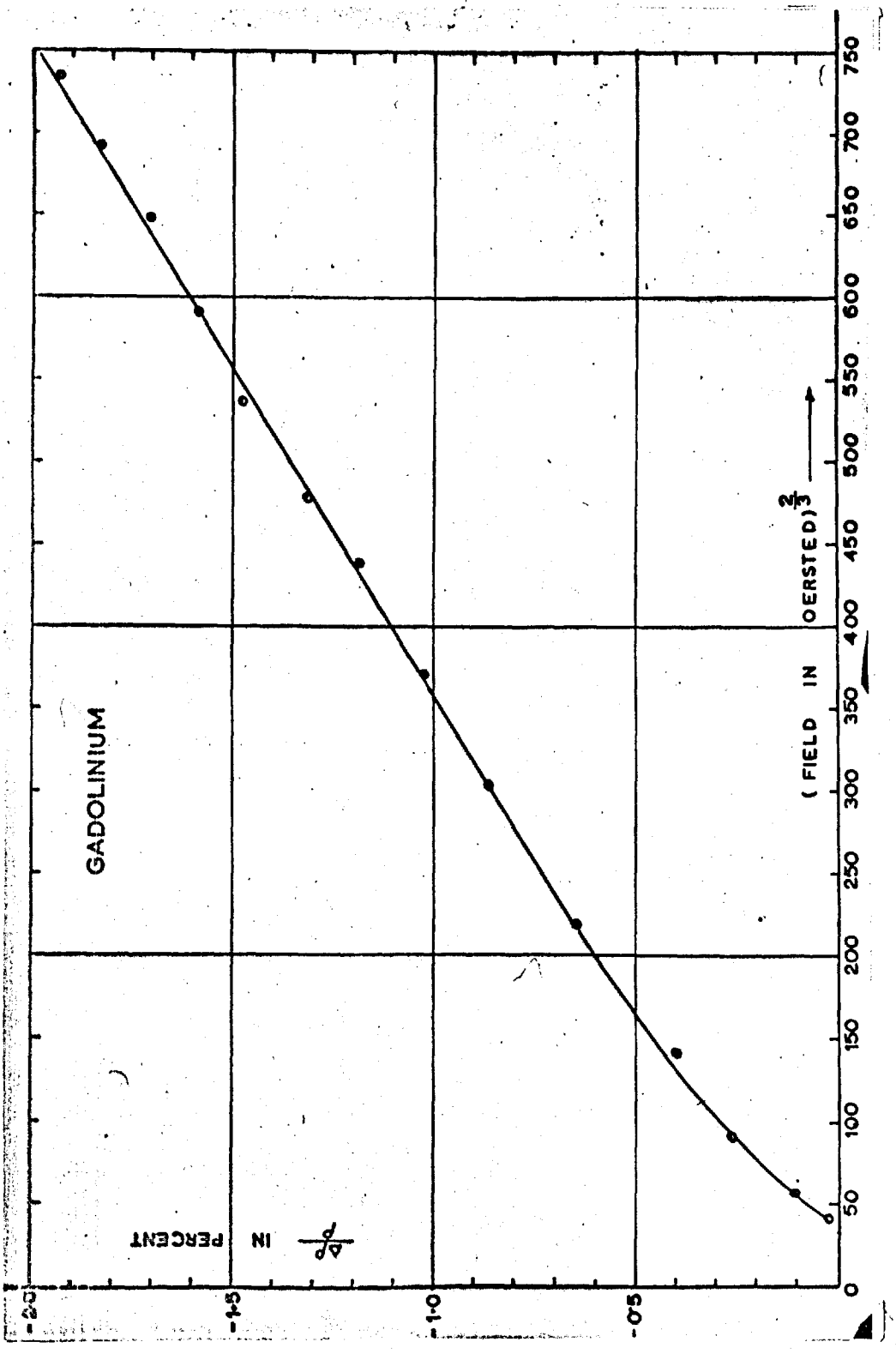

Fig. 35. Magnetoresistivity of gadolinium plotted against two-third power of the magnetic field. The graph shows a linear variation near the Curie temperature.

and the magnetic field can be immediately derived from the thermodynamic relation connecting the pressure dependence of magnetization to magnetostriction, thus

$$\left(\frac{\partial \omega}{\partial H}\right)_{P,T} = -\left(\frac{\partial I}{\partial P}\right)_{H,T} , \qquad (6.28)$$

where $\omega = \frac{\Delta V}{V}$. With $I = \chi H$ where χ is a constant, equation (6.28) gives on integration

$$\frac{\Delta V}{V} = \frac{1}{2}\left(-\frac{\partial \chi}{\partial P}\right) H^2 . \qquad (6.29)$$

Belov's theory[100] on the other hand indicates that near the Curie temperature, the magnetization and the magnetostriction are given by

$$A + B\sigma^2 = H/\sigma \qquad \text{and} \qquad \lambda = \text{const} \times \sigma^2 , \qquad (6.30)$$

where σ = magnetization per gm. and $\lambda = \delta l/l$. This means that an $H^{2/3}$ dependence of λ is expected. The measurement of the temperature dependence of the magnetoresistivity[21] indicates a similar H^2 variation at temperatures above 346° K. Since the susceptibility at these temperatures is field independent, this means that

$$\frac{\Delta \rho}{\rho} \propto \chi^2 H^2 \propto \sigma^2 , \qquad (6.31)$$

implying a square law relation between the magnetization and magnetoresistance. The present investigations give a large 'forced' magnetoresistance effect, being near the Curie temperature, and the negative slope is found to be substantially isotropic for all orientations of the field as can be seen from the following values

$$\left(\frac{\partial \frac{\Delta\rho}{\rho}}{\partial H}\right)_{\parallel} = -5.79 \times 10^{-7}\ \text{Oe}^{-1}$$

$$\left(\frac{\partial \frac{\Delta\rho}{\rho}}{\partial H}\right)_{\perp} = -5.96 \times 10^{-7}\ \text{Oe}^{-1} .$$

Unlike all previous cases, the difference $\left(\frac{\Delta\rho_{\parallel} - \Delta\rho_{\perp}}{\rho}\right)$ is found to be negative which is one of the most important features in the present investigation. Such behaviour has been reported by Bates[18] in his measurements of magnetoresistance on cast alnico, but for a different reason. In the present case a longitudinal field might induce a greater ordering of the spins near the Curie temperature and the shape-anisotropy of the specimen may also be important.

In Fig. 33 are given the values of $\frac{\Delta\rho}{\rho}$ as taken from Fig. 32 after correcting for the demagnetizing field so as to correspond to the saturation magnetic state at zero internal field. The dotted curve is obtained by the direct evaluation of the values of P and Q from the data of $\left(\frac{\overline{\Delta\rho}}{\rho}\right)_{\parallel}$ and $\left(\frac{\overline{\Delta\rho}}{\rho}\right)_{\perp}$ without attempting a Fourier analysis. The solid curve results from Fourier analysis in which the cos 4 x term is included and the value of the coefficient of this term is found to be about 10% of that of the cos 2 x term and is of the opposite sign. In view of the enlarged scale of the $\frac{\overline{\Delta\rho}}{\rho}$ axis, the difference between the solid curve and the magnetoresistivity value at $x = 90^{\circ}$ corresponds to about 4%. This difference can be explained by the fact that near the Curie temperature the magnetic field has a pronounced ordering effect on the randomly oriented spins, and that a more rigorous calculation of the demagnetizing field therefore becomes necessary in order that the values of $\frac{\overline{\Delta\rho}}{\rho}$ under consideration should conform to the same magnetic state of the material. It is also felt that a still higher field is desirable to get the true saturation effect.

The dependence of magnetoresistance on field at this temperature (273° K) is found to be more near to $H^{2/3}$ than to H. This is depicted in Fig. 35 in which the relationship between $(\frac{\Delta\rho}{\rho})_{11}$ and $H^{2/3}$ is seen to be almost linear above the low field region up to the maximum value of the field used. In this respect, and in relation to the earlier finding of an H^2 variation at high temperatures, the magnetoresistivity of gadolinium has been found to follow the corresponding magnetostriction behaviour rather closely.

PART II

C H A P T E R V I I

INTRODUCTION

7.1 Summary

The subject of exchange interactions in magnetic materials has been extensively investigated since the first introduction of the theory and concept of 'ferrimagnetism' in 1948 by Néel[1] to describe the magnetic properties of a group of developing, technically important, ferromagnetic oxide materials - the ferrites. The subject was further stimulated by the appearance of neutron diffraction as a powerful means for observing magnetic order in ferro-, ferri- and particularly antiferromagnetic materials[2,3,4] and by the development, lately, of the Mössbauer technique[5,6] as an additional experimental tool in such investigations.

According to Néel, the simplest ferrimagnetic material is composed of two inter-penetrating sublattices and with interactions only between nearest neighbours (n.n.). A sublattice is defined, in such a case, as constituting all the magnetic ions of a given kind on a given type of site, and these ions are all grouped together as a single magnetic unit in the description of their magnetic behaviour The negative exchange interaction between the two sublattices causes their spins to align in an antiparallel manner resulting in a net

magnetic moment equal to the difference between the two individual sublattice magnetizations. If, however, the two moments are equal, the net magnetization is zero giving rise to what is called 'antiferromagnetism', a state which was earlier postulated by Néel[7] and Van Vleck[8]. Antiferromagnetism may therefore be regarded as a special case of balanced ferrimagnetism. Landau[9] first stressed the phenomenological similarity of ferro- and antiferromagnetism in respect of spin ordering below the thermal transition point and suggested the existence of the Néel point analogous to the Curie temperature.

The theoretical model of antiferromagnetism or ferrimagnetism is such as to give a detailed account of the ordering of the spin moments and how the degree of order changes with temperature and the effect this has on the magnetic and thermal properties such as susceptibility, magnetic anisotropy, specific heat and changes in lattice parameter with temperature. In view of the importance of the molecular field theory of antiferromagnetism as the groundwork for all subsequent developments, a brief account is included in Chapter VIII starting with a generalization of the Weiss theory of ferromagnetism.

Since Néel's original hypothesis, the term ferrimagnetism has been extended to include materials with more than two sublattices and those with triangular, spiral or canted spin arrangements. In the Néel model[7], there is no allowance for any crystalline anisotropy. Van Vleck[8] postulated the presence of some kind

of anisotropy forces whose magnitude, however, was just sufficient to keep the axis of the antiferromagnetism along this direction but was negligibly small in comparison with the strong exchange couplings. Nagamiya[10] and Yosida[11] have explicitly introduced an anisotropy energy term in their theory to explain the discrepancy between the theoretical predictions and the experimental results.

Néel in his original treatment also showed how the existence of next nearest neighbour (n.n.n.) interactions would partly account for the difference observed in many cases between the Néel temperature and the asymptotic Curie temperature which is obtained from the extrapolation of the Curie-Weiss law. More recent studies of the effect of n.n.n. interactions made by Van Vleck[12], Street[13], Smart[14] and Anderson[15] reveal that the type of order which sets in below the Néel point is primarily determined by the n.n.n. interactions if the latter is predominant over the n.n. interactions.

While it is reasonable to anticipate that the molecular field in antiferromagnetism or in ferrimagnetism has the same basic origin as in ferromagnetism, that is, in a quantum mechanical exchange interaction, a consideration of the magnitude of the spin aligning forces in many compounds (e.g. MnO and MnS) leads to the conclusion that the interaction is not of a simple direct exchange type. For instance, in most ferrites, the cations are separated by much larger distances than those necessary, on the bases of Slater-Bethe curve[16], to account for the observed degree of couplings between adjacent spins. It must therefore be concluded that the

exchange interactions occur indirectly via non-magnetic oxygen ions. This mechanism, now called super-exchange, was first introduced by Kramers[17] in an attempt to account for the results of adiabatic demagnetization which indicated that small exchange couplings existed even between ions separated by one or several diamagnetic groups. The theory has since been developed further by Anderson[15] and Van Vleck[12]. Another mechanism in which the oxygen ion plays an important role is the double-exchange proposed by Zener[18] to account for the interaction between adjacent parallel spins via an oxygen intermediary. Zener's theory, therefore, does not explain the negative interaction in ferrites but may be a contributing factor to the observed ferromagnetic (positive) interactions in certain manganites and cobaltites. A somewhat different indirect exchange interaction (negative) has been proposed by Goodenough[19] to account for the partial covalent or homopolar bonding between cation and anion in spinel-like structures and is called the semi-covalent exchange interaction.

A description of several important crystal structures in non-metals which illustrate many significant features of magnetism is given by Goodenough[20]. The most important of these, from the point of view of antiferromagnetism, may be summarized as: the rocksalt (e.g. MnO, NiO, FeO, CoO) and zinc-blende (e.g. chalcopyrite $CuFeS_2$) type of lattices in the cubic crystal structure, corundum

type (e.g. Cr_2O_3, α-Fe_2O_3) in the rhombohedral structure, rutile type (e.g. MnF_2, FeF_2, CoF_2, NiF_2, MnO_2) in the tetragonal structure, and the $CdCl_2$ (e.g. $FeCl_2$, $CoCl_2$, $NiCl_2$) and NiAs (e.g. CrSb, MnAs, MnBi) types in the hexagonal structure. Ferrimagnetism, on the other hand, has been widely studied in oxides and compounds having crystal structures of spinel (e.g. ferrites with general formula $MOFe_2O_3$), and garnets (e.g. compounds with general formula $2R_3X_2(ZO_4)_3$ where R is usually a large ion such as calcium, yttrium or a rare-earth, and X and Z are transition elements), hematite-ilmenite, mineral magnetoplumbite (e.g. M type compound with general formula $MO.6Fe_2O_3$ where M represents a large divalent ion such as Ba^{2+}, Sr^{2+}, Pb^{2+}), in NiAs-type compounds and finally in perovskite-type oxides (e.g. of general formula $MFeO_3$ where M is a large metal ion such as La^{3+}, Ba^{2+} or Sr^{2+}).

The discovery of the fact that some antiferromagnetic materials also exhibit weak ferromagnetism (the historical example is α-Fe_2O_3) set a new trend in the development of the antiferromagnetic theory and eventually led to the concept of the canted spin mechanism. According to this theory, first proposed by Dzialoshinsky[21] and later supported by Moriya[22], the magnetic moments of the antiferromagnetic sublattices are not exactly antiparallel but are turned towards each other resulting in a net moment which is perpendicular to the antiferromagnetic axis. However, a canted spin arrangement is possible only if the magnetic crystal symmetry is the same as that when the spins are antiparallel. For α-Fe_2O_3, Dzialoshinsky showed

that this condition is satisfied when the moments lie in the basal (111) plane above the Morin transition[23] at about 250° K, and is not satisfied when the spin orientation is along the ternary [111] axis below this transition. Lin[24] suggested that Dzialoshinsky's idea could be extended by assuming a general model of a canted antiferromagnetism with unequal sublattice moments but there is yet no general acceptance of this. Quite apart from this phenomenological approach, two mechanisms were suggested by Moriya to explain the origin of the canting of the spins, which are different in materials like NiF_2[25] and in materials like α-Fe_2O_3 or the orthoferrites[26]. The first requires the presence in the crystal of two non-equivalent sites for the interacting magnetic ions. The crystalline field acting on the ions in the two sites is then different and hence the magnetocrystalline easy direction of magnetization is different for the non-equivalent ions, energetically favouring spin canting. The second mechanism invokes the combined effects of the spin-orbit and the super-exchange interaction phenomena and leads to a term in the anti-symmetric exchange interaction of the form $\underline{D}_{ij} \cdot \underline{S}_i \times \underline{S}_j$. This term tends to align the two interacting spins $\underline{S}_i$ and $\underline{S}_j$ perpendicular to each other and perpendicular to the constant vector $\underline{D}_{ij}$. For α-Fe_2O_3, $\underline{D}$ lies along the ternary [111] direction. Other antiferromagnetic materials exhibiting weak ferromagnetism include $MnCO_3$[27], $CoCO_3$[27], $KMnF_3$[28] and CrF_3[29].

The problem of canted spin in ferrimagnetism has been dis-

cussed by Dwight and Menyuk[30] in their study of the magnetic properties of single-crystal samples of hausmannite Mn_3O_4 which is known to become ferrimagnetic at about 42° K. Compounds of mixed cadmium manganites, which have the general formula $(Cd_x^{2+} Mn_{1-x}^{2+})Mn_2^{3+}O_4$ and are isomorphous with Mn_3O_4, are the materials which have been studied in the present investigations. In addition to these, the antiferromagnetic behaviour of the ordered and disordered phases of lithium ferrite, $LiFeO_2$, has also been studied. Both types of materials were in the form of crushed single-crystal powder. The present investigations have led to some new and interesting results which are included in the discussion. In particular, the generally complex susceptibility curves of the manganite compounds, all of which have a tetragonally distorted spinel-like structure, call for a detailed account of some of the more advanced theories of ferrimagnetism and of the possibility of the simultaneous existence of ferro- or ferrimagnetic and antiferromagnetic phases. For example, as first observed in the Co-CoO system[31], the rotational hysteresis or the shifted hysteresis loop is now believed to be the result of the exchange interaction that acts across the interface between the antiferromagnetic and ferromagnetic single-domain particles. Interfacial exchange interactions have also been found to be present in antiferromagnetic-ferromagnetic and ferrimagnetic-ferromagnetic systems[32].

As stated earlier, one of the most important groups of ferrimagnetic materials is the ferrite by which is understood materials of the composition MFe_2O_4, where M is a divalent metal ion

and Fe is a trivalent ferric ion. These materials form the spinel structure in which the oxygen ions are much the largest, occupying most of the volume, and in themselves form a close-packed cubic array. The cation sites are of two kinds, called respectively tetrahedral, or A, sites each of which is surrounded by four oxygen ions and octahedral, or B, sites each of which is co-ordinated by six oxygen ions. A unit cell consists of eight formula units; of the 64 tetrahedral sites, 8 are occupied, while of the 32 octahedral sites, 16 are occupied. Each anion site is co-ordinated by one A site and three B sites. Furthermore, the occupied A sites form in themselves, two interpenetrating fcc lattices having an edge 'a' (equal to that of the unit cell) which are displaced relative to each other over a distance $\frac{\sqrt{3}}{4}a$ in the direction of the body diagonal of the elementary cube. The occupied B sites, on the other hand, lie on four fcc lattices with side 'a' which are displaced relative to each other over a distance $(\sqrt{2}/4)a$ in the direction of the face diagonal of the cube.

In the normal spinel structure, the 8 divalent ions occupy the A sites and the 16 trivalent ions occupy the B sites. In the inverse spinel structure, half of the trivalent ions are on the A sites while the other half plus the 8 divalent ions are on the B sites. Intermediate arrangements are also possible and are called 'partially inverted'. Ferrimagnetism implies the existence of at least two non-identical sublattices, A and B and usually at least three different exhange interactions J_{AA}, J_{AB} and J_{BB}. A simplif-

ication, however, is sometimes afforded by the fact that the divalent metal ion is non-magnetic, e.g. Zn, Cd. There is thus only one type of interaction, namely B-B in the case of a normal spinel. Néel in his theory of ferrimagnetism[1] assumed the existence in the material of one type of magnetic ion only, of which a fraction appeared on the A sites and the other fraction on the B sites. An unequal distribution of the ions may occur if there are unequal numbers of sites on the two sublattices, or if there is some kind of site preference which is generally determined by (a) the size of the ions involved (b) the electron configuration of the ion and (c) the symmetry and strength of the crystalline field at a site. It is obvious that with two or more different types of magnetic ions in various mixtures between the A and B sites, there can be a very large number of sublattices which may be needed to describe the system properly. For example, with two non-identical ions on the A sites and further two different types on the B sites, there could be a total of ten different interactions that would in general require ten molecular field constants. In the present investigations on the ordered phase of $LiFeO_2$, a total of 16 sublattices has been considered. However, in many cases it is often found possible to suppress a large number of them and still get an adequate description in terms of a smaller number of sublattices.

The simple Néel theory, based on a two sublattice model, is quite adequate in illustrating many important general features of ferrimagnetism but unfortunately does lead to conflict with the third

law of thermodynamics in the prediction of a finite slope of the net magnetization curve at the absolute zero. Yafet and Kittel[33] removed this difficulty by extending Néel theory to accommodate the postulate of a triangular spin configuration. In this, the A sublattice is divided into two interpenetrating fcc lattices while the B sublattice is similarly divided into four such interpenetrating sublattices. Neglecting anisotropy, they showed that the four B sublattices could be lumped together to form two equivalent sublattices. Yafet and Kittel found, among other possibilities, that when the A-A or B-B antiparallel interactions become comparable to the A-B interactions, the two sublattice magnetizations no longer remain exactly antiparallel but make an angle with each other. There is thus a resultant magnetization on that site and it is this which sets antiparallel with the magnetization of the other site. The triangular spin arrangements predict a linear increase in net magnetization with field at high field and also at low temperature - an important point of difference from that of Néel theory - and still give values of reduced magnetization of the same order of magnitude. The Yafet-Kittel theory has been applied qualitatively by Gorter to several series of ferrimagnetic compounds[34]. Lotgering[35] discussed the possibility of one or more transitions from one type of magnetic ordering to another during the course of heating and found evidence for the triangular configurations in $MnCr_2O_4$, $FeCr_2O_4$ and possibly $NiCr_2O_4$. Neutron diffraction data, however, have given mixed evidence for such a theory. For example, Prince[36]

concluded that the data on $CuCr_2O_4$ are in agreement with a triangular arrangement, while Pickart and Nathans[37] found no such evidence in nickel and manganese ferrite-chromites whose magnetizations are abnormally low and therefore easily accountable by this theory. On the other hand, Jacobs[38] studied a series of tetragonally distorted spinel compounds $MO.Mn_2O_3$ (where M = Mn, Co, Zn and Mg) and obtained results in good agreement with the triangular model. The Yafet-Kittel theory is further discussed in section 8.5 .

It was suggested by Kaplan[39] that the possible spin configurations in cubic spinels can be a magnetic spiral (or helical) in which case the ground state has a lower energy than that given by the triangular arrangements. In other words, the spin vector rotates as one advances from one magnetic ion to the next retaining, of course, the same sense and magnitude for its component along a given direction. The Yafet-Kittel type configurations were shown to be the stable ground state only under appropriate conditions for cubic spinels which are tetragonally distorted[40]. A helical spin configuration is also proposed by Yoshimori[41] in relation to the antiferromagnetic spin structure of MnO_2 and further evidence comes from other workers[42,43,44].

Finally, mention may be made of the concept of super-super-exchange in explaining some of the dominant magnetic exchange interactions involving two oxygen ions or one oxygen and one diamagnetic ion between the pairs of paramagnetic cations. This type of exchange interaction has been suggested by Osmond to account for

the antiferromagnetic ordering in ilmenite, $MnTiO_3$[45], and also in the magnetic structure of spinels containing paramagnetic octahedral cations but diamagnetic tetrahedral cations[46].

7.2 Purpose of the present study

Interest in the magnetic behaviour of lithium ferrite, $LiFeO_2$, arises mainly because of the apparently complicated nature of the phase transformation between its two crystallographic forms, a disordered rock-salt structure (α-$LiFeO_2$) and an ordered tetragonal structure. According to latest investigations carried out by Anderson (J.C.) and Schieber[47], the final ordered phase is the γ-phase, into which the unstable disorderd α-phase transforms via an intermediate body-centred tetragonal form, called the β-phase. The γ-phase, in turn, disorders to form the α-phase. Fayard[48] and Collongues[49], on the other hand, proposed the sequence $\beta \rightarrow \alpha \rightarrow \beta$ where the $\beta \longmapsto \alpha$ process proceeds via a less ordered γ-phase.

Neutron diffraction and Mössbauer study experiments[50] have revealed antiferromagnetic spin arrangements both for the ordered γ-phase in which there is cation order similar to that in chalcopyrite, $CuFeS_2$, with a Néel temperature at 315° K and for the α-phase with a transition temperature in the region of 90° K. The former corresponds to a magnetic superstructure of tetragonal symmetry with + and - spins alternating in the (001) planes, while the latter gives antiferromagnetic ordering in the (111) planes, the

spins being ferromagnetically coupled in the individual planes.

Previous magnetic susceptibility measurements in the transition region, however, had either failed to reveal any antiferromagnetic peak or given unusually large values for the magnetic moment of the Fe^{3+} ion when calculated from the Curie-Weiss law[51]. This, according to the present investigation, may be attributed to two reasons. Firstly, there is always present in the samples a minute trace of ferro- or ferrimagnetic impurity like $LiFe_5O_8$ which is reflected by the manifestation of a spontaneous moment in the magnetization versus field graph, and which renders the interpretation of the magnetic results difficult, and secondly, the previous measurements were not extended up to a sufficiently high temperature to get a true slope of the susceptibility graph. It was therefore decided to prepare a fresh sample of these materials and measure the magnetic susceptibility of all the three phases over an extended temperature range and as a function of field from 4-1000° K. The remanent magnetization, however, could not be entirely eliminated and was assumed to be due to the presence of approximately 1% of $LiFe_5O_8$ which would not be observed in the X-ray analysis. Transition temperatures were observed at 42° K for α and β phases and at 295° K for the γ phase after making necessary corrections for the impurity. The generally antiferromagnetic behaviour of all the three phases are consistent with the earlier neutron diffraction results[50] and yield values of the magnetic moment for Fe^{3+} that are in good agreement with the theoretical value. The departure

from Curie-Weiss law, which is observed above the transition temperature for up to a certain range, has been discussed in the published results of these investigations[52] (Appendix III).

The second part of the work is devoted to the experimental study of the magnetic properties of powder compounds of the series $Cd_xMn_{3-x}O_4$. As stated earlier, these compounds are isomorphous to hausmannite, Mn_3O_4, and are formed by partial to complete substitution of the paramagnetic Mn^{2+} ions by diamagnetic Cd^{2+} ions in the A sites of Mn_3O_4. This series was chosen for study because Mn_3O_4 is known to become ferrimagnetic at 42° K[53] and has a saturation moment at absolute zero which is nearly half of that predicted by the Néel model of ferrimagnetism and is generally attributed to Yafet and Kittel angles on the B sites[30,38,40]. Jacobs[38] observed the high field differential susceptibility in the series $Co_xMn_{3-x}O_4$, $Zn_xMn_{3-x}O_4$ and $Mg_xMn_{3-x}O_4$ as further evidence for triangular arrangements. The case of diamagnetic ions occupying the A sites appears to be particularly interesting since at the end point x = 1, both $ZnMn_2O_4$ and $MgMn_2O_4$ are found to exhibit antiferromagnetism on the basis of susceptibility[54] and neutron diffraction[55] experiments. In addition to these results, unidirectional anisotropy is also found in these two mixed manganites ($0 < x < 1$) when the material is cooled down to low temperatures in the presence of magnetic fields of several kilo-oersteds[55]. This suggests the existence of interactions between ferrimagnetic and nearly antiferromagnetic regions brought about by the random

distribution of diamagnetic cations among the tetrahedral sites and again points to the antiferromagnetic ordering of the spins.

It will thus be clear that with non-magnetic ions occupying most of the A sites, the predominant B-B exchange interactions have a direct influence on the magnetic behaviour of the substance. The cadmium manganite series thus provides a further excellent means to test the validity of the Yafet-Kittel theory and may even probe the applicability of the theory of spiral spin configuration in similar structures. In particular, the much larger size of the cadmium ions compared to that of Zn or Mg may have a significant effect on the super-super-exchange interactions if the latter prove important or may act as a more effective screen in the formation of the isolated clusters of the magnetic ions on the B sites. In either case, a departure from the usual antiferromagnetic behaviour at low temperatures may be expected. Another interesting feature is provided by the fact that the antiferromagnetic susceptibility may remain temperature independent below the Néel point in some cases with the spinel-like structure having only diamagnetic cations on the A sites. The antiferromagnetism of zinc ferrite is shown to exhibit this feature[56] which was explained on the assumption of negligible anisotropy in the plane perpendicular to the tetragonal c-axis. On rather incomplete experimental evidence, Rosenberg and Nicolae[57] had suggested that $CdMn_2O_4$ also exhibit temperature-independent antiferromagnetic susceptibility. The present investigations over the temperature range 4 - 1000° K have

revealed a generally complex behaviour with more than one transition temperature. The results are given in the published paper[58], a reprint of which is attached to this thesis (Appendix IV).

CHAPTER VIII

ANTIFERROMAGNETISM AND FERRIMAGNETISM

8.1 The generalization of the Weiss molecular field theory of antiferromagnetism

The starting point for the theoretical description of a co-operative magnetic phenomenon (ferro-, ferri- or antiferromagnetism) is the quantum mechanical exchange interaction of the Heisenberg-Dirac-Van Vleck model on the origin of the Weiss molecular field. According to this model, the exchange interaction energy V_{ij} between the spins of the i^{th} and j^{th} atoms or ions in the crystal, which are neighbours, is given by

$$V_{ij} = - 2 J \underline{S_i} \cdot \underline{S_j} \quad , \tag{8.1}$$

J being the exchange integral. In the general treatment of the antiferromagnetic theory, an atom or ion of a given sublattice is considered to be surrounded by a number of neighbours, some of which may belong to the same sublattice and some to others, so that the Weiss field acting on this ion depends upon the various sublattice magnetizations and may be expressed by the usual summation convention as

$$H_i^{int} = b_{ij} M_j \quad (j = 1,2,3,\ldots,n) \quad , \tag{8.2}$$

where M_j is the magnetic moment of the j^{th} sublattice, n is the number of sublattices considered and the b_{ij}'s are the Weiss molecular field coefficients and are a measure of the strength of

the exchange interaction between the spin of an ion from the i^{th} sublattice with that of an ion from the j^{th} sublattice and expressed by the equation (8.1). For this to be more realistic, $\underline{S}_j$ should be replaced by the mean value, $(\underline{S}_j)_{Av}$, which is proportional to M_j; the interaction then acts as an effective field due to magnetization of the sublattice containing j. In other words, the customary practice is to replace all the spins except the one under consideration by their averages and treat the statistical behaviour of this one spin alone. For an antiferromagnetic medium, b_{ij} is negative $(= -|b_{ij}|)$.

It may be pointed out that equation (8.2) is only useful if all the ions on a given sublattice have the same spin; if each sublattice contains equal numbers of positive and negative spins then clearly $M_j = 0$ and the equation is not helpful unless the sublattice is further divided.

At thermal equilibrium, the average value of the spin $\underline{S}_j$ is

$$(\underline{S}_j)_{Av} = S\, B_s(a_j) \ , \tag{8.3}$$

where S is the total spin quantum number, $B_s(a_j)$ is the Brillouin function and its argument a_j is given by

$$a_j = Sg\, \mu_B\, H^{eff}/kT \ . \tag{8.4}$$

Here

$$H^{eff} = H_i^{int} + H_{applied} \ . \tag{8.5}$$

The external field is included for the purpose of calculating susceptibility. The j^{th} sublattice magnetization is therefore given by

$$M_j = \text{constant} \times S\, B_s(a_j) \ , \tag{8.6}$$

which, for small values of the argument a_j, reduces to

$$M_j = \gamma \frac{H^{eff}}{T} \quad , \tag{8.7}$$

where all the constants are included in the symbol γ. Equation (8.7) holds for each sublattice separately. At high temperatures, the spontaneous magnetization is zero and the Curie temperature, T_c, is obtained by substituting the Weiss fields from equation (8.2) for H^{eff} in equation (8.7) and putting $T = T_c$. For the i^{th} sublattice, one therefore obtains

$$M_i - \gamma_i \frac{b_{ij} M_j}{T_c} = 0 \quad (j = 1,2,3,\ldots,n) \; . \tag{8.8}$$

The resulting set of n homogeneous linear equations in M, however, are not all independent and will give a non-zero solution for the sublattice magnetizations if the determinant of the coefficients of M is zero. In general, this determinantal equation yields more than one solution for T_c. The kind of magnetic ordering which actually exists below the Curie temperature will be that which corresponds to the highest value of T_c as this gives the lowest energy at the absolute zero.

8.2 Case of the simplest antiferromagnet

Van Vleck theory[8] deals with the simplest case, namely that of a body-centred cubic lattice in which there are two sublattices, one comprising the corner positions and the other the body positions. This arrangement has the special feature that the nearest neighbour of an ion or atom on sublattice 1 always lies on

sublattice 2 and vice versa. The internal field on one sublattice is then given entirely by the average magnetization of the other.

8.2.1 Behaviour above the Néel temperature, T_N

For the usual values of the applied field, the approximation made in equation (8.7) is true and this yields

$$M_1 = (H + b_{11} M_1 + b_{12} M_2) \gamma / T ,$$
$$M_2 = (H + b_{11} M_2 + b_{12} M_1) \gamma / T , \qquad (8.9)$$

where the same type of ions are involved in the two sublattices. On adding these two equations and solving, one gets

$$\text{Susceptibility } \lambda = \frac{M_1 + M_2}{H} = \frac{C}{T + \theta} , \qquad (8.10)$$

where

$$C = 2\gamma = 2\frac{g^2 \mu_B^2 S(S + 1)}{3k} , \qquad (8.11a)$$

after substituting the value of γ, and where

$$\theta = -(b_{11} + b_{12})\gamma = -(b_{11} + b_{12}) \frac{g^2 \mu_B^2 S(S + 1)}{3k} . \qquad (8.11b)$$

A relationship between the Weiss molecular field constant b_{ij} and the corresponding exchange integral J_{ij} is readily obtained by[59] equating the two expressions of the exchange Hamiltonian, containing the terms J_{ij} and b_{ij} respectively. This yields

$$b_{ij} = \frac{2zJ_{ij}}{g^2 \mu_B^2} , \qquad (8.12)$$

where z is the number of neighbours involved. Equation (8.11b) may therefore be expressed as

$$\theta = -\frac{2}{3k} (z'J_{11} + zJ_{12}) S(S + 1) . \qquad (8.13)$$

The antiferromagnetic Néel point, T_N, is obtained from equation (8.8)

as

$$\begin{vmatrix} b_{11} - 2T_N/C & b_{12} \\ b_{12} & b_{11} - 2T_N/C \end{vmatrix} = 0 \ , \qquad (8.14a)$$

giving

$$T_N = \tfrac{1}{2}C\,(b_{11} - b_{12}) = \frac{2}{3k}\,(z'J_{11} - zJ_{12})\,S(S+1). \qquad (8.14b)$$

Hence,

$$\frac{\theta}{T_N} = \frac{b_{12} + b_{11}}{b_{12} - b_{11}} = \frac{zJ_{12} + z'J_{11}}{zJ_{12} - z'J_{11}} \ . \qquad (8.15)$$

The effect of the intra-sublattice interaction is therefore to make θ, the Curie-Weiss temperature, different from the Néel temperature. If, however, the intra-sublattice (n.n.n.) interaction becomes too large in comparison to the inter-sublattice (n.n.) interaction, the simple two-sublattice arrangement becomes unstable. This is discussed in section 8.2.2.

8.2.2 Susceptibility below the Néel temperature

Van Vleck postulated the existence of some kind of easy axis of spontaneous antiferromagnetism below the Néel point and considered the effect of an applied field parallel and perpendicular to this preferred direction. Thus for H = 0, one obtains from equation (8.6) the two expressions

$$M_1 = \text{constant} \times S\,B_s\left[\frac{Sg\mu_B}{kT}\,(b_{11}M_1 + b_{12}M_2)\right] \ , \qquad (8.16a)$$

$$M_2 = \text{constant} \times S\,B_s\left[\frac{Sg\mu_B}{kT}\,(b_{11}M_2 + b_{12}M_1)\right] \ , \qquad (8.16b)$$

By symmetry, $M_1 = -M_2 = M$, so that

$$M = \text{constant} \times S B_s \left\{ \frac{Sg\mu_B}{kT} (b_{11} - b_{12}) M \right\}, \qquad (8.16c)$$

giving the same magnetization curve as ferromagnetism for the two sublattices separately. It follows therefore that at the absolute zero all the spins will be set parallel or antiparallel to H in the case of parallel susceptibility and the field induced magnetization will be zero, that is, $\chi_{\parallel} = 0$.

When H is perpendicular to the antiparallel spins, the field tends to rotate the sublattice magnetizations and this is opposed by the molecular field (Fig. 36). Since $\underline{H} \ll \underline{H}^{eff}$, the parallel molecular field, to a first approximation, is constant at $H_{\parallel}^{eff} = (b_{11} - b_{12})M$ while the perpendicular molecular field is given by $H_{\perp}^{eff} = H + (b_{11} + b_{12})\,\delta M$ where δM is the change produced in M by the application of H. Hence

$$\frac{H_{\perp}}{H_{\parallel}} = \frac{\delta M}{M} = \frac{H + (b_{11} + b_{12})\,\delta M}{(b_{11} - b_{12})M}, \qquad (8.17a)$$

which gives

$$\chi_{\perp} = \frac{2\,\delta M}{H} = -\frac{1}{b_{12}} = \text{constant}. \qquad (8.17b)$$

The perpendicular susceptibility thus only depends on the inter-sublattice interaction. The susceptibility of the powdered sample is now given by (averaging over all random crystallites)

$$\chi_{poly} = \chi_{\parallel}\overline{\sin^2\theta} + \chi_{\perp}\overline{\cos^2\theta} = \frac{1}{3}\chi_{\parallel} + \frac{2}{3}\chi_{\perp}. \qquad (8.18)$$

It follows, therefore, that at the absolute zero, $\chi_{poly} = \frac{2}{3}$ of χ at the Néel point. The experimental support to Van Vleck theory is

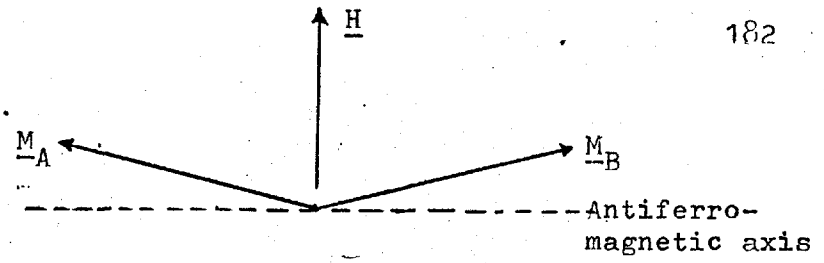

Fig. 36. Diagram illustrating the perpendicular susceptibility, $\chi_\perp$.

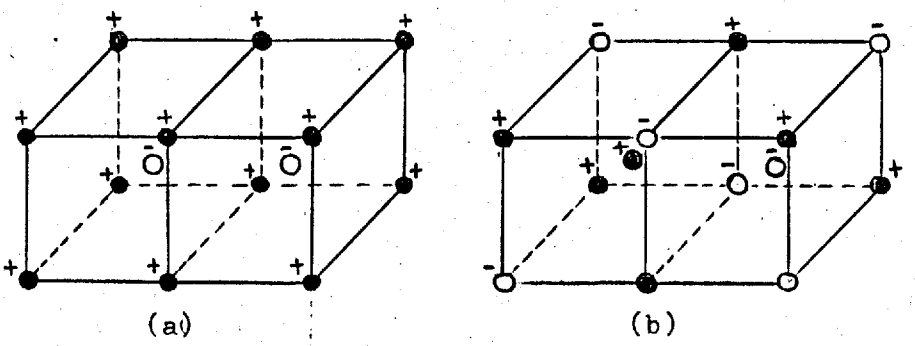

Fig. 37. Antiferromagnetic spin arrangements in a bcc lattice: (a) First kind of order (b) Second kind of order.

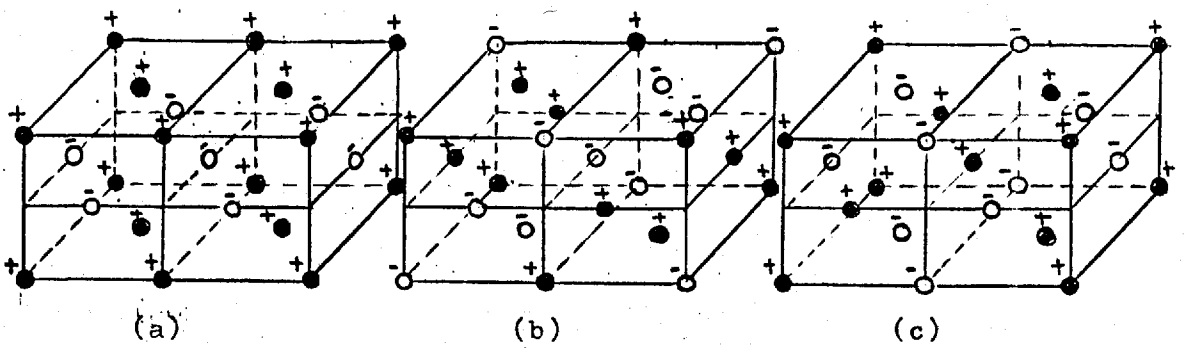

Fig. 38. The three possible kinds of magnetic ordering for a fcc lattice: (a) First kind of order (b) Second kind of order (MnO structure) (c) Third kind of order. After Smart (14).

provided by the results of Bizette, Squire and Tsai[60] on MnO although an attempt to fit the results of MnSe into the theory failed. Nagamiya, Yosida and Kubo[61] have given a list of most of the antiferromagnetic materials studied in which the value of $\chi(0)/\chi(T_N)$ can be seen to vary from 0.2 to 0.93. It is thus clear that some antiferromagnets behave more like the predictions of the Van Vleck theory than do the others and that these latter type of materials require a more rigorous theory involving the anisotropy field and the use of more complicated lattices. Anderson[15] has pointed out that with more than one antiferromagnetic axis within a single domain, it is possible to account for the ratio $\chi(0)/\chi(T_N)$ being different from $\frac{2}{3}$.

Fig. 37a gives the spin arrangements for the bcc structure of the foregoing discussion in which the plus and minus signs indicate moments aligned parallel and antiparallel to the easy direction respectively. However, no antiferromagnetic compounds are known in which the magnetic lattice is body-centred cubic. The second kind of order, shown in Fig. 37b results when the intrasites interaction becomes comparable to the intersites interaction (long range order) and is antiferromagnetic. The arrangements now need four sublattices to describe the magnetic behaviour. Following the same procedure as that outlined earlier, it is easy to show that the ratio of the Curie-Weiss temperature, θ, to the Néel temperature, T_N, is given by

$$\frac{\theta}{T_N} = -\frac{b_{12} + b_{ii}}{b_{ii}}, \text{ where } T_N = \tfrac{1}{2} C b_{ii}, \qquad (8.19)$$

and corresponds to the fact that the spin arrangements with the highest Néel point give the stable solution. Thus for $b_{ii} < \frac{1}{2} b_{12}$, equation (8.14b) gives a larger value for T_N and θ/T_N lies between 1 and 3 while for $b_{ii} > \frac{1}{2} b_{12}$ the second kind of ordering is stable. An example of the latter is provided by the rutile structure (body-centred tetragonal) in which the corner atoms are the n.n.n.'s to the body-centred atom and the corresponding interactions are the important ones.

8.3 The face-centred cubic structure

Anderson[15] extended the Weiss field treatment to the more complicated case of the fcc structure and showed that this should be divided into no less than four sublattices having the property that each sublattice contains four n.n.'s in each of the other three and six n.n.n.'s in its own. Smart[14], in a further generalization of Anderson's method, suggested that while the method of subdivision depends on the symmetry of the specific lattice, there should be enough sublattices so that a given atom has neither nearest nor next nearest neighbours on its own. The fcc lattice was accordingly divided into 8 fcc sublattices. This division is particularly important for the MnO structure in which, according to neutron diffraction studies[3], any Mn^{2+} ion has six parallel and six anti-parallel n.n.'s whereas the six n.n.n.'s are antiparallel. Hence

the important interaction which produces the antiferromagnetism is between the n.n.n.'s and is provided by the super-exchange.

The inclusion of a sufficient number of sublattices in a generalized treatment such as given by Smart has the advantage that the Curie temperature for a specified type of magnetic ordering may be obtained directly without solving the determinantal equation. For instance, if the interactions, B_{ij}'s, are all defined as positive and the signs of the interactions are explicitly given by the notation ε_{ij}, where $\varepsilon_{ij} = \pm 1$ denotes whether the i-j neighbour interaction is ferromagnetic or antiferromagnetic, and if the ordering is further specified by the relation $S_i = (\eta_{ij})\, S_j$ where $\eta_{ij} = \pm 1$, then one may write

$$\theta = C \sum_{i \neq j} \varepsilon_{ij} \; b_{ij} \; , \tag{8.20a}$$

and

$$T_c = C \sum_{i \neq j} \eta_{ij} \; \varepsilon_{ij} \; b_{ij} \tag{8.20b}$$

which are equivalent to equations (8.11b) and (8.14b). Thus θ and T_c may be obtained directly once the molecular field coefficients and the type of ordering are assigned. Fig. 38 shows the three types of antiferromagnetic order possible in a fcc lattice with only n.n. and n.n.n. interactions. The first kind of ordering occurs if the n.n.n. interactions are ferromagnetic. The third kind occurs if $b(\text{n.n.})/b(\text{n.n.n.}) > \frac{4}{3}$, otherwise it is of the second kind as observed in MnO. In addition, θ/T_N is found to lie between 1 and 5 for the

fcc structure. It may be pointed out that while T_c depends on the type of magnetic ordering below the order-disorder transition point, θ only indicates the effect of the internal field in aiding (θ = + ve; ferro-) or opposing (θ = - ve; antiferro-) the applied field which tends to align the moments. It is interesting to note that the usually accepted procedure to look for the highest Néel point assumes the impossibility of transitions from one type of magnetic order to another at some intermediate temperature unless the molecular field (m.f.) coefficients are temperature dependent such as those due to thermal changes of the lattice parameters. Thus, the simple m.f. theory cannot explain such complex behaviour as ferro- or ferri-magnetic-antiferromagnetic transitions etc. in the simple Bravais lattices described above.

8.4 Ferrimagnetism

In a ferrimagnetic material, the sublattices into which the magnetic structure is divided are not identical because there are different kinds of magnetic ions, different types of crystallographic sites for the ions, or both. Unequal numbers of magnetic ions on the sublattices may also contribute to the lack of symmetry. Néel, using the simplest two-sublattice model, assumed the existence of one type of magnetic ion only, of which a fraction λ appeared on the A sites and a fraction μ on the B sites, so that

$$\lambda + \mu = 1. \qquad (8.21)$$

For a normal spinel, $\lambda = 0$, $\mu = 1$ whereas for an inverse spinel,

$\lambda = \mu = 0.5$. In general, the AB interaction is negative and is much stronger than either AA or BB interactions, each one of which may in principle be positive or negative but apparently positive for a great number of ferrimagnetic materials. The local field at sublattice, say, 1 is thus opposite to the magnetization of sublattice 2 and the magnetizations at the two sites are antiparallel.

In the theoretical treatment of ferrimagnetism, the customary practice is to denote the molecular field coefficients corresponding to the three types of interactions by the notations n, $n\alpha$, and $n\beta$ respectively, where n is taken as a positive quantity and a plus or minus sign is used explicitly to indicate whether the AB interaction is positive or negative and where the parameters α and β are given by

$$\alpha = \frac{\text{AA interactions}}{\text{AB interactions}} \quad ; \quad \beta = \frac{\text{BB interactions}}{\text{AB interactions}} \quad . \qquad (8.22)$$

The m.f. analysis of a simple ferrimagnet thus becomes formally the same as that for an antiferromagnet and a similar procedure yields the expression for the susceptibility in the paramagnetic region (with - ve AB interaction) as

$$\frac{1}{\chi} = \frac{1}{C} \cdot \frac{T^2 - nC(\lambda\alpha + \mu\beta)T + \lambda\mu n^2C^2(\alpha\beta - 1)}{T - \lambda\mu nC(\alpha + \beta + 2)} \quad , \qquad (8.23a)$$

$$= \frac{T - \theta}{C} - \frac{\zeta}{T - \theta'} \quad , \qquad (8.23b)$$

where

$$\theta = - Cn(2\lambda\mu - \lambda^2\alpha - \mu^2\beta) \quad , \qquad (8.23c)$$

$$\theta' = n\lambda\mu C\,(2 + \alpha + \beta) \quad , \qquad (8.23d)$$

and $$\zeta = n^2\lambda\mu C\left[\lambda(1+\alpha) - \mu(1+\beta)\right]^2 . \qquad (8.23e)$$

The last term of the equation (8.23b) has no ferromagnetic counterpart and gives the characteristic parabolic shape of ferrimagnetism. The forms of the $1/\chi$ versus T curves for the various cases, namely $J = 0$ (para-), $J > 0$ (ferro-) and $J < 0$ (antiferro- and ferrimagnetism) are now depicted in Fig. 39 together with the geometrical interpretations of the parameters of the equation (8.23b). The curve (b) is for a ferrimagnet with an antiferromagnetic Néel point above the Curie temperature. The influence of the short range order which may persist even after the Curie temperature has been shown by Smart[62] to result in a smaller slope for the $1/\chi$ versus T curve than that obtained from the Weiss field approximation and consequently in a lowering of the Curie point.

The ferrimagnetic Curie temperature, T_c, may be calculated by putting equation (8.23a) equal to zero at $T = T_c$. Alternatively, the numerator in the equation may be put in the form

$$(T - T_c)(T - T_c') = 0 , \qquad (8.24a)$$

where

$$T_c = \tfrac{1}{2} Cn\left[\lambda\alpha + \mu\beta + \sqrt{(\lambda\alpha - \mu\beta)^2 + 4\lambda\mu}\right] , \qquad (8.24b)$$

and

$$T_c' = \tfrac{1}{2} Cn\left[\alpha\lambda + \mu\beta - \sqrt{(\lambda\alpha - \mu\beta)^2 + 4\lambda\mu}\right] \qquad (8.24c)$$

If the two sublattices are identical, then $\lambda = \mu = \frac{1}{2}$ and $\alpha = \beta$ in which case $\zeta = 0$ and the hyperbola reduces to a straight line with $\theta \neq T_c$. It is easy to show that if the AB interaction is positive, the $1/\chi$ versus T curve is again of the parabolic form where the

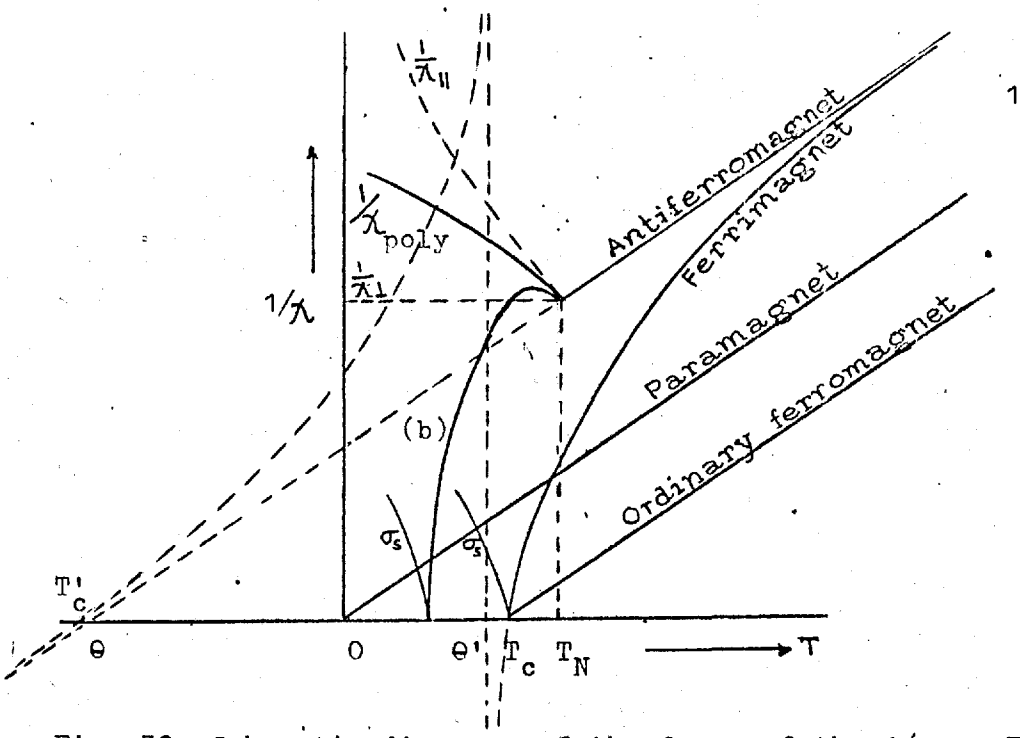

Fig. 39. Schematic diagrams of the forms of the $1/\chi$ vs T curves for a para-, ferro-, ferri- and an antiferromagnetic material. Curve (b) shows a ferrimagnetic with an antiferromagnetic Néel point above the Curie point.

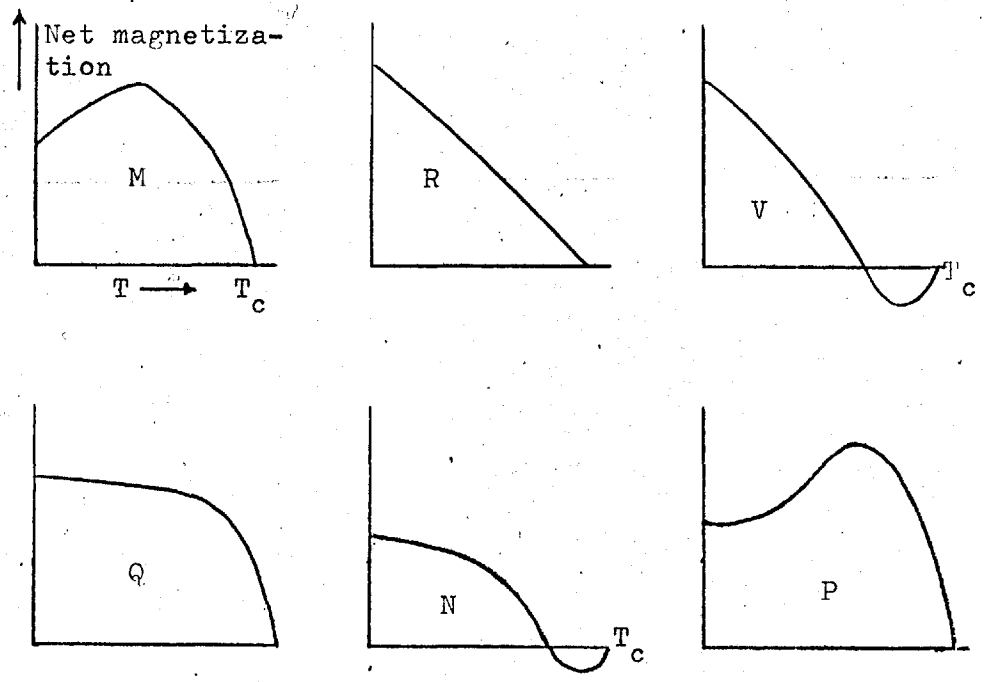

Fig. 40. The six possible forms of spontaneous magnetization curves on a two sublattice theory. (After Néel[1]).

associated parameters may be directly obtained from equations (8.23a) to (8.23e) by applying the transformations $n \rightarrow -n$, $\alpha \rightarrow -\alpha$ and $\beta \rightarrow -\beta$. This also results in the interchange of the expressions for T_c and T_c' but in this case $\theta = T_c$ when the two sublattices are identical, and this result corresponds to the case of ferromagnetism.

The condition for obtaining ferrimagnetism is that T_c should be positive which implies, from equation (8.24b), that either α, β are both positive or

$$\alpha\beta < 1, \text{ for negative } \alpha \text{ and } \beta. \qquad (8.25)$$

The physical significance of this is that large negative AA or BB interaction is unfavourable for ferrimagnetism. In fact, Néel[1] suggested that the material remains paramagnetic at all temperatures under this condition - a prediction which is considered somewhat unlikely since for strong interactions one would expect some kind of ordering at low temperatures. This is further considered in section 8.5.1.

8.4.1 The spontaneous magnetization

For the spontaneous magnetization, one is interested in the values of the sublattice magnetizations in the absence of an external field. For a general case, these are given by the expressions

$$M_A = \lambda\, g_1 \mu_B\, S_1\, B_s\left[\frac{g_1\, \mu_B\, S_1}{kT}\,(\alpha\, n\, M_A + n\, M_B)\right], \qquad (8.26a)$$

$$M_B = \mu\, g_2 \mu_B\, S_2\, B_s\left[\frac{g_2\, \mu_B\, S_2}{kT}\,(\beta\, n\, M_A + n\, M_B)\right]. \qquad (8.26b)$$

The variations of M_A and M_B with temperature thus depend on the

relative magnitudes of λ, α and β and will, in general, be different for the two sublattices since the arguments of the Brillouin functions involve different combinations of the sublattice magnetizations and the m.f. coefficients. Hence the form of the resultant magnetization curve can be quite anomalous, particularly in the case of negative AB interactions. The problem was considered by Néel who obtained six possible forms of spontaneous magnetization curves under various combinations of λ, α and β. These are shown in Fig. 40 with Néel's original notations. It will be seen that type Q is of the 'normal' form. An experimental P-type curve is found in $NiCr_2O_4$ and in some mixed ferrite-aluminates[34,63] while the R-type temperature dependence is observed in most of the commercial ferroxcube III materials[64]. A magnetization curve of type N or V, exhibiting a zero net moment at some temperature below the Curie temperature was first observed by Gorter[34] and the existence of the compensation point was first experimentally demonstrated by Gorter and Schulkes[65]. Later, Bertaut and Pauthenet[66] found similar results in various kinds of ferrimagnetic iron garnets.

8.4.2 Limitations of the Néel theory

It will thus be apparent that the Néel theory explains quite satisfactorily many of the salient features of ferrimagnetism. However, there are also discrepancies. For example, the slope of the $1/\chi$ - T curve, calculated from the high temperature region, does not generally give a correct value for 1/C as predicted by the

theory. One probable explanation may be that a given magnetic ion behaves differently in its magnetic properties on the A and B sites. If the orbital contributions to the magnetic moments are not fully quenched, this may lead to different g values. Also, the distribution of magnetic ions between A and B sites may be a function of temperature. Néel himself tried to remove some of the difficulties by assuming a temperature variation of the molecular field coefficients. The ambiguity regarding the choice between a positive and a negative AB interaction is, however, ruled out by consideration of the values for spontaneous moments at low temperatures (which in most of the ferrite and other ferrimagnetic materials are far less than those which simple summations of the two moments will give) and also by direct neutron diffraction experiments. The most important theoretical objection to the Néel theory comes from the fact that magnetization curves of the types M, R and V, displaying non-zero slopes of dM/dT at 0° K, violate the third law of thermodynamics. This difficulty was later removed by Yafet and Kittel[33] (hereafter referred to as Y.K.).

8.5 The Y.K. theory

Y.K. extended the Néel theory to take into account the antiferromagnetic exchange interactions within the two magnetic sublattices. Accordingly, the A and B lattices were further divided into two more sublattices, A_1, A_2 and B_1, B_2. Actually, the B lattice was subdivided into four fcc lattices, B_1', B_2', B_3', B_4', all having the

same side as the spinel unit cell. The sub-division was carried out on the assumption that the order in both A and B lattices is determined by the n.n. interactions only. Any given ion from A_1 then has four n.n.'s from A_2 while an ion from, say, B_1', has six n.n.'s, two from each of the other three B_i' s. It will thus be clear that the interactions between any two B_i' s, which are of the super-exchange type P-X-Q (where X is the intermediate anion and the angle PXQ is 90°), are all identical.

It is perhaps worthwhile to consider here the relative strengths of the other interactions since super-exchance predicts strongest and weakest interactions at angles of 180° and 90° respectively and is also determined by the distances of the cations from the anion. On this basis, the next favourable BB interaction is that between the face-centred ion of say the B_1' sublattice and the nearest corner ion of the B_2' sublattice where the angle is 125° and the two distances are 1; 1.73 where the values are obtained after dividing by the shortest distances, i.e. $\frac{1}{8}\,a\sqrt{3}$ for A-X and $\frac{1}{4}\,a$ for B-X[35]. For increasing distances, the interactions cease to be of the super-exchange type because of the screening effects of the surrounding ions and other mechanisms such as super-super-exchange, symbolized by the notation P-X-X-Q, must be invoked.

On the A sites, the inter-sublattice interaction is again via super-exchange in which the angle is 70° and the cation distances are 1;1.92. The n.n.n. interaction between the corner ion and the face-centred ion on a given sublattice is considerably

weaker, the angle being 118° and the distances being 1.92;1.92.

For the AB interactions, the angles are more favourable; for instance, that between the corner ions of the A_1 and B_1' sublattices is 125° with distances 1:1; that between the face-centred ion on A_1 and the corner atom on B_2' is 180° with distances 1;1.73 and so on. The general conclusion is that the intersites interactions are stronger than those within the sublattices, and further, that the interactions between ions in the A sites are weakest of all. The possibility of an angle occurring between the spins on the A_1 and A_2 sublattices is therefore considered rather unlikely[35] (see also section 8.5.1 (2c)).

Following Lotgering[35], if $\underline{M}_{a_i}$ and $\underline{M}_{b_i'}$ denote the magnetization vectors of the sublattices A_i and B_i' respectively and if n, $n\alpha_1$, $n\alpha_2$, $n\beta_1'$, $n\beta_2'$ are the Weiss constants for the interactions A_iB_j', A_iA_i, $A_iA_{j\neq i}$, $B_i'B_i'$ and $B_i'B_{j\neq i}'$ respectively, then the molecular fields on the six lattices may be written:

$$\underline{H}_{a_1} = -n\left[\alpha_1 \underline{M}_{a_1} + \alpha_2 \underline{M}_{a_2} + \sum \underline{M}_{b_i'}\right],$$

$$= -n\left[(\alpha_1 - \alpha_2)\underline{M}_{a_1} + \alpha_2 \sum \underline{M}_{a_i} + \sum \underline{M}_{b_i'}\right], \quad (8.27a)$$

$$\underline{H}_{b'_1} = -n\left[\sum \underline{M}_{a_i} + \beta_1' \underline{M}_{b_1'} + \beta_2' (\underline{M}_{b_2'} + \underline{M}_{b_3'} + \underline{M}_{b_4'})\right],$$

$$= -n\left[(\beta_1' - \beta_2')\underline{M}_{b_1'} + \sum \underline{M}_{a_i} + \beta_2' \sum \underline{M}_{b_i'}\right], \quad (8.27b)$$

---

in which all the interactions are taken as negative and where $\alpha_1 < \alpha_2$, $\beta_1' < \beta_2'$. Since $\underline{M}_{a_1}$ should be parallel to $\underline{H}_{a_i}$ and so also, $\underline{M}_{a_2}$ should be parallel to $\underline{H}_{a_2}$, it follows from equations (8.27a) and (8.27b) that if $\underline{M}_{a_1}$ and $\underline{M}_{a_2}$ are not parallel to each other then

$$\alpha_2 \sum \underline{M}_{a_i} + \sum \underline{M}_{b_i'} = 0 \quad ; \tag{8.28a}$$

similarly, if the vectors $M_{b_i'}$ are not parallel then

$$\sum \underline{M}_{a_i} + \beta_2' \sum \underline{M}_{b_i'} = 0. \tag{8.28b}$$

For simultaneous angles on both A and B sites, the condition then is

$$\alpha_2 \, \beta_2' = 1 \, . \tag{8.29}$$

For arbitrary α_2 and β_2', this situation therefore does not arise. Equation (8.28b) further implies that for angles appearing on the B sites, all configurations with the same resultant magnetic moment have the same self-energy and also the same exchange energy in the presence of the A lattices. Thus one can make $\underline{M}_{b_1'}$, $\underline{M}_{b_3'}$ and $\underline{M}_{b_2'}$, $\underline{M}_{b_4'}$ respectively collinear. The four sublattices B_1', B_2', B_3', B_4' are therefore equivalent to two, B_1 and B_2, referred to earlier and these are associated with the magnetization vectors $\underline{M}_{b_1}$ and $\underline{M}_{b_2}$ respectively, where

$$\begin{aligned} \underline{M}_{b_1} &= 2 \, \underline{M}_{b_1'} = 2 \, M_{b_3'} \quad , \\ \underline{M}_{b_2} &= 2 \, \underline{M}_{b_2'} = 2 \, M_{b_4'} \quad . \end{aligned} \tag{8.30}$$

8.5.1 Ground state at 0° K

Y.K. considered the interactions within the A and B lattices to be separately antiferromagnetic in which case the four molecular field equations are

$$\begin{aligned}
\underline{H}_{a_1} &= n\left[\alpha_1\underline{M}_{a_1} + \alpha_2\underline{M}_{a_2} - \underline{M}_{b_1} - \underline{M}_{b_2}\right], \\
\underline{H}_{a_2} &= n\left[\alpha_2\underline{M}_{a_1} + \alpha_1\underline{M}_{a_2} - \underline{M}_{b_1} - \underline{M}_{b_2}\right], \\
\underline{H}_{b_1} &= n\left[-\underline{M}_{a_1} - \underline{M}_{a_2} + \beta_1\underline{M}_{b_1} + \beta_2\underline{M}_{b_2}\right], \\
\underline{H}_{b_2} &= n\left[-\underline{M}_{a_1} - \underline{M}_{a_2} + \beta_2\underline{M}_{b_1} + \beta_1\underline{M}_{b_2}\right],
\end{aligned} \tag{8.31}$$

where β_1, β_2 are connected with the primed coefficients by the relations

$$\beta_1 = \tfrac{1}{2}(\beta_1' + \beta_2') \; ; \qquad \beta_2 = \beta_2' \tag{8.32}$$

Lotgering[35] assumes $\alpha_1 = \beta_1' = 0$ and obtains 0, $\alpha_2 n$, $\tfrac{1}{2}\beta_2 n$, $\beta_2 n$ and n respectively for the five interactions. Furthermore, the constants α, β of the simple two sublattice model of Néel are related to the new constants by the expressions

$$\alpha = \tfrac{1}{2}(\alpha_1 + \alpha_2) \; ; \qquad \beta = \tfrac{1}{2}(\beta_1 + \beta_2) \, . \tag{8.33}$$

The exchange energy is given by

$$\begin{aligned}
E &= -\tfrac{1}{2}\sum \underline{H}_i \cdot \underline{M}_i \\
&= -n\left[\alpha_1 \underline{M}_{a_1}^2 + \alpha_2 \underline{M}_{a_1} \cdot \underline{M}_{a_2} + \beta_1 \underline{M}_{b_1}^2 + \beta_2 \underline{M}_{b_1} \cdot \underline{M}_{b_2}\right. \\
&\quad \left. - (\underline{M}_{a_1} + \underline{M}_{a_2}) \cdot (\underline{M}_{b_1} + \underline{M}_{b_2})\right],
\end{aligned} \tag{8.34}$$

Assuming that the sublattices are saturated at 0° K and that one kind of magnetic ion occupies the A and the B sites, then

$M_a/M_b = \lambda/\mu = y$ where y changes from 0 to 1. Equation (8.34) thus reduces to (Fig. 41)

$$E = -n M_b^2 \left[(\alpha_1 - \alpha_2 \cos 2\phi)\, y^2 + (\beta_1 - B_2 \cos 2\Psi) + 4y \sin\phi \sin\Psi \right] . \qquad (8.35)$$

The values of ϕ and Ψ that minimize the energy can be readily obtained by applying the usual rule for finding the minima of a function of two variables. The results are summarized below

(1) when $\alpha_2 \beta_2 > 1$, $\phi = \Psi = 0$, the doubly antiferromagnetic arrangements constitute the ground state for all y with each site, in turn, becoming antiferromagnetically ordered at its characteristic Curie temperature T_{cA} and T_{cB}. The configuration may be expressed by the notation $\updownarrow\updownarrow$ (Fig. 43 a)

(2) when $\alpha_2 \beta_2 < 1$, three possibilities arise:

(a) $\phi = \frac{1}{2}\pi$, $\sin\Psi = y/|\beta_2|$ for $0 < y < |\beta_2|$, the ground state then has the triangular spin arrangements, symbolized by $\triangleright$ with angles on the B sites. The value of $\sin\Psi$ is also given by the equation (8.28b). The physical meaning of the condition $|\beta_2| > M_a/M_b$ is that the molecular field of B_2 acting on B_1 is stronger than the field of A_1 (or A_2) acting on B_1.

(b) $\phi = \Psi = \frac{1}{2}\pi$ for $|\beta_2| < y < 1/|\alpha_2|$, this is the Néel ferrimagnetic state $\downarrow\uparrow$ in which the spins at the two sites are antiparallel to each other (collinear spins). The ordering takes place at the Curie temperature T_c given by equation (8.24b) or (8.38c).

(c) $\Psi = \frac{1}{2}\pi$, $\sin\phi = 1/|\alpha_2|\, y$ for $y > 1/|\alpha_2|$; this configuration with the angle on the A site and symbolized by $\triangleleft$, occurs

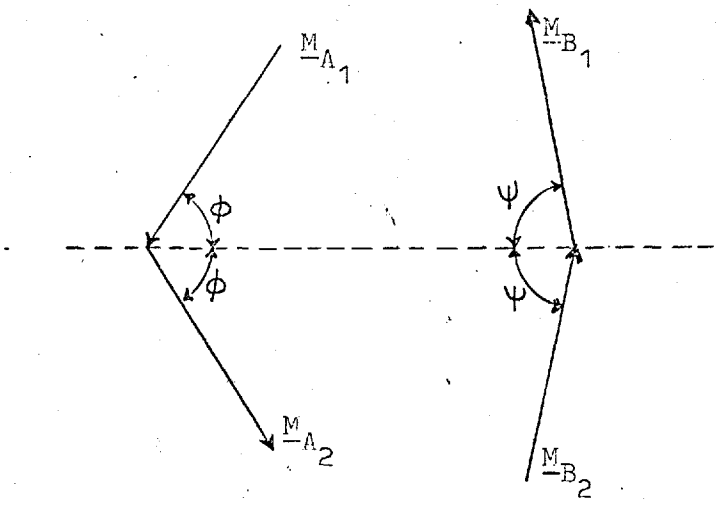

Fig. 41. The canting of the sublattice magnetizations of the A and B sites

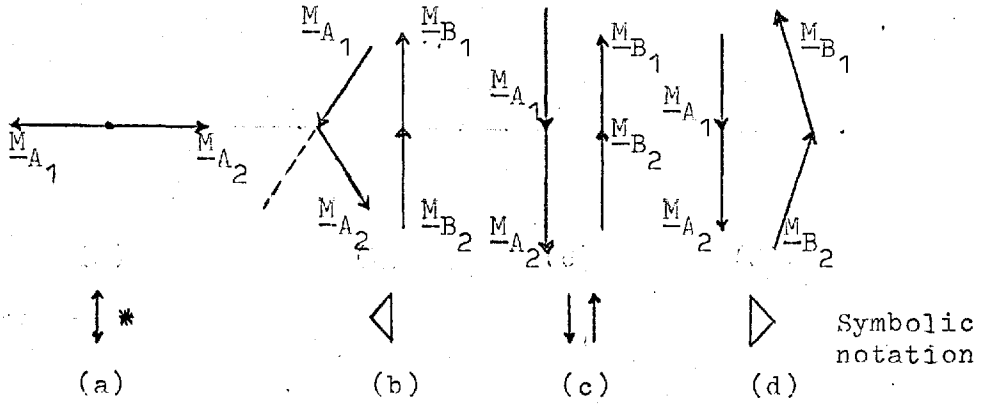

Fig. 42. Diagrams illustrating the successive phases of the transitions from the paramagnetic to the Yafet-Kittel ferrimagnetic state.

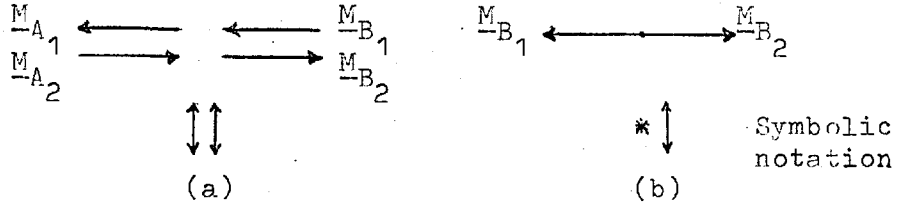

Fig. 43. (a) The doubly-antiferromagnetic spin alignments, (b) the antiferromagnetic B site with A site remaining paramagnetic.

when $|\alpha_2| > M_b/M_a$ and the corresponding Curie temperature is given by[33] $T_c = \mu\, Cn\, (\beta + \frac{1}{|\alpha_2|})$.

8.5.2 Evaluation of the Curie temperatures

At high temperatures, the various sublattice moments are given from equation (8.7) as

$$M_{a_1} = \frac{\lambda\, C\, H_{a_1}}{2T} \quad , \tag{8.36a}$$

$$M_{b_1} = \frac{\mu\, C\, H_{b_1}}{2T} \quad , \tag{8.36b}$$

The possible Curie points can be determined by finding what temperatures allow non-zero solutions for M_a and M_b in accordance with the rule set out in (8.8). The determinantal equation is then of the form

$$\begin{vmatrix} U & \alpha_2 & -1 & -1 \\ \alpha_2 & U & -1 & -1 \\ -1 & -1 & V & \beta_2 \\ -1 & -1 & \beta_2 & V \end{vmatrix} = 0 \quad , \tag{8.37a}$$

where

$U = \alpha_1 - \frac{2T}{\lambda Cn}$ and $V = \beta_1 - \frac{2T}{\mu Cn}$. The equation may be factorized into the form

$$(U - \alpha_2)\,(U + \alpha_2)\,(V - \beta_2)\,(V + 2\beta_2 - \frac{4}{U + \alpha_2}) = 0, \tag{8.37b}$$

giving four solutions

$$T_{cA} = \tfrac{1}{2}\, Cn\, \lambda\, (\alpha_1 - \alpha_2) \quad , \tag{8.38a}$$

$$T_{cB} = \tfrac{1}{2} Cn\, \mu\, (\beta_1 - \beta_2)\ , \qquad (8.38b)$$

$$T_c = \tfrac{1}{2} Cn \left[\lambda\alpha + \mu\beta \pm \sqrt{(\lambda\alpha - \mu\beta)^2 + 4\lambda\mu} \right]. \qquad (8.38c)$$

The last one is the same as equation (8.24) and becomes the only Curie temperature if $\alpha_1 = \alpha_2$; $\beta_1 = \beta_2$. The kind of magnetic ordering which appears below the highest Curie point is, as shown by Y.K., not always such as to lead to the lowest state at 0° K. Thus considering the case $\alpha_2\beta_2 < 1$, if T_c is the largest root and the ferrimagnetic arrangement $\downarrow\uparrow$ is the ground state, then only one transition (at T_c) occurs. On the other hand, if T_{cA} is the largest root and the triangular arrangement with the angle on the B site is the ground state, the spin configurations may undergo four successive transitions as shown in Fig. 42 . The first phase is the one in which there is an antiferromagnetic order of the A spins whereas the B spins are in a paramagnetic state and this is followed by the other types of ordering as the substance is gradually cooled down to 0° K. If, however, T_{cB} is the highest root and the triangular configuration with the B site angle is the ground state, there are two transitions starting from the state in which the A site is paramagnetic and the B site is antiferromagnetic (Fig.43 b). It is this possibility which has been taken into account in the discussion of the experimental results on $Cd_xMn_{3-x}O_4$. The derivation of the above results leads to one important conclusion, namely, that a direct transition from the triangular arrangement to the paramagnetic state is not possible and that at least one intermediate state must

exist. Another interesting point is that the Y.K. theory allows transitions among the various configurations at different temperatures without the assumptions of temperature-dependent interactions. This may be compared with the theoretical investigations by Smart[67] who suggested that magnetic phase transitions between ferromagnetism and antiferromagnetism, or between two different kinds of antiferromagnetic ordering, would occur only if the molecular field coefficients vary with temperature.

8.5.3 Comparison between the Néel theory and Y.K. theory

By putting $\alpha_1 = \beta_1' = 0$ (i.e. considering only the intersublattice interactions), it can be readily derived from equations (8.32), (8.33) and (8.35) that the Néel ferrimagnetism occurs when

$$\alpha_2 \beta_2 < \frac{8}{3} , \qquad (8.39)$$

whereas Y.K. theory predicts collinear spins only when $\alpha_2 \beta_2 < 1$. The Y.K. ferrimagnetic region is thus considerably smaller than the Néel region. This difference arises because of the neglect, by Néel, of the antiferromagnetic arrangements within the A or B sites. Thus, if the paramagnetic state is to have as low an energy as an antiferromagnetic state either on the A or B site, then clearly from equation (8.35), $\alpha_1 = \alpha_2 = \alpha$ and $\beta_1 = \beta_2 = \beta$; in other words, no subdivision of the A or B lattice is possible. The two cases are illustrated in Fig. 44 in which the regions of unsaturated Néel lattice magnetizations are indicated by the dashed arrows. The lack of saturation in the Néel case is also responsible for a non-zero

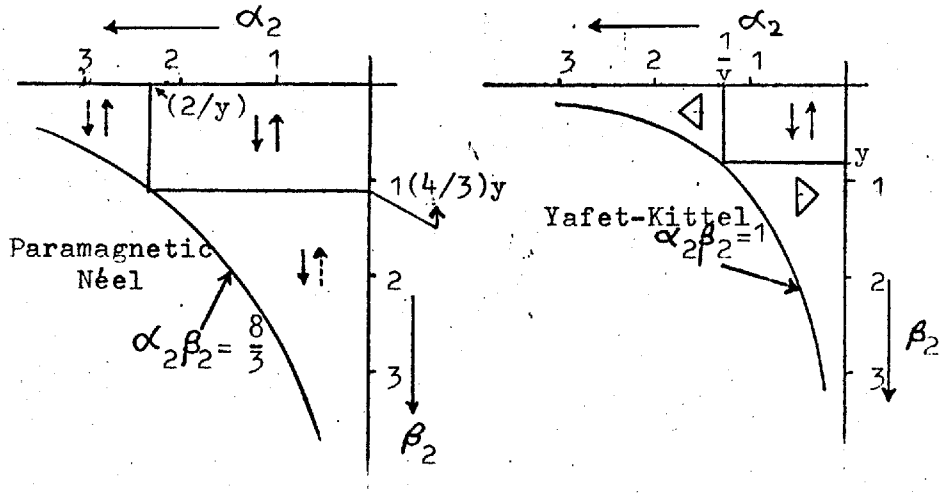

Fig. 44. The $\alpha - \beta$ diagrams for T = 0, according to Néel and Yafet-Kittel theories respectively, both for the same value of y = 0.8. (After Lotgering[35]).

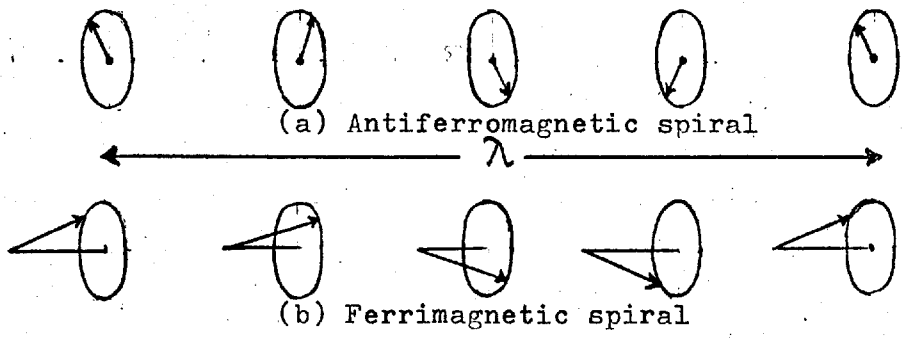

Fig. 45. The helical spin configurations.

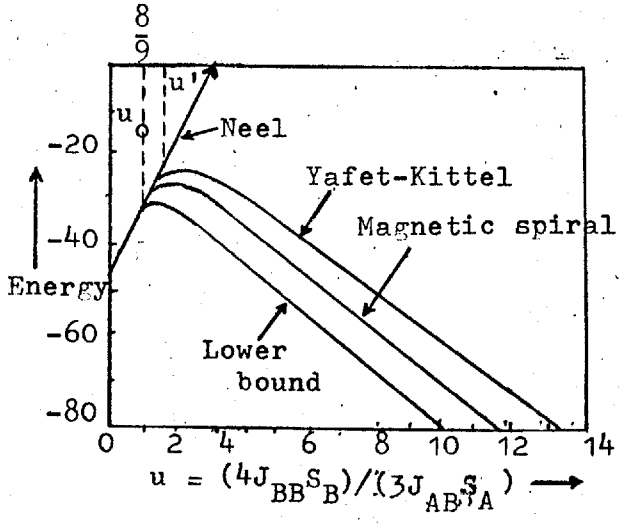

Fig. 46. Energy as a function of the parameter u for the various models in cubic spinel. (After Kaplan et al[40]).

entropy at 0° K, giving a non-zero slope of the net magnetization versus T curve referred to earlier.

8.6 The helical (or spiral) spin configurations for the cubic and the tetragonally distorted cubic spinels

It has been shown that for large enough AA and/or BB interactions compared with the AB interaction (all negative), the triangular configuration would have appreciably lower energy than that of the Néel collinear spins and would also explain the lower spontaneous magnetizations observed in many ferrimagnetic materials. For the special case of zero AB interaction, Anderson[68] showed that there would be no long-range ordering of the B spins in a cubic spinel and that for non-zero AB interaction there should also be no long-range ordering of angles between the spins. The latter argument was based on the assumption that the Y.K. state has the minimum energy.

However, Kaplan[39] and later, with his co-workers[40], made a detailed study of the ground state problem and showed that the Y.K. configurations do not minimize the exchange energy in the cubic spinel. In their treatment, the sublattice assumptions are all withdrawn and only n.n. AB and BB antiferromagnetic interactions with one spin type, S_A, on the A sites and one, S_B, on the B sites (normal spinel) are considered. The method is based on the generalized approach, made by Lyons and Kaplan[39], to the Luttinger-Tisza[69] method for finding the rigorous minimum of a quadratic form - in this case -

the classical Heisenberg exchange energy function. The mathematical analysis is lengthy and complex and so only the results are summarized here. By introducing a single exchange parameter, u, defined by

$$u = \frac{4\ J_{BB}\ S_B}{3\ J_{AB}\ S_A} \tag{8.40}$$

Lyons et al.[40] showed that in the cubic spinel, the Néel configuration is the ground state for only $u < u_o = \frac{8}{9}$ in which case it is locally stable (i.e. for all arbitrary small deviations of the spin vectors from their direction in the configuration, the energy increases). The important derivation is that for all BB interactions large enough to destabilize the Néel alignment, a ferrimagnetic spiral spin configuration has considerably lower energy than that of any previously known configuration, including the collinear and triangular models. A magnetic spiral is referred to as ferrimagnetic or antiferromagnetic depending on whether the net moment is non-zero or zero. In the former case, all the spins lie on a cone of semi-vertical angle ø but the spin vector rotates as one advances from one magnetic ion to the next according to a definite phase relation. When $ø = \pi/2$, the antiferromagnetic spiral results. These are illustrated in Fig. 45 . Over the range $\frac{8}{9} < u < u'' = \sim 1.3$, it was shown that the ferrimagnetic spiral has a propagation vector in the [110] direction, is locally stable and, possibly, is the ground state. For $u > 1.3$, the spiral is definitely not the ground state and over a finite range of u in this region, the calculations indicated the existence of spin ordering which is much more complex

than the magnetic spiral. However, the method succeeded in proving that the spiral provides the lowest energy of all the known spin configurations and in addition, yielded a rigorous lower bound to the ground state energy. A comparison of the three types of models discussed so far is given in Fig. 46 .

In a further extension of the generalized treatment to a class of tetragonally distorted spinels, Kaplan et al.[40] showed that the Y.K. triangular configuration can be the stable ground state for certain limited ranges of AB and BB interactions starting from the boundary of the Néel region. As is known, the tetragonal distortion in the spinel is caused by the fact that most A site cations are too large to be filled in the relatively small A sites without expanding the sites. This expansion is accomplished by a displacement of the four neighbouring anions away from the cations along their bond axes and by a possible simultaneous shrinkage of the anions in the B site octant. The distortions are of two types, one for which $c/a < 1$ as in $CuCr_2O_4$[36] and the other for which $c/a > 1$ as in Mn_3O_4[70]. In both materials, experimental evidence for the existence of the Y.K. state has been reported, the former by Prince[36] and the latter by Jacobs[38].

Outside the Néel and Y.K. stability region, the ground state is shown to be an antiferromagnetic $[100]$ spiral for most parts of the limited ranges of AB and BB interactions which were considered. Furthermore, Menyuk et al.[40] examined the corresponding stability regions for temperatures approaching the highest transition temp-

erature and concluded that in tetragonal spinels neither Y.K. nor ferrimagnetic-spiral configurations can exist at the highest transition temperature. In other words, ferrimagnetic material with a non-collinear ground state at 0° K must possess at least two transitions. It is interesting to note that these conclusions were earlier derived in connection with the derivation of the Y.K. theory (section 8.6.2). The results of neutron diffraction on manganese chromite have been reported by Corliss and Hastings[71] to be in good agreement with the postulate of a ferrimagnetic spiral rather than a triangular ground state, and the presence of more than one transition temperature. The experimental results, on mixed cadmium manganites, reported in this thesis, seem to substantiate these predictions by providing additional evidence.

CHAPTER IX

EXPERIMENTAL

9.1 Introduction

Many methods are now available for determining the magnetic susceptibilities of weakly magnetic materials, following the classical works of Faraday, Curie and Gouy. The modern devices are either improvements of the earlier methods employing the principle of a force balance with sensitive optical or transducer operated indicator systems[72,73,74,75,76,77,78,79,80] or are so-called vibrating coil and vibrating sample magnetometers[81,82,83,84]. The use of a strain gauge balance and of an electromagnetic balance using a differential transformer have also been reported, the former by Lundquist and Mayers[85] and the latter by Scheringer[86] and Butera[87]. Strakhov and Shan'tsze[88], on the other hand, have used a ferro-electric sensor element in place of a Hall transducer to give greater sensitivity and stability of operation.

9.2 Theory of the force balance

Despite certain disadvantages arising from the use of an inhomogeneous field, the Faraday method of measuring susceptibility is still one of the best of the existing measuring techniques where only small samples are available. The method depends simply on measuring the force experienced by the material when it is placed in a magnetic field gradient. It can be shown (see, for instance,

Bleaney and Bleaney[89]) that the x-component of the force on the sample with magnetic moment I is given by

$$F_x = I_x(\partial H_x/\partial x) + I_y(\partial H_y/\partial x) + I_z(\partial H_z/\partial x) \ . \qquad (9.1)$$

If the material has a volume susceptibility χ and volume V, its moment I will be

$$\underline{I} = \chi V \underline{H_i} \ , \qquad (9.2)$$

where $\underline{H_i}$, the field inside the sample, is given by

$$\underline{H_i} = \underline{H} - N\chi\underline{H_i} \ , \qquad (9.3)$$

assuming that the shape of the sample is such as can be described by a demagnetizing coefficient N. Thus

$$F_x = \frac{\chi V}{1 + N\chi}(H_x\, \partial H_x/\partial x + H_y\, \partial H_y/\partial x + H_z\, \partial H_z/\partial x)$$

$$= \tfrac{1}{2}\frac{\chi V}{1 + N\chi}\left(\frac{\partial}{\partial x}\ \underline{H}^2\right) \ . \qquad (9.4)$$

If the field is so arranged as to give a large value of $\partial H_y^2/\partial x$ while the quantities $\partial H_x^2/\partial x$ and $\partial H_z^2/\partial x$ are negligibly small, then

$$F_x = \tfrac{1}{2}\frac{\chi V}{1 + N\chi}\left(\frac{\partial}{\partial x}\ H_y^2\right) \ . \qquad (9.5)$$

Since, with the values of χ (10^{-3} or less) ordinarily encountered, $N\chi \ll 1$, the magnetic field inside the specimen can be taken to be the same as the value measured before the specimen was introduced. Hence the x-component of the force becomes

$$F_x = \tfrac{1}{2}\chi V\left(\frac{\partial}{\partial x}\ H_y^2\right) \ , \qquad (9.6a)$$

$$= \tfrac{1}{2}\chi_g\, m\left(\frac{\partial}{\partial x}\, H_y^2\right) \quad \text{where } \chi_g = \text{susceptibility per gm.}$$

and m = mass of the sample in gm. (9.6b)

Strictly speaking, equation (9.6a) is correct for a sample of infinitesimal size. For a finite sample, one obtains

$$F_x = \tfrac{1}{2}\chi \iiint \left(\frac{\partial}{\partial x} H_y^2\right) dV \ . \qquad (9.7)$$

The integration should be carried out in cases where large field gradients and large specimens are used to increase the sensitivity and accuracy. Experimentally, a simplification is provided by making $H_y \partial H_y/\partial x$ constant over the specimen and this is accomplished by using shaped pole-faces in the electromagnet. The main difficulty arises from the fact that the value of $H_y \partial H_y/\partial x$ is usually constant over only a rather small volume in the case of a large field gradient, and different specimens must therefore be placed accurately in the same position relative to the field to obtain correct results.

An alternative approach is that due to Gouy which provides a better method if large quantities of a substance are available. The specimen is made into a long cylinder of uniform cross-section with one end hanging between the poles of a magnet. The vertical force in the x direction is then found, by integrating equation (9.4) over the length of the specimen, to be

$$F_x = \tfrac{1}{2} \alpha \chi (H_1^2 - H_2^2) \ , \qquad (9.8)$$

where α is the cross-section of the rod and H_1, H_2 are the values of the field at the lower and upper ends of the rod respectively. If $H_2 \ll H_1$, only the homogeneous field at the centre of the magnet, H_1, need be known, although the force is developed from the inhomogeneity of the field.

It is, perhaps, of some interest to discuss the relative merits of the two methods before arriving at a final decision as to which is to be used. For the same material, the Gouy method gives

greater sensitivity, but it is often difficult to make specimens in the form of a long cylinder of uniform cross-section and density. With the small quantities of powdered samples available in the present investigation, the Faraday method was the obvious choice. The small size of the sample was also helpful in realizing an almost constant $H_y \partial H_y/\partial x$ over its volume and enabled studies of field and temperature dependences of the magnetic susceptibility to be easily made. In addition, with the Faraday method, the Honda correction[90] for ferromagnetic impurities can be applied much more accurately. The great advantage of the Gouy method is that it permits absolute measurement of susceptibility to be made with considerable accuracy. By contrast, a precise knowledge of the value and the variation of the non-uniform field and of the position of the sample in the Faraday method is difficult to obtain (and relative measurements with respect to a known sample are usually carried out).

9.3 The Sucksmith ring balance

9.3.1 Design requirements

Having selected the Faraday method, the problem was now to make a decision on the type of balance to be constructed. To make a rough estimate of the magnitude of the force involved, it would be seen that for $\chi_g \simeq 10^{-4}$ emu/gm, H = 5 kOe and $\partial H/\partial x \simeq 10^3$ Oe/cm, the force is 500 dyne per gm of the sample. With about 50 mgm of the specimen placed in the inhomogeneous field, the total force is only 25 dyne and the balance should be sensitive

enough to detect at least 0.1 dyne and preferably 0.05 dyne. The force detector should be capable of recording this in the presence of a standing load of about 5-10 gm caused by the weight of the suspension and other ancilliary attachments. Though sensitive versions of torsion balances or chemical balances can be made to fulfil these requirements, it was decided to set up a modified Sucksmith ring balance equipped with a split-photocell amplifier device to give the desired sensitivity and accuracy. The advantages of simplicity, ease of operation and a quick-reading device suitable for measurements in varying temperatures and fields are all combined in this balance, while the major problems of mechanical vibrations and thermal instabilities such as drift can be overcome to a large extent by the use of suitable materials.

The design requirements for the balance should also include the necessary adjustments to be made for its use at low temperatures down to liquid helium and at high temperatures up to about 1000° K. The magnet used was a large 7" Newport electromagnet. Although a specially designed low-temperature cryostat and a small high-temperature furnace were used to keep the pole-gap to a minimum, it could not be reduced to less than 2" owing to heat insulation problems associated particularly with the high temperature measurements. Using about 20 amp current per coil, fields of the order of 9 kOe and 6 kOe were obtained at the centre of the pole-gap and at the edge of the (cylindrical) pole-tips respectively. In a preliminary experiment using a Hall probe, the region of maximum $H\,\partial H/\partial x$ was found to lie on a radius about one cm outside the edges

of the pole-tips and in the plane bisecting the pole-gap. The value of $H\,\partial H/\partial x$ was about 12×10^6 Oe^2/cm.

9.3.2 The balance

The ring was made from a $\frac{1}{2}$" wide and 0.006" thick phosphor-bronze strip and supported by an adjustable hook as shown in Fig. 47. A circular disc of 'dural' alloy, $\frac{1}{2}$" thick and 14" in diameter formed the base plate which had its top side finely turned on a lathe. The support for the ring and for the lifting mechanism for the calibrating weight was provided by means of a brass strip, 1" wide and $\frac{1}{4}$" thick, bent into a U-shape as shown in Fig. 47 , and screwed into the base plate. The diameter of the ring was 10 cm. Two concave mirrors, each of focal length 50 cm, were attached to the ring at M_1 and M_2 where the lines joining the mirrors to the centre of the ring made angles of 49° with the horizontal - the condition for maximum sensitivity[91]. An electromagnetically operated lever arrangement placed the calibrating weight (30 mgm) on the mica shelf P attached to the lowest point of the ring. The weight was kept hanging away from the balance when not in use, by means of the spring Q.

The base plate was mounted on the top of a rigid dexion frame using foam rubber pads for the anti-vibration mounting. The arrangement considerably reduced mechanical vibrations. In addition, the balance was provided with a system of eddy current damping by means of four aluminium discs which were attached to the suspension and held in the narrow gap of each of four small galvanometer-

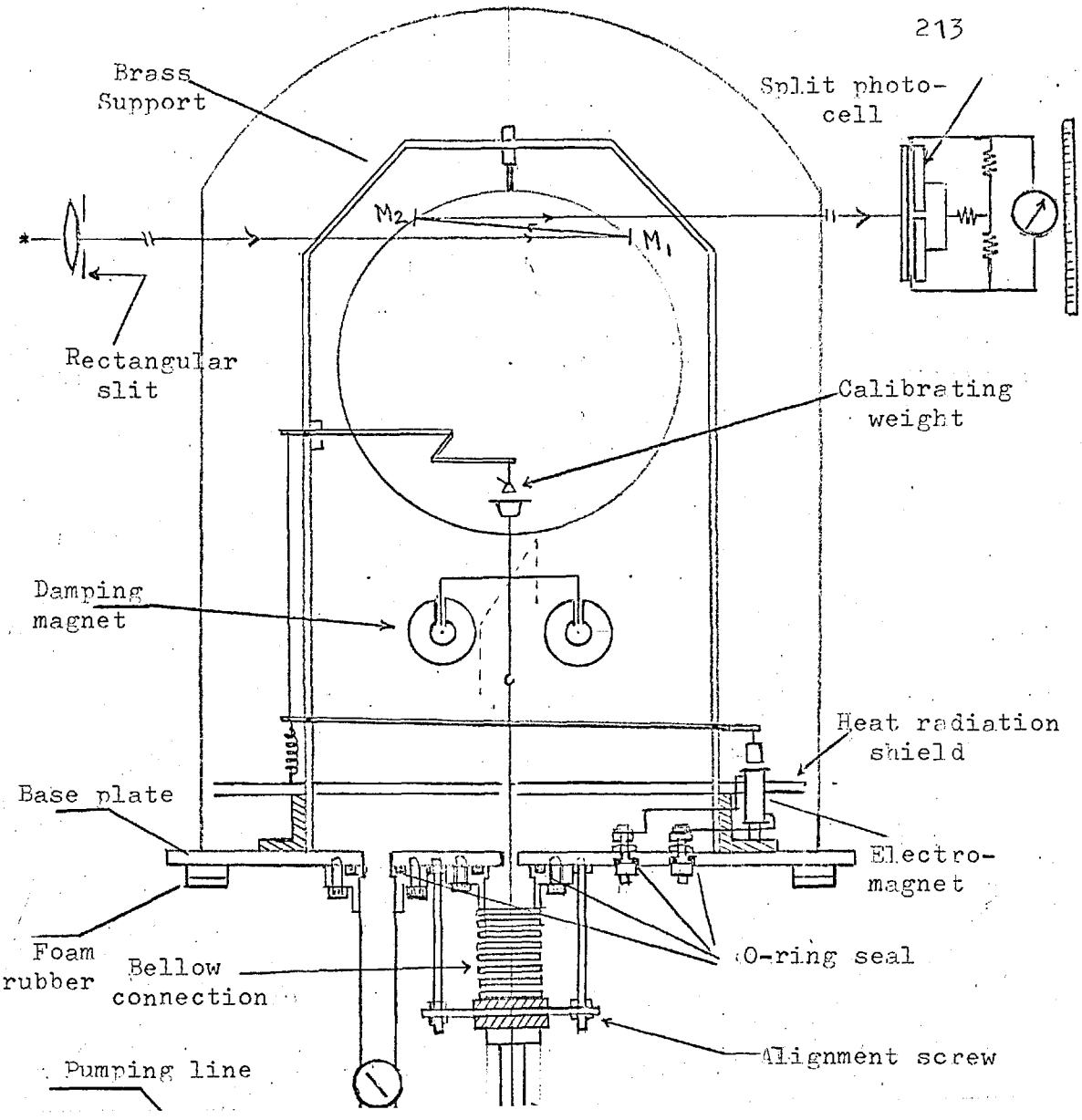
Brass Support
Split photo-cell
M_2
M_1
Rectangular slit
Calibrating weight
Damping magnet
Heat radiation shield
Base plate
Electro-magnet
Foam rubber
Bellow connection
O-ring seal
Alignment screw
Pumping line

magnets. The suspension, about 90 cm in overall length, consisted of three separate pieces. The top part was made of thin brass wire ending in a hook and this in turn supported the other two pieces which were quartz. By fusing the quartz tube into the shape of a tiny ring or hook at the end, the pieces could be easily joined together or dismantled. By this arrangement, any disturbance imparted to one end of the suspension was found to be greatly attenuated while travelling to the other end. It was thus possible to maintain the specimen holder freely in suspension inside the narrow space of the 1 cm diameter vacuum tube enclosing the specimen. The weight of the whole suspension assembly was about 4-5 gm. A glass bell-jar, 12" in diameter and fitted with an L-shaped rubber gasket was made to sit under a vacuum seal on the base plate when the pump was in operation. All connections to the inside of the chamber were made through holes cut in the base plate and sealed by Edward's standard metal flanges, joints and o-rings. Plate 1 gives a general view of the balance and the optical system.

9.3.3 The optical system

The optical part of the balance consisted of a 4V, 8 watt lamp assembly and a split photo-cell amplifier device both rigidly mounted on either side of the balance at approximately the same height as the mirrors. A rectangular slit placed close to the focussing lens produced, after reflections at the two mirrors, a sharp image on the photo-cell covering an area equal to that of either half of the cell. This resulted in maximum sensitivity and linearity of

response of the photo-cell. The principle of operation of the photo-cell has been described in section 4.3.3 of part I of this thesis. The recording galvanometer in this case was a Cambridge type (L-371173), of resistance 830 Ω and period 3.4 sec and of 4500 mm/μA current sensitivity and 20,000 Ω damping resistance. The photo-cell used was of the selenium rectifier type (barrier layer), 27 mm by 40 mm and was split parallel to the shorter side. The damping resistance was equally distributed between the two halves of the photo-cell circuit as shown in Fig. 47 . With an unregulated 4V a.c. supply to the primary lamp and a uniform light intensity over the spot focussed on the photo-cell, the overall performance of the galvanometer amplifier was found to be quite satisfactory. The stability and degree of freedom from zero drift were further improved by covering the whole optical system in cardboard boxes with their insides painted black. The stray light from the room or the associated temperature fluctuations had no effect whatsoever on the photo-cell and the thermostatic stability of the balance was attained easily and quickly without any external power regulation.

9.3.4 The measurement technique

Fig. 48 shows the relationship between the net photo-current and the displacement of the light spot across the cell; it exhibits linearity for the full range of the scale. However, in actual practice, much larger deflections had to be dealt with so as not to alter the sensitivity and a null method was considered

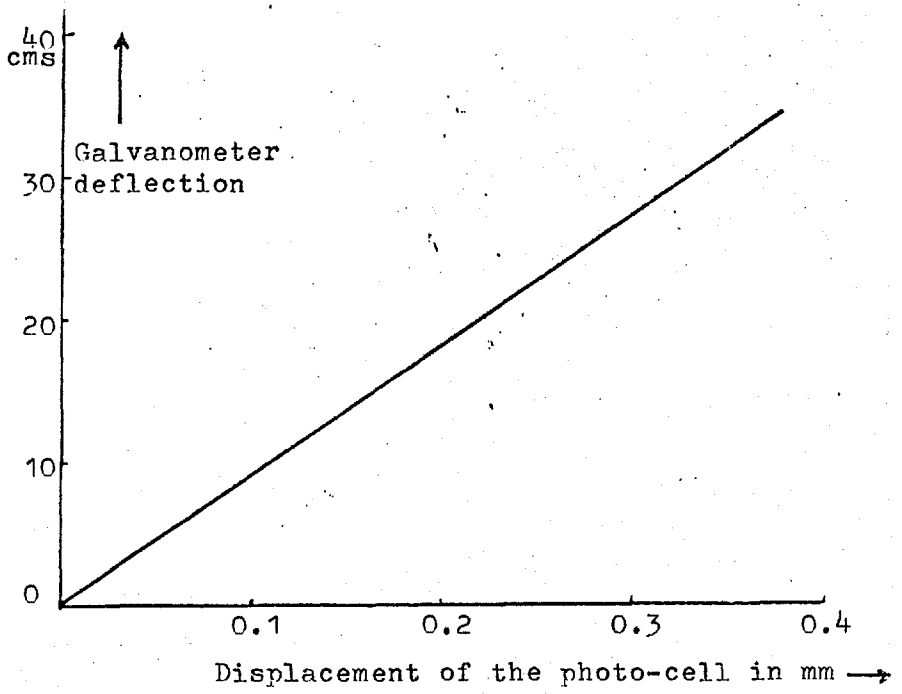

Fig. 48. Calibration of the galvanometer amplifier

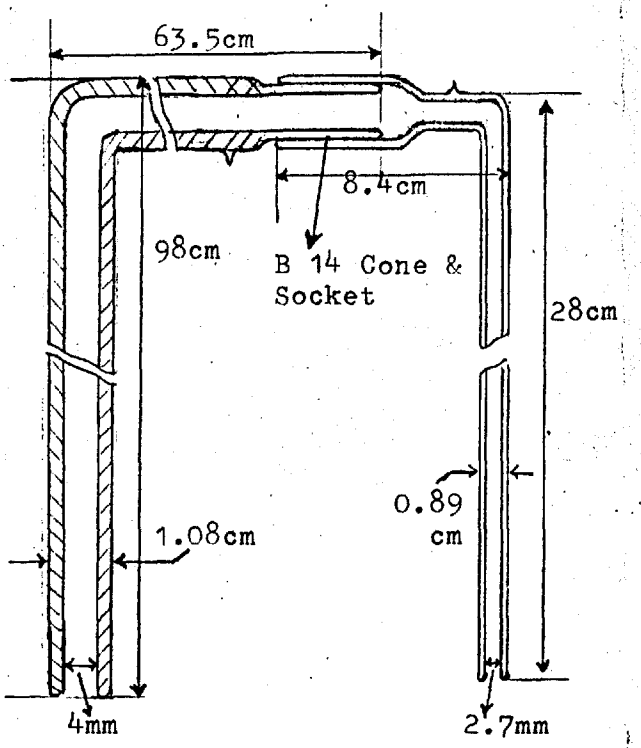

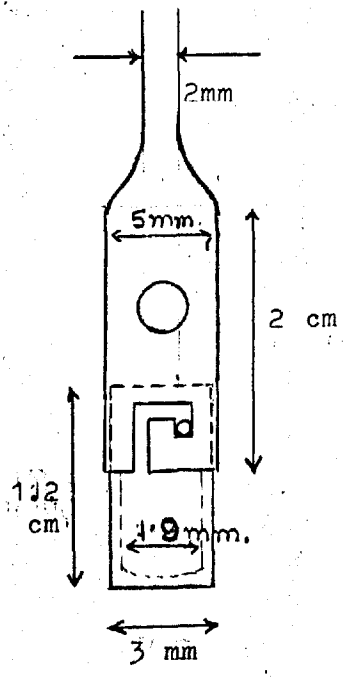

Fig. 49. The specimen holder

Fig. 50. The glass transfer syphon with the demountable coupling

necessary. This can be achieved in two ways, namely, by counter-balancing the magnetic pull on the specimen with the force exerted on a small current-bearing coil by a permanent magnet or, secondly, by moving the photo-cell unit parallel to itself until the zero of the reading scale is restored. While the former method incorporates the basic advantage of the latter, that is, it brings the light-spot to the same position on the photo-cell each time, the sensitivity of the balance is generally reduced by the connection of the current leads to the moving parts of the balance. If however, the displacement of the specimen is so small that $H\,\partial H/\partial x$ can be made substantially independent of x, the second method is preferable to the first. With an estimated value of x of about 10^{-3} cm corresponding to a 1 mm shift of the light on the photo-cell, the condition of constant $H\,\partial H/\partial x$ is sufficiently maintained to justify the use of the second method. The photo-cell was therefore mounted on a metal frame which could be moved vertically upward or downward on a guide track, its movement being recorded by means of a micrometer. For convenience of zero adjustment, a transverse motion of the photo-cell was also provided by setting up the unit on a travelling stage. The device thus measured the actual shift of the light spot at the cell rather than the galvanometer deflection and no tacit assumption regarding the proportionality of the photo-current to displacement was necessary.

9.3.5 The sensitivity of the balance

The smallest force detectable was about 0.08 dyne which

corresponded to less than 5×10^{-5} emu in magnetic moment or 10^{-8} cgs in susceptibility for a 1 gm sample in a field of 6 kOe. The accuracy in measurement of susceptibility was estimated to be 1 - 1.5%.

9.3.6 The specimen holder

Several attempts were made to design the most suitable sample holder which could easily be operated within the narrow space available and be made of quartz or silica. The help of a competent glass blower was necessary to make one that was satisfactory for the purpose. As shown in Fig. 49, the lower end of the quartz suspension tube was first blown into a wide-necked outer tubing. A slot was then cut inward from the end of the quartz tube and this had a right angle bend as shown. A small quartz capsule measuring 12 mm by 1.9 mm was drawn out of a larger piece and a tiny hook was attached to it near the open end. The capsule containing the sample could then be held in position by the hook entering the slot and a close-fitting outer case prevented the capsule from moving. The overall diameter of the assembly was just less than 6 mm which left a clearance of about 2 mm between the capsule and the inner wall of the vacuum enclosure. The specimen holder had a thin wall to give poor thermal insulation to the material under study. In actual experiments, the mass of the specimen used varied from 40 mgm to 100 mgm and this covered approximately lengths of 4 to 8 mm inside the capsule.

9.4 The magnet and the power unit

All measurements were done using a Newport 7" electromagnet with a pole-gap of 2". At the maximum power of 6 kilo-watt, this gave a field of 6 kOe at the edge of the pole-tips and a field gradient of 2×10^3 Oe/cm that was substantially constant over the length of the specimen. The magnet was mounted on a trolley running on rails which allowed it to be removed from the rest of the apparatus when placing the specimen in position. For precision location of the sample in the field, vertical and sideways movements of the magnet were also provided by including a sliding base, fitted with levelling screwbolts, between the magnet turntable and the trolley. The whole arrangement thus provided extreme flexibility in three dimensions in addition to the rotatory motion afforded by the turntable.

The power unit for the magnet was designed and built by E. M. Wareham (Measuring Systems) Ltd. specifically to give a stabilized current supply, with very low ripple content, up to 6 kilo-watt. It essentially consisted of a series of condenser banks and silicon controlled rectifiers (SCR) in which the stored energy derived from the rectified input voltage was used to deliver power to the load. The output current had a short term stability better than 2 mA (minute to minute), long term stability (hour to hour) better than 10 mA and a regulation of less than 0.1% for a 10% change of either mains input voltage or load voltage. Plate 1 gives a general view of the magnet in position.

9.5 Low temperature measurements

The low temperature measurements involving the use of liquid helium made it necessary to set up a complete helium conservation system including a storage vessel, transfer syphon, cryostat, low pressure gas storage, compressor and high pressure gas cylinders.

9.5.1 The design of the cryostat

The conventional helium cryostat based on a double-dewar design was unsuitable for use with a narrow pole gap. The most promising of the new designs consists of an inner dewar of which only the upper portion is surrounded by a liquid nitrogen jacket[92]. The liquid helium in the lower part is shielded by a copper cylinder which is suspended from, and cooled by, conduction to the nitrogen reservoir. Thus there are only three walls separating the working space in the lower portion from the outside and these can be arranged to be close together resulting in considerable reduction in the size of the lower portion. Although metal dewars enable further economy of space, it was decided to make a glass dewar for reasons of inherent simplicity, economy of construction and ease of disassembly for cleaning, etc. The final dewar, made of Pyrex, is shown in Fig. 51 . The nitrogen jacket runs down to the point at which the cryostat narrows, thus giving an adequate storage volume for the liquid. Below this level, the shielding is provided by the copper cylinder made from 0.012" thick sheet and rolled into the desired shape and size. It was important that the shield did

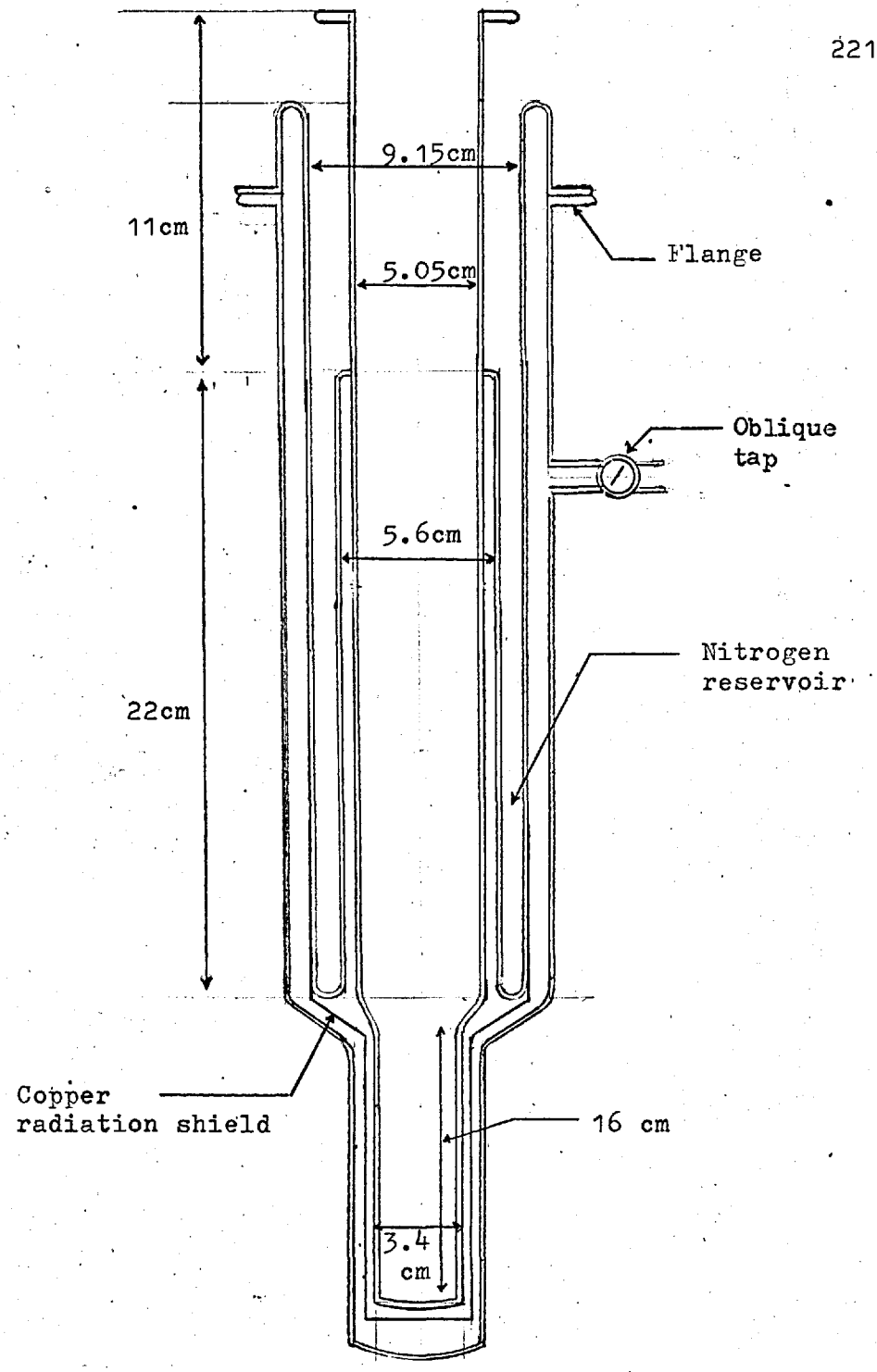

Fig. 51. The glass dewar for liquid helium

not touch any part of the inner or outer wall of the dewar when finally assembled. A ground flange joint in the outer glass near the top permitted easy demounting as well as a support for the assembled dewar during use. Since, however, Pyrex is somewhat permeable to helium gas, a side vacuum line with a tap was provided which enabled evacuation of the gas from time to time. An oblique tap was found more satisfactory as the large pressure difference caused by liquid helium between the inlet and outlet sides of the tap sometimes opened up fine leaks along the curved portion of the greased surfaces of the ordinary tap. For the flange joint at the top, Edwards high vacuum silicon grease was found satisfactory as this has a greater heat stability over a temperature range of -40° C to 200° C. It was however found that the close proximity of the flange joint to the open end of the nitrogen reservoir resulted in freezing of the grease due to prolonged exposure to the cold nitrogen vapour and also by conduction developing occasional leaks in the vacuum. To off-set this, a small 10 watt heater coil with a thermo-couple regulated power supply was set up which maintained the neck of the dewar at a substantially uniform temperature. Plate 2 shows the disassembled dewar parts. The cryostat was sealed at the top by means of a metal cap which rested against a rubber washer over the flanged end of the innermost vessel and was clamped together by terry clips. The transfer syphon into the cryostat was introduced through one of the two off-centre holes made in the cap while the other hole was connected to the gas return pipe through a valve.

9.5.2 The heat losses in the cryostat

Although it is often difficult to calculate accurately the total heat loss in cryostats unless the physical properties of the various materials operating at temperatures vastly different from the ambient temperature are well known, a rough upper limit can always be quoted. The main factors contributing to the heat loss in the present arrangement are summarized below together with their estimated value in each case:

(i) the radiation across the vacuum space - the heat transfer by radiation between the innermost wall at 4.2° K and the adjacent wall at 77° K is found to be equal to 4.28×10^{-3} watt.

(ii) the conduction down the neck of the vessel - this is estimated to be about 0.0133 watt (from room temperature to 4.2° K).

(iii) the conduction down the central $\frac{1}{2}$" german-silver tube - taking the average value of the thermal conductivity as 0.18 between 300° K and 4° K, the corresponding heat transfer is calculated to be 0.14 watt.

(iv) the room temperature radiation entering the german-silver tube along the optical reflection path - assuming a perfect specular reflection from the inner wall of the tube, this loss is estimated to be 0.0408 watt. In practice, isolation from room temperature radiation can be effected by means of a bend in the tube or insertion of a small radiation baffle.

(v) conduction through the low-pressure exchange helium gas inside the german-silver tube or inside the cryostat - the total heat transfer in the latter case is calculated to be 0.442p watt approximately where p is the pressure of the gas in microns. For $p = 10^{-6}$ cm of Hg, this is equal to 0.0044 watt. The heat loss in the former case is estimated at 0.026 watt for a pressure of 10 microns which indicates that helium can be conveniently used for the exchange gas without seriously impairing the thermal insulation.

(vi) Joule heating in and conduction through the electrical leads - the total loss is estimated at 0.014 watt.

The total heat leak to the cryostat system thus comes to 0.243 watt which is equivalent to 208 cal/hour. If it is assumed that this quantity of heat is all used to evaporate the liquid, it would mean that 320 c.c. of liquid helium would boil off per hour neglecting the fact that the cold evaporating gas cools the wall of the german-silver tube and the vessel's exit and thereby reduces the heat leak. On the other hand, if there were complete heat exchange with the outflowing gas so that the latter had increased its enthalpy from 4.2° K while gaining heat from the various sources described above and had finally left the vessel's exit at room temperature, the liquid would have evaporated at a rate of only 4.2 c.c. per hour. In the actual experimental set up, test measurements showed that, after precooling to 4.2° K, an initial filling of 200 c.c. of helium would last for about 3 - 4 hours. The heat exchanger for the

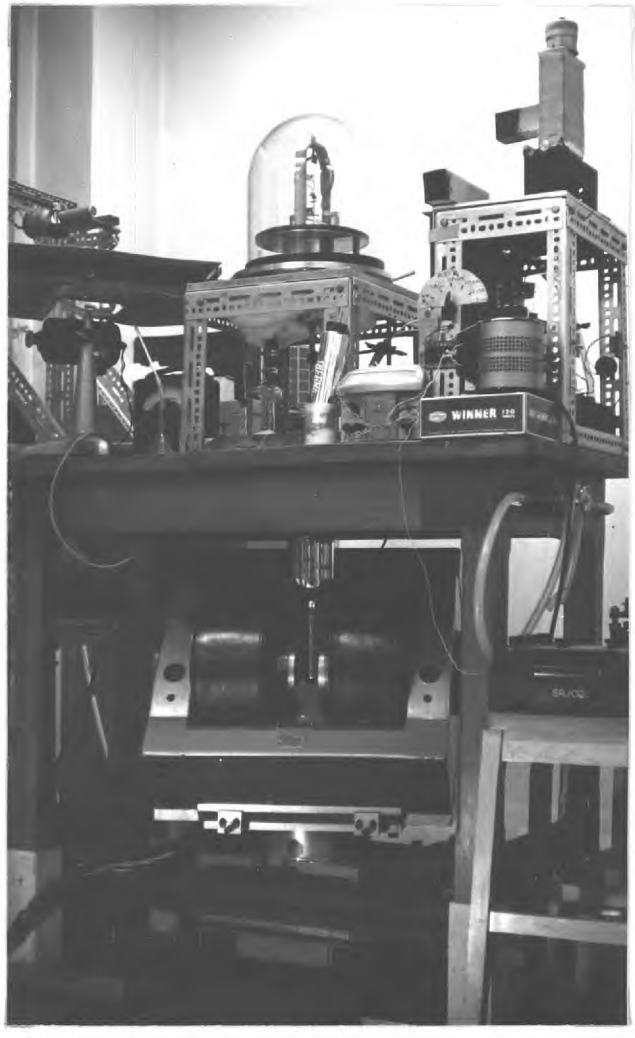

Plate 1. Showing a general view of the balance, the dewar and the 7" electromagnet.

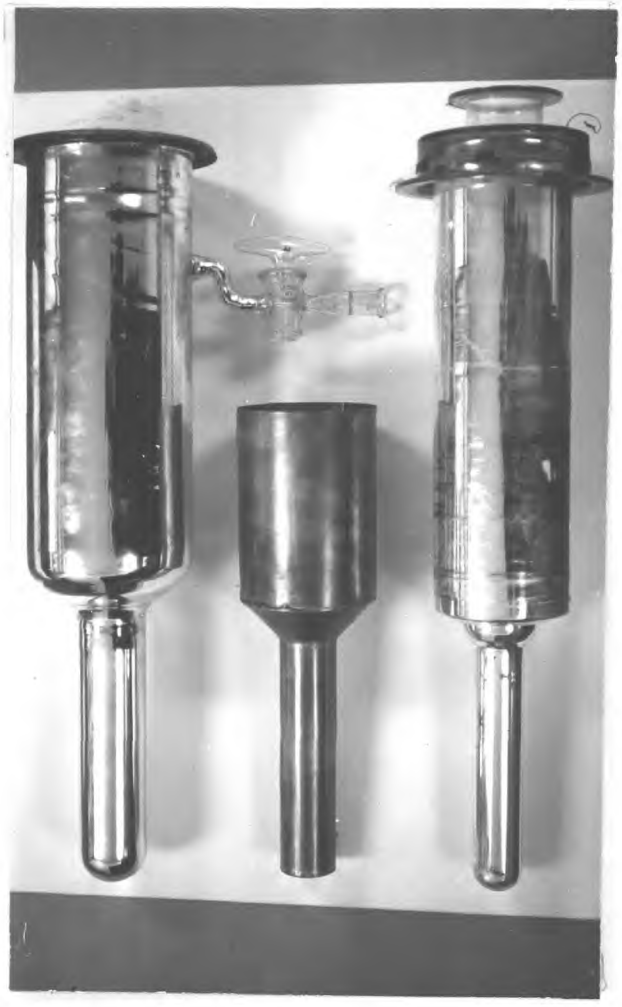

Plate 2. Showing the disassembled parts of the helium dewar.

out-flowing gas consisted of a perforated copper shield, half way down the neck of the vessel and closely fitting the inside of the dewar. The empty space above the heat exchanger was filled with a block of foamed polysterene leaving narrow passages for the transfer tube and for gas collection.

9.5.3 Access to the specimen

The lower end of the german-silver tube (63 cm long, 1.1 cm i.d., and 0.008" thick) was soldered to a copper end cap which consisted of two pieces with a truncated joint as shown in Plate 3. The whole unit was 7.5 cm long and 1.8 cm in o.d. and provided an effective thermostatic bath for the specimen. The pieces could be sealed together by means of vacuum grease or low temperature solder, e.g. Wood's metal, in which case the lead solder used for fixing the upper piece to the supporting tube remained intact. Access to the specimen was obtained by undoing the low temperature seal and then taking the capsule out of the specimen holder.

9.5.4 The transfer syphon

Owing to the close proximity of the balance to the cryostat assembly, the transfer syphon had to be provided with a demountable coupling. For reasons of low cost, simplicity of construction and good insulation properties, it was again decided to make a glass transfer tube of the desired specifications. The demountable coupling was effected by using a standard glass B14 cone and socket which were made double-walled and fused to the respective main tubes

as shown in Fig. 50. The diameter of the shorter section of the syphon was made smaller than that of the other part so as to fit into the limited space inside the cryostat and yet offer no substantial resistance to the flow of the liquid. The co-axial tubes were thin walled 'Pyrex' separated from each other by insulating spacers of triangular shape, used sparingly along the tube. The differential thermal contraction between the inner and outer walls of the syphon was not serious and this was taken account of by allowing some looseness between the spacers and the outer casing so that the contraction did not subject the assembly to undue stress. In addition to this, the tube was thoroughly annealed before silvering. Although the syphon was permanently sealed off after initial evacuation and worked perfectly well under the efficient "getter" action of the liquid helium, it needed re-evacuation after some 80-100 hours of use when it tended to go 'soft' due to slow diffusion of the gas inside the evacuated annulus. This was observed as formation of cold spots at each spacer position during the transfer, indicating heat leaks. It was found desirable to mount the socket portion of the union on the low pressure side to ensure a free flow of helium. By sealing the exterior of the union with a rubber sleeve or sellotape, the enclosed gas prevented the liquid from flowing outward. The use of vacuum grease for the ground glass surfaces of the union was not helpful as the grease hardened on cooling and cracked causing leaks to the coupled system.

The dimensions of the glass syphon are given in Fig. 50. The tube was found to start transferring liquid in about 5-7 minutes

and in a typical run about 800 c.c. of helium would be consumed in precooling the cryostat and the syphon and in collecting about 200 c.c. of liquid in the cryostat. In cases where the liquid level had fallen low enough to need refilling, some helium was inevitably used up in this operation as the relatively warm gas, blowing out of the syphon tube, caused evaporation of a considerable quantity of helium already present in the vessel. For this reason, the transfer was generally carried out in one single operation after which all magnetic measurements were started.

9.5.5 Level indicator

The level indicators were of two types, (i) a rubber diaphragm level finder for use in the Dupree Swift Duplex storage vessel and (ii) a carbon resistor and thermistor for use in the cryostat.

It has been known for some time[93] that thermal oscillations may occur in a narrow gas filled tube which has one end at room temperature and the other at the temperature of liquid helium. A dipstick probe working on this principle was reported earlier[94] and Fig. 52 shows the design of the probe used here. When the open end was gradually lowered into the storage vessel, oscillations began to occur and then decreased abruptly in intensity (about 60%) and frequency (about 30%) upon touching the liquid surface. The level was detected by feeling or watching this sudden change in the vibration of the diaphragm and the level could be measured to within $\pm$ 1 mm with care. With a smaller diameter tube than that used here,

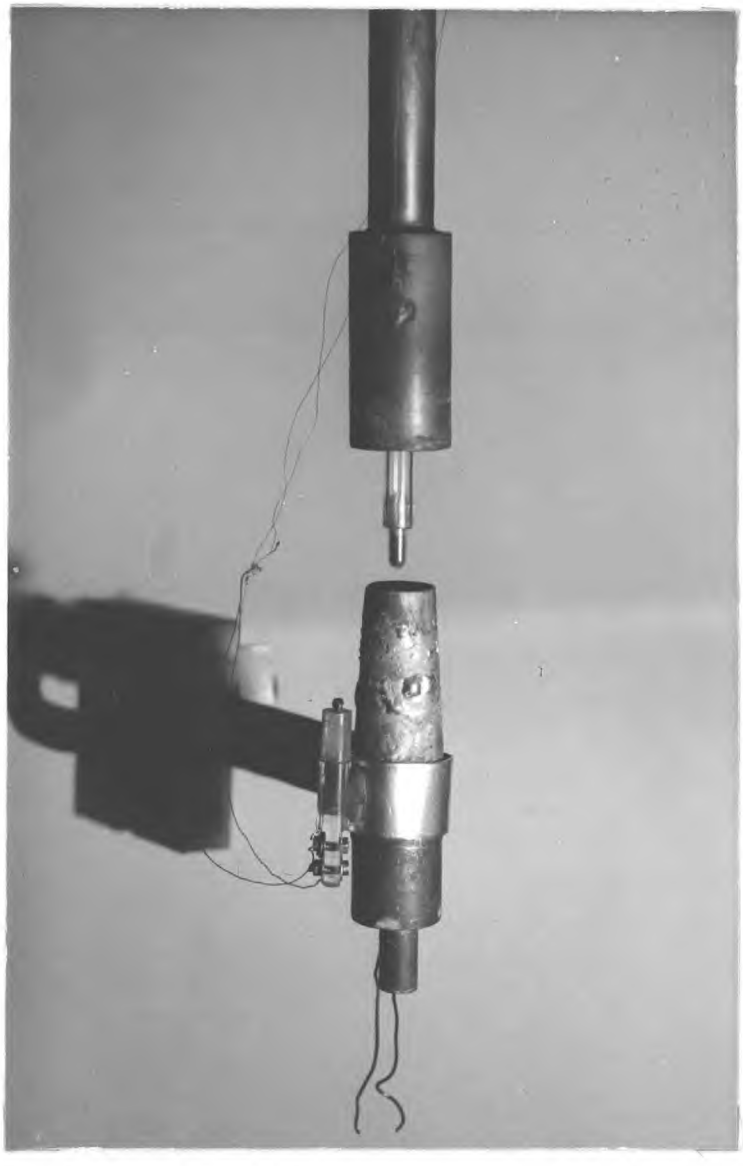

Plate 3. A view of the detached copper end-cap which encloses the specimen holder; the lower narrow tube holds the thermistor which is also shown in the photograph.

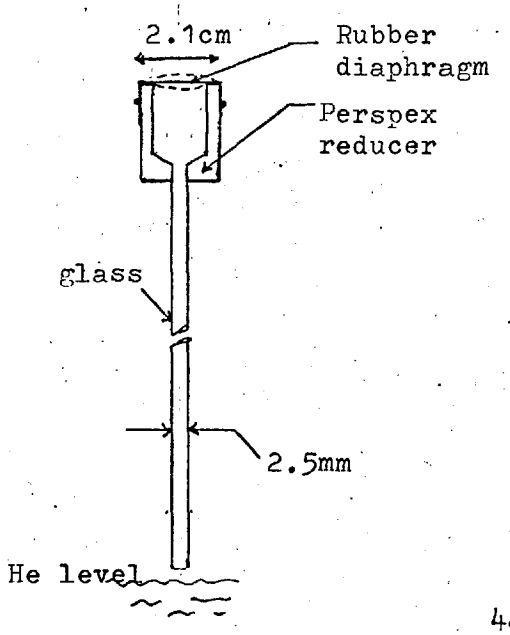

Fig. 52. The level indicator

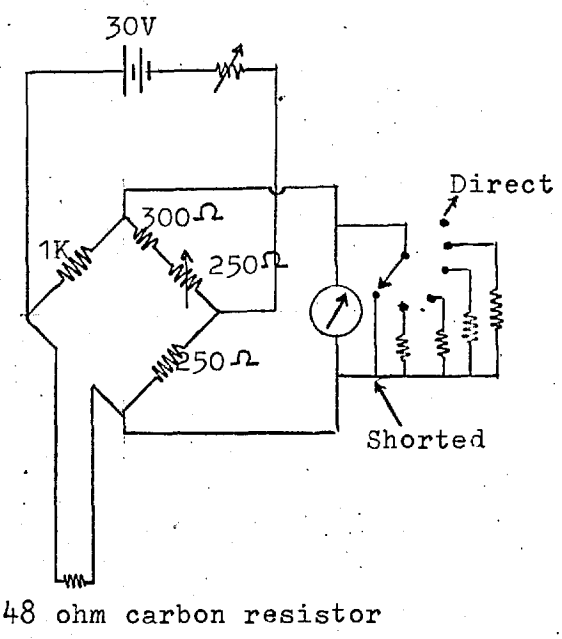

Fig. 53. The bridge circuit for the carbon resistor

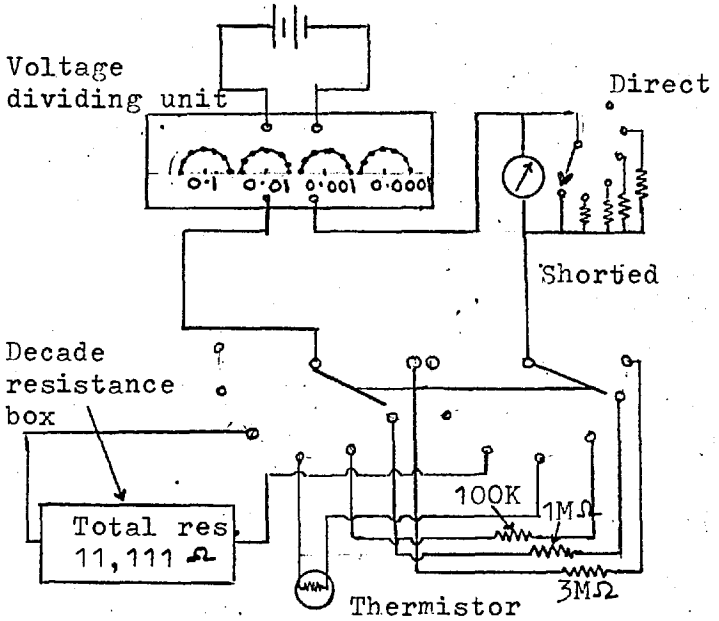

Fig. 54. The circuit for the thermistor level finder

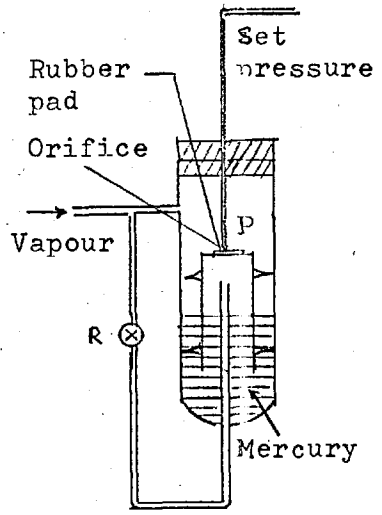

Fig. 55. The Cartesian Manostat

the loss of helium was found to be less but the air occasionally got frozen inside the tube stopping the oscillations altogether. With a larger diameter tube, the intense oscillations could disturb the level so much that no reliable indication of level was possible.

The second device depended for its operation on the high (negative) temperature coefficient of resistance of a carbon resistor at low temperatures and also on the fact that electrical heating is greater when the resistor is in the helium gas than when it is in the liquid[95]. The heating current is rather critical because when it is too low, the resistor does not heat up sufficiently in the gas and when it is too high, it heats up even when inside the liquid.

Fig. 53 shows the bridge circuit used for the 48Ω carbon resistor used here. The latter was fixed to the german-silver tube at the appropriate height and was thermally insulated from it. The bridge was balanced when the liquid filled up to that level and the out-of-balance current produced the deflection as soon as the resistor came out of the liquid.

A highly sensitive sensing element - a thermistor with a greatly reduced energy gap - was later set up for level indication near the specimen as well as for use as a supplementary means of temperature measurement below 20° K. The thermistor, supplied by Keystone Carbon Company, U.S.A. was in the shape of a small disc 0.1" in diameter and fitted with two silver leads. It had a nominal resistance of 11.6Ω at 90° K rising to 2.86 MΩ at 4.2° K with a standard tolerance figure of about 20%. The sensitivity increased

nearly proportionally to $1/T^2$ and the high value of resistance at low temperatures eliminated the need for correction for lead resistance. The large temperature coefficient together with the very low specific heat of the material below 20° K permitted a temperature increment of only a few degrees above the environment (corresponding to a transition from liquid to vapour phase) to be sufficient to produce a large signal. For the purpose of temperature measurement, its resistance was determined by comparison with standard known resistances in the circuit as shown in Fig. 54 . The calibration curve of the thermistor is given in Fig. 56 .

Plate 3 shows the method of mounting the sensor element to the specimen enclosure. A perspex rod with two small holes drilled right along the length was used for holding the disc and for taking out the connections. The unit could then be supported by the copper head which was permanently soldered to the copper enclosure of the specimen. Thus good thermal contact was ensured.

9.5.6 Temperature measurement and control

The temperature of the sample was measured using a copper-constantan thermocouple from room temperature down to 77° K and a thermocouple of silver containing 0.37 atomic percent gold and gold containing 2.1 atomic percent cobalt, from 77° K down to 4.2° K. Below about 20° K, the latter was supplemented by the thermistor thermometer described in the previous section. The thermo-electric power of the silver-gold gold-cobalt thermocouple is about 16 μV at 20° K decreasing linearly with temperature below that point. Since

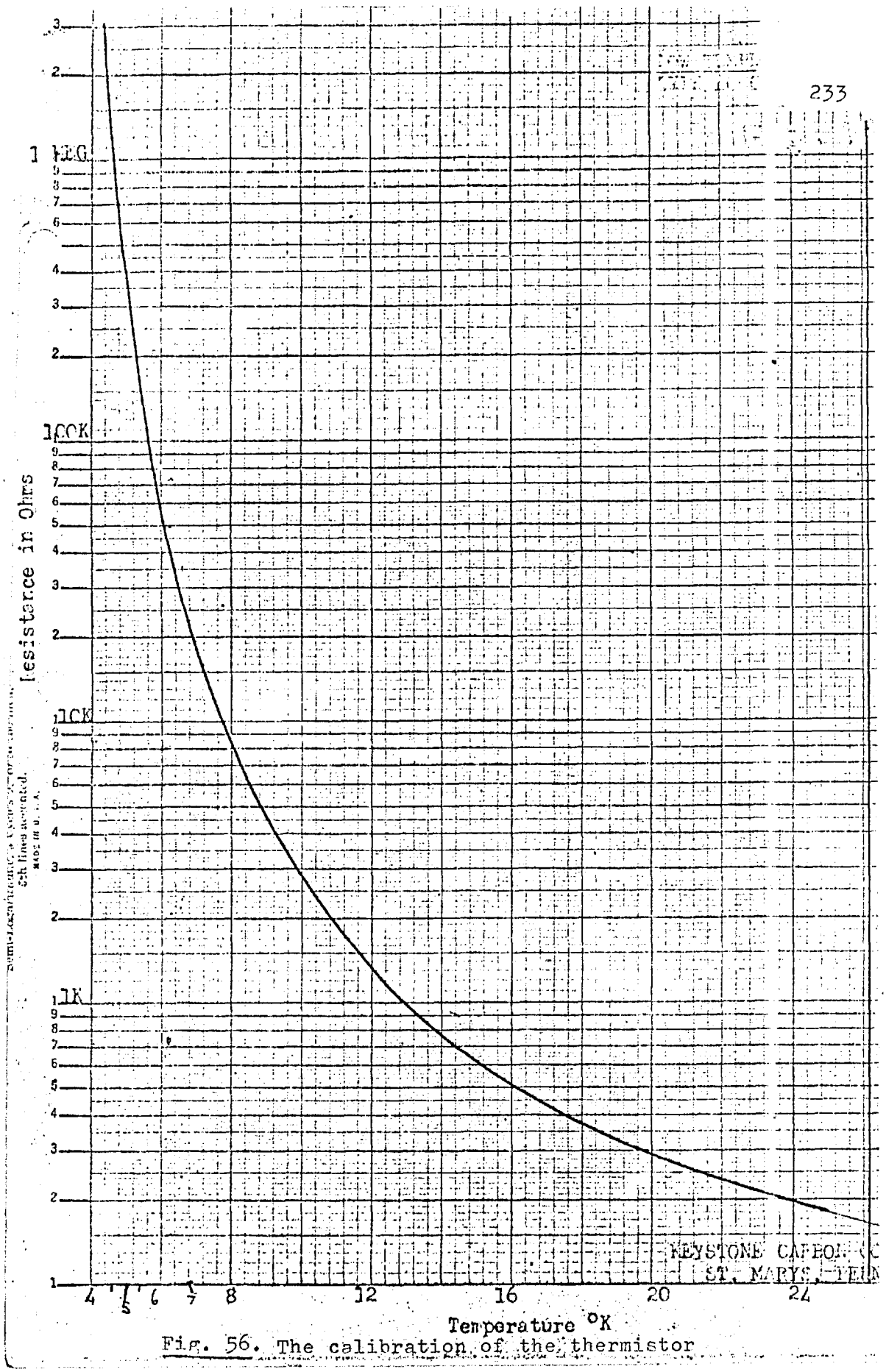

Fig. 56. The calibration of the thermistor

the composition of the alloy is known to be far less homogeneous than that of the pure metals, the thermocouple was re-calibrated (reference junction at liquid oxygen temperature which is 90° K) against the copper-constantan thermocouple (reference junction 0° C) over the temperature range 90° - 77° K and independently at the freezing point of nitrogen (63° K), boiling point of liquid helium (4.2° K) and finally against the semiconductor resistance thermometer over the range 4.2° - 10° K. By a combination of the analytical and graphical results, a smooth curve was finally drawn covering the entire range of low temperatures and which served as a satisfactory secondary standard for the same sets of thermocouples. The use of low temperature for reference improved the accuracy of measurement since now a much smaller voltage had to be measured within the desired limit than when the reference junction was at 0° C.

The thermojunction was soldered to the copper enclosure to achieve a good thermal contact with the metal surface, the temperature of which was closely followed by the specimen due to its immediate vicinity, to the radiation effect and to conduction through the exchange helium gas. All electrical leads were taken out of the cryostat cap through holes pricked in a rubber bung which was fitted into a side tube and then sealed with wax.

The measuring equipment for the thermocouples consisted of a Diesselhorst thermoelectric-free potentiometer (type 3589R), a thermo-electric free reversing switch (type 4092), an auxiliary compensator to cancel spurious e.m.f.'s in the circuit, built-in photocell galvanometer amplifier (Tinsley 5214) and a liquid oxygen

bath for the reference junction. The galvanometer amplifier increased the overall sensitivity by a factor of about 200 to give 3-4 cm deflection for a change of 1 μV in input voltage. This actually far exceeded the present requirements in sensitivity as will be clear from the following illustration. The silver-gold gold-cobalt thermocouple gave an e.m.f. of 2.288 mV at 4.2° K with the reference junction at 90° K. For a sensitivity of 5% at 4.2° K, this voltage needed to be measured to about 0.003 mV, that is, to a precision of 1 part in 760. The measuring equipment was in fact capable of detecting 1 part in 10^4 corresponding to a sensitivity of 0.5% or to a change of temperature of 0.02° K at 4.2° K.

It would thus appear that the best use of the sensitive detector was only possible when all sources of spurious e.m.f.'s and temperature drift were eliminated from the circuit. One source of error was the possible slight variation in the temperature of the reference junction caused by fluctuations of the vapour pressure of the boiling oxygen. A suitable pressure control device - the Cartesian manostat(96) - was therefore set up and is shown in Fig. 55. In operation, the pressure above the liquid oxygen was set up at the desired control pressure by opening the tap R. Then R was closed and any fluctuations, subsequently developed, was smoothed down by the let-off valve. With this arrangement, the oxygen temperature was stabilized to within 0.01° K. Screened copper leads were used for the connection between the reference junction and the potentiometer and in the amplifier circuit while the thermocouple wires were carefully lagged and protected against irregular heating or

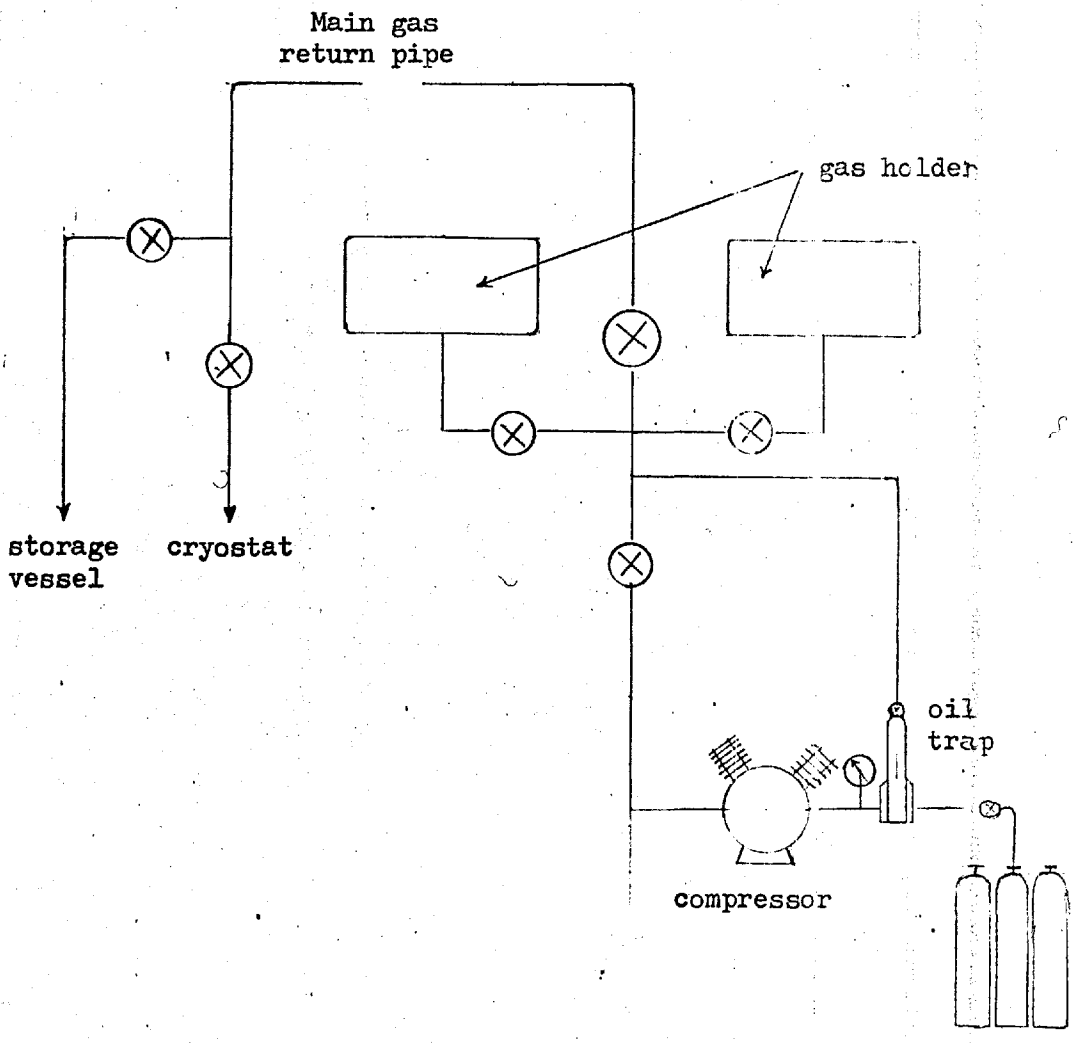

Fig. 57. Layout of the helium conservation system

cooling.

Control of temperature was mainly achieved by providing a suitable thermal link between the copper enclosure and the level of liquid as it dropped below the height of the enclosure. This consisted of two 20 S.W.G. copper wires hanging from the bottom of the metal, so that conduction along the wires tended to keep the specimen chamber at the temperature of liquid helium against the heat loss. The large thermal mass of the chamber also contributed towards a very slow rise of temperature. This arrangement was quite satisfactory and hence no provision was made for a heater. The practice usually followed was to cool down the specimen to 4.2° K and then to make measurements as the temperature gradually rose to 300° K. In a typical run, the temperature would rise at a rate of 0.2° K/min between 8° - 16° K, 0.5° K/min between 26° - 42° K and about 1° K/min between 45° - 65° K.

9.5.7 The helium conservation system

The evaporating helium gas was collected by connecting the outlets of the storage vessel and the cryostat to the main gas return pipe. (Fig. 57). Standard $\frac{1}{2}$" Edwards diaphragm valves were used for the various controls. The low pressure storage consisted of polythene gas holders, each of 1 cubic meter capacity and of a concertina-like construction with heat sealed joints. Connection between the bags and the pipe line was made through 1" diameter nylon embedded P.V.C. tubings. For pumping the gas into the high pressure cylinders, a 'Bristol' Duplex high pressure air

compressor, type 308/BM4S was used. This is a 4-stage air-cooled compressor capable of giving an output pressure of 2000 lb/sq. in. (140 atmos.). Taking a simple 1 to 1000 ratio for the conversion of 1 litre of liquid helium into gaseous phase at N.T.P., this would mean that about 6 litres of the liquid could be used to fill up a 200 cu.ft. cylinder at this pressure.

To prevent oil from the compressor getting into the cylinders, an oil-trap was inserted in the high pressure line. This had a pressure release valve which was operated to let the compressed air in the pipe flow back into the gasholder when the cylinder had to be disconnected.

9.5.8 Experimental procedure at low temperature

The first step in the use of liquid helium was to ensure a leak-proof vacuum system both in the specimen chamber and in the cryostat. The removal of all traces of helium gas from the inside of the dewar was important and this was done by alternate evacuation and admission of air. Before syphoning in liquid helium, the cryostat was precooled by filling the outer jacket with liquid nitrogen. Some nitrogen was also poured into the helium space to speed up the rate of cooling. Since however, it was neither easy nor convenient to remove the excess liquid from the narrow portion of the dewar after precooling, only a small quantity of nitrogen was used, the size of which was soon determined by experience. The precooling operation usually took two to three hours. The transfer syphon was then gently introduced inside the cryostat and the storage vessel.

The two pieces of the syphon were now joined together and all leaks sealed off carefully. With the outlet valve of the storage vessel shut, an overpressure was immediately built up inside and this forced the liquid through the syphon into the cryostat and a large volume of cold gas began to appear. On a few occasions, the transfer tube was choked by ice but this happened only when the system cooled down before all traces of air or nitrogen could be replaced by the helium gas. At the outset, the football bladder, which was used to provide the overpressure, was inflated hard and a gentle touch on it was sufficient to increase the transfer rate of the liquid. When the transfer was too fast, this was regulated by opening the outlet valve of the storage vessel. The initial syphoning was done rather slowly in order to ensure that the cold gas had sufficient time to cool the contents of the cryostat before being driven out. This was checked by the observation that no ice was formed on the cryostat head or the gas return tube. As soon as the temperature reached 4.2° K, liquid began to collect in the bottom of the dewar and this was accompanied by a drop in the pressure. The bladder was then squeezed to increase the rate of flow. The transfer was preferably completed in one operation as a refilling at a later stage always involved evaporation of a considerable portion of the liquid already present in the vessel. In a typical run, it took about 10 minutes to cool the syphon before liquid began to collect in the dewar. After the transfer was completed, the syphon was left attached to the cryostat until all measurements were finished. The practice of keeping a continuous

watch on the readings of temperature indicators was a great help while the transfer operation was being carried out.

A small quantity of helium gas, of about 5 - 10 micron pressure was introduced in the balance chamber to provide a better thermal link with the specimen. The exchange gas did not interfere with the normal functioning of the cryogenic system. The susceptibility measurements were not started until preliminary tests had revealed that the specimen had reached the helium temperature. Some difficulties were experienced in making good soft soldered joints between the two copper surfaces of the end cap enclosing the specimen. Due to unequal strains set up on cooling, leaks were sometimes opened up when the system was tested in liquid nitrogen. However, by fresh attempts with properly tinned surfaces a satisfactory result was obtained. Since oxygen is strongly paramagnetic, it was necessary to ensure that the specimen chamber was free from leaks and the exchange helium gas had effectively replaced the air of the chamber.

The various samples investigated were all cooled down to liquid helium temperature in the zero magnetic field and the measurements were taken both as functions of field and temperature. In cases where the samples became ferrimagnetic at low temperatures, e.g. $Cd_{0.4}Mn_{2.6}O_4$, a small hysteresis was found to be present and accordingly the specimens were demagnetized before making measurements in the presence of the field. The balance was calibrated only at room temperature using standard materials, e.g. $FeNH_4(SO_4)_2,12H_2O$,

and for various magnetic fields. Diamagnetic correction for the sample holder was applied, wherever necessary, in the calculation of the susceptibility. Since the thermistor showed some magneto-resistance effects in the measuring field the latter was switched off before making any temperature measurements.

9.6 High temperature measurements

Measurements at high temperatures were carried out using a specially designed water-cooled furnace which is shown in Fig. 58 . A long silica tube, 0.62" o.d. and 31" in length, provided the core of the furnace and also acted as the vacuum enclosure for the specimen. The lower end of the tube was wound with the heater coil, which lay between two layers of alumina paste and the unit was completely detachable from the rest of the furnace. The heating element extended over 7" giving a hot zone length of about 3" inside the tube. Twin bore alumina tubes were embedded in the paste and these served to carry the electrical leads. The whole assembly could be easily introduced into another silica tube, 0.99" i.d. and 11" long. The latter was permanently fixed in mica-fil (vermiculite) to give a surrounding insulation, 5/16" thick, contained in a brass cylinder, 1.86" i.d. and 12" long. Two syndano spacers were used for holding the sheath centrally. The furnace was water cooled by making the metal case doubly jacketed. This had a wider cylindrical top and a narrower bottom with the water pipes running along two opposite ends so as to enable the lower portion to get into the 2" pole gap of the magnet. All metal joints were

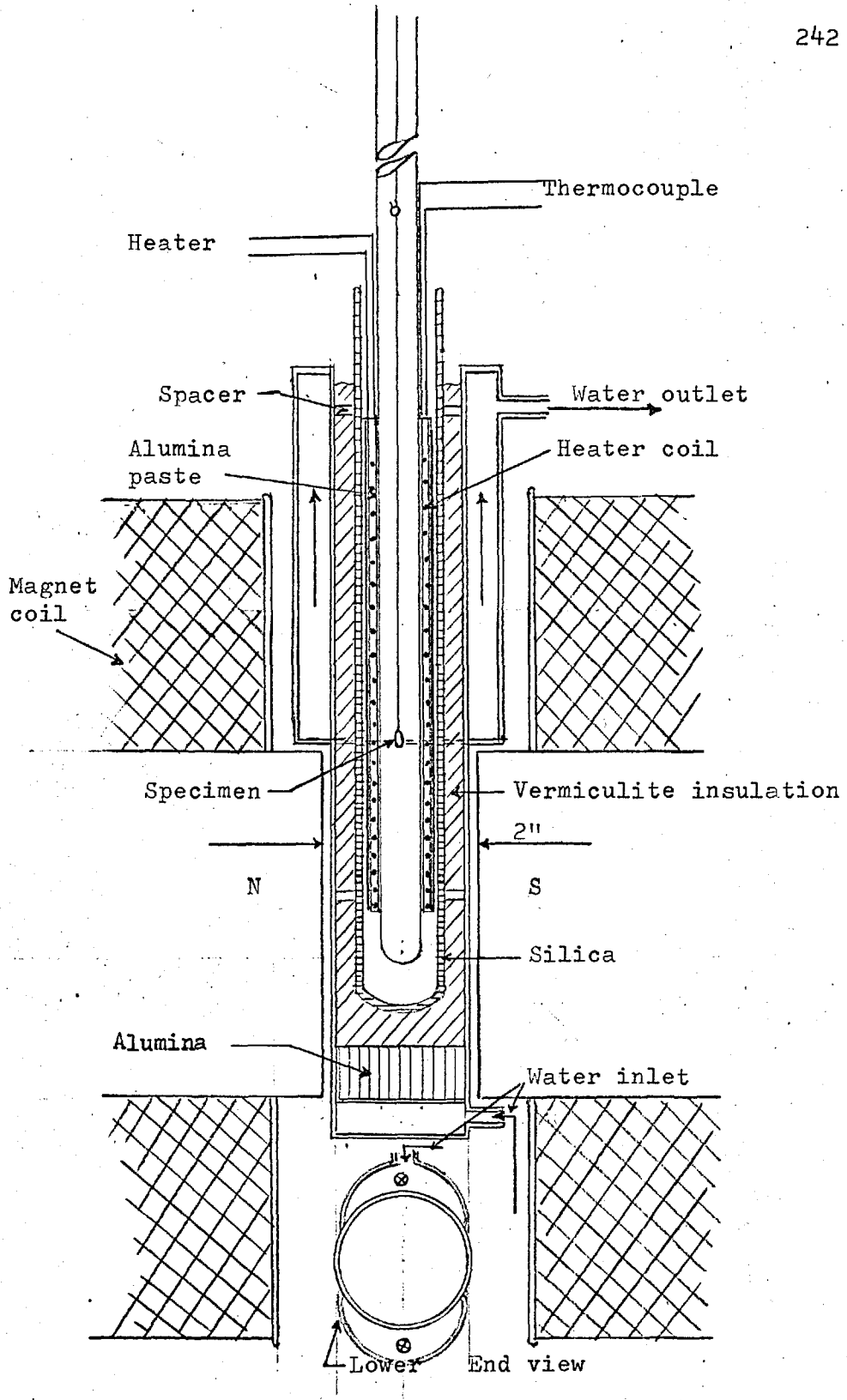

Fig. 58. The high-temperature furnace

silver soldered which had to be done by a careful process of selection and controlled heating.

For the high temperature measurements, the german-silver tube was replaced by the silica tube and was sealed at the top by an O-ring pressure seal. The rest of the furnace could then be quickly assembled by sliding the metal case from underneath and closing the gap between the two silica tubes with glass wool or other heat insulating material. The support to the furnace was provided by an adjustable clamp the holder of which was screwed into the table. The temperature was measured with a Chromel-Alumel thermocouple, the thermojunction being fixed right inside the core of the heating element. A preliminary magnetic measurement using pure nickel had indicated that the thermocouple was recording the correct temperature of the specimen in spite of being located outside the tube. In actual measurements, sufficient time was allowed (20 - 30 min) for the sample to attain temperature stability after each new setting of the furnace current.

Tests carried out with this furnace showed that a temperature of 1000° K could be attained by only 450 watt power and that with a water flow rate of 1 litre/min the outside temperature was within 30° C at this power dissipation. The balance section, however, had to be shielded from the heat radiation from below and this was done by setting up a radiation baffle as shown in Fig. 47. It consisted of two parallel discs of copper and aluminium, each of 10" diameter, and spaced about 1 cm apart. The copper disc at the top helped in stabilizing the temperature of the ring and thus improved

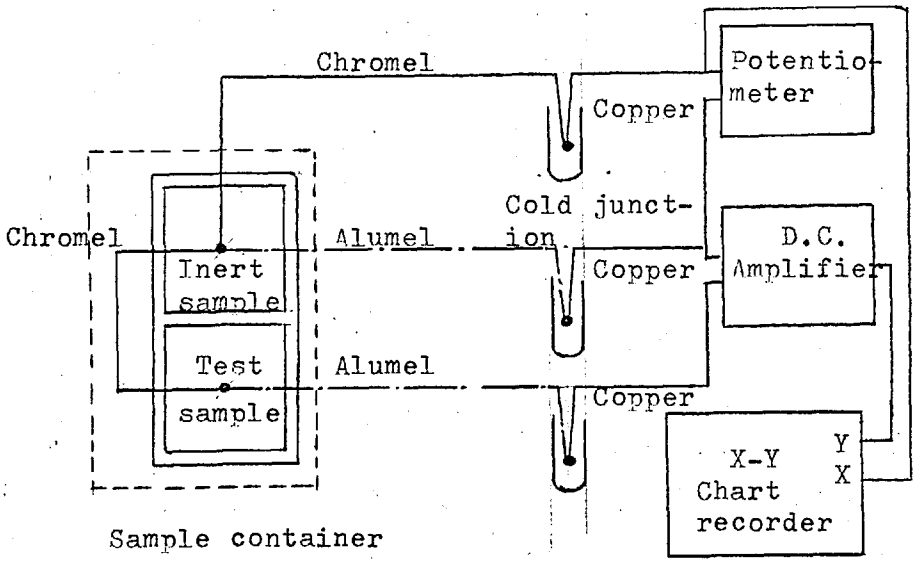

Fig. 59a. The block diagram of the simple D.T.A. circuit

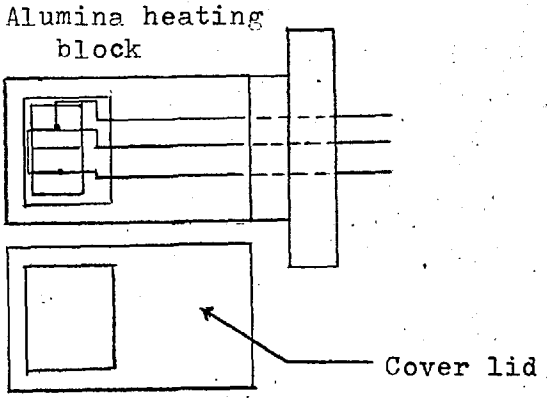

Fig. 59b. The heating block

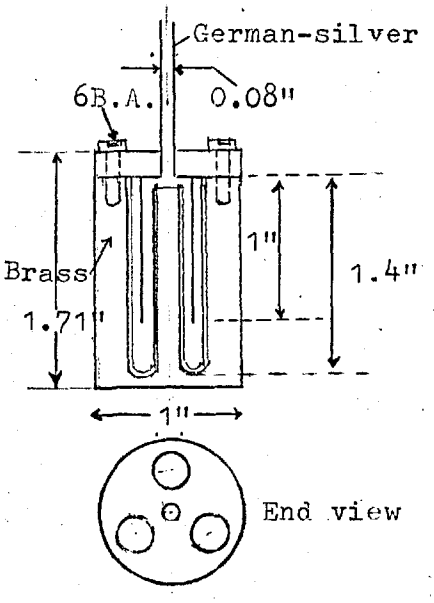

Fig. 59c. The cooling block

the zero stability of the balance.

9.7 Differential thermal analysis (D.T.A.)

The method is based on the detection of the heat evolved or absorbed when a material, on being heated or cooled, undergoes physical or chemical changes involving changes in specific heat[97]. A temperature difference ΔT is thus established between the material under test and an inert reference substance, both of which are heated or cooled side by side at uniform rate. Two thermocouple systems are usually employed to determine the temperature difference as well as the actual temperature of the inert sample (Fig. 59 a). Exothermic and endothermic reactions of the test sample are thus observed and recorded as series of peaks and valleys in the continuous plot of ΔT against T.

The experimental arrangements for carrying out such tests at high and low temperatures are shown in Figs. 59b and 59c. As the primary task in the analysis was to provide supplementary evidence to the results of the susceptibility measurements on some materials, the present D.T.A. investigations were made on a much simpler scale. Basically the equipment consisted of a sample container with two adjacent cells, a heating or cooling block, a suitable d.c. amplifier, temperature measuring equipment and an X-Y recorder. The furnace should be preferably programme controlled to give a uniform heating rate.

CHAPTER X

CONCLUSIONS

PART I

The objective at the commencement of the project was to investigate the field dependence of the magnetoresistance of the ferromagnetic materials and to determine what the influence the geometry of the specimen has on the magnetoresistivity, especially at low fields. To obtain a clearer insight into the problem, a detailed theoretical analysis was carried out which led to the derivations of sixth-rank tensor expressions for the saturation magnetoresistivity of cubic and hexagonal materials, for both single crystals and polycrystals, together with their inter-relationships in the two cases. This material is presented in Chapters II and III. The measurements were performed on rod-shaped specimens of Ni, Fe, Co and Gd, using static fields of up to 21,500 Oe and a liquid bath of para-Xylene which was cooled by a continuous stream of ice-cold water (an arrangement which provided a temperature constant to within 0.005° C). A pair of Helmholtz-type a.c. demagnetizing coils were used to demagnetize the specimens completely. The various points discussed in section 1.3 about the care needed to provide an unambiguous description of the magnetoresistive behaviour were fully taken into account in interpreting the experimental results.

It was discovered that the usually accepted practice of

representing the polycrystalline magnetoresistance of cubic materials by an expression of the form $P + Q\cos^2 x$ was reasonably accurate for nickel but not for iron. In the latter case, a further term of the form $R\cos^4 x$, gave a much better fit with the experimental data when Fourier analysis of the latter is used. The coefficient R was found to be about one-sixth of Q in magnitude for iron. In both cases, however, the simple two-constant (k_1 and k_2) equation of magnetoresistivity gave poor, or only approximate, agreement with the polycrystalline values at saturation (Table 4). On the other hand, the experimental values of Q, for both iron and nickel, gave better agreement with those derived from the single-crystal saturation constants than hitherto obtained (Table 5). The values of the constants for iron were taken from previously published data while for nickel original measurements were made which, incidentally, provided an excellent opportunity to study the forced magnetoresistance effect.

The single crystal, in the form of a rectangular bar, was cut along the $\langle \bar{2}11 \rangle$ axis with the two adjacent side faces lying in the $\{111\}$ and $\{110\}$ planes. Measurements of the magnetoresistivity in these two planes and also in the $\{\bar{2}11\}$ plane at right angles to the axis of the specimen gave three sets of data which were just sufficient to evaluate the five saturation magnetoresistive constants of nickel (equation 6.16). The new values of the constants are lower than those previously obtained (Table 6) and give excellent agreement for Q, when compared with the polycrystalline measurement carried out in the present investigation.

The other aspect of the investigation of cubic materials was the 'forced' magnetoresistance, which is analogous to the isotropic linear effect in volume magnetostriction. Both are caused by a field-induced increase in the spontaneous domain magnetization. The forced magnetoresistance in iron, unlike that in nickel, was found to be influenced slightly by the orientation of the field relative to the specimen axis. However, in view of the high demagnetizing field associated with the transverse magnetization in iron, it was considered likely that the anisotropy arose because the specimen did not exhibit true saturation within the range of the fields studied. It proved possible, in the case of nickel, to correlate theoretically the forced magnetoresistance with the forced magnetization and with the variation of resistivity with the spontaneous magnetization. The final expression, so developed, contains the Weiss molecular field coefficient, q, (equation 6.25) and the substitution of the appropriate experimental data in that equation yields the value q = 17,200. This compares favourably with the figure of 18,500 obtained from the Curie temperature and by taking $J = \frac{1}{2}(60)$.

In all measurements on the rod-shaped specimens, the demagnetizing field was found to influence the magnetoresistive behaviour considerably. Extrapolation of the results to zero internal field (so as to correspond to the same magnetic state at saturation) was accomplished by considering the case of uniform magnetization for all orientations of the specimen axis relative to the field.

In the measurements on hexagonal materials, $(\frac{\overline{\Delta\rho}}{\rho})_{\parallel}$ and $(\frac{\overline{\Delta\rho}}{\rho})_{\perp}$ were found to have the same sign even when these values were extrapolated to the zero effective field. In cobalt, the magnetoresistance was found to be positive over the entire range of the field irrespective of the angle of orientation of the specimen axis relative to the field. For gadolinium, the ferromagnetic anisotropy, $(\Delta\rho_{\parallel} - \Delta\rho_{\perp})/\rho$, was shown to have a negative value - an important result of the present investigation. Similar behaviour was reported by Bates[18] in his measurements of magnetoresistance of cast alnico, but for a different reason. In the present case, the resistivity anomaly is considered to be associated mainly with the exchange interaction between the conduction electrons and the unpaired electrons localized in the 4f shell. The extra resistance arising from the spin-disorder scattering is therefore affected by an external field, particularly near the Curie temperature, but above it, the resistivity should remain temperature-independent. As the Curie point of gadolinium is 289° K and the present investigation was carried out at 273° K, a longitudinal field can be imagined to induce a greater ordering of the spins than a transverse one.

Finally, the dependence of magnetoresistivity of gadolinium on field (H) at 273° K was shown to correspond more nearly to $H^{2/3}$ than to H. This is in good agreement with the Belov's theory[100] which predicts a similar $H^{2/3}$ variation in magnetostriction near the Curie temperature. In this respect, and in relation to the earlier finding of an H^2 variation at high temperature[21], the magnetoresistivity of gadolinium follows the corresponding magneto-

striction behaviour very closely.

PART II

The experimental results together with the relevant graphs and discussions relating to this part of the thesis are given in the two attached reprints on $LiFeO_2$ and $Cd_xMn_{3-x}O_4$ (referred to as Appendix III and IV respectively). The diagrams, contained therein, have not been reproduced in the thesis, the bulk of which has thereby been reduced. The results on $Cd_xMn_{3-x}O_4$ are, however, further discussed here in order to bring out the main aspects of the present investigation.

As mentioned in sections 7.1 and 7.2, the magnetic measurements on Mn_3O_4 support the Y.K. configurations at 0° K. According to the helical spin theory[40], a tetragonally distorted cubic spinel can have the triangular arrangement but the stability exists only for a limited range of the ratio of BB to AB interactions. The Y.K. angle on the B site is given by the expression $\sin\Psi = 1/\beta_2(M_A/M_B)$, where $M_A = \frac{1}{2}N\mu_B gS_A$ and $M_B = N\mu_B gS_B$ (taking the 'spin-only' values for the moments and assuming g to be constant). Thus, if an applied field large compared with the anisotropy field of the crystal can alter the canting angle Ψ, a linear increase is to be expected in the net magnetization (given by the expression $gS_A(1 - 1/|\beta_2|)$) with field. Such a high-field differential susceptibility was observed by Jacobs[38] in Mn_3O_4 at low temperatures and in pulsed fields of up to 140 kOe, but not in Fe_3O_4. This is generally taken as evidence for the triangular model. In the case of Fe_3O_4, the Néel

collinear spin arrangement is believed to be the stable state at 0° K. Another fact lending support to the Y.K. configuration is that the saturation moment of Mn_3O_4 is found to be 1.56 μ_B per molecule[38] whereas a simple antiparallel alignment of moments on the A and B sites would lead to a value of $|5 - 2x4| = 3\mu_B$ per molecule. It is therefore concluded that the B site moments must be divided to give this reduced magnetization.

The gradual replacements of the Mn^{2+} ions on the A sites by the non-magnetic divalent ions, Zn^{2+}, Mg^{2+} or Cd^{2+}, has the effect of weakening the AB interaction compared with the BB interaction. If it is assumed that the Y.K. state still minimizes the energy, then the above process will result in a decrease in the B site angle and a lowering of both the A site moment and the net magnetization. It is suggested here that the highest transition temperature corresponds to the antiferromagnetic ordering on the B sites with the A sites remaining paramagnetic. However, as is seen from Fig. 2a of Appendix IV, the $1/\chi_g$ vs. T curves do not show minima at the Néel point but decrease rapidly with decrease in temperature. This effect may be explained by taking into account the presence of Mn^{2+} ions on the A sites. In fact, these ions are very much diluted when x tends to 1 and they are assumed to remain paramagnetic down to the lowest transition temperature, that is, the ferrimagnetic Curie point. The paramagnetic contribution to the susceptibility increases in importance as the concentration of the magnetic ions on the A sites increases and there is some evidence for this in the results.

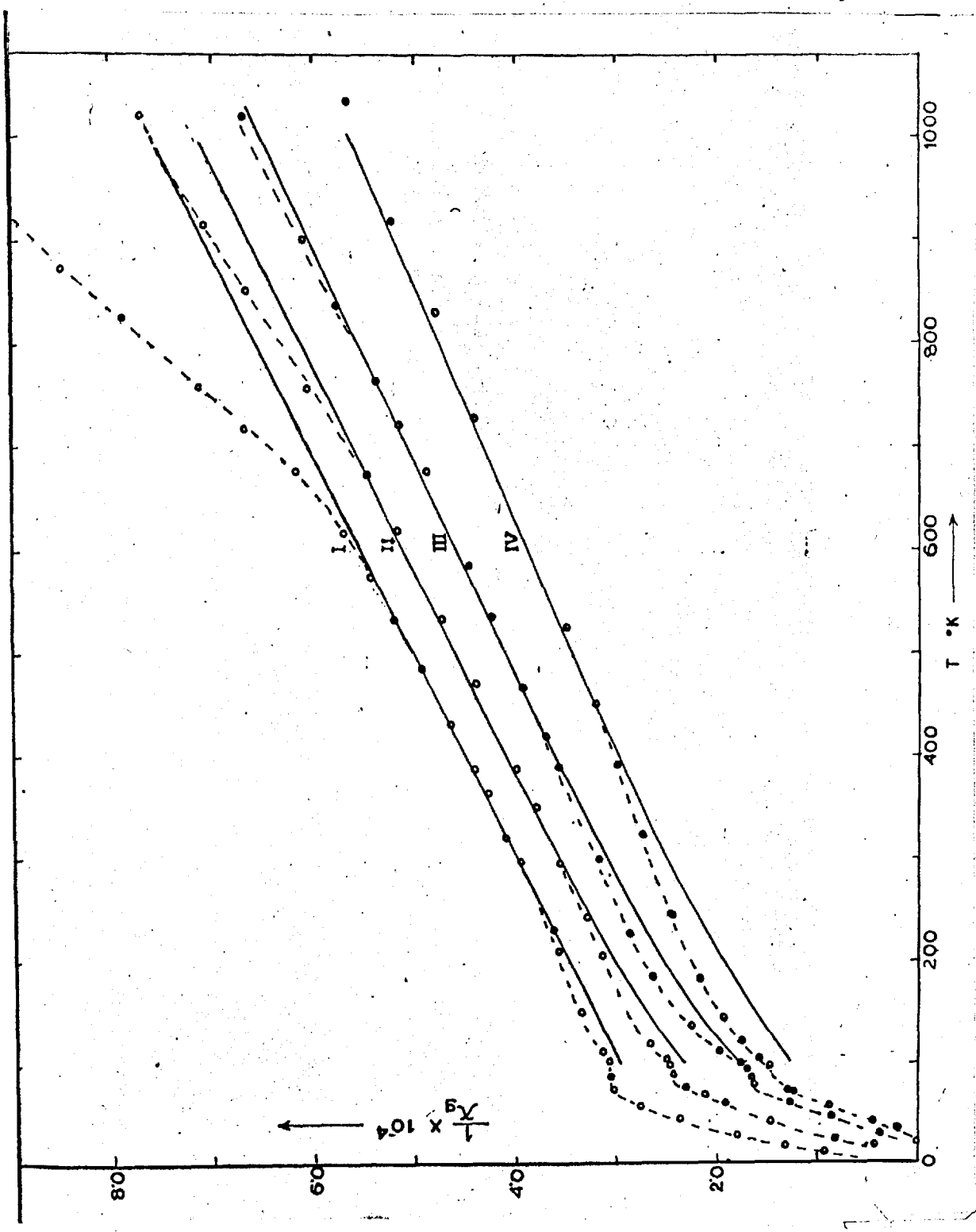

Fig. 60. $1/\chi_g$ vs. T graphs for $Cd_xMn_{3-x}O_4$. The solid lines are represented by the equation $\chi = C/(T+\theta) + C'/T$, while the open circles are the experimental points. (x = 0.4, 0.6, 0.8 and 1.0 respectively for the curves IV, III, II & I).

If the above ideas are correct, then it should be possible to express the susceptibility at high temperatures by an equation of the form

$$\chi = \frac{C}{T + \theta} + \frac{C'}{T} \quad ,$$

where C and C' are the Curie constants for the Mn^{3+} and Mn^{2+} ions respectively and θ is the asymptotic Curie temperature for the Mn^{3+} ions only. Moreover, C and θ should not vary significantly as the value of x is decreased from 1. In Fig. 60 , the inverse susceptibility given by the above equation has been plotted as a function of T together with some of the experimental points taken from Fig. 2a in Appendix IV and using the following values for the constants in cgs units; $C = 193.4 \times 10^{-4}$; $C' = 45 \times 10^{-4}$, 22×10^{-4}, 9×10^{-4} and zero for the cases x = 0.4, 0.6, 0.8 and 1.0 respectively. The values of C and θ are obtained from the experimental curve for x = 1, over the temperature range 200 - 600° K, where the Curie-Weiss law is found to be strictly observed. The deviation of the experimental points from linearity at very high temperatures suggests the possible onset of crystallographic phase transformations and it may therefore be ignored in the present discussion.

The temperature-independent antiferromagnetic susceptibility below the Néel point was considered by Sinha and Sinha[98] for the case of tetragonalized spinels having only diamagnetic cations on the A sites. Their conclusion was that if the exchange interaction in the (001) plane is stronger than that in the (010) plane, the molar susceptibility below the Néel point can be written in the form $\chi_M = 0.3752 \times \frac{k}{z(J_{12} + J_{13})}$, where J_{12} and J_{13} denote the BB

interactions between cations which lie in the (001) and (010) planes and where z = 2 for such a model. Also, the asymptotic Curie temperature is given as

$$\theta = \frac{2S(S+1)}{3} \times \frac{z(J_{12} + 2J_{13})}{k} \quad .$$

Assuming that the above two equations are correct, an estimate of J_{12} and J_{13} may be made from the present experimental data. Thus, if $\chi_M = 46.5 \times 10^{-4}$ and $\theta = -470^\circ$ K then

$$J_{12}/k = -22^\circ \text{ K} \; ; \qquad J_{13}/k = -18^\circ \text{ K}.$$

These values for $CdMn_2O_4$ may be compared with those obtained by Blasse[99] ($J_{12}/k = -42^\circ$ K and $J_{13}/k = -5^\circ$ K) from his measurements on $ZnMn_2O_4$ and by Rosenberg and Nicolae[57] from their measurements on $Cd_{0.8}Mn_{2.2}O_4$. Both investigators used the expressions for χ_M and θ given above in their calculations. Blasse, however, considered his value of θ to be not very accurate because a Curie-Weiss law behaviour was found only at very high temperatures. Rosenberg and Nicolae's data of J, on the other hand, contradict Sinha and Sinha's assumptions. On the basis of the present values of the two interactions, it seems unlikely that the model of a one-dimensional antiferromagnet such as the Ising linear-chain considered by Blasse, will correctly represent the magnetic structure.

With $C = 193.4 \times 10^{-4}$, the magnetic moment of the Mn^{3+} ion is found to be 4.71 μ_B as against the calculated value of 4.90 μ_B, assuming a 'spin-only' moment. Using the constants for the case x = 0.4, the Mn^{2+} moment is obtained as 3.84 μ_B which is also somewhat lower than the calculated value of 5.92 μ_B. The lowering of the Curie constants (also observed by Blasse in the system

$ZnMn_xFe_{2-x}O_4$) may be ascribed to various causes, such as (a) the clustering of the Mn^{3+} ions as a result of increasing isolation imposed by the diamagnetic matrix of the Cd ions, (b) the temperature variation of the molecular field coefficients, (c) the non-quenching of the orbital moment of the magnetic ions, and so on. However, in view of the complexity of the problem, no attempt will be made at further discussion.

A physical picture of the temperature-independent susceptibility has been outlined in Appendix IV. It may be suggested that, provided there are few magnetic ions on the A sites, the paramagnetic-like susceptibility behaviour of $CdMn_2O_4$ below the second transition can be explained, at least partly, by the presence of these ions. This is, however, considered to be unlikely, and an alternative explanation has been given in terms of the appearance of a canted spin structure. A more extended study of $CdMn_2O_4$ may be necessary fully to confirm this point.

Finally, it may be pointed out that the Yafet-Kittel triangular model has been shown to be a stable state at 0° K for a tetragonalized spinel only for a limited range of the ratio of BB to AB interactions[40]. Above this range, the spin ordering transforms to an antiferromagnetic spiral, which in turn soon destabilizes to pass on to a far more complex system as the BB interaction continues to dominate. Whilst the existence of a helical or spiral spin model does not impair the validity of the above discussions, the complexity of the spin structure may, perhaps, account for some of the discrepancies observed between the theory and the results presented here.

PART I

BIBLIOGRAPHY

1. SMIT, J. Physica 17(6), 612 (1951)

2. STIERSTADT, O. Physik. Z. 31, 561 (1930)

3. WEBSTER, W. L. Proc. Roy. Soc. A113, 196 (1926); A114, 611 (1927), see also Proc. Phys. Soc. 42, 431 (1930)

4. SHIRAKAWA, T. Sci. Repts. Tôhoku Imp. Univ. 29, 132 (1940); 29, 152 (1940)

5. GONDO, Y. and FUNATOGAWA, Z. J. Phys. Soc. Japan 7, 41 (1952)

6. KAYA, S. Sci. Repts. Tohoku Imp. Univ. 17, 1027 (1928)

7. DÖRING, W. Ann. Physik 32, 259 (1938)

8. GERLACH, W. and SCHNEIDERHAHN, K. Ann. Physik 6, 772 (1930); GERLACH, W. ibid. 8, 649 (1931); SCHNEIDERHAHN, K. ibid. 11, 385 (1931); see also GERLACH, W. Physik. Z. 33, 953 (1932); Ann. Physik 12, 849 (1932)

9. POTTER, H. H. Proc. Roy. Soc. A132, 560 (1931)

10. POTTER, H. H. Phil. Mag. 13(7), 233 (1932)

11. MATUYAMA, T. Sci. Repts. Tôhoku Imp. Univ. 23, 537 (1934)

12. FEDENEV, D. and USKOV, A. Tech. Phys. U.S.S.R. 5, 309 (1938); Zhur. Tekh. Fiz. 8, 73 (1938)

13. KIMURA, H. and TATSUMOTO, E. J. Sci. Hiroshima Univ. A23(1), 113 (1959)

14. ÔHARA, T. Sci. Rep. Insts. Tôhoku Univ. Japan A15(2), 55 (1963)

15. KIKOIN, I. K. and IGOSHEVA, T. N. Zh. Eksper. Teor. Fiz. 46(5), 1923 (1964) (Soviet Physics - JETP 19(5), 1296)

16. COLEMAN, R. V. and ISIN, A. Abs. 11th Annual Conf. Magnetism and Mag. materials, San Francisco (1965)

17. ALAM, M. S. Z. Physik 93, 556 (1935)

18. BATES, L. F. Proc. Phys. Soc. 58, 153 (1946)

19. de MANDROT, R. Helv. Phys. Acta 26, 563 (1953)

20. LÜTHI, B. and GRÜNEISEN, F. Physics Letters 10(2), 161 (1964)

21. BABUSHKINA, N. A. Dokl. Akad. Nauk S.S.S.R. 155(6), 1290 (1964) (Soviet Physics - Doklady 9(4), 299)

22. BELOV, K. P. Proc. Int. Conf. Magnetism, Nottingham (1964) p.266

23. AKULOV, N. S. Z. Physik 59, 254 (1930)

24. PEIERLS, R. Ann. Physik 10, 97 (1931)

25. ENGLERT, E. Ann. Physik 14, 589 (1932); see also Z. Physik 74, 748 (1932)

26. JONES, H. and ZENER, C. Proc. Roy. Soc. A145, 268 (1934)

27. DAVIS, L. Phys. Rev. 56, 93 (1939)

28. BOZORTH, R. M. Phys. Rev. 70, 923 (1946)

29. SONDHEIMER, E. H. and WILSON, A. H. Proc. Roy. Soc. A190, 435 (1947)

30. KÖHLER, M. Ann. Physik 6, 18 (1949)

31. SNOEK, J. L. Nature 163, 837 (1949)

32. SMIT, J. Thesis, University of Leiden, April (1956)

33. GANS, R. and HARLEM, J. V. Ann. Physik 15, 512 (1933)

34. HIRONE, T. and HORI, N. Sci. Repts. Tôhoku Imp. Univ. 30, 125 (1942)

35. PARKER, R. Phil. Mag. 1, 1133 (1956)

36. CHIKAZUMI, S. J. Phys. Soc. Japan 5, 327 (1950)

37. HAJDU, J. Z. Physik Pt. I 160(1), 47 (1960); Pt. II 160(5), 481 (1960); Pt. III 163(1), 108 (1961)

38. KONDO, J. Progr. Theor. Phys. Japan 27(4), 772 (1962)

39. JONES, M C. and SONDHEIMER, E. H. Physics Letters 11(2), 122 (1964)

40. BOZORTH, R. M. and HAMMING, R. W. Phys. Rev. 89, 865 (1953)

41. JAN, J.-P. Solid State Physics (New York : Acad. Press Inc.) 5, 1 (1951)

42. MATTHEWS, H. and DOHERTY, W. R. J. Electron. Contr. 10(4), 273 (1961)

43. van der PAUW, L. J. Philips Res. Repts. 13, 1 (1958)

44. SVENSSON, B. Ann. Phys. 22(5), 97 (1935); 25(5), 263 (1936)

45. POTTER, H. H. Proc. Phys. Soc. 49, 671 (1937)

46. GRÜNEISEN, E. Ann. Physik 16, 530 (1933)

47. BLOCH, F. Z. Physik 52, 555 (1930)

48. MOTT, N. F. Proc. Phys. Soc. 47, 571 (1935); Proc. Roy. Soc. A153, 699 (1936); A156, 368 (1936)

49. WILSON, A. H. Proc. Roy. Soc. A167, 580 (1938)

50. COLES, B. R. Advanc. Phys. 7(25), 40 (1958)

51. KASUYA, T. Progr. Theor. Phys. Japan 16, 45 (1956); 16, 58 (1956)

52. YOSIDA, K. Phys. Rev. 107, 396 (1957)

53. DE GENNES, P. G. and FRIEDEL, J. J. Phys. Chem. Solids 4, 71 (1958)

54. MANNARI, I. Progr. Theor. Phys. Japan 22, 335 (1959)

55. MOTT, N. F. and STEVENS, K. W. H. Phil. Mag. 2, 1364 (1957)

56. ALLISON, F. E. and PUGH, E. M. Phys. Rev. 102, 1281 (1956)

57. SCHINDLER, A. I., SMITH, R. J. and SALKOVITZ, E. I. Phys. Rev. 108, 921 (1957)

58. OVERHAUSER, A. W. and SCHINDLER, A. I. J. Appl. Phys. 28, 544 (1957); N.R.L. Report 4920 (1957)

59. BECKER, R. and DÖRING, W. "Ferromagnetismus". Springer, Berlin, 1939.

60. BOZORTH, R. M. Ferromagnetism (New York : Van Nostrand) 1951.

61. GERRITSEN, A. N. Handbuch der Physik 19, 137 (1956)

62. ZIMAN, J. M. Electrons and phonons (Oxford Univ. Press) 1960.

63. BIRSS, R. R. and DEY, S. K. Proc. Roy. Soc. A263, 473 (1961)

64. JONES, H. Handbuch der Physik 19, 227 (1956)

65. FLETCHER, G. C. Proc. Phys. Soc. 65, 192 (1952)

66. WEISS, R. J. and DE MARCO, J. J. Rev. Mod. Phys. 30, 59 (1958); Phys. Rev. Letters 2, 148 (1959)

67. BATTERMAN, B. W. Phys. Rev. Letters 2, 47 (1959)

68. KOMURA, Y., TOMIIE, Y. and NATHANS, R. Phys. Rev. Letters 3,268(1959)

69. GRIFFITH , J. S. J. Inorg. and Nuclear Chem. 3, 15 (1956)

70. LOMER, W. M. and MARSHALL, W. Phil. Mag. 3, 185 (1958)

71. BIRSS, R. R. Proc. Phys. Soc. 75, 8 (1960)

72. WHITE, G. K. and WOODS, S. B. Phil. Trans. Roy. Soc. A251, 273 (1959)

73. ONSAGER, L. Phys. Rev. 37, 405 (1931); 38, 2265 (1931)

74. CASIMIR, H. B. G. Rev. Mod. Phys. 17 (343) 1945

75. MAZUR, P. and de GROOT, S. R. Physica 19, 961 (1953)

76. FIESCHI, R., de GROOT, S. R. and MAZUR, P. Physica 20, 67, 259 (1954)

77. BIRSS, R. R. Symmetry and Magnetism (Amsterdam: North Holland Publishing Co.) 1964.

78. JEFFREYS, H. and JEFFREYS, B. S. Methods of Mathematical Physics (Cambridge Univ. Press) 1950.

79. BIRSS, R. R. Rep. Progr. Phys. 26, 307 (1963)

80. FIESCHI, R. and FUMI, F. G. Nuovo Cim. 10(7), 865 (1953)

81. FIESCHI, R. Physica 23, 972 (1957)

82. PEARSON, G. L. and SUHL, H. Phys. Rev. 83, 768 (1951)

83. SEITZ, F. Phys. Rev. 79, 372 (1950)

84. MASON, W. P. Phys. Rev. 96, 302 (1954)

85. BOZORTH, R. M. and SHERWOOD, R. C. Phys. Rev. 94, 1439 (1954)

86. AMER. INST. OF PHYSICS HANDBOOK, Second Edition (McGraw-Hill).

87. BIRSS, R. R. and BROWN, C. G. The School Science Review 43, 474 (1961-62)

88. HILL, A. V. J. Sci. Instrum. 8, 262 (1931); 11, 281 (1934); 25, 225 (1948)

89. PRESTON, J. S. J. Sci. Instrum. 23, 173 (1946)

90. LOW, G. G. E. J. Sci. Instrum. 36, 197 (1959)

91. BOZORTH, R. M. and CHAPIN, D. M. J. Appl. Phys. 13, 320 (1942)

92. STONER, E. C. Phil. Mag. 36, 803 (1945)

93. BROWN, W. F. Magnetostatic Principles in Ferromagnetism (Amsterdam: North-Holland) 1962.

94. BATES, L. F. Modern Magnetism (Cambridge Univ. Press) 1963.

95. WEISS, P. and FORRER, R. Ann. Phys. 5(10), 153 (1926); 12(10), 279 (1929)

96. MOTT, N. F. and JONES, H. The Theory of the Properties of Metals and Alloys (Oxford Univ. Press) 1958.

97. DARNELL, F. J. Phys. Rev. 130, 1825 (1963)

98. SPEDDING, F. H., LEGVOLD, S., DAANE, A. H. and JENNINGS, L. D. Progress in Low Temperature Physics (Amsterdam : North Holland) 1957.

99. CORNER, W. D. and HUTCHINSON, F. Proc. Phys. Soc. 75, 781 (1960)

100. BELOV, K. P., LEVITIN, R. Z., NIKITIN, S. A. and PED'KO, A. V. Soviet Physics-JETP 13, 1096 (1961)

101. BOZORTH, R. M. and WAKIYAMA, T. J. Phys. Soc. Japan 18, 97 (1963)

102. ALSTAD, J. and LEGVOLD, S. J. Appl. Phys. 35, 1752 (1964)

103. COLEMAN, W. E. and PAVLOVIC, A. S. J. Phys. Chem. Solids 26, 691 (1965); Phys. Rev. 135, A426 (1964)

PART II

1. NÉEL, L. Ann. Phys. 3,137 (1948)

2. SHULL, C. G. and SMART, J. S. Phys. Rev. 76, 1256 (1949)

3. SHULL, C. G., STRAUSER, W. A. and WOLLAN, E. O. Phys. Rev. 83, 333 (1951)

4. SHULL, C. G., WOLLAN, E. O. and KOEHLER, W. C. Phys. Rev. 84, 912 (1951)

5. MÖSSBAUER, R. L. Z. Physik 151, 124 (1958)

6. WERTHEIM, G. K. J. Appl. Phys. 32, 110S (1961)

7. NÉEL, L. Ann. Phys. 18, 5 (1932); 5, 232 (1936)

8. VAN VLECK, J. H. J. Chem. Phys. 9, 85 (1941)

9. LANDAU, L. D. Physik, Z. Sowjetunion 4, 675 (1933)

10. NAGAMIYA, T. Progr. Theor. Phys. 6, 342 (1951)

11. YOSIDA, K. Progr. Theor. Phys. 6, 691 (1951)

12. VAN VLECK, J. H. J. Phys. Radium 12, 262 (1951)

13. STREET, R. Sci. Progr. 39, 258 (1951)

14. SMART, J. S. Phys. Rev. 86, 968 (1952)

15. ANDERSON, P. W. Phys. Rev. 79, 350, 705 (1950)

16. BETHE, H. Handbuch der Physik 24 (2), 595 (1933)

17. KRAMERS, H. A. Physica 1, 182 (1934)

18. ZENER, C. Phys. Rev. 82, 403 (1951)

19. GOODENOUGH, J. B. Phys. Rev. 100, 564 (1955); GOODENOUGH, J. B. and LOEB, A. ibid. 98, 391 (1955); see also KANAMORI, J. J. Phys. Chem. Solids 10, 87 (1959)

20. GOODENOUGH, J. B. in "Magnetism" Vol. III (Rado, G. T. and Suhl, H., eds.), Academic Press, New York 1963

21. DZYALOSHINSKY, I. J. Phys. Chem. Solids 4, 241 (1958); Zh. Eksper. Teor. Fiz. 33, 1454 (1958) (Soviet Physics - JETP 6, 1120)

22. MORIYA, T. Phys. Rev. 120, 91 (1960)

23. MORIN, F. J. Phys. Rev. 78, 819 (1950)

24. LIN, S. T. Phys. Rev. 116, 1447 (1959)

25. MORIYA, T. Phys. Rev. 117, 635 (1960)

26. TREVES, D. Phys. Rev. 125, 1843 (1962); GORODETSKY, G. and TREVES, D. ibid. 135(1A), A97 (1964)

27. BOROVIK-ROMANOV, A. S. and ORLOVA, M.P. Zh.Eksper. Teor. Fiz. 31, 579 (1956)

28. HEEGER, A. J., BECKMAN, O. and PORTIS, A. M. Phys. Rev. 123, 1652 (1961)

29. HANSEN, W. N. and GRIFFEL, M. J. Chem. Phys. 30, 913 (1959)

30. DWIGHT, K. and MENYUK, N. Phys. Rev. 119, 1470 (1960)

31. MEIKLEJOHN, W. H. and BEAN, C. P. Phys. Rev. 102, 1413 (1956); 105, 904 (1957)

32. MEIKLEJOHN, W. H. J. Appl. Phys. 33, 1328 (1962)

33. YAFET, Y. and KITTEL, C. Phys. Rev. 87, 290 (1952)

34. GORTER, E. W. Philips Res. Repts. 9, 295, 321, 403 (1954)

35. LOTGERING, F. K. Philips Res. Repts. 11, 190, 337 (1956)

36. PRINCE, E. Acta Cryst. 10, 554 (1957)

37. PICKART, S. J. and NATHANS, R. Phys. Rev. 116, 317 (1959); Bull. Amer. Phys. Soc. 3, 231 (1958)

38. JACOBS, I. S. J. Appl. Phys. 30, 301S (1959); J. Phys. Chem. Solids 11, 1 (1959)

39. KAPLAN, T. A. Phys. Rev. 116, 888 (1959); 119, 1460 (1960); LYONS, D. and KAPLAN, T. A. ibid. 120, 1580 (1960)

40. KAPLAN, T. A., DWIGHT, K., LYONS, D. and MENYUK, N. J. Appl. Phys. 32, 13S (1961); LYONS, D., KAPLAN, T. A., DWIGHT, T. and MENYUK, N. Phys. Rev. 126, 540 (1962); MENYUK, N., DWIGHT, K., LYONS, D. and KAPLAN, T. A. ibid. 127, 1983 (1962); see also LYONS, D. H. ibid. 132, 122 (1963)

41. YOSHIMORI, A. J. Phys. Soc. Japan 14, 807 (1959)

42. VILLAIN, J. J. Phys. Chem. Solids 11, 303 (1959)

43. MIWA, H. and YOSIDA, K. Progr. Theoret. Phys. 26, 693 (1961)

44. ENZ, U. J. Appl. Phys. 32, 22S (1961)

45. OSMOND, W. P. British J. Appl. Phys. 15, 1377 (1964)

46. OSMOND, W. P. Proc. Phys. Soc. 85, 1191 (1965)

47. ANDERSON, J. C. and SCHIEBER, M. J Phys. Chem. Solids 25, 961 (1964)

48. FAYARD, M. Thesis. University of Paris (1962)

49. COLLONGUES, E. C. R. Acad. Sci., Paris 241, 1577 (1955)

50. COX, D. E., SHIRANE, G., FLINN, P. A., RUBY, S. L. and TAKEI, W.J. Phys. Rev. 132, 1547 (1963)

51. SCHIEBER, M. private communication

52. ANDERSON, J. C., DEY, S. K. and HALPERN, V. J. Phys. Chem. Solids 26, 1555 (1965)

53. BOROVIK-ROMANOV, A. S. and ORLOVA, M. P. Zh. Eksper. Teor. Fiz. 32, 1255 (1957) (Soviet Physics - JETP 5, 1023)

54. BONGERS, P. F. Thesis, Leiden (unpublished) 1957

55. JACOBS, I. S. and KOUVEL, J. S. Phys. Rev. 122, 412 (1961)

56. TACHIKI, M. and YOSIDA, K. Progr. Theoret. Phys. 17, 223 (1957)

57. ROSENBERG, M. and NICOLAE, I. Phys. Stat. Sol. 127 (1964); Proc. Int. Conf. Magnetism, Institute of Physics and Physical Society, 1964

58. DEY, S. K. and ANDERSON, J. C. Phil. Mag. 12, 975 (1965)

59. NEWELL, G. E. and MONTROLL, E. W. Rev. Mod. Phys. 25, 353 (1953)

60. BIZETTE, H., SQUIRE, C. and TSAI, B. Compt. rend (Paris) 207, 449 (1939)

61. NAGAMIYA, T., YOSIDA, K. and KUBO, R. Adv. Phys. 4, 1 (1955)

62. SMART, J. S. Phys. Rev. 101, 585 (1956)

63. MAXWELL, L. R. and PICKART, S. J. Phys. Rev. 92, 1120 (1953)

64. SMART, J. S. Amer. J. Phys. 23, 356 (1955)

65. GORTER, E. W. and SCHULKES, J. A. Phys. Rev. 90, 487 (1953)

66. BERTAUT, F. and PAUTHENET, R. Proc. I.E.E. Suppl. B104, 261 (1957); PAUTHENET, R. J. Appl. Phys. 29, 253 (1958)

67. SMART, J. S. Phys. Rev. 90, 55 (1953)

68. ANDERSON, P. W. Phys. Rev. 102, 1008 (1956)

69. LUTTINGER, J. M. and TISZA, L. Phys. Rev. 70, 954 (1946); LUTTINGER, J. M. ibid. 81, 1015 (1951)

70. KASPER, J. S. Bull. Amer. Phys. Soc. 4, 178 (1959)

71. CORLISS, L. and HASTINGS, J. J. Appl. Phys. 33S, 1138 (1962); HASTINGS, J. and CORLISS, L. Phys. Rev. 126, 556 (1962)

72. PEPPER, A. R. and SMITH, J. H. J. Sci. Instrum. 42, 328 (1965)

73. GRIFFITHS, D. J. Sci. Instrum. 38, 463 (1961)

74. SHUTLEWORTH, R. A. Rev. Sci. Instrum. 32, 1327 (1961)

75. CLARK, C. A. and WHITTLE, J. E. J. Sci. Instrum. 36, 190 (1959)

76. CHANDRASEKHAR, B. S. Rev. Sci. Instrum. 27, 967 (1956)

77. McMILLAN, J. A. Amer. J. Phys. 27, 352 (1959)

78. CHEN, W. K., KOCH, F. B. and SIVERSTEN, J. M. Rev. Sci. Instrum. 31, 1157 (1960)

79. VICKERY, R. C. and SEXTON, W. C. Rev. Sci. Instrum. 31, 647 (1960)

80. SVECHKAREV, I. V. Instrum. Exper. Tech (U.S.A.) No. 4, 734 (1964)

81. SMITH, D. O. Rev. Sci. Instrum. 27, 261 (1956)

82. DWIGHT, K., MENYUK, N. and SMITH, D. J. Appl. Phys. 29, 491 (1958)

83. FONER, S. Rev. Sci. Instrum. 30, 548 (1959)

84. FREDERICH, N. V. I.R.E. Trans. Instrumentation (USA) No. 2, 194 (1960)

85. LUNDQUIST, N. and MYERS, H. P. J. Sci. Instrum. 39, 154 (1962)

86. SCHERINGER, C. Rev. Sci. Instrum. 35, 515 (1964)

87. BUTERA, R. A., CRAIG, R. S. and CHERRY, L. V. Rev. Sci. Instrum. 32, 708 (1961)

88. STRAKHOV, L. P. and SHAN'TSZE, T. Instrum. Exper. Tech (USA) No. 2, 326 (1963)

89. BLEANEY, B. and BLEANEY, B. Electricity and Magnetism (Oxford, Clarendon Press) 1965

90. See ref. 94 of Part I

91. SUCKSMITH, W. and PEARCE, R. R. Proc. Roy. Soc. 167A, 189 (1938)

92. SCHOEN, L. J. and BROIDA, H. P. NBS Report No. 7359, U.S. Dept. of Commerce; see also HELLWEGE, K. H., JOHNSON, U. and SCHNEIDER, B. Z. Angew. Phys. 14, 481 (1962)

93. KEESOM, W. H. Helium (Elsevier Pub. Co. Texas) 1942

94. GAFFNEY, J. and CLEMENT, J. R. Rev. Sci. Instrum. 26, 620 (1955)

95. ROSE-INNES, A. C. (English U.P.) 1964 Low temperature techniques

96. WHITE, G. K. Experimental techniques in low-temperature physics (Oxford Clarendon Press) 1961

97. GRIMSHAW, R. W., HEATON, E. and ROBERTS, A. L. British Ceramic Soc. 44, 69 (1945)

98. SINHA, K. P. and SINHA, B. P. J. Phys. Soc. Japan, Suppl. B-I, 17, 218 (1962)

99. BLASSE, G. Philips Res. Repts. 20, 528 (1965)

A P P E N D I X I

Derivations of the expressions for magnetoresistivity in the (111), $(0\bar{1}1)$ and $(\bar{2}11)$ planes which are used to evaluate the five saturation magnetoresistance constants of nickel:-

The direction cosines α_1, α_2, α_3 and β_1, β_2, β_3 respectively of the magnetization vector, OQ, and of the direction of current i used for measuring the resistance, OP, relative to the crystallographic axes, x, y, z, are given by Fig. 61a ,

$$\beta_1 = \sin\theta \cdot \cos\phi \ ,$$

$$\beta_2 = \sin\theta \cdot \sin\phi \ ,$$

$$\beta_3 = \cos\theta \ ,$$

$$\alpha_1 = \cos\eta \cdot \sin\theta \cdot \cos\phi + \sin\eta\,(\cos\theta \cdot \cos\phi \cdot \cos\psi + \sin\phi \cdot \sin\psi),$$

$$\alpha_2 = \cos\eta \cdot \sin\theta \cdot \sin\phi + \sin\eta\,(\cos\theta \cdot \sin\phi \cdot \cos\psi - \cos\phi \cdot \sin\psi),$$

$$\alpha_3 = \cos\eta \cdot \cos\theta - \sin\eta \cdot \sin\theta \cdot \cos\psi \ . \qquad (I\text{-}1)$$

Equation (I-1) in conjunction with (3.42) gives a general expression for the magnetoresistance in any direction of a cubic crystal for which the easy directions of magnetization are the ternary axes. $k_1 \ldots k_5$ are the five saturation magnetoresistance constants to be evaluated. The general expression is now applied to the three specific cases:

(a) In this case, $\langle \bar{2}11 \rangle$ is the measuring direction and the magnetization vector is contained in the (111) plane. Hence ψ is fixed and is given by Fig.61 b ,

$$\cos\psi = \sqrt{\frac{3}{5}} \ ; \qquad \sin\psi = \sqrt{\frac{2}{5}} \ .$$

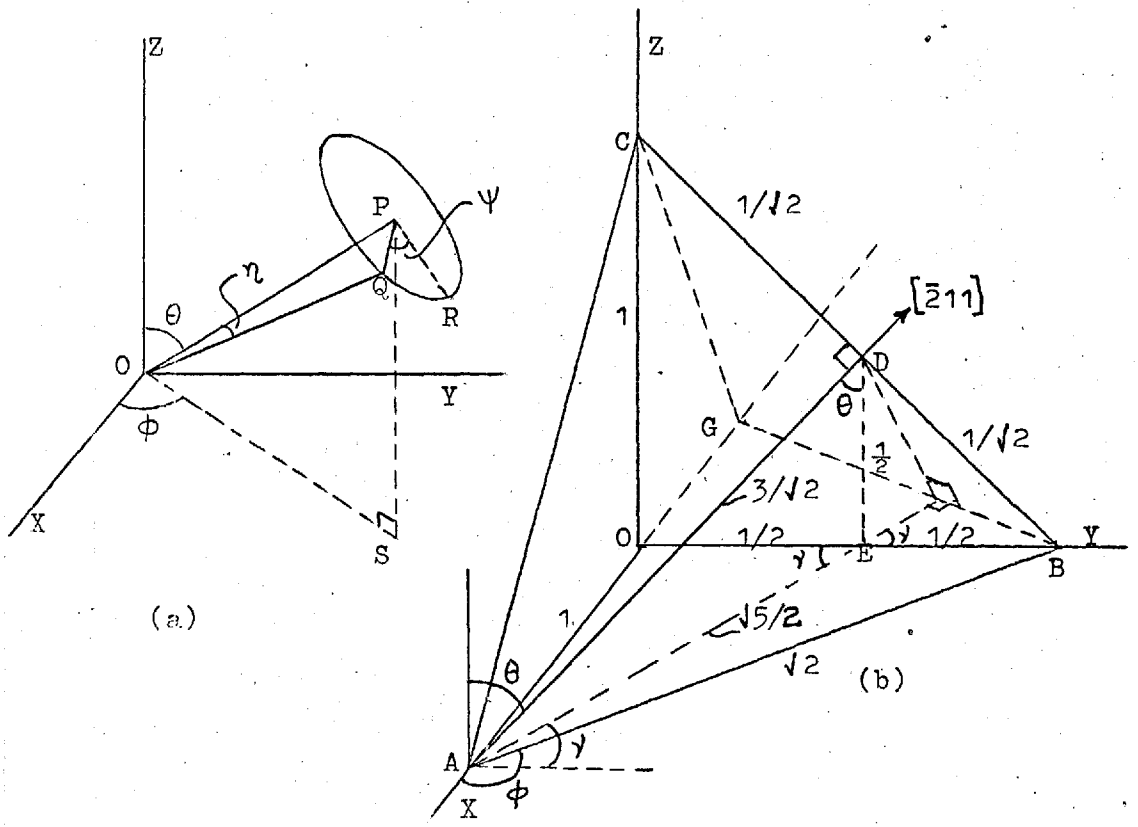

Fig. 61. Schematic diagrams illustrating the various angles occuring in Appendix I

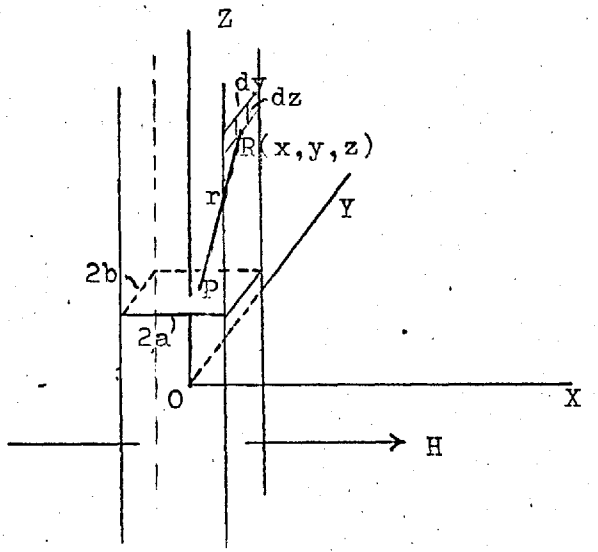

Fig. 62. Diagram illustrating the calculation of the demagnetizing field of a rectangular bar for uniform magnetization.

Also

$$\sin\theta = \sqrt{\frac{5}{6}}\ ; \qquad \cos\theta = \sqrt{\frac{1}{6}}\ ,$$

$$\cos\phi = -\sin\gamma = -\sqrt{\frac{2}{5}}\ ; \qquad \sin\phi = \cos\gamma = \sqrt{\frac{1}{5}}\ .$$

Substitution of these values in equation (I -1) gives

$$\beta_1 = -\sqrt{\frac{2}{3}}\ ; \qquad \alpha_1 = -\sqrt{\frac{2}{3}}\cos\eta\ ,$$

$$\beta_2 = \sqrt{\frac{1}{6}}\ ; \qquad \alpha_2 = \sqrt{\frac{1}{6}}\,(\sqrt{3}\sin\eta + \cos\eta)\ ,$$

$$\beta_3 = \sqrt{\frac{1}{6}}\ ; \qquad \alpha_3 = \sqrt{\frac{1}{6}}\,(\cos\eta - \sqrt{3}\sin\eta)\ , \quad \text{(I -2)}$$

where η is the angle between the magnetization vector and the direction of measurement. Combining now the relations (I -2) and (3.42) and arranging in terms of $\cos 2\eta$ and $\cos 4\eta$, the saturation magnetoresistance is given by

$$\frac{\Delta\rho}{\rho} = \left(\frac{1}{6}k_2 - \frac{1}{12}k_3\right) + \left(\frac{1}{6}k_1 + \frac{1}{3}k_2 + \frac{1}{9}k_4 + \frac{1}{18}k_5\right)\cos 2\eta + \left(\frac{1}{36}k_4 + \frac{1}{18}k_5\right)\cos 4\eta\ , \quad \text{(I -3)}$$

$$= A_1 + B_1\cos 2\eta + C_1\cos 4\eta\ , \quad \text{(I -4)}$$

where the values of the coefficients A_1, B_1, C_1 are given by the expressions within the corresponding brackets.

(b) The direction of measurement is again $\langle\bar{2}11\rangle$ but the magnetization vector now lies in the $(0\bar{1}1)$ plane. The value of ψ is now given by

$$\cos\psi = -\sqrt{\frac{2}{5}}\ ; \qquad \sin\psi = \sqrt{\frac{3}{5}}\ .$$

The β's are the same as before but the α's now take the values

$$\alpha_1 = \sqrt{\frac{1}{3}}\,(\sin\eta - \sqrt{2}\cos\eta),$$

$$\alpha_2 = \alpha_3 = \frac{1}{\sqrt{3}} \left(\sin \eta + \sqrt{\frac{1}{2}} \cos \eta\right) , \qquad (I-5)$$

Introducing these values in the expression (3.42) and arranging in the form of sine and cosine terms, the saturation magnetoresistance is given by

$$\begin{aligned}\frac{\Delta \rho}{\rho} = &\left(\frac{1}{12} k_2 + \frac{1}{12} k_1 - \frac{11}{96} k_3 + \frac{3}{32} k_4 + \frac{1}{48} k_5\right) \\ &+ \cos 2\eta \left(\frac{1}{12} k_1 + \frac{5}{12} k_2 - \frac{1}{24} k_3^{*} + \frac{5}{72} k_4 + \frac{1}{9} k_5\right) \\ &+ \cos 4\eta \left(\frac{7}{96} k_3^{*} - \frac{7}{288} k_4 - \frac{1}{48} k_5\right) \\ &+ \sin 2\eta \left(-\frac{2}{6} k_1 + \frac{2}{6} k_2 + \frac{2}{12} k_3^{*} - \frac{52}{36} k_4 + \frac{2}{36} k_5\right) \\ &+ \sin 4\eta \left(\frac{2}{24} k_3^{*} - \frac{2}{72} k_4 + \frac{2}{24} k_5\right) \qquad (I-6a)\end{aligned}$$

$$= A_2 + B_2 \cos 2\eta + C_2 \cos 4\eta + D_2 \sin 2\eta + E_2 \sin 4\eta \qquad (I-6b)$$

$$= A_2 + \frac{B_2}{\cos \varepsilon} \cos (2\eta - \varepsilon) + \frac{C_2}{\cos \lambda} \cos (4\eta - \lambda), \qquad (I-7)$$

where

$$\cos \varepsilon = \frac{B_2}{(B_2^2 + D_2^2)} ; \qquad \cos \lambda = \frac{C_2}{(C_2^2 + E_2^2)}$$

and the coefficients, A_2, B_2, C_2, D_2, E_2, are given by the expressions within the corresponding brackets. As before η is the angle between the magnetization vector and the direction of measurement.

(c) As before, the direction of measurement is fixed in the $\langle \bar{2}11 \rangle$ direction but the magnetization vector now lies always in the $(\bar{2}11)$ plane. Since the latter is always perpendicular to the former, $\eta = 90^\circ$ and so if θ is the angle the magnetization vector makes with the $\langle 1\bar{1}1 \rangle$ direction (Fig.61b), then

$$\cos\Psi = \sqrt{\frac{3}{5}}\sin\theta - \sqrt{\frac{2}{5}}\cos\theta \ ,$$

$$\sin\Psi = \sqrt{\frac{2}{5}}\sin\theta + \sqrt{\frac{3}{5}}\cos\theta \ .$$

The β's are the same as before but the values of α's are given by

$$\alpha_1 = \frac{1}{\sqrt{3}}\cos\theta$$

$$\alpha_2 = \frac{1}{\sqrt{2}}\sin\theta + \frac{1}{\sqrt{3}}\cos\theta \ ,$$

$$\alpha_3 = -\frac{1}{\sqrt{2}}\sin\theta + \frac{1}{\sqrt{3}}\cos\theta \ , \qquad \text{(I -8)}$$

and also, $\alpha_1\beta_1 + \alpha_2\beta_2 + \alpha_3\beta_3 = 0$. (I -9)

Substitution of the relations (I -8) and (I -9) in equation (3.42) gives

$$\frac{\Delta\rho}{\rho} = \left(-\frac{1}{12}k_1 - \frac{1}{4}k_2 - \frac{11}{96}k_3^{*} - \frac{7}{96}k_4 - \frac{1}{48}k_5\right)$$

$$+ \cos 2\theta\left(+\frac{1}{12}k_1 - \frac{1}{12}k_2 + \frac{1}{24}k_3^{*} + \frac{1}{24}k_4 - \frac{1}{18}k_5\right)$$

$$+ \cos 4\theta\left(\frac{7}{96}k_3^{*} + \frac{1}{32}k_4 - \frac{5}{144}k_5\right) \qquad \text{(I -10a)}$$

$$= A_3 + B_3\cos 2\theta + C_3\cos 4\theta \ , \qquad \text{(I -10b)}$$

where the constants A_3, B_3, C_3 are given by the expressions inside the corresponding brackets. It is to be noted that the cases $\theta = 90^\circ$ ($\langle 011\rangle$ direction) and $\theta = 0$ ($\langle 111\rangle$ direction) correspond to $\eta = 90^\circ$ in the first and second positions of the crystal respectively.

APPENDIX II

The demagnetizing factor of a uniformly magnetized isotropic medium in the shape of an infinitely long bar of rectangular cross-section:-

If a ferromagnetic body of irregular shape is brought into a uniform applied field, H , the magnetising force, H_i, inside the material, differs in magnitude from the applied field and varies in direction throughout the body in an unknown manner. For a uniformly magnetized body, the relation is given by

$$H_i = H - NI \ , \qquad \text{(II-1)}$$

where the demagnetizing field, NI, is assumed proportional to the intensity of magnetization I and is co-directional with H_i and H. Except in the special case where the specimen is magnetized to saturation in very strong fields, uniformity of magnetization is possible only for homogeneous, isotropic bodies whose surfaces are of the second degree, although H_i and I are not necessarily in the same direction as H.

Inside any ellipsoid, the field H_d due to magnetization alone (putting H = 0 in (II-1)) is co-directional with I for magnetization along the three principal axes; taking these components as I_x, I_y, I_z along the co-ordinate axes x, y, z, the components of the demagnetizing field due to magnetization I are therefore N_xI_x, N_yI_y, N_zI_z respectively where N_x, N_y, N_z are the corresponding demagnetizing coefficients of the ellipsoid and are

determined by the ratios of the principal axes. It is thus clear that except for the sphere, the resultant field H_i due to magnetization alone will not be co-directional with the intensity I. Using the demagnetizing factor, defined as $D = N/4\pi$, the relations among the three components are

$$N_x + N_y + N_z = 4\pi, \quad \text{or} \tag{II-2a}$$

$$D_x + D_y + D_z = 1 . \tag{II-2b}$$

For a sphere, $D_x = D_y = D_z = \frac{1}{3}$; for an infinitely long bar or cylinder, $D_x = D_y = \frac{1}{2}$, $D_z = 0$, whilst for an infinitely long flat plate magnetized perpendicular to its surface, $D_x = D_y = 0$, $D_z = 1$.

It has been shown (see, for example, Jeffreys and Jeffreys[78]) that the potential of a magnetized body at any external point, in general, is given by the equation

$$U = \iiint \left\{ I_x \frac{\partial}{\partial x}\left(\frac{1}{r}\right) + I_y \frac{\partial}{\partial y}\left(\frac{1}{r}\right) + I_z \frac{\partial}{\partial z}\left(\frac{1}{r}\right) \right\} dx\,dy\,dz , \tag{II-3}$$

where I_x, I_y, I_z are the components of magnetization I at the point x,y,z of the magnetized body. For a uniformly magnetized body, the magnetization is solenoidal and (II-3) reduces, by the familiar volume-to-surface integral transformation, to the form

$$U = \int \frac{I \cos\theta}{r} \, dS , \tag{II-4}$$

where θ is the angle between the direction of magnetization and the outward-drawn normal to the element dS of the surface. If the magnetization of the body is not uniform, the potential is then given by a distribution of magnetic charges throughout the interior of volume-density ρ together with a distribution over the surface of

surface-density σ as expressed in the following relation

$$U = \int_{\tau} \frac{\rho}{r} d\tau + \int_{s} \frac{\sigma}{r} dS \ . \qquad \text{(II-5)}$$

When the point P (ξ, η, ζ) at which the potential is being calculated, is <u>outside</u> the region of integration and provided that the integrand has at all points of the region and for all values of say, ξ', a differential coefficient with respect to ξ, which is a uniformly continuous function of ξ throughout the region, it can be shown that the differential coefficient of the integral is the same as the integral of the differential coefficient.

At <u>interior</u> points, however, the integral expressions are generally improper since the factors $1/r^k$ become infinite within the region of integration. The integral is convergent for $k < 3$, divergent for $k > 3$ and may be divergent, semi-convergent or convergent for $k = 3$. Differentiation under the integral sign is permissible only when the integrals both before and after differentiation are convergent.

By considering a small spherical cavity of surface S_2, surrounding the point P inside a magnetized body of (outside) bounding surface S_1, the potential at this point may be written as

$$U = U_1 + U_2 \ , \qquad \text{(II-6)}$$

where

$$U_1 = \int_{S_1} \frac{\sigma}{r} dS \quad \text{and} \quad U_2 = \int_{S_2} \frac{\sigma}{r} dS$$

But

$$U_2 = \int_{S_2} \frac{\sigma \, r d\theta . r \sin\theta \, d\phi}{r}$$

$$= \int_{S_2} k\, r\, d\theta\, d\phi \ , \qquad \text{(II-7)}$$

where ϕ is the azimuthal angle.

Thus U_2 vanishes as $r \longrightarrow 0$. This result is true even if the surface S_2 is not spherical and so the only contribution is from S_1 i.e. from U_1.

In the case of a uniformly magnetized bar, magnetized along the x direction perpendicular to its axis (Fig. 62), the field at the point P (ξ, η, ζ) due to pole densities of $\pm \sigma$ on the faces $x = \pm a$, $|y| \leqq b$, is then given by

$$F_\xi = \sigma \int_0^b \int_{-\infty}^{+\infty} \frac{\partial}{\partial x} (r^{-1})\, dy\, dz$$

remembering that $\frac{\partial}{\partial x} \left(\frac{1}{r}\right) = - \frac{\partial}{\partial \xi} \left(\frac{1}{r}\right)$. This gives

$$F_\xi = 2\sigma \left[\tan^{-1} \frac{b - \eta}{a - \xi} - \tan^{-1} \frac{-\eta}{a - \xi} \right]. \qquad \text{(II-8)}$$

The average demagnetizing field over the interior of the body is obtained as

$$\langle F_\xi \rangle_{av} = \frac{2}{ab} \int_0^b \int_0^a F_\xi\, d\eta\, d\xi \ . \qquad \text{(II-9)}$$

By solving this integral, it may be shown that

$$\langle F_\xi \rangle_{av} = \frac{4\sigma}{ab} \left[2b^2 \left\{ \tfrac{1}{2} \ln (1 + p^2) + p \tan^{-1} \frac{1}{p} \right\} - \frac{a^2}{2} \ln \left(1 + \frac{1}{p^2}\right) - \frac{b^2}{2} \ln (1 + p^2) \right] ,$$

$$= 2\sigma \left[4 \tan^{-1} \frac{1}{p} + 2p \ln p + \frac{1 - p^2}{p} \ln (1 + p^2) \right], \qquad \text{(II-10a)}$$

$$= 4\pi D\sigma \ , \qquad \text{(II-10b)}$$

where $p = \frac{a}{b}$ and D = demagnetizing factor. This gives the expression (5.4) appearing on page 123. Since $D_z = 0$ for an infinitely long bar, the values of D for $p = p_1$ and for $p = \frac{1}{p_1}$ add to unity in the above expression. For any arbitrary direction of magnetization,

$$\sigma_x = \sigma \sin\theta \cos\phi$$

$$\sigma_y = \sigma \sin\theta \sin\phi$$

$$\sigma_z = \sigma \cos\theta$$

and if $D_z = 0$, the demagnetizing field is given by

$$H_d = 4\pi \sqrt{D_x^2 \sigma_x^2 + D_y^2 \sigma_y^2}$$

$$= 4\pi \sigma \sin\theta \sqrt{D_x^2 - (2D_x - 1) \sin^2\phi}\ , \qquad \text{(II-11)}$$

and this makes an angle Ψ with the x direction where

$$\tan\Psi = \frac{D_y}{D_x} \tan\phi = \tan\phi \left(\frac{1}{D_x} - 1\right)$$

since $D_x + D_y = 1$.

APPENDIX III

J. Phys. Chem. Solids Pergamon Press 1965. Vol. 26, pp. 1555–1560. Printed in Great Britain.

THE MAGNETIC SUSCEPTIBILITIES OF $LiFeO_2$

J. C. ANDERSON, S. K. DEY and V. HALPERN

Materials Section, Department of Electrical Engineering, Imperial College, London S.W.7

(*Received* 8 *January* 1965; *in revised form* 9 *April* 1965)

Abstract—The temperature and field dependence of susceptibility for α, β and γ phases of $LiFeO_2$ have been measured. Transition temperatures are observed at 42°K for α and β and at 295°K for γ phases, which are identified as Néel temperatures. The temperature dependence of susceptibility curves show departures from Curie–Weiss behaviour for each phase. This is explained in terms of short-range ordering of Fe and Li ions in the cases of α and β. The γ structure is ordered and the Weiss molecular field theory is applied to it, using a 16-sublattice model. The results of the calculation illustrate the limitations of the Weiss model in this structure.

INTRODUCTION

FOLLOWING an earlier investigation, by ANDERSON and SCHIEBER,[1] into the morphology of $LiFeO_2$, magnetic susceptibilities have now been measured, in the range 4–1000°K for the three crystallographic phases α, β and γ.

The α form is a rock-salt structure whilst β is a body-centred tetragonal structure, both with disordered metal ions. These show antiferromagnetic behaviour at low temperatures both with transitions at 42°K. The γ structure is ordered and has a transition temperature at 295°K$\pm$5°K. In each case there are deviations from the 'normal' type of susceptibility. The limitations of the Weiss molecular field theory in respect of the γ-phase structure are pointed out.

APPARATUS AND SAMPLES

The samples were powdered single-crystals, grown from a flux as described by ANDERSON and SCHIEBER.[2] Heat treatments were carried out to produce the three phases as described in ref. (1), the same samples being used as were the subject of the X-ray investigation.

Measurements were made on a Sucksmith ring balance, in conjunction with a split-photocell amplifier device, detecting a minimum magnetic moment of 10^{-4} e.m.u. corresponding to a susceptibility of 10^{-8} c.g.s. for a 1 gm sample in a field of 6 K Oe. A 7 in. electromagnet provided fields up to 6 kG across a 2 in. gap. Calibration of the balance was carried out using six different materials for which accurate susceptibility values were available in the literature.

Temperature measurement in the range 4·2–300°K was provided by means of a gold–cobalt/gold–silver thermocouple, using liquid oxygen as the reference point. Above 300°K a Chromel–Alumel thermocouple was used. Estimated accuracy of temperature measurement was $\pm$0·25°K in the range 20–60°K and $\pm$0·1°K elsewhere. Accuracy in measurement of susceptibility was estimated at 1–1·5%.

RESULTS

In Figs. 1, 2 and 3 are given the field-dependence of magnetization curves, for the three phases, over a range of temperatures. Extrapolation of these reveal, for each phase, a remanent moment σ_0 at absolute zero, so that the magnetization may be represented by $\sigma = \sigma_0 + \chi H$. At room temperature the values of σ_0 are 0·542 e.m.u./gm for α, 0·615 e.m.u./gm for β and 0·484 e.m.u./gm for γ.

From Fig. 3 the temperature-dependence of σ_0 for the γ-phase has been deduced and is plotted in Fig. 4, from which it is seen that σ_0 falls to zero at 960°K. This result strongly suggests that the remanent moment is due to a ferromagnetic impurity having a Curie temperature of the order of 960°K. The possible ferromagnetic impurities are Fe_3O_4 or $LiFe_5O_8$. These have Curie temperatures of 585°C and 670°C respectively, so that $LiFe_5O_8$

is the most probable of the two. The remanent moment of 0·484 e.m.u./gm in γ would be accounted for by approximately 1% of $LiFe_5O_8$, which would not be observed by X-ray analysis. It is assumed that this type of impurity is present in all the samples despite the apparently higher Curie temperature observed for σ_0. On this basis, curves of reciprocal susceptibility as a function

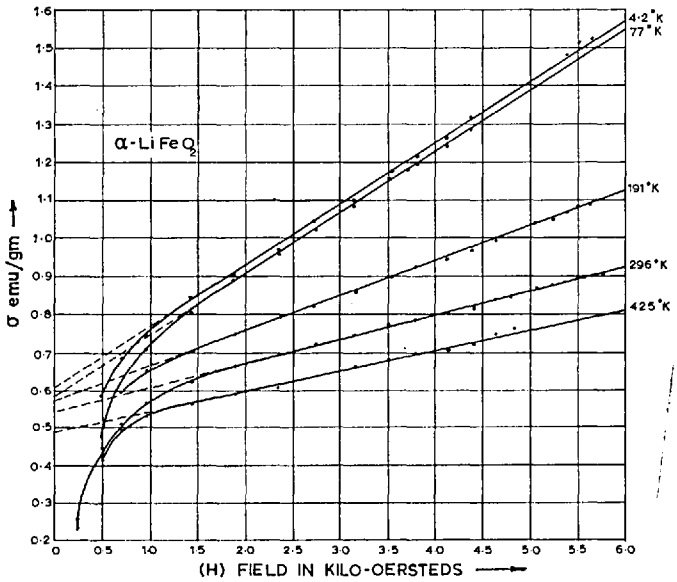

FIG. 1. Magnetization, σ, as a function of field and temperature for α-$LiFeO_2$

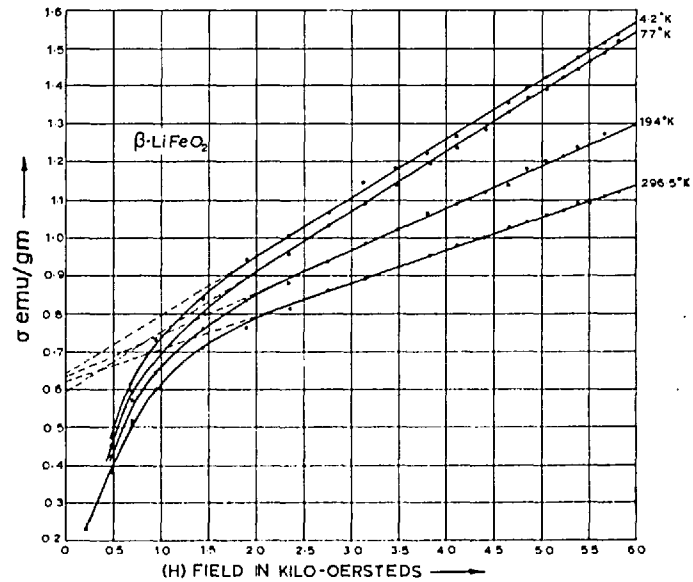

FIG. 2. Magnetization, σ, as a function of field and temperature for β-$LiFeO_2$.

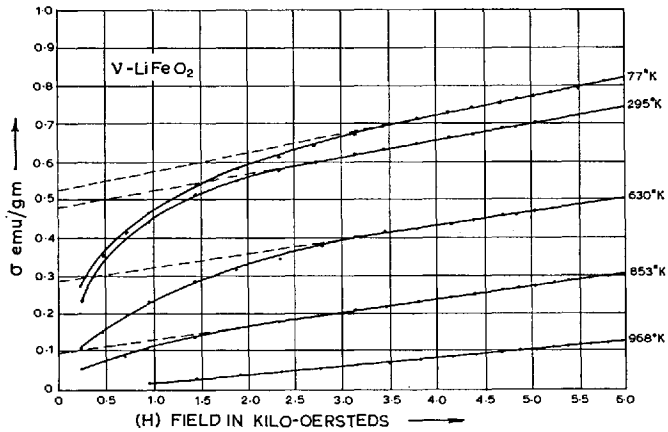

FIG. 3. Magnetization, σ, as a function of field and temperature for γ-$LiFeO_2$.

temperature have been deduced from Figs. 1, 2 and 3 with the remanent moment contributions subtracted; the results are shown in Figs. 5, 6 and 7 for the α, β and γ phases respectively.

In the cases of both α and β there is a transition at 42°K. However, the Curie–Weiss law of susceptibility above the transition temperature is only properly obeyed above about 250°K, and calculations for this part of the curves yield a moment for the Fe^{3+} ions in the α-phase of 5·91 Bohr magnetons and in the β-phase of 5·48 Bohr magnetons. For the γ-phase the Curie–Weiss law is obeyed above the transition temperature and yields a moment for the Fe^{3+} ions of 5·94 Bohr magnetons in good agreement with the theoretical value of 5·92 for Fe^{3+} ions.

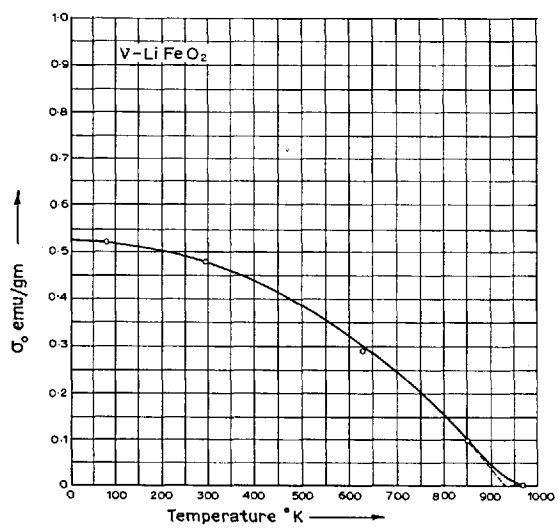

FIG. 4. Remanent moment, σ_0, as a function of temperature for γ-$LiFeO_2$.

DISCUSSION OF RESULTS

Neutron diffraction and Mossbauer data on the α and γ forms of $LiFeO_2$ have been published by Cox *et al.*[3] They give a magnetic structure for α at low temperature in which the spins are coupled ferromagnetically in [111] planes but alternate planes are antiparallel giving a net antiferromagnetic distribution, as shown in Fig. 8(a). They found some evidence of a tendency for Fe and Li ions to order on alternate [111] planes. From the Mossbauer data they obtained a transition temperature in the region of 90°K, compared with 42°K from the present measurements. This discrepancy, together with the departure from the Curie–Weiss law between 42°K and about 250°K in the present measurements could be accounted for by assuming that some spin-ordering, possibly in local clusters, may occur at higher temperatures due to a proportion of the ordered Fe–Li distribution proposed by Cox, but that complete spin-ordering with a disordered Fe–Li distribution cannot occur until the true transition temperature of 42°K is reached.

The β-phase exhibits similar behaviour to that of the α-phase and, in the absence of neutron

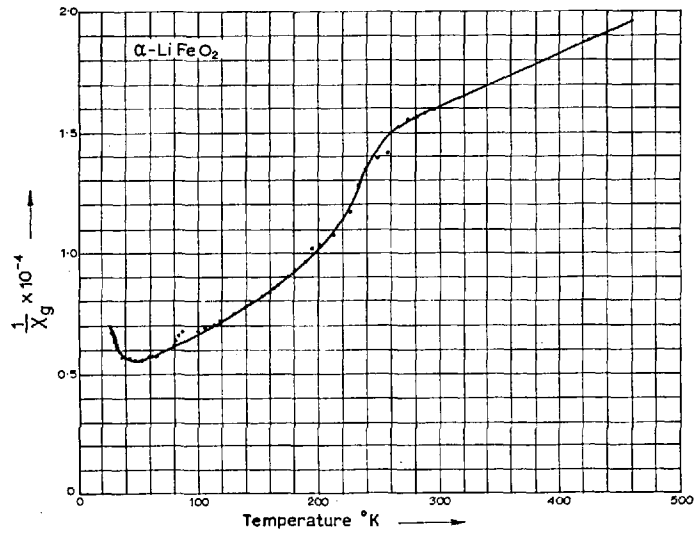

FIG. 5. Reciprocal susceptibility as a function of temperature for α-$LiFeO_2$.

diffraction data, a speculative model of the spin distribution, obtained by interpolation between the known α and γ distributions, is shown in Fig. 8(b). This is based upon the assumption that the predominant interaction is the negative superexchange through 180°, via an oxygen ion, between Fe ions. This leads to an arrangement with the spins ferromagnetically coupled in [110] planes and antiferromagnetically between adjacent [110] planes. The possibility of Fe–Li ordering in these planes, as in the case of α, clearly exists and would account for the departure from the Curie–Weiss law between the transition temperature and 250°K.

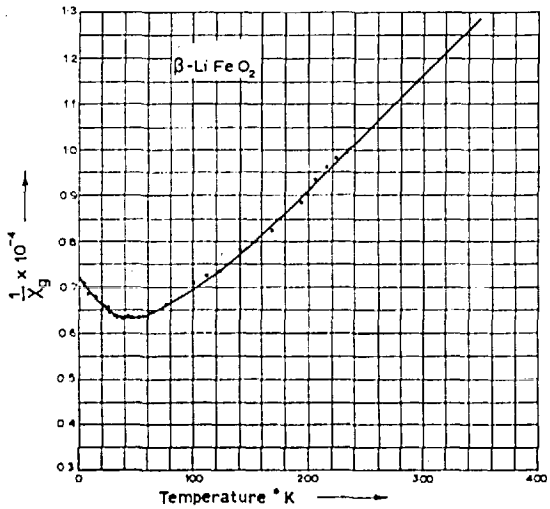

FIG. 6. Reciprocal susceptibility as a function of temperature for β-$LiFeO_2$.

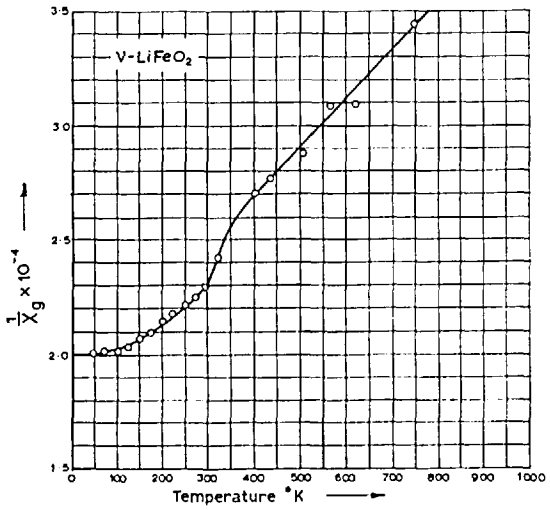

FIG. 7. Reciprocal susceptibility as a function of temperature for γ-$LiFeO_2$.

The γ structure, as reported by Cox *et al.*, is given in Fig. 8(c), and is characterized by antiferromagnetic coupling in the basal plane, with a magnetic symmetry $I\bar{4}2d$. From Mossbauer data they obtained a transition temperature in the region of 290°K, in good agreement with the present result of 295°K. The form of the susceptibility curve, however, departs markedly from that normally expected; comment on this is provided in the next section.

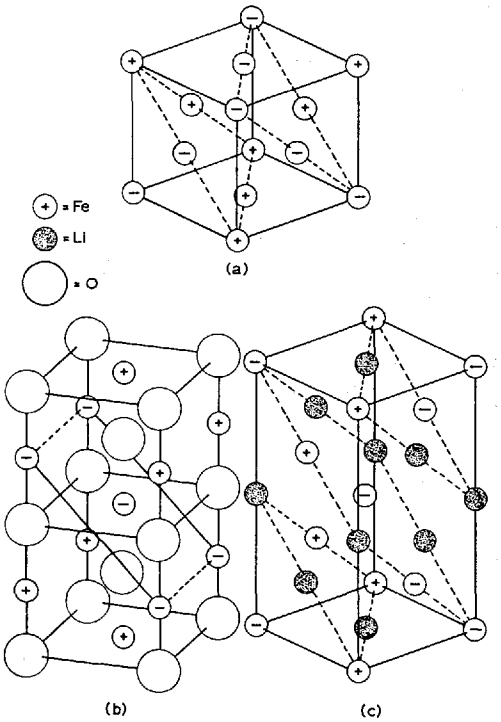

FIG. 8. Spin distributions for (a) α-$LiFeO_2$, (b) β-$LiFeO_2$, (c) γ-$LiFeO_2$. Structures (a) and (c) are from Cox *et al.*[3]

THEORETICAL CONSIDERATIONS

VAN VLECK[4] and NÉEL[5] have given a general treatment in terms of molecular field theory of antiferromagnetism, based on a two-sublattice model. P. W. ANDERSON[6] has generalized this treatment by the use of four sublattices and the inclusion of next-nearest neighbour interactions, and has dealt specifically with the face-centred cubic structure. YAFET and KITTEL[7] have applied the four-sublattice model specifically to ferrites and SINHA and SINHA[8] have considered the spinel structure. In all these treatments a Weiss internal field model is used. For n lattices, the field experienced by the ith lattice is given by

$$H_i^{\text{int}} = \sum_{j=1}^{n} b_{ij} M_j \tag{1}$$

where M_j is the magnetic moment of the jth sublattice. It should be noted that such an equation is only useful if all the atoms on a given sublattice have the same spin; if each sublattice contains equal numbers of positive and negative spins then $M_j = 0$, and the equation is not very valuable.

The γ-phase has a chalcopyrite structure with the magnetic unit cell four times as large as the ordinary crystallographic unit cell and containing 16 Fe atoms. As a result each iron atom can be associated with one of 16 interpenetrating simple cubic sublattices, each of which has all atoms of the same spin. Following P. W. Anderson the moment of the ith sublattice is given approximately by

$$M_i = \gamma \cdot \frac{H_i^{\text{eff}}}{T} \tag{2}$$

Then, in the absence of an external field, from equation (1),

$$TM_i = \gamma \sum_{j=1}^{16} b_{ij} \cdot M_j \tag{3}$$

Equation (3) has a solution in which not all M_j are zero only for certain values of T, and the highest such value corresponds to the transition temperature T_c for that arrangement of spins which gives the lowest energy at temperatures less than T_c. If we assume that each M_j is either parallel or antiparallel to the z-axis, in accordance with the symmetry $I\bar{4}2d$ to which the γ-phase belongs, then the coefficients b_{ij} are scalars and T_c is γ times the highest eigenvalue of the matrix (b_{ij}). If only the sixteen nearest neighbours of each iron atom are assumed to interact appreciably with it, then if the sublattices are suitably labelled the matrix $B = (b_{ij})$ has the form

$$B = \begin{bmatrix} \alpha & \beta & \gamma & \delta \\ \beta & \alpha & \delta & \gamma \\ \gamma & \delta & \alpha & \beta \\ \delta & \gamma & \beta & \alpha \end{bmatrix} \tag{4}$$

where α, β, δ and γ are 4×4 matrices. If we assume that the interaction between second-neighbour iron atoms is the largest in magnitude of all the interactions considered, and is antiferromagnetic, then the state of lowest energy is just that found by Cox *et al.* for the γ structure, in which second-nearest neighbours have opposite spins. This state is quadruply degenerate because of an arbitrariness in the choice of the x, y and z axes, but in one of these states there is a positive spin on all Fe atoms in the first eight sublattices and a negative spin on the other eight. Thus if each set of eight is treated as a single sublattice, the two-lattice theory of Van Vleck can be applied and we should expect the Van Vleck form for the temperature dependence of susceptibility.

Since in the α and β phases the metal atoms are disordered, it is not practicable to apply to them a theory depending on long-range order. Some antiferromagnetism associated with short-range order would be expected, so that it might be possible to relate the magnetic properties of these phases with the deviations of the γ-phase from the Van Vleck theory.

CONCLUSION

All three phases of the lithium ferrite $LiFeO_2$ have been shown to be antiferromagnetic at low temperatures. A remanent moment in each has been ascribed to an impurity, possibly the magnetic spinel $LiFe_5O_8$. It has been shown that the γ-phase, having a chalcopyrite structure, departs from the simple Van Vleck theory of antiferromagnetism. Possible reasons for this deviation require further investigation.

Acknowledgements—It is a pleasure to acknowledge the contribution of M. SCHIEBER, who initiated the research and supplied the samples. One of the authors (V. HALPERN) was supported by a grant from the Worshipful Company of Clothworkers of the City of London.

REFERENCES

1. ANDERSON J. C. and SCHIEBER M., *J. Phys. Chem. Solids* **25**, 961 (1964).
2. ANDERSON J. C. and SCHIEBER M., *J. Phys. Chem. Solids* **25**, 1838 (1964).
3. COX D. E., SHIRANE G., FLINN P. A., RUBY S. L. and TAKEI W. J., *Phys. Rev.* **132**, 1547 (1963).
4. VAN VLECK J. H., *J. Chem. Phys.* **9**, 85 (1941).
5. NÉEL L., *Ann. de Phys.* **3**, 137 (1948).
6. ANDERSON P. W., *Phys. Rev.* **79**, 705 (1950).
7. YAFET Y. and KITTEL G., *Phys. Rev.* **87**, 290 (1952).
8. SINHA K. P. and SINHA A. P. S., *J. Phys. Soc. Japan* **17**, B.I., 218 (1962).

APPENDIX IV

Reprinted from
PHILOSOPHICAL MAGAZINE, Vol. 12, No. 119, p. 975, November 1965

The Magnetic Properties of Cadmium Manganite

By S. K. DEY and J. C. ANDERSON
Department of Electrical Engineering, Imperial College, London, S.W.7

[Received 9 June 1965]

ABSTRACT

The magnetic susceptibilities of cadmium manganites, $(Cd_x^{2+}Mn_{1-x}^{2+})Mn_2^{3+}O_4$, have been measured between 4·2°K and 1000°K as functions of field and temperature. All the samples except $x=1$ become ferrimagnetic at low temperatures and show three transition points. As the temperature is lowered, the first transition corresponds to paramagnetic antiferromagnetic ordering and the second to the appearance of a canted spin structure. The lowest transition corresponds to the appearance of spontaneous moment. Between the first and second transitions the susceptibility remains temperature independent, a feature which becomes more evident as x is increased. The presence of each transition is confirmed by differential thermal analysis. The generally complex behaviour is explained in the light of the existing theories.

§ 1. INTRODUCTION

THE magnetic properties of manganites having the general formula $(D_x^{2+}Mn_{1-x}^{2+})Mn_2^{3+}O_4$, where D is a diamagnetic cation, have been studied widely (Bongers 1957, Jacobs 1959, Jacobs and Kouvel 1961, Rosenberg and Nicolae 1964). These compounds are isomorphous with the mineral hausmannite (Mn_3O_4) and are characterized by replacement of the Mn^{2+} ions on the tetrahedral sites by Zn^{2+}, Mg^{2+} or Cd^{2+}. The crystal structure is a tetragonally distorted spinel with $c/a \sim 1{\cdot}15$ (Jacobs and Kouvel 1961, Mason 1947) with only Mn^{3+} ions on the octahedrally coordinated B sites, the A sites being randomly occupied by Mn^{2+} and diamagnetic ions (Dunitz and Orgel 1957, Goodenough and Loeb 1955, Wojtowicz 1959). Yafet and Kittel (1952) have proposed a model for low temperatures in which the spin distribution is described in terms of four sub-lattices, on two of which the spins are parallel and on the other two they are canted, so that there is a net triangular spin arrangement. On the basis of measurements down to 77°K, Rosenberg and Nicolae (1964) have suggested that the cadmium manganites exhibit, instead, antiferromagnetic behaviour as predicted by Sinha and Sinha (1962). This was for tetragonalized spinels having only diamagnetic cations on tetrahedral sites, and involves a spin arrangement on the octahedral sites giving rise to a temperature-independent antiferromagnetic susceptibility below the Néel point.

§ 2. Measurements and Results

Samples of $Cd_xMn_{(3-x)}O_4$ were prepared with $x=0{\cdot}4$, $0{\cdot}5$, $0{\cdot}6$, $0{\cdot}7$, $0{\cdot}8$, $0{\cdot}9$ and $1{\cdot}0$. All samples were checked by x-ray analysis and were found to have approximately the same tetragonal distortion from spinel structure with $a=8{\cdot}074$ Å, $c=9{\cdot}554$ Å and $c/a=1{\cdot}18$ for $CdMn_2O_4$. Measurements on this compound by Sinha *et al.* (1957) gave $a=8{\cdot}22$ Å, $c=9{\cdot}87$ Å and $c/a=1{\cdot}2$. The magnetic measurements were carried out on a Sucksmith ring balance capable of measuring a minimum magnetic moment of 10^{-4} emu/g with better than $1{\cdot}5\%$ accuracy. The field was provided by

Fig. 1

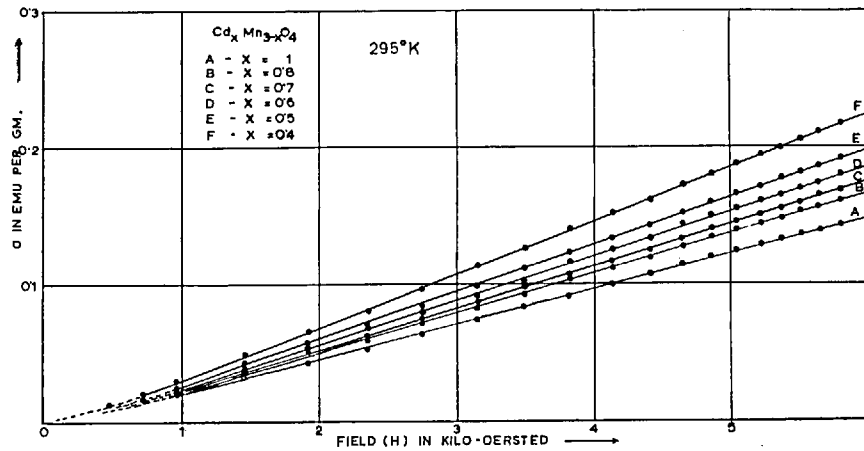

(*a*)

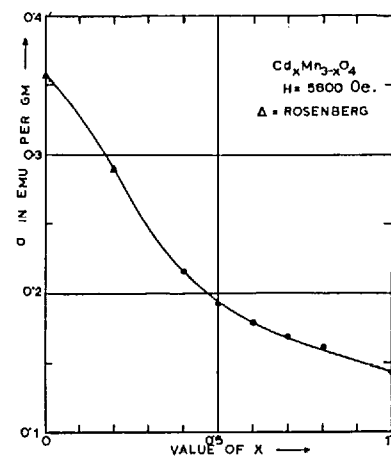

(*b*)

(*a*) Magnetization, σ, as a function of field at room temperature for samples $Cd_xMn_{3-x}O_4$ with $x=0{\cdot}4$, $0{\cdot}5$, $0{\cdot}6$, $0{\cdot}7$, $0{\cdot}8$ and $1{\cdot}0$. (*b*) Magnetization, σ, as a function of cadmium concentration x at $H=5800$ oe for $Cd_xMn_{3-x}O_4$.

Fig. 2

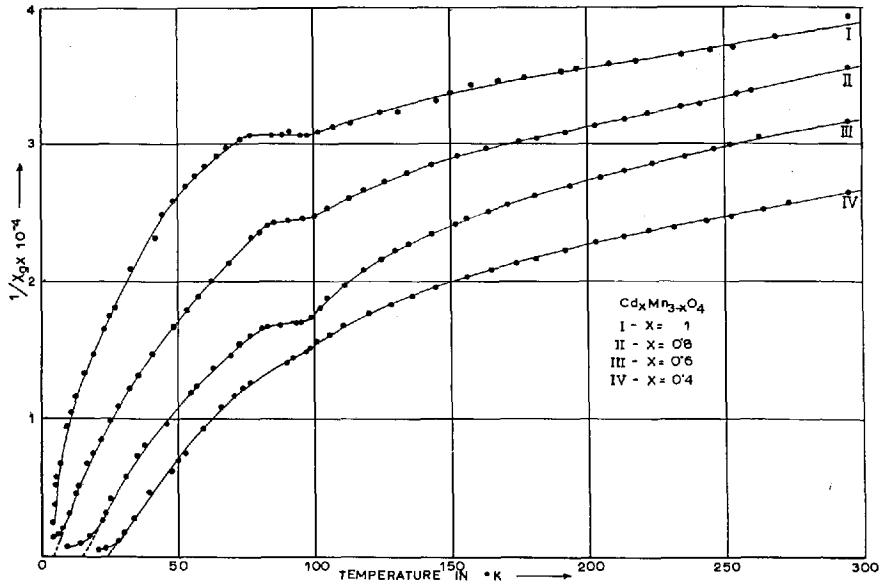

(*a*)

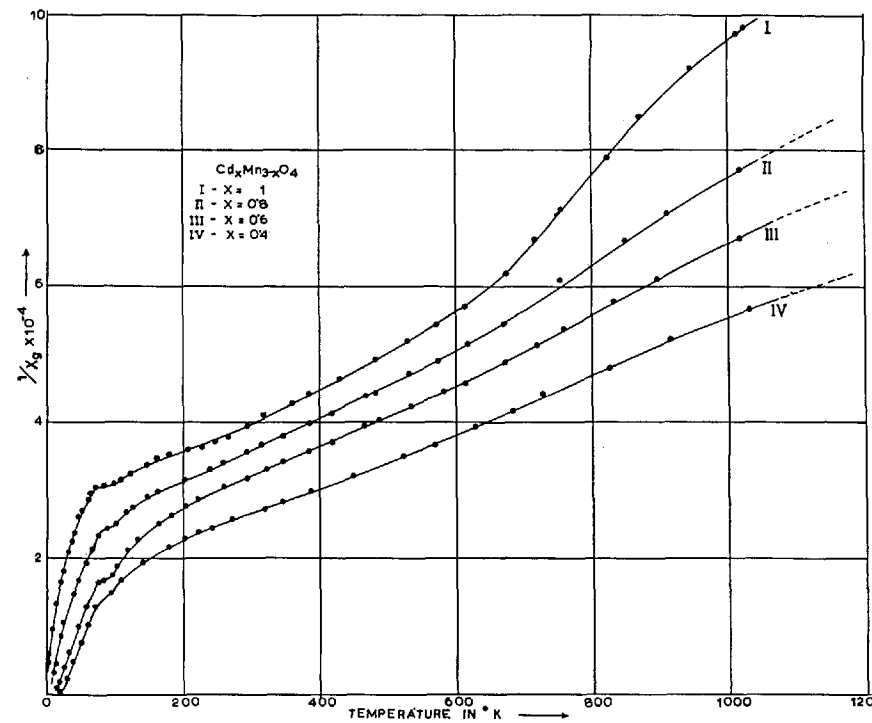

(*b*)

(*a*) Inverse susceptibility, $1/\chi_g$, as a function of temperature for $Cd_xMn_{3-x}O_4$ with $x=1{\cdot}0$, $0{\cdot}8$, $0{\cdot}6$ and $0{\cdot}4$ in a field $H=5200$ oe and below room temperature. (*b*) Inverse susceptibility, $1/\chi_g$, as a function of temperature for $Cd_xMn_{3-x}O_4$ with $x=1{\cdot}0$, $0{\cdot}8$, $0{\cdot}6$ and $0{\cdot}4$ in a field $H=5200$ oe and above room temperature.

a 7 in. electromagnet producing a maximum field of 6 koe across the sample. The susceptibility values are given for σ/H per gram, rather than for the incremental susceptibility.

Magnetization was measured as a function of temperature by cooling the specimen to 4·2° K in zero field and then making measurements in a fixed field of 5220 oe as the temperature rose to 300° K. A water-jacketed furnace provided the means for high temperature measurements up to 1000° K. Magnetization was also measured as a function of field from zero to 6 koe at 4·2° K, 77° K and at room temperature.

In fig. 1 (*a*) are shown magnetization versus field curves, taken at room temperature, for samples with $x = 0{\cdot}4$, 0·5, 0·6, 0·7, 0·8 and 1·0, from which it will be seen that there is a linear increase of magnetization with field throughout the range in agreement with normal paramagnetic behaviour. Figure 1 (*b*) shows the magnetization plotted against various values of x at $H = 5800$ oe taken from the previous graph. In figs. 2 (*a*) and 2 (*b*) the reciprocal of susceptibility ($1/\chi_g$) is plotted as a function of temperature, in a field of 5200 oe for samples with $x = 1{\cdot}0$, 0·8, 0·6 and 0·4. Below $\sim 70°$ K, these curves exhibit typical ferrimagnetic behaviour with Curie temperatures of $< 4°$ K, 5° K, 15° K and 24·5° K respectively. In the range 80–100° K, there appears a range of temperature-independent susceptibility which progressively increases in temperature range as x increases from 0·4 to 1·0. For each sample this region ends at 99° K, after which $1/\chi_g$ increases with increasing temperature. This is taken to be a transition temperature from an ordered spin arrangement to the paramagnetic state and is referred to as the first transition. However, this characteristic was not evident when measurements were repeated in a field of 3000 oe. The curves also exhibit deviation from linearity at high temperatures which becomes more pronounced with increasing x, suggesting the possible onset of crystallographic phase transformations. For $CdMn_2O_4$, this occurs at about 670° K, a temperature which gradually moves towards higher values as x is decreased (fig. 2 *b*).

In figs. 3 (*a*) and 3 (*b*) are shown susceptibility versus field curves for $x = 0{\cdot}4$, 0·6, 0·8 and 1·0 at 77° K and 4·2° K respectively. At 77° K the susceptibility tends to drop markedly in low fields. Figure 3 (*b*) gives results below the Curie temperature for each sample and is typical of ferrimagnetic behaviour which decreases in magnitude as x increases from 0·4 to 0·8, with the exception that the low field initial susceptibility for $x = 1{\cdot}0$ decreases with decreasing field in a normal antiferromagnetic manner. Magnetization curves as a function of temperature at a fixed field are shown in fig. 4 for the various compounds, at temperatures near to the Curie points. The evaluation of Curie temperatures from the slope of these curves is considered unreliable because the maximum available field is not sufficiently high and determination from the temperature intercept of each $1/\lambda_g$ versus T curve is preferred. As is seen from the graphs, the presence of Cd on the spinel A sites has a marked effect upon the Curie temperature. Within the range of the present investigation,

Fig. 3

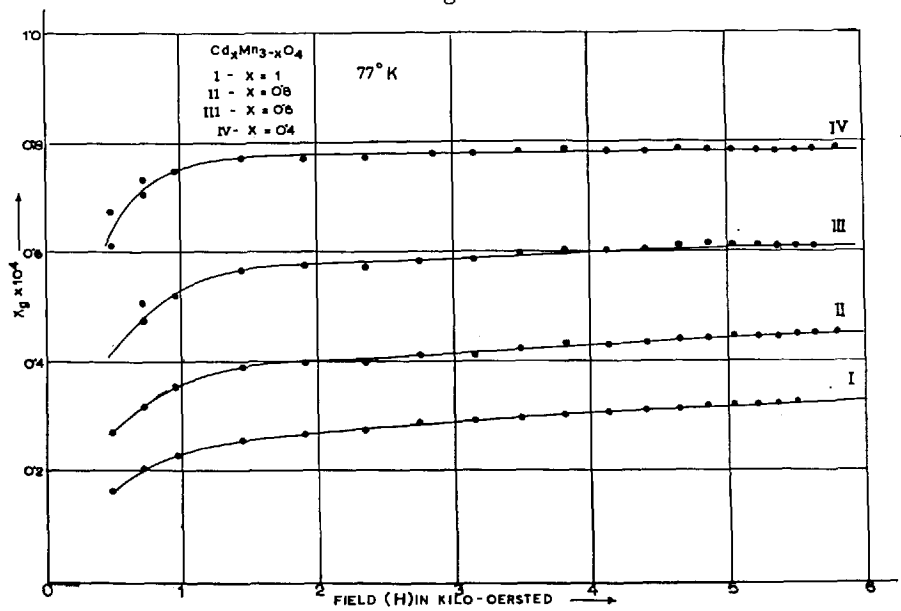

(*a*)

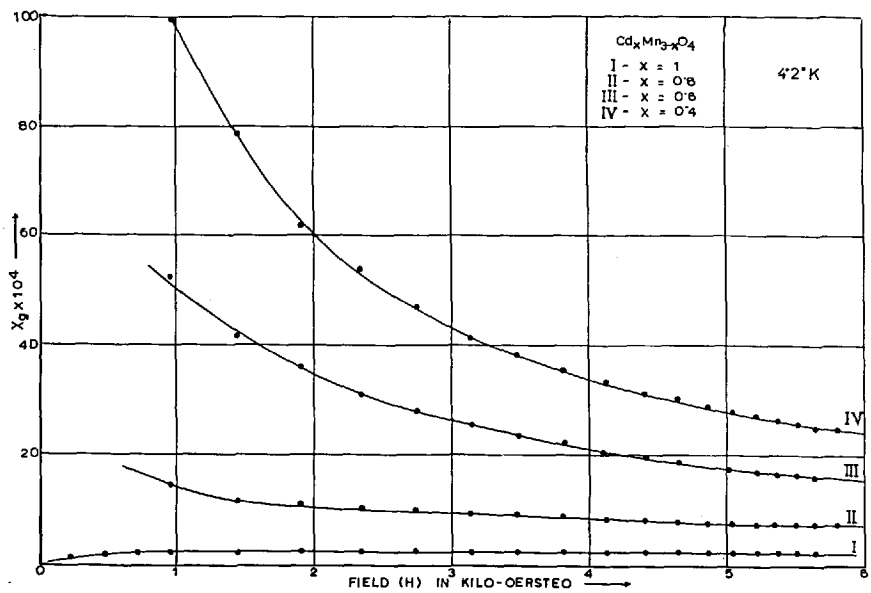

(*b*)

(*a*) Magnetic susceptibility, χ_g, as a function of field at 77°K for $Cd_xMn_{3-x}O_4$ with $x=0{\cdot}4$, 0·6, 0·8 and 1·0. (*b*) Magnetic susceptibility, χ_g, as a function of field at 4·2°K for $Cd_xMn_{3-x}O_4$ with $x=0{\cdot}4$, 0·6, 0·8 and 1·0.

Fig. 4

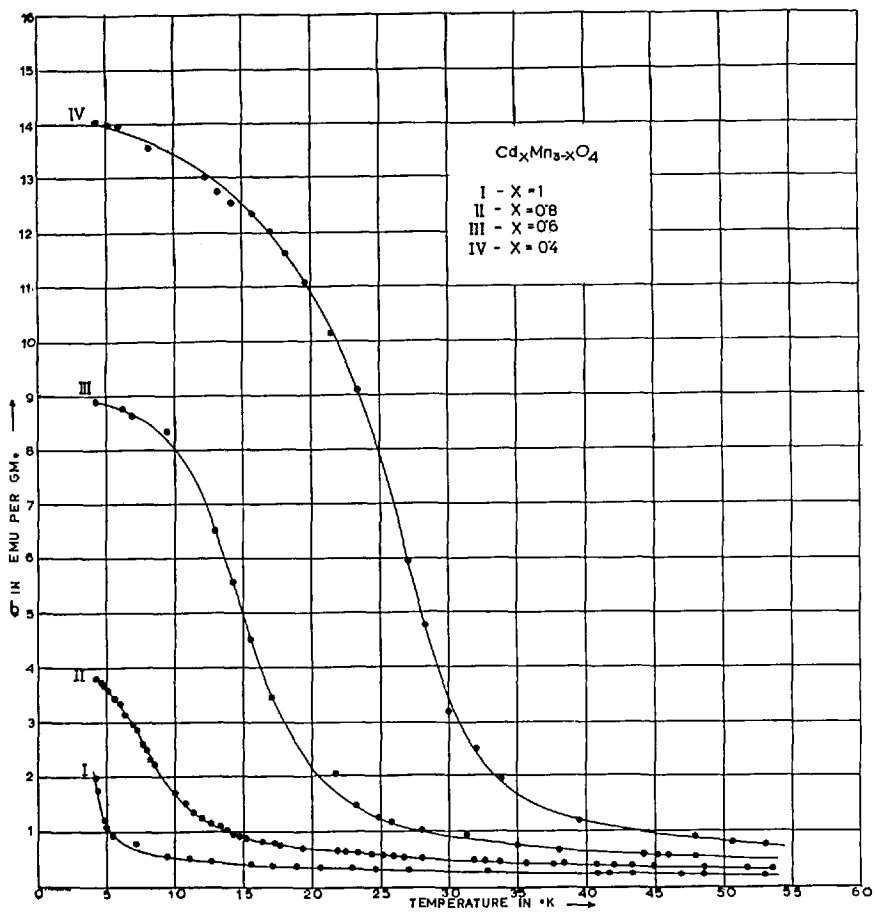

Magnetization, σ, as a function of temperature for $Cd_xMn_{3-x}O_4$ with $x = 0{\cdot}4$ 0·6, 0·8 and 1·0 below the Curie points.

the dependence of the Curie temperature upon the Cd concentration shows a strictly linear relationship as in fig. 5. However, fig. 6 shows that the variation of the spontaneous magnetization with x is non-linear. This behaviour is discussed later.

Differential thermal analysis was also carried out on the present samples in the temperature range 77°–1000°K and the results appear to be in good agreement with the magnetic measurements. Below room temperature, two peaks were obtained, at 95·2°K and 86·2°K for $x = 1$, but only one asymmetric peak at 91·7°K for all $x < 1$ was observed. Further, for $x = 1$, the first peak at the higher temperature is about seven times bigger than the second peak and of the opposite sign. These results suggest that two different kinds of magnetic transformation are involved as the temperature

Fig. 5

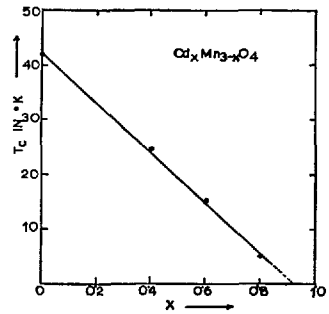

Variation of the Curie temperature, T_c, with the cadmium concentration x in the samples $Cd_xMn_{3-x}O_4$.

is gradually lowered. The absence of a double peak for $x < 1$ may be explained by the low resolution of the D.T.A. method and corresponds to the super-imposition of the two peaks. High temperature D.T.A. on $CdMn_2O_4$ had initially shown a peak at 465°K and a sharp discontinuity at 763°K but subsequent runs involving approximately the same hours of heating as in the case of susceptibility measurements indicated a broad discontinuous peak at about 600°K which is ascribed to crystallographic phase change.

The crystal structure of $CdMn_2O_4$ below the order–disorder transition temperature was further investigated by x-ray powder photograph taken at 77°K. The low temperature camera consisted of a simple Laue plate

Fig. 6

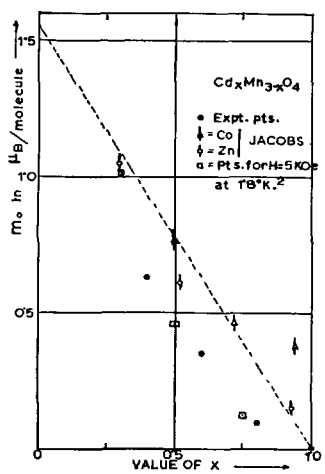

Variation of the spontaneous magnetization, m_0, with the cadmium concentration in the samples $Cd_xMn_{3-x}O_4$.

employing the back reflection technique and an arrangement for a fine stream of liquid nitrogen to flow constantly over the rotating specimen during the exposure time. A comparison of the photograph with that taken at room temperature showed that no crystallographic phase transformations occur in this temperature range. McGuire *et al.* (1952) have reported a kink in the $1/\chi$ versus T curve for $NiCr_2O_4$ at 310°K where the unit cell is found to change from cubic to tetragonal; such a transformation does not occur in the present compounds.

§ 3. Discussion of Results

A conclusion of the Yafet–Kittel theory is that the transition from a triangular spin arrangement to a paramagnetic state must be via an intermediate state. There are two possibilities for this intermediate state:

(*a*) an antiparallel Néel ferrimagnetic state for the A and B sub-lattices;
(*b*) a state in which the A lattice is paramagnetic and the B lattice antiferromagnetic.

The former case should lead to normal antiferromagnetic behaviour with a negative slope to the $1/\chi$ curve over the intermediate range. In the present case this range corresponds to a temperature-independent susceptibility so that the second possibility would appear the more probable. In this connection we refer to the differential thermal analysis results (D.T.A.). As the temperature is lowered the first transition corresponds to a lowering of entropy, which could be accounted for by the appearance of antiferromagnetic ordering on the B sites. The second transition corresponds to a slight increase in entropy which would be expected if there appeared a canted or spiral spin arrangement on the B sites. For both the first and second transitions it is assumed that the A sites remain paramagnetic.

The temperature-independent susceptibility would be accounted for, neglecting the A site contribution for the moment, if the antiparallel spins all lie in planes having low crystalline anisotropy. This is known to be the case in Mn_3O_4 in which the spins all lie in the x–z planes where the y direction is one of high anisotropy (Dwight and Menyuk 1959). When this is the case the antiparallel pairs of spins will be able to minimize their energy in an applied field by turning perpendicular to it, when the field is sufficiently high to overcome the (small) anisotropy in the plane. This would mean that the susceptibility measured is always $\chi_\perp$ which, in accordance with the Néel theory, is temperature-independent. There would be a paramagnetic contribution to the susceptibility from the A sites, of increasing importance as the concentration of magnetic ions on the A sites increased and there is some evidence of this in the results. This behaviour and spin configuration are of the type predicted by Sinha and Sinha (1962) for tetragonalized spinels, but it should be noted that the Sinhas' calculation is not in agreement with that of Yosida (1953) which is generally accepted as correct.

Below the second transition temperature the susceptibility increases as temperature falls, reaching a maximum at the Curie temperature, providing there are some magnetic ions on the A sites, below which a spontaneous moment appears, which rapidly increases as the temperature falls further. In the region between the second transition and the Curie temperature the paramagnetic-like susceptibility behaviour may be ascribed to lack of long-range order on the B sites. For the special case of zero A–B interaction, Anderson (1956) has shown that no long-range ordering of the B spins in the ground state is possible in a cubic spinel and that there is also no long-range ordering of angles between spins. When $x=1$, the A site ion has no magnetic moment and, in the absence of any appreciable long-range order, the magnetic configuration of the B sites in $CdMn_2O_4$ may be likened to groups of four magnetic ions which are exchange coupled amongst themselves but are isolated in a diamagnetic matrix, if super–superexchange is neglected. Thus only local structures are involved rather than a cooperative phenomenon among many ions. Following Jacobs and Kouvel (1961) it can be argued that if the local structures exhibit weak net magnetization, behaving like canted or spiral antiferromagnets below the transition temperature and making differing angles with the field direction, it is possible that an applied field can align them to produce a net spontaneous magnetization. A subsequent paper by Kaplan (1960) however, points out that, for mixed compounds like $D_xMn_{3-x}O_4$, it is reasonable to expect that the comparative importance of the B–B interaction, with regard to magnetic properties, is due to the weakening of the A–B interaction by the diamagnetic ions. This mechanism might therefore be expected to operate in all the present compounds and would be expected to lead to a fall in susceptibility in low fields, as is observed (fig. 3*a*) at 77°K, above the Curie temperatures.

At the Curie temperature it is assumed that the A sites become ordered and that long-range order then appears on the B sites, leading to a ferrimagnetic state in all but the $CdMn_2O_4$ case where there are no magnetic ions on the A sites.

On the basis of simple molecular field assumptions, the variation of spontaneous moment with the substitution of non-magnetic ions in A sites should follow a linear decrease. This assumes that the interaction field of A site ions on B site ions is proportional to the net A site moment. With the applied field of 5200 oe, the observed moments are shown in fig. 6 from which it is seen that this proportionality is not fulfilled. However, in view of the very high uniaxial anisotropy field in Mn_3O_4 crystals at 4·2°K($\sim$70 koe) (Dwight and Menyuk 1959), it is clear that saturation measurements on polycrystalline samples will require very large fields. Assuming the absence of anisotropy fields exceeding 70 koe, the spontaneous moment of Mn_3O_4 was found by Jacobs to be $1{\cdot}56 \pm 0{\cdot}04\,\mu_B$/molecule at 4·2°K by extrapolation to $H=0$ from measurements taken with 170 kG pulsed fields. In the present work the spontaneous moments were measured in comparatively low fields but do

show a linear variation within the range of investigation. For the sake of comparison, values of magnetic moments calculated from the hysteresis loop curves of Jacobs and Kouvel (1961) measured at 1·8°K for various manganite compounds in 5 koe field are plotted alongside our experimental values for cadmium manganite, and are in good agreement.

§ 4. Conclusion

The complex behaviour of the reciprocal magnetic susceptibility of the cadmium manganites as a function of temperature indicates the existence of three transition temperatures. As temperature is lowered the first transition corresponds to paramagnetic/antiferromagnetic ordering and the second the appearance of a canted spin structure. The lowest transition temperature corresponds to the appearance of a spontaneous moment and is taken to be a ferrimagnetic Curie temperature. The susceptibility is independent of temperature between the first and second transitions and is accounted for by the assumption that the B-site spins are all antiferromagnetically ordered in low-anisotropy planes. Between the second transition and the Curie temperature there is evidence of the absence of long-range order, the magnetic properties being accounted for by a model postulating local clusters of canted or spiral antiferromagnets.

Acknowledgments

It is a pleasure to acknowledge the assistance of M. Rosenberg, of the Institute of the Academy of Sciences, Bucharest, who provided the samples, and of Dr. V. Halpern for advice on the theoretical interpretation of the results.

References

Anderson, P. W., 1956, *Phys. Rev.*, **102,** 1008.
Bongers, P. F., 1957, Thesis, Leiden (unpublished).
Borovik-Romanov, A. S., 1957, *Soviet Phys., JETP*, **5,** 1023.
Dunitz, J. D., and Orgel, L. E., 1957, *J. Phys. Chem. Solids*, **3,** 20, 318.
Dwight, K., and Menyuk, N., 1959, *Phys. Rev.*, **119,** 1470.
Goodenough, J. B., and Loeb, A. L., 1955, *Phys. Rev.*, **98,** 391.
Jacobs, I. S., 1959, *J. Phys. Chem. Solids*, **11,** 1.
Jacobs, I. S., and Kouvel, J. S., 1961, *Phys. Rev.*, **122,** 412.
Kaplan, T. A., 1959, *Phys. Rev.*, **116,** 888 ; 1960, *Ibid.*, **119,** 1460.
Kanamori, J., 1960, *J. appl. Phys.*, **31,** 14S.
Kasper, J. S., 1959, *Bull. Amer. phys. Soc.*, **4,** 178.
Kouvel, J. S., 1960, *J. appl. Phys.*, **31,** 142S.
Lotgering, F. K., 1956, *Philips Res. Rep.*, **11,** 190.
McGuire, T. R., Howard, L. N., and Smart, J. S., 1952, *Ceramic Age*, **60,** 22.
Mason, B., 1947, *Amer. Min.*, **32,** 426.
Moruzzi, V. L., 1961, *J. appl. Phys.*, **32,** 59S.
Néel, L., 1948, *Ann. Phys.*, **3,** 137.
Rosenberg, M., and Nicolae, I., 1964, *Phys. Stat. Sol.*, K, 127.
Sinha, A. P. B., Sanjana, N. R., and Biswas, A. B., 1957, *Acta Cryst.*, **10,** 439.
Sinha, K. P., and Sinha, B. P. 1962, *J. phys. Soc., Japan*, Suppl. B–I, **17,** 218.
Wojtowicz, P. J., 1959, *Phys. Rev.*, **116,** 32 ; 1960, *J. appl. Phys.*, **31,** 265S.
Yafet, Y., and Kittel, C., 1952, *Phys. Rev.*, **87,** 290.
Yosida, K., 1953, *Annual Report of Scientific Works from the Faculty of Science*, Osaka University, Vol. 1 for 1952, p. 20.